Development of mineralogical and geochemical exploration techniques for carbonatite-related Nb (±Ta) and REE deposits in the Canadian Cordillera

by

Duncan Alisdair Robert Mackay
BSc, Simon Fraser University, 2012

A Thesis Submitted in Partial Fulfillment
of the Requirements for the Degree of

MASTER OF SCIENCE

in the School of Earth and Ocean Sciences

© Duncan Alisdair Robert Mackay, 2015
University of Victoria

All rights reserved. This thesis may not be reproduced in whole or in part, by photocopy
or other means, without the permission of the author.

Supervisory Committee

Development of mineralogical and geochemical exploration techniques for carbonatite-related Nb (±Ta) and REE deposits in the Canadian Cordillera

by

Duncan Alisdair Robert Mackay
BSc, Simon Fraser University, 2012

Supervisory Committee

Dr. George Simandl, Supervisor
(School of Earth and Ocean Science, University of Victoria; British Columbia Geological Survey)
Supervisor

Dr. Dante Canil, Co-Supervisor
(School of Earth and Ocean Science, University of Victoria)
Co-Supervisor

Dr. Laurence Coogan, Departmental Member
(School of Earth and Ocean Science, University of Victoria)
Departmental Member

Abstract

Supervisory Committee

Dr. George Simandl, Supervisor
(School of Earth and Ocean Science, University of Victoria; British Columbia Geological Survey)

Dr. Dante Canil, Co-Supervisor
(School of Earth and Ocean Science, University of Victoria)

Dr. Laurence Coogan, Departmental Member
(School of Earth and Ocean Science, University of Victoria)

Niobium and rare earth elements (REE) are considered as strategic metals in industrialised countries, and are mainly derived from carbonatite-related deposits. Indicator mineral methods for carbonatites using of portable XRF and Quantitative Evaluation of Materials by Scanning Electron Microscopy (QEMSCAN®), shows promise in exploration for Nb and REE. Portable XRF analysis of stream sediments from the Aley, Lonnie, and Wicheeda carbonatites identified 125-250 μm as the ideal size fraction for indicator mineral studies. QEMSCAN® provides (with no additional processing) detection and characterisation of indicator minerals (when found in high concentrations) from carbonatite deposits. Preconcentration by Mozley C800 separator is recommended for sediment samples with low concentrations of indicator minerals. Discrimination diagrams for pyrochlore supergroup and columbite-tantalite series minerals show that minerals from carbonatites occupy the pyrochlore field and extend slightly into the betafite field. Columbite-tantalite series minerals from carbonatites have Mn/(Mn+Fe) atomic ratios ≤0.25 and Ta/(Ta+Nb) ≤0.20. The compositional fields for pyrochlore supergroup and colubmite-tanatlite series minerals from different deposit types partially overlap.

Table of Contents

Supervisory Committee ..... **ii**

Abstract ..... **iii**

Table of Contents ..... **iv**

List of Tables ..... **vii**

List of Figures ..... **x**

Acknowledgments ..... **xvi**

Dedication ..... **xvii**

1 Introduction and objectives **1**
1.1 Statement of problem 1
1.2 Objectives 1
1.3 Outline 2

2 Geology, market, and supply chain of niobium and tantalum – a review **3**
2.1 Introduction 3
2.2 Geology of Ta- and Nb-bearing deposits 10
2.2.1 Pegmatite-related Ta deposits 12
2.2.2 Carbonatite-related Nb-Ta deposits 21
2.2.3 Peralkaline complex-hosted Nb-Ta-REE deposits 26
2.2.4 Peraluminous granite-related Ta±Nb deposits 29
2.2.5 Secondary Ta sources 32
2.3 Grade and tonnage 33
2.4 Ta and Nb concentrate considerations 35
2.5 Summary 36

3 Stream sediment orientation survey and QEMSCAN® study **37**
3.1 Stream sediment orientation surveys 37
3.1.1 Aley carbonatite stream sediment orientation survey 37
3.1.1.1 Introduction 37
3.1.1.2 Geological setting 38
3.1.1.3 Geology of the Aley carbonatite complex 40
3.1.1.4 Methods 42
3.1.1.5 Results 45
3.1.1.6 Discussion 46
3.1.1.7 Conclusions 55
3.1.2 Wicheeda carbonatite stream sediment orientation survey 57
3.1.2.1 Introduction 57
3.1.2.2 Geological setting 58
3.1.2.3 Geology of the Wicheeda carbonatite complex 58
3.1.2.4 Methods 60
3.1.2.5 Results 62

3.1.2.6 Discussion ... 66
3.1.2.7 Conclusions ... 71
3.2 Assessment of QEMSCAN® in specialty metal indicator mineral studies ... 72
3.2.1 Introduction ... 72
3.2.1.1 Potential indicator minerals ... 73
3.2.1.2 Geological setting and characterization of carbonatite-related deposits 73
3.2.1.3 Sampling, portable XRF analysis, and processing methodology ... 74
3.2.2 Methodology ... 75
3.2.2.1 QEMSCAN® methodology ... 75
3.2.2.2 Chemical analysis ... 76
3.2.3 Results ... 76
3.2.3.1 QEMSCAN® ... 76
3.2.3.2 Geochemistry ... 77
3.2.4 Discussion ... 78
3.2.4.1 Aley ... 78
3.2.4.1.1 Indicator mineral abundances ... 78
3.2.4.1.2 Particle size distribution ... 85
3.2.4.1.3 Mineral abundance and pathfinder element concentration ... 87
3.2.4.1.4 Mineral association ... 92
3.2.4.2 Lonnie mineral abundances ... 95
3.2.4.3 Wicheeda mineral Abundances ... 95
3.2.5 Conclusions ... 95

4 Pyrochlore and columbite-tantalite discrimination diagrams ... 97
4.1 Introduction ... 97
4.2 Pyrochlore supergroup ... 98
4.3 Columbite-tantalite solid solution series ... 99
4.4 Methodology ... 100
4.5 Results ... 100
4.6 Discussion ... 107
4.6.1 Pyrochlore supergroup Nb-Ti-Ta ternary diagrams ... 108
4.6.2 Columbite-tantalite quadrilateral ... 110
4.6.3 Discrimination diagrams ... 112
4.7 Conclusions ... 115

5 Conclusions ... 116

Bibliography ... 119

Appendix A Pyrochlore supergroup and columbite-tantalite series minerals ... 151

Appendix B Standards and data quality ... 156
B.1 Portable X-ray fluorescence data quality ... 156
B.2 Laboratory chemical analysis ... 162

Appendix C Heavy mineral processing by Mozley C800 mineral separator ... 164
C.1 Introduction ... 164
C.2 Assessment of the Mozley C800 laboratory mineral separator procedure ... 164
C.3 Processing procedure ... 165
C.4 Optimizing operating conditions based on synthetic and natural samples ... 167

C.5 Mozley C800 laboratory mineral separator and geochemical analysis results 169
C.6 Discussion 171
C.7 Conclusions 177

Appendix D Heavy mineral processing by Wilfley shaking table 179
D.1 Introduction 179
D.2 Assessment of Wilfley mineral separator 179
D.3 Processing procedure 180
D.4 Results of Wilfley table separation and geochemical analysis 180
D.5 Discussion of Wilfley table heavy mineral separation..... 182
D.6 Conclusions 187

List of Tables

Table 2.1 Selected properties of Nb and Ta metals. Atomic radii and valence for both metals is virtually the same, resulting in the very similar chemical and physical properties of the elements. From Slater (1964), Lide (2008), and Winter (2011). 4

Table 2.2 Key Nb- and Ta-bearing minerals. 6

Table 2.3 Major Ta and Nb deposits. 13

Table 3.1 Characteristics of stream channel and sample sites. Sample AL-13-09 was collected upstream of the deposit. Samples Al-13-04, AL-13-05, AL-13-06, and AL-13-07 were collected directly over the deposit. Remaining samples are in order of increasing distance downstream of the deposit. 47

Table 3.2 Relative concentrations of major and trace element analysed by factory-calibrated pXRF. Samples are listed in order of increasing distance downstream of the deposit. Concentrations in ppm excepted were otherwise indicated. The data are internally consistent but have not been recalibrated as described in Simandl et al. (2014) to improve accuracy by correcting for matrix effects and biases. Based on strong positive correlation between 11 U and 15 Th pXRF analysis and corresponding ICP-MS analyses of stream sediments from Aley, Lonnie, and Wicheeda (unpublished) processed in exactly the same manner as those in the present study, systematic overestimation of U and Th, of the order of 35% and 90% respectively, is expected. [a]Total Fe as ferric oxide (Fe_2O_3). 52

Table 3.3 Characteristics of stream channel and sample sites. Samples are in order of increasing distance downstream of the Wicheeda carbonatite complex. UTM zone 10, NAD 83. 63

Table 3.4 Relative major oxide and trace element concentrations analysed by pXRF. This pXRF data has acceptable precision; however, it has not been recalibrated using results of standard laboratory analyses (as described in Simandl et al., 2014) to correct for matrix effects and analytical biases to improve accuracy. Portable XRF is not a substitute for conventional laboratory analyses. Eight size fractions reported for sample WI-13-71H. Six size fractions reported for WI-13-66H. The + 125 μm fraction is reported for all other samples. Results are in ppm except where otherwise noted. Samples are in order of increasing distance downstream of the Wicheeda carbonatite complex. 64

Table 3.5 Potential indicator minerals for carbonatite-related deposits, their density, and corresponding pathfinder elements. 74

Table 3.6 Indicator and major rock forming mineral concentrations (wt. %) for the RAW stream sediment samples and corresponding CON from the Aley (AL), Lonnie (LO), and Wicheeda (WI) carbonatites. “Other” includes all other minor minerals and undefined minerals detected. Mineral abbreviations: pyrochlore (Pcl); columbite-(Fe) (Cmb); fersmite (Fer); REE-fluorocarbonates (REE-Fl); zircon (Zrc); apatite (Ap); magnetite

(Mag); hematite (Hem); rutile (Rt); amphibole/pyroxene (Amp/Px); barite (Brt); calcite (Cal); dolomite (Dol); quartz (Qtz); feldspar (Fsp). n.d. = not detected..... 79

Table 3.7 Indicator mineral concentrations (particle count) for the RAW stream sediment samples and corresponding CON from the Aley (AL), Lonnie (LO), and Wicheeda (WI) carbonatites. Proportion for each indicator minerals (%) of total grain count are shown in brackets. Mineral abbreviations same as Table 3.6. 80

Table 3.8 Concentration of Nb, LREE, and Fe_2O_3 in polished smear sections determined by QEMSCAN®. 81

Table 3.9 Bulk chemical analysis of the RAW stream sediments and corresponding CON from the Aley carbonatite drainage..... 82

Table 3.10 Bulk chemical analysis of the RAW stream sediments and corresponding CON from the Lonnie carbonatite drainage..... 83

Table 4.1 Representative electron microprobe analyses for pyrochlore supergroup minerals. Oxides are in wt. %. 101

Table 4.2 Representative electron microprobe analyses for columbite-tantalite series minerals. Oxides are in wt. %. 104

Table A.1 Mineral chemistry database sources..... 151

Table B.1 Results of repeated analyses on the NIST Standard Reference Material 2780. From Luck and Simandl (2014). 158

Table B.2 Repeated analyses on the Certified Reference Material “TRLK” rare earth ore CGL 124. From Luck and Simandl (2014). 159

Table B.3 Statistical assessment of repeated analyses of the reference material OKA-1. From Luck and Simandl (2014). 160

Table B.4 Portable XRF limits of detection (LOD) for elements pertinent to carbonatite exploration. From Luck and Simandl (2014)..... 161

Table B.5 Lower and upper limits of detection for analytical methods from ALS Limited. From ALS Limited (2015). 162

Table C.1 Relative concentrations (in ppm) of major and minor elements associated with carbonatite from Mozley C800 laboratory mineral separator concentrates, middlings, and tailings from stream sediment samples, analyzed by portable X-ray fluorescence spectrometer. Samples are listed from upstream of, to directly over, and with increasing distance downstream of the Aley carbonatite, northeastern British Columbia. See Fig. 3.2 for sample locations. Error propagation and elemental concentrations near the limit of detection greatly reduce the reliability of calculated values. 172

Table D.1 Selected major and minor elemental composition (ppm) of the 125–250 μm size fraction of stream sediments from the Aley area, analysed by portable XRF. Phosphorous content was determined by lab analysis using fused bead, acid digestion, and ICP-AES analysis. Modified from Section 3.1.1. 185

Table D.2 Selected major and trace element composition (ppm) of Wilfley table concentrates from the Aley area, analysed by portable XRF. Phosphorous was determined by ICP-AES analysis..... 185

List of Figures

Figure 2.1 World mine production of contained Ta metal (excluding Ta recovered as a by-product of Sn mining) by country for the period of 1994 to 2012. Data from Cunningham (1996a, 1997a, 1999a, 2001a, 2003a, 2005a), Magyar (2007a), and Papp (2009a, 2011a, 2013a)..... 8

Figure 2.2 Price of contained Ta_2O_5 in concentrate for 1991 to 2012. Prices are adjusted for inflation to 2012 US dollars. Data from Cunningham (1996a, 1997a, 1999a, 2001a, 2003a, 2005a), Magyar (2007a), and Papp (2009a, 2011a, 2013a). 9

Figure 2.3 World mine production of contained Nb metal by country from 1994 to 2012. Data compiled from Cunningham (1996b, 1997b, 1999b, 2001b, 2003b, 2005b), Magyar (2007b), and Papp (2009a, 2011b, 2013b)..... 10

Figure 2.4 Historic price of contained ferroniobium alloy in concentrate for the period 1998 to 2012. Prices are adjusted for inflation to 2012 US dollars. Data compiled from Cunningham (2003b, 2005b), Magyar (2007b), and Papp (2009b, 2011b, 2013b)..... 11

Figure 2.5 Schematic representations of granite-pegmatite relationship within a pegmatite field. Arrow denotes increasing complexity of zonation, extent of replacement (albitization) and increasing Ta/Nb ratio with distance from the source granite. Modified from Trueman and Černý (1982), Černý and Meintzer (1988), and Černý (1991b). 18

Figure 2.6 Lithologic map of the Wodgina and Mt. Cassiterite pegmatite groups, Western Australia. Only Li is currently extracted from the Mount Cassiterite and Tinstone pits. The Wodgina pit is essentially mined out. Modified from Sweetapple et al. (2001b), Sweetapple and Collins (2002), and Fetherston (2004). 20

Figure 2.7 Cross section of the Wodgina pegmatite across the north end of the pit (area of highest Ta grades). Modified from Sweetapple et al. (2001b) and Fetherston (2004). 21

Figure 2.8 Block diagram of the St. Honoré carbonatite complex displaying conical, circular, or crescent shapes. The two units currently mined for niobium are denoted by "Nb." The REE mineralization is concentrated in the brecciated Fe–Mn carbonatite core. The diorite host rock is strongly fenitized in contact with the carbonatite and syenite intrusions. Modified from Lafleur and Ayad (2012). 24

Figure 2.9 Schematic lithologic map of the Araxá Carbonatite (Barreiro), Brazil. Modified from Grozzi-Sad and Torres (1976), Issa Filho et al. (1984), and Traversa et al. (2001)..... 25

Figure 2.10 Lithologic map and schematic cross section of the Strange Lake peralkaline complex. The locations of strongest Zr–Y–Nb–REE mineralization are denoted by yellow stars. Modified From Miller (1986, 1990), Salvi and Williams-Jones (1990, 1996, 2006), Daigle et al. (2011) and Boily and Gosselin (2012). 27

Figure 2.11 Geologic map and cross section of the Nechalacho (Thor Lake) deposit based on drill hole data. Location of the cross section is identified by the black line (A,

B). The cross section depicts the domal layered igneous complex. The contact between the upper and basal zones is based on a sharp increase in HREE and total REE content. The basal zone-bottom has TREO >1 % and HREO >0.15 % with a HREE/LREE ratio of 0.25; the basal zone-top has TREO >1 % and HREO >0.15 % with HREE/LREE ration of 17 % (Ciuculescu et al., 2013). Modified from Möller and Williams-Jones (2013), Sheard et al. (2012), and Ciuculescu et al. (2013). 29

Figure 2.12 Vertical cross section of the Orlovka deposit. Tantalum mineralization is hosted in apical, highly differentiated units. Tantalum content increases upwards. Modified from Seltmann et al. (2010). 32

Figure 2.13 Grade and tonnage characteristics of (a) Ta and (b) Nb deposits associated with carbonatite complexes, pegmatites, peralkaline complexes and rare-element granites. Diagonal lines indicate tonnage of Ta_2O_5 and Nb_2O_5, respectively. Numbers correspond to deposits listed in Table 2.3. 34

Figure 3.1 Location and tectonic setting of the Aley, Lonnie, and Wicheeda carbonatites (yellow stars). Modified from Colpron and Nelson (2011). British Columbia Alkaline Province (red in inset map) is base on Pell (1994). 39

Figure 3.2 Geological setting of the Aley carbonatite and locations of stream sediment samples. Yellow markers (A-B-C) denote location of profile in Figure 3.6. Modified after Pride (1983), Mäder (1986), Massey et al. (2005), and McLeish (2013). UTM zone 10, NAD 83. 41

Figure 3.3 Al-13-05 sample site; dry pool below chute over fenite bedrock. Sampled material forms matrix between cobbles and boulders. Looking north up the dry stream bed valley toward the Aley Carbonatite. Shovel is 1 m long. 44

Figure 3.4 Al-13-08 sample site; Al creek, downstream of the Aley carbonatite. Sampled material constitutes matrix between cobbles and boulders, which form the predominant substrate. Stream is 3.5 m wide; looking east upstream. 45

Figure 3.5 Portable XRF analyses for selected trace elements and grain size fraction distributions of samples AL-13-02, AL-13-18, and AL-13-18B. The + 250 μm, + 125 μm, and + 63 μm size fractions are enriched in Nb, Ta, Y, La, Ce, Pr, Nd, P, U, and Th relative to other size fractions. Analyses below detection limits are not shown. Error bars based on average 2σ values determined from multiple analyses of standards by pXRF (Appendix B). 49

Figure 3.6 Downstream variation in carbonatite pathfinder elements concentrations (+ 125 μm size fraction) with increasing distance from the Aley carbonatite. Yellow star-fenite, carbonatite, and Ospika diatreme boulders. Green arrow-landslides. A thick layer of overburden is located downhill of the Aley carbonatite. Legend for geology is the same as in Figure 3.2. For location see yellow markers (A-B-C) on Figure 3.2. Error bars based on average 2σ values determined from multiple analyses of standards by pXRF (Appendix B). 50

Figure 3.7 Carbonatite pathfinder elements in creeks draining the Aley carbonatite complex. a) Location of samples and landslides (greater than 200 m^2). b) Nb and Ta. c) La, Ce, and Y. d) P, U, and Th. e) Ba and Sr. All concentrations in ppm. Concentrations of Nb, Ta, La, Ce, Y, U, Th, and Sr show a decreasing trend with increasing distance

downstream of the deposit. Sample AL-13-07 shows the effects of significant dilution of source detritus. Sample AL-13-09 (upstream of the deposit) shows the background concentrations of trace elements. 53

Figure 3.8 Correlations between concentrations of a) Nb and FeO. b) Nb and Ta. c) Nb and La. d) Nb and TiO_2. Error bars based on average 2σ values determined from multiple analyses of standards by pXRF (Appendix B). 54

Figure 3.9 Geological setting of the Wicheeda carbonatite complex, associated dikes, and locations of stream sediment samples. Base map modified after Massey et al. (2005). Thorium radiometric anomalies from Bruland (2011) shown by yellow traces. Cerium soil anomaly from Lane (2009) shown by green traces. UTM zone 10, NAD 83. 59

Figure 3.10 Location of stream sediment samples and local topography around the Wicheeda carbonatite complex. Samples are downhill of the Wicheeda carbonatite complex. Elevation contours denoted by brown lines (100 m contour interval). Modified after Massey et al. (2005). 61

Figure 3.11 Portable XRF analyses for selected trace elements and grain size fraction distributions of samples WI-13-66H and WI-13-71H. The + 250 μm, + 125 μm, and + 63 μm size fractions are enriched in Nb, La, Ce, and Th relative to other size fractions. 65

Figure 3.12 Selected trace element concentrations in stream sediment samples. a) Sample numbers. b) Nb, Ta, and Th. c) La, Ce, and Y. d) Ba and Sr concentrations in ppm. The edge of the cut block and the area of low topographic relief are denoted by the green dotted line. 66

Figure 3.13 Profiles of SiO_2, CaO, Ba, and Sr concentrations in the + 125 μm size fraction; elevation (m above sea level). The approximate position of the calcite carbonatite dike outcrop is projected onto the profile. 67

Figure 3.14 Profiles of key pathfinder elements concentration in the + 125 μm size fractions; and elevation (m above sea level). The approximate position of the calcite carbonatite dike outcrop is projected onto the profile. 68

Figure 3.15 Correlations between the concentrations of selected elements in the + 125 μm size fraction of samples. a) Ce and Th. b) Nb and Ce. c) Nb and TiO_2. d) Nb and FeO. 70

Figure 3.16 Flow chart for QEMSCAN® analysis. Based on QEMSCAN® software help file. 77

Figure 3.17 Mineral abundance (wt. %; determined by QEMSCAN®) for RAW and corresponding Mozley C800 concentrates (CON) for selected samples a) AL-13-01, b) AL-13-04, and c) AL-13-16. Concentration factors for CON relative to corresponding unprocessed (RAW) samples are shown in parentheses. Mineral abbreviations are the same as in Table 3.6. 84

Figure 3.18 Particle size distribution in terms of particle count and wt. % for pyrochlore (a and b), columbite-(Fe) (c and d), REE-fluorocarbonates (e and f), monazite (g and h), and apatite (i and j). RAW samples and corresponding CON samples are each ordered from west (away from the deposit) to east (nearest the deposit). Particle sizes are in μm. 86

Figure 3.19 Comparison of a) Nb, b) LREE, and c) Fe_2O_3 content of stream sediments from the Aley drainage area, determined by QEMSCAN® and traditional chemical analysis. 89

Figure 3.20 Relationship between indicator mineral concentrations (determined by QEMSCAN®) and corresponding pathfinder element content for: a) Nb vs. pyrochlore; b) Nb vs. columbite(Fe); c) Nb vs. fersmite; d) Nb vs. niobates (includes pyrochlore, columbite-(Fe), and fersmite); e) LREE vs. monazite; f) LREE vs. REE-fluorocarbonates; g) P_2O_5 vs. apatite; and h) P_2O_5 vs. monazite. Results are for unprocessed samples (blue circles) and Mozley C800 concentrates (red circles). 90

Figure 3.21 Comparison of columbite-(Fe) and pyrochlore concentrations (determined by QEMSCAN®) for RAW (blue circles) and corresponding Mozley C800 concentrate (red circles) samples. 92

Figure 3.22 Proportions of monomineralic (Mono) and composite grains with predominant mineral associations (in terms of particle count and wt. %) for: a) and b) pyrochlore; c) and d) columbite-(Fe); e) and f) REE-fluorocarbonates; g) and h) monazite; i) and j) apatite. Results are for RAW samples and corresponding CON. Sample distance increases from directly over the deposit (AL-13-04) to 11.5 km downstream (AL-13-01). 'Others' refers to very complex composite grains, and those containing unidentified mineral phases. Abbreviations: pyrochlore (Pcl); columbite-(Fe) (Cmb); fersmite (Fer); REE-fluorocarbonates (REE-Fl); zircon (Zrc); apatite (Ap); magnetite (Mag); hematite (Hem); rutile (Rt); amphibole/pyroxene (Amp/Px); barite (Brt); quartz (Qtz); dolomite (Dol); calcite (Cal); feldspar (Fsp); hematite (Hem); goethite (Gth); chlorite (Chl); biotite (Bt); and muscovite (Ms). 93

Figure 4.1 Chemical compositions of pyrochlore supergroup minerals from the Upper Fir, Roadside, Verity, Mount Grace, Wicheeda, Lonnie, Aley, Oka, and St. Honoré carbonatites plotted on Nb-Ti-Ta ternary diagrams. Solid lines bound the pyrochlore, betafite, and microlite fields as defined by Atencio et al. (2010). Inset map of Canada shows the location of carbonatite occurrences. 106

Figure 4.2 Chemical compositions of columbite-(Fe) from the Upper Fir, Aley, and Lonnie carbonatites. Inset shows the full columbite-tantalite series quadrilateral with all new analyses from Upper Fir, Aley, and Lonnie (red dots). Mineral classification is according to Černy and Ercit (1985) and Černy and Ercit (1989). The empirically derived tantalite-tapiolite miscibility gap is from Černy et al. (1992). 107

Figure 4.3 Chemical compositions of pyrochlore supergroup minerals from (a) British Columbia and Quebec carbonatites supplemented by those of pyrochlore supergroup minerals from other North and South American, African, European, and Asian carbonatite complexes; (b) peralkaline complexes; (c) LCT pegmatites; (d) peraluminous granites; and (e) a synthesis of all of the above data. Contour shading refers to number of data points per unit area. Sources for the worldwide data compilation are in Appendix A. 109

Figure 4.4 Chemical composition of columbite-tantalite minerals from British Columbia carbonatites supplemented by data available from other carbonatite complexes, LCT

pegmatites, peralkaline complexes, and peraluminous granites. Sources for the worldwide data compilation are in Appendix A. 111

Figure 4.5 Discrimination diagram for the pyrochlore supergroup minerals from carbonatite complexes, peraluminous granites, LCT pegmatites, and peralkaline complexes. The yellow star denotes the composition of a pyrochlore grain from a hypothetical sample. A corresponding columbite-(Fe) grain from the same sample is denoted by a yellow star in Fig. 4.6. 113

Figure 4.6 Discrimination diagram for minerals belonging to columbite-tantalite series from carbonatite complexes, peraluminous granites, LCT pegmatites, and peralkaline complexes. 114

Figure C.1 A sample being poured onto a Mozley C800 laboratory mineral separator. Water is supplied to the v-profile tray by the wash water pipe (copper tube) and the irrigation pipes (two white plastic tubes with water outlets at regular intervals). The direction of water flow is denoted by black arrows. 166

Figure C.2 View of the surface of the Mozley C800 laboratory mineral separator table and sample material after a completed run. Concentrate, middlings, and tailings are separated based on pattern and colour of the material stream. 167

Figure C.3 Comparison of the weight of magnetite contained in unprocessed synthetic standards with corresponding weight of magnetite in Mozley C800 laboratory mineral separator concentrates. 168

Figure C.4 Proportions of concentrate, middlings, and tailings in five subsamples of AL-13-16 (Fig. 3.2) after processing on the Mozley C800 laboratory mineral separator for 5, 10, 15, 20, and 25 minutes. 169

Figure C.5 Proportions of Mozley C800 laboratory mineral separator concentrates, middlings, and tailings for stream sediment samples from the Aley carbonatite drainage area, northeastern British Columbia. Samples were processed for 15 minutes. Samples appear in order of their geographic location from west to east (see Fig. 3.2 for sample locations). 170

Figure C.6 Comparison of a) Nb, b) Ta, and c) LREE (ΣLa, Ce, Nd, Pr) concentrations in Mozley C800 laboratory mineral separator concentrates, tailings, and corresponding raw samples. Samples appear in order of their geographic location from west to east (see Fig. 3.2 for sample locations). 174

Figure C.7 Comparison of the concentrations of a) Nb, b) Ta, c) light rare earth elements (LREE), d) Y, e) Sr, and f) Ba in Mozley C800 laboratory mineral separator concentrates versus raw samples (from Aley carbonatite drainage area, northeastern British Columbia). Error bars (2σ) are based on repeated portable X-ray fluorescence analyses of standards as described in Appendix B. 175

Figure C.8 Weight percent distribution of material for different size fractions in dry sieved stream sediment samples from the Aley carbonatite drainage area, northeastern British Columbia. 177

Figure D.1 Wilfley shaking table with adjustable launder trays. Slope and incline axes (angle from horizontal) are shown. 181

Figure D.2 Close-up of the Wilfley table. Heavy minerals (black) are separated from middlings and tailings as material moves from the top-right to bottom-left. 182

Figure D.3 Proportion of original wt. % in Wilfley table concentrates, middlings, and tailings for Aley carbonatite area stream sediments. 183

Figure D.4 Comparison of a) Nb, b) Ta, and c) LREE (Σ La, Ce, Nd, Pr) concentrations in Wilfley table concentrates relative to corresponding raw samples from Aley. Concentration factors for each element or group of elements for individual samples are shown in parentheses. 184

Figure D.5 Comparison of Wilfley table concentrates relative to raw samples from the Aley carbonatite. a) Nb. b) Ta; for raw samples Ta is near the lower detection limit, resulting in large errors relative to the concentrates. c) LREE; error propagation for ΣLREE results in larger margins relative to La, Ce, Pr, and Nd individually. d) Y. e) Sr. f) Ba. Error bars (2σ) are based on repeated analyses of standards as described in Appendix B. 186

Acknowledgments

I owe my deepest gratitude to my supervisor, Dr. George Simandl. I could not have done this thesis without his knowledge, advice, and enthusiastic support throughout.

I am indebted to my co-supervisor, Dr. Dante Canil, and other committee members, Dr. Laurence Coogan, and Dr. Paul Bédard, for their constructive review of the thesis manuscript. I would also like to thank Pearce Luck for all his help in the lab, keen insight on analytical techniques, and help with editing manuscripts.

The support, expertise, and laboratory access from John Gravel at Bureau Veritas Commodities Canada Ltd., Geo-analytical Division and Mike Redfearn, Boja Grcic, Wendy Ma, and Cheng Li at Bureau Veritas Commodities Canada Ltd., Inspectorate Metallurgical Division are greatly appreciated. I would like to thank Dr. Mati Raudsepp and Edith Czech for their guidance while preforming electron microprobe analysis at the University of British Columbia. My field work experience was greatly improved thanks to Joel Trofanenko, who braved the devil's club and bugs at the Wicheeda carbonatite.

This project was funded by the Targeted Geoscience Initiative 4 (2010-2015), a Natural Resources Canada program carried out with collaboration between the Geological Survey of Canada and the British Columbia Geological Survey. I would like to thank Geoscience BC for awarding me a scholarship. The logistical and helicopter support provided by Taseko Mines Ltd. is greatly appreciated. I would also like to thank Spectrum Mining Corp, Rara Terra Minerals Corporation, Commerce Resource Corp., IAMGOLD Corporation, and NIOCAN Inc. for access to their deposits and samples.

The faculty and staff at in the School of Earth and Ocean Science at the University of Victoria and the British Columbia Geological Survey created a truly wonderful and welcoming environment in which to work and learn during my time there.

Finally, I would like to thank my family and friends for supporting me throughout my degree. This would not have been possible without you.

Dedication

This thesis is dedicated to my parents, Alisdair and Faith, who have supported me through all my endeavours, and to my former teachers, Ron Crosby and Rod Carr, who inspired me to pursue scientific research.

1 Introduction and objectives

1.1 Statement of problem

Specialty metals such as Nb in high-strength low-alloy (HSLA) steels used extensively in the automotive and petroleum industries, Ta used as Ta-powders in capacitors used in many modern electronic applications, and rare earth elements (REE) essential for modern high-technology manufacturing and in environmental applications (Simandl, 2014; Chapter 2). These metals are also considered economically and strategically important to industrialised economies (European Commission, 2011, 2014). Canada has excellent potential for discovery of new specialty metal deposits (Simandl et al., 2012). Potential shortages in specialty metal supply have cause price spikes in the price of Ta_2O_5 and a steady increase in the price of ferroniobium. This has fueled interest in carbonatite-related deposits. To improve the effectiveness of Canadian companies, there is a need for development of new, or customisation of existing, exploration methods.

1.2 Objectives

The main objectives of this thesis are:

1) to contribute to the characterisation of specialty metal deposits;
2) development and optimization of an indicator mineral technique specific to specialty metal deposits in the Canadian Cordillera;
3) development of discrimination diagrams that permit identification of deposit type from which these indicator minerals were derived.

1.3 Outline

Chapter 2 provides an introduction to specialty metals (including Nb, Ta, rare earth elements (REE), Y, Li, Cs, and Zr), Nb and Ta markets, and to deposits containing these metals. Besides carbonatite-related deposits, Nb-, Ta-, and REE-bearing minerals are found in Li-Cs-Ta pegmatites, peraluminous granites, and peralkaline complexes (Simandl, 2014). Chapter 2 was published as a peer reviewed paper in a scientific journal (Mackay and Simandl, 2014a).

Chapter 3, section 3.1, describes stream sediment orientation surveys from the drainage areas of the Aley and Wicheeda Lake carbonatites, British Columbia. These surveys demonstrate that portable X-ray fluorescence (pXRF) can be used to streamline indicator mineral studies by identifying the most favourable grain size fraction for detailed study. The orientation surveys for Aley and Wicheeda were published as peer reviewed government publications (Mackay and Simandl, 2014b,c). Section 3.2 establishes that Quantitative Evaluation of Materials by Scanning Electron Microscopy (QEMSCAN®) can substitute for traditional indicator mineral methodologies that involve hand-picking of minerals, which are relatively time consuming and costly. The QEMSCAN® study has been submitted for peer reviewed publication (Mackay et al., in Review).

***Chapter* 4** presents discrimination diagrams useful for predictive deposit targeting (deposit type from which indicator minerals were derived can be identified) based on the chemical composition of pyrochlore supergroup and columbite-tantalite series minerals. These diagrams are part of a peer reviewed scientific paper (Mackay and Simandl, 2015).

2 Geology, market, and supply chain of niobium and tantalum – a review

Submitted 7 March 2014/ Accepted 17 August 2014/ Published online 9 September 2014: Mackay, D.A.R. and Simandl, G.J., 2014. Geology, market and supply chain of niobium and tantalum – a review. Mineralium Deposita, 49, 1025-1047.

2.1 Introduction

Tantalum (Ta) and niobium (Nb) are transition metals in group V of the periodic table, and have nearly identical atomic radii and similar electrical, physical and chemical properties (Table 2.1; Slater, 1964; Nowak and Ziolek, 1999; Winter, 2011). They are considered rare-elements, a group consisting of high-field strength elements (HFSE; Ti, Zr, Hf, Nb, and Ta), some large ion lithophile elements (LILE; Rb, Sr, Cs, and Ba), rare-earth elements (REE; lanthanides+Y), Li, U, Th, and Be. Pegmatites, rare-element-enriched peraluminous granites, and placers remain most favourable settings to host future economically significant Ta resources (Simandl 2002). The main ore minerals of Ta are tantalite (Ta-rich end member of the columbite-tantalite solid solution series) and microlite (Ta-rich pyrochlore; Table 2.2). Pyrochlore (Nb-rich variety) and columbite (Nb-rich end member of the columbite-tantalite series) are the main Nb ore minerals (Table 2.2). Other common Ta- and Nb-bearing minerals are betafite (Ti-rich pyrochlore), loparite, lueshite, fersmite, fergusonite, strüverite, euxenite, samarskite, and wodginite (Table 2.2).

Table 2.1 Selected properties of Nb and Ta metals. Atomic radii and valence for both metals is virtually the same, resulting in the very similar chemical and physical properties of the elements. From Slater (1964), Lide (2008), and Winter (2011).

	Ta	Nb
Atomic Number	73	41
Atomic Weight	180.94788	92.90638
Melting Point (°C)	2996	2468
Boiling Point (°C)	5425	4930
Density (g/cm^3)	16.7	8.57
Atomic Radius (pm)	145	145
Electrical resistivity (nΩm) at 25°C	134	144
Thermal Conductivity (W·m^{-1}·K^{-1})	57	54

Tantalum is a hard but ductile metal, with a high melting point (2,996 °C), high density (16.7 g/cm^3), and high resistance to corrosion (Table 2.1; Lide, 2008). In recent years, 50–60% of Ta was used in the production of Ta-oxide powders for the manufacture of electronic components such as capacitors (Roskill, 2013a; Tantalum-Niobium International Study Center, 2013a). Components made with Ta are essential in most portable electronic devices, such as mobile phones, laptop computers, computer hard drives, digital cameras, GPS navigation systems, and airbag triggers. Tantalum is also used in medical implants, super alloys used in jet turbine, and rocket nozzle production, corrosion prevention in chemical and nuclear plants, as a sputtering target, and in optical lenses (Tantalum-Niobium International Study Center, 2013a). These applications make Ta economically and strategically important to most industrialised countries (European Commission, 2011, 2014; Brown et al., 2012; Papp, 2012).

World production of Ta from mining (excluding production from Ta contained in Sn slags) for 2012 (Fig. 2.1) was estimated at 764 tonnes of metal content (Papp, 2013a). Until 1999, world Ta production was relatively stable and slightly increasing in Australia. While Ta production for 2012 is much lower (in terms of tonnage) than other important metals such as Cu (17 million metric tonnes of Cu content; Brininstool, 2013) and Fe (2,950 million metric tonnes of metal; Tuck 2013), its economic importance is ranked as

comparable to Fe and higher than Cu (European Commission, 2011, 2014). The supply risk for Ta is ranked higher than that of Fe and Cu.

Since 1999, a substantial portion of Ta ore and concentrate was sourced in politically unstable regions of West and Central Africa. Introduction of conflict Ta (Coltan) resulted in several major past producers, such as Wodgina, Mt. Cattlin (Australia), and Tanco (Canada), being placed on care and maintenance. Tantalum production at the massive Greenbushes pegmatite (Australia) has stopped, though Li production continues. The recently introduced Conflict-Free Smelter Program allows for voluntary review of smelters by a third party to verify the source of material as conflict free (EICC, 2013). Should consumers and manufacturers of electronic devices resist the use of Coltan, mines currently on care and maintenance will be the first to restart. Infrastructure and permitting are already in place for care and maintenance projects, foregoing the start-up time for new operations. The Kenticha mine (Ethiopia) is a past producer that may re-enter production in the near future. Favourable market conditions could see projects on care and maintenance reopen, avoiding the immediate need for new Ta resources.

Individual feasibility studies (or prefeasibility studies on new developments) are required in any mine as price levels vary for each deposit and are dependent on negotiated contracts with concentrate buyers. In western countries, a typical mine may take more than three years to put into production, assuming the advanced stage of exploration is complete and there are no unforeseen problems with permitting. Up to 40 % of total Ta production in 2012 was from primary concentrates while 30 % came from scrap recycling and synthetic concentrates, 20 % as a by-product of Sn mining and 10 % was sourced from secondary concentrates (Tantalum-Niobium International Study Center 2013a). The main Ta producers are currently the Mibra Mine, Volta Grande (Brazil), the Pitinga Mine (Brazil), and Marropinno (Mozambique). The Yichun mine (China) is another well-known source of Ta, as well as Nb and Li (Lin et al. 1995), though grade, tonnage, and production are not reliably known.

Table 2.2 Key Nb- and Ta-bearing minerals.

Mineral Name	Chemical Formula	Wt. % Nb_2O_5	Wt. % Ta_2O_5	Crystal System	Hardness	Density (g/cm^3)	Associated Deposits	Reference
Columbite[a]	$(Fe,Mn)(Nb,Ta)_2O_6$	46.8-81.2	5.3-31.2	Orthorhombic	6	5.3-7.3	Carbonatite, Pegmatite, Peralkaline	Wenger et al. 1991; Anthony et al. 2014
Tantalite[a]	$(Fe,Mn)(Ta,Nb)_2O_6$	0.3-26.8	56.5-86.2	Orthorhombic	6-6.5	6.65-7.95	Pegmatite, Granite, Peralkaline	Černý et al. 1992; Anthony et al. 2014
Pyrochlore	$(Ca,Na)_2(Nb,Ti,Ta)_2O_6(O,OH,F)$ ± 1% REE-oxides	34.3-86.8	Trace-4.3[b]	Isometric	5.0-5.5	4.2-6.4	Carbonatite, Pegmatite, Peralkaline,	Hogarth 1977; Anthony et al. 2014; Atencio et al. 2010
Betafite	$(Ca,U)_2(Ti,Nb,Ta)_2O_6(OH)$	34.8	Trace-1.0	Isometric	3-5.5	3.7-4.9	Pegmatite, Carbonatite	Hogarth 1977; Anthony et al. 2014; Atencio et al. 2010
Microlite	$(Na,Ca)_2(Ta,Ti,Nb)_2O_6(O,OH,F)$	Trace-3.4	73.7-86.0	Isometric	5.0-5.5	4.2-6.4	Pegmatite, Peralkaline, Granite	Hogarth 1977; Anthony et al. 2014; Atencio et al. 2010
Loparite (Perovskite)	$(Ce,La,Na,Ca,Sr)(Ti,Nb)O_3$	9.7-15.1	0.8-1.0	Isometric	5.5-6	4.60-4.89	Peralkaline, Carbonatite	Ferguson 1978; Kramm and Kogarko 1994; Anthony et al. 2014
Lueshite (Perovskite)	$NaNbO_3$	79.7-81.1	Trace	Orthorhombic	5-5.5	4.44	Peralkaline, Carbonatite	Fleischer 1960; Anthony et al., 2014
Fersmite	$(Ca,Ce,Na)(Nb,Ta,Ti)_2(O,OH,F)_6$	66.0-70.1	Trace-16.9	Orthorhombic	4-4.5	4.69-4.79	Pegmatite, Carbonatite	Cummings and Simonsen 1970; Anthony et al., 2014
Fergusonite-(Y)	$YNbO_4$	44.5-54.1	6.30	Tetragonal	5.5-6.5	5.6-5.8	Pegmatite, Placer	Graham and Thornber 1974; Anthony et al. 2014
Fergusonite-(Nd)	$(Nd,Ce)(Nb,Ti)O_4$	39.8		Tetragonal	5.5-6.5	N.A.	Carbonatite	Jambor and Vanko 1989; Anthony et al. 2004
Strüverite	$(Ti,Ta,Nb,Fe)_2O_6$	6.5-9.3	33.1-35.5	Tetragonal	6-6.5	5.4	Pegmatite, Placer	Černý et al., 1981; Anthony et al. 2014
Euxenite-(Y)	$(Y,Ca,Ce,U,Th)(Nb,Ta,Ti)_2O_6$	41.3	3.8	Orthorhombic	5.5-6.5	4.3-5.9	Pegmatite	Ewing 1976; Anthony et al. 2014
Samarskite-(Y)	$(Y,Fe^{3+},U)(Nb,Ta)O_4$	38.3	11.2	Orthorhombic	5-6	5.2-5.7	Pegmatite	Sugitani et al. 1985; Anthony et al. 2014
Wodginite	$MnSnTa_2O_6$	3-15	45-56	Monoclinic	5.5	7.3	Pegmatite	Ercit et al. 1992; Anthony et al. 2014

[a] Pure columbite and tantalite are unknown in nature; they are theoretical end members of the columbite-tantalite solid solution series.
[b] Ta content of pyrochlore is representative of Nb ores. Pyrochlore of some deposits, such as Upper Fir, Canada, have much higher Ta content.

During the 1990s, the price of Ta_2O_5 concentrate was relatively stable at approximately US$100/kg (Fig. 2.2). In the year 2000, spot prices reached US$647/kg of contained Ta_2O_5 due to an increase in demand and perceived shortfall in supply (Simandl, 2002). In response, production increased in Australia, which was the dominant supplier at the time. By 2002, prices dropped and remained stable under US$120/kg until 2010. This more recent price spike is correlated to instability and loss of production in Australia and Canada (Fig. 2.1). Shortages of conflict free concentrate, the high economic importance of Ta and high supply risk (European Commission, 2011) have led to higher Ta_2O_5 concentrate prices (Fig. 2.2). Since 2014, Ta is no longer considered a critical metal, but its supply risk remains elevated relative to other economically important metals such as Cu or Fe (European Commission, 2014).

Niobium is a soft, ductile metal. It has a high melting point (2,468 °C) and is also corrosion resistant, though to a lesser degree than Ta (Lide, 2008). By far the most common use for Nb is in the production of micro-alloyed or high-strength low-alloy (HSLA) steel (containing at most 0.1 % Nb, commonly approximately 0.03 % Nb). The HSLA steels are used extensively in high-pressure pipeline construction, offshore petroleum drilling platforms and as major components in the automotive industry (Roskill, 2013b; Tantalum-Niobium International Study Center, 2013b). In the USA, as much as 58 % of Nb is used in the productions of HSLA steels while nearly 42 % is used in the production of super alloys (Papp, 2013b). The high-strength and corrosion resistance of these super alloys make them essential to the space and aviation industries in the production of components for rocket and jet engines. There is also minor use of Nb in superconducting alloys (Tantalum-Niobium International Study Center, 2013b).

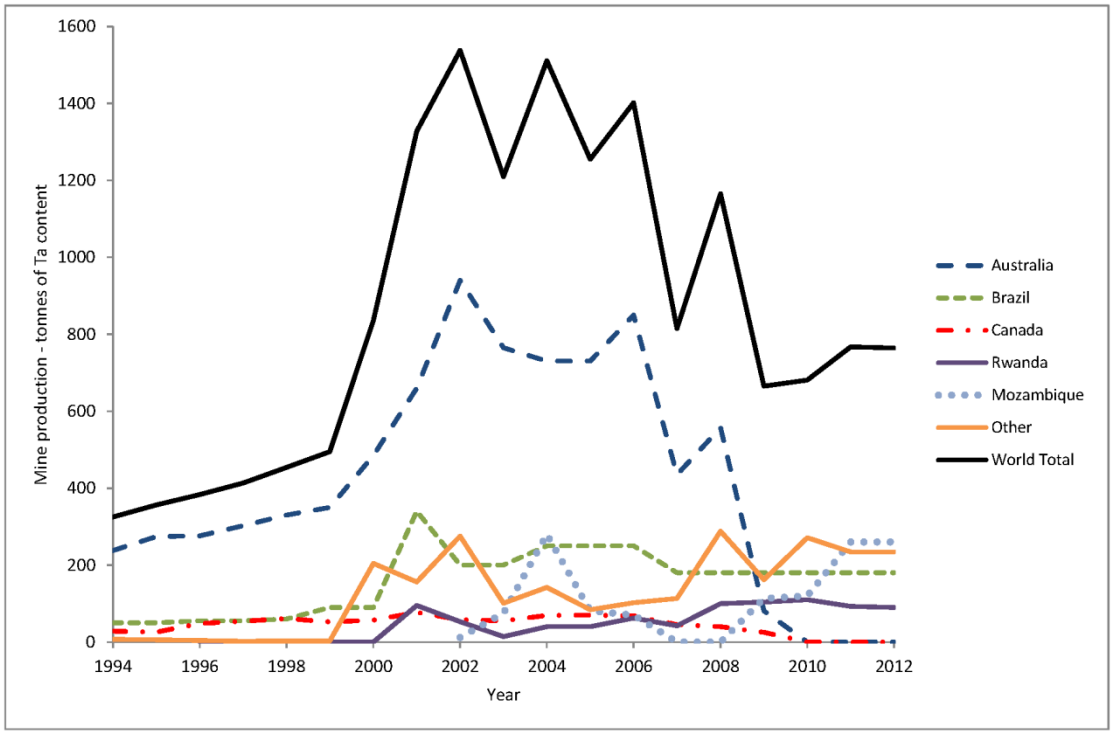

Figure 2.1 World mine production of contained Ta metal (excluding Ta recovered as a by-product of Sn mining) by country for the period of 1994 to 2012. Data from Cunningham (1996a, 1997a, 1999a, 2001a, 2003a, 2005a), Magyar (2007a), and Papp (2009a, 2011a, 2013a).

Mine production of Nb has increased rapidly over the last 15 years, from 18,323 to 68,700 tonnes of contained Nb (Fig. 2.3), driven by demand from modernization and pipeline building in China, Russia, and India. Production comes primarily from Brazil. Production from Canada and other countries has remained relatively constant for the period from 1994 to 2012. Steel production in the USA, Japan, South Korea, Brazil, and EU countries currently utilises higher concentrations of Nb than in China, India, and Russia (Roskill 2013a). It is expected that demand for Nb will continue to rise until concentrations in Chinese, Indian, and Russian steel reach the same levels as those in EU- and US-produced steels.

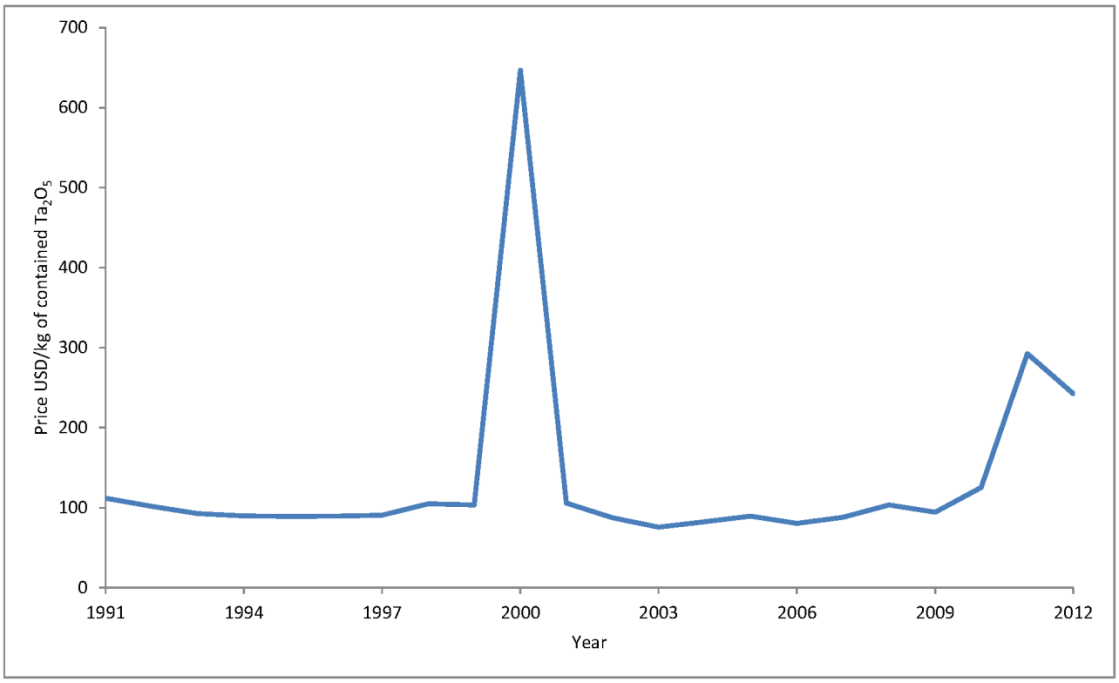

Figure 2.2 Price of contained Ta_2O_5 in concentrate for 1991 to 2012. Prices are adjusted for inflation to 2012 US dollars. Data from Cunningham (1996a, 1997a, 1999a, 2001a, 2003a, 2005a), Magyar (2007a), and Papp (2009a, 2011a, 2013a).

The price of ferroniobium (Fe-Nb alloy containing 65% Nb_2O_5) was declining slightly until 2006, when it began to rise rapidly (Fig. 2.4). Higher prices since 2006 coincide with increased production (Fig. 2.3), indicating a growing demand for Nb in HSLA steel. Similar to Ta, Nb is considered to have high economic importance in comparison to other major metal commodities (e.g. Cu) and is considered a critical metal because it is subject to higher supply risk (European Commission, 2011, 2014). Carbonatite complex-related weathered ores in Brazil account for about 92 % of Nb mine production (Papp, 2013b). The main producers in Brazil are Araxá and Catalão I and II. The St. Honoré mine (Canada) accounts for most of the remaining global Nb production. Only 20 % of Nb is sourced from recycled material (Papp, 2013b). Unforeseen circumstances that limit or curtail Nb production in Brazil would drastically impact the economies of most modern industrialised nations. Unlike the Ta market where several mines can be rapidly restarted, there are few Nb deposits that are on care and maintenance or with existing infrastructure. To improve supply chain security, new deposits outside of Brazil need to be developed. Niobium co-production from peralkaline complexes (e.g. Nechalacho or

Strange Lake) is possible, but conditional on the extraction of REE or Zr as principal commodities. Multiple co-products can help insulate a project from economic downturns, as REE, Nb, Ta, and Zr, typically follow different market cycles; however, complex metallurgy is commonly reflected by high capital and plant operating costs.

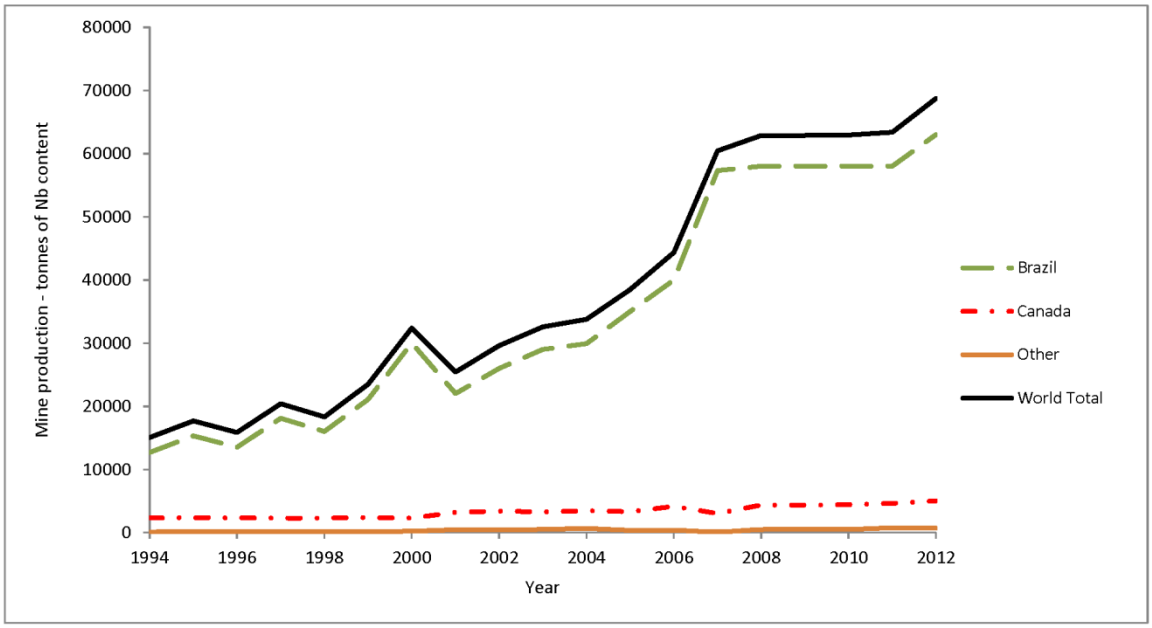

Figure 2.3 World mine production of contained Nb metal by country from 1994 to 2012. Data compiled from Cunningham (1996b, 1997b, 1999b, 2001b, 2003b, 2005b), Magyar (2007b), and Papp (2009a, 2011b, 2013b).

2.2 Geology of Ta- and Nb-bearing deposits

Ta is or was produced from pegmatites (e.g. Greenbushes and Wodgina, Australia; Tanco, Canada; Keticha, Ethiopia; and Marropino, Mozambique), rare-element-enriched peraluminous granites (e.g. Yichun, China, and Orlovka, Russia), their weathering-enriched equivalents, artisanally mined placer deposits (e.g. Rwanda, Congo, and Burundi), and as a by-product of Sn mining (Table 2.3; Simandl 2002; Shaw and Goodenough 2011; Papp 2012; Pohl 2012). The Pitinga deposit, Brazil, is hosted in a peralkaline unit (Nardi et al., 2012) within a predominantly peraluminous granite (Horbe et al., 1991; Bastos Neto et al., 2009), and does not fit any of the above-listed deposit types. The proportion of ore reserves contained within ‘granite’, pegmatites or colluvium is not clear. Several junior mining companies are evaluating carbonatite complexes to

recover Ta as a co-product of Nb (e.g. Upper Fir [Chong et al., 2012], and Crevier, Canada [Duplessis and Girard, 2010]).

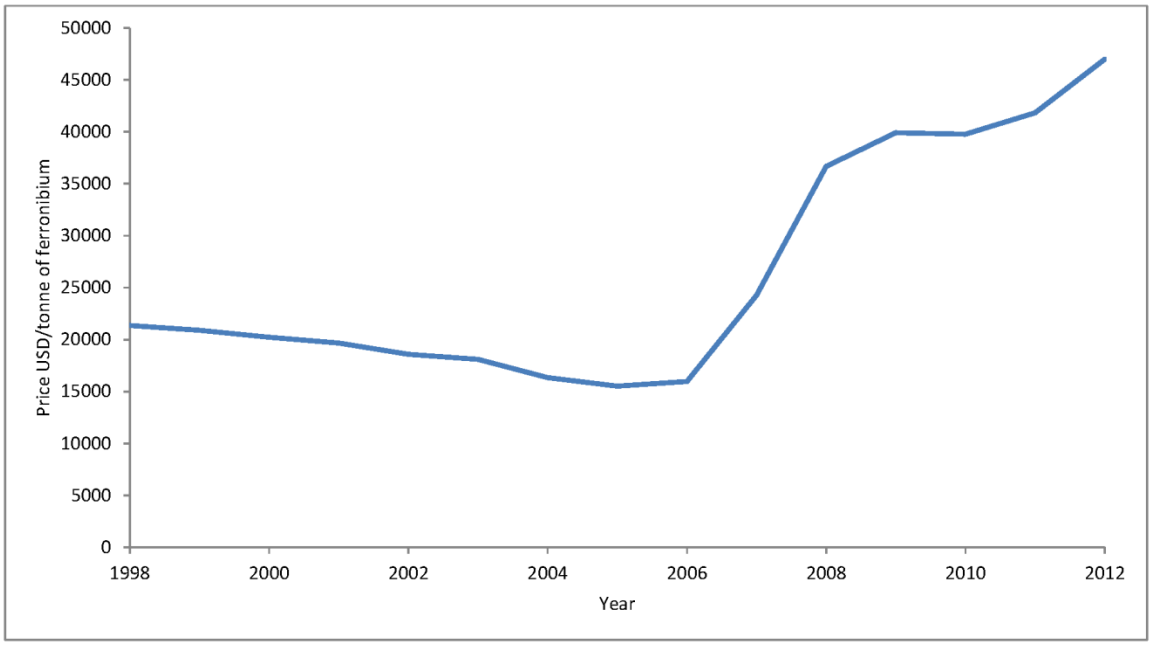

Figure 2.4 Historic price of contained ferroniobium alloy in concentrate for the period 1998 to 2012. Prices are adjusted for inflation to 2012 US dollars. Data compiled from Cunningham (2003b, 2005b), Magyar (2007b), and Papp (2009b, 2011b, 2013b).

Nb is currently derived mainly from weathering-enriched material associated with carbonatite complexes (e.g. Araxá and Catalão I and II, Brazil). Few present and past Nb producing mines extract ore from unweathered hard rock carbonatite deposits (e.g. St. Honoré and Oka, Canada). Coproduction of REEs and Nb is also being investigated at several peralkaline complex-related deposits and carbonatite complexes (e.g. St. Honoré; Table 2.3). In other cases, junior exploration companies are hoping to recover Nb as a by-product of phosphate (e.g. Prairie Lake [Nuinsco Resources Ltd., 2014], Nkombway Hill [v. Straaten, 2002], and Sukulu [Karagambe-Kaliiza, 1989]) or REE production (e.g. Nechalacho [Ciuculescu et al., 2013] and Iron Hill [Staatz et al., 1979; v. Gosenm 2009]).

Known major Nb and Ta deposits vary in age from ~2.8 Ga to ~85 Ma (Table 2.3). Many of the ages reported in Table 2.3 correspond to emplacement of intrusive rocks and represent only approximate time of mineralization. The methods used to obtain these ages were potassium–argon (K/Ar), argon–argon (Ar/Ar), uranium–lead (U/Pb), lead–lead

(Pb/Pb), rubidium–strontium (Rb/Sr), samarium–neodymium (Sm/Nd) and fission track radiometric methods.

2.2.1 Pegmatite-related Ta deposits

Pegmatites are coarse-grained igneous rocks, with most crystals larger than 1 cm, found in a variety of tectonic and metamorphic settings. They form small stocks, sills, dikes, and irregularly shaped pods and lenses that are usually less than 1 m thick and tens to hundreds of metres along strike (Jahns, 1955; Varlamoff, 1972; Černý, 1975, 1982). Only exceptional pegmatite bodies (e.g. Greenbushes and Wodgina, Australia, and Tanco, Canada) display kilometre-scale extent along strike and reach tens of metres in thickness. Pegmatites consist mainly of K-feldspar, albite, and quartz ± muscovite and/or biotite (Černý, 1991a). Reviews of pegmatite mineralogy are provided in Černý (1991a) and Černý and Ercit (2005); that of Ta-bearing minerals is provided by Černý and Ercit (1985). Pegmatites have been the subject of many detailed studies, numerous descriptive and genetic reviews and a variety of classification schemes (Ginsberg, 1984; Černý, 1982, 1991a; Černý and Ercit, 2005; and references herein). They can be divided into five classes: abyssal, muscovite, muscovite-rare-element, rare-element, and miarolitic, based on geological environment and geochemistry (Černý and Ercit, 2005). From a Ta exploration standpoint, the rare-element class is the most important.

Granitic pegmatites are similar in terms of major element composition, rock-forming mineralogy and tectonic setting to the granitoids from which they are derived; however, they are commonly more enriched in rare-elements. Based on petrogenetic criteria, they can be subdivided into three families (Černý, 1991a; Černý and Ercit, 2005): the LCT family (enriched in Li, Cs and Ta), the NYF family (enriched in Nb, Y, and F), and the relatively rare mixed NYF+LCT family with overlapping mineralogical or chemical characteristics (Černý, 1991a; Černý and Ercit, 2005). The degree of fractionation increases with distances from co-genetic parental granites (Fig. 2.5; Černý, 1991a, b; Černý and Ercit, 2005).

Table 2.3 Major Ta and Nb deposits.

No.	Deposit, Country	Tonnage and Grade	Co-Products [potential]	Production Capacity	Age (method)	References
	CARBONATITE COMPLEX-RELATED					
1	Aley, Canada (*HR*)	285.8Mt @ 0.37% Nb_2O_5 144.2Mt[3] @ 0.32% Nb_2O_5			366-400 (U/Pb)	Simpson (2012) McLeish (2013)[5]
2	Araxá, Brazil (*W*)	808 Mt[1] @ 2.3% Nb_2O_5	[P_2O_5, REE]	70000 t/yr Fe-Nb, 3000 t/yr Ni-Nb and Fe-Nb, 210 t/yr Nb metal	97-89 (K/Ar)	Hasui and Cordani (1968)[5] CBMM (2014)
3	Araxá, Brazil (*HR*)	1800 Mt[1] @ 1.5% Nb_2O_5	[P_2O_5, REE]		97-89 (K/Ar)	CBMM (2014) Hasui and Cordani (1968)[5]
4	Argor, Canada (*HR*)	62.5 Mt[1] @ 0.52% Nb_2O_5				Stockford (1972) Sage (1988) Kamitani and Hirano (1990)
5	Bayan Obo, China (*HR*)	16.92 Mt[1] @ 0.1859% Nb_2O_5	REE		1426±40 (Sm/Nd) 1580 (Sm/Nd)	Nakai et al. (1989)[5] Yuan et al. (1992)[5] Smith and Spratt (2012)
6	Bonga, Angola (*HR+W*)	824 Mt[1] @ 0.48% Nb_2O_5	[P_2O_5]		130.8±1.4 (Rb/Sr)	Allsopp and Hargraves (1985)[5] Pena (1989) Kamitani and Hirano (1990)
7	Catalão I, Brazil (*HR+W*)	14.9 Mt[2] @ 0.70% Nb_2O_5 22.9Mt[3] @ 1.15% Nb_2O_5	[P_2O_5]	4500 t/yr (Nb_2O_5)	85±6.9 (K/Ar)	Sonoki and Garda (1988)[5] Anglo American plc. (2014)
8	Catalão II, Brazil (*HR+W*)	25.2 Mt[2] @ 0.96% Nb_2O_5 19.5 Mt[3] @ 1.15% Nb_2O_5	[P_2O_5]	Production included with Catalão I	85±6.9 (K/Ar)	Sonoki and Garda (1988)[5] Anglo American plc. (2014)
9	Clay-Howells, Canada (*HR*)	40.4 Mt[3] @ 0.11% Nb_2O_5	[TREO+Y, 0.48%] [Fe_2O_3, 34.6%]		1072±16 (Rb/Sr)	Bell and Blenkinsop (1980)[5] Daigle (2011)
10	Crevier, Canada (*HR*)	25.396 Mt @ 0.0234% Ta_2O_5 0.196% Nb_2O_5 15.423 Mt[3] @ 0.0252% Ta_2O_5 0.17% Nb_2O_5			879 (K/Ar)	Harrisson (1981)* Duplessis and Girard (2010)
11	Elk Creek, United States (*HR*)	19.3 Mt @ 0.67% Nb_2O_5 83.3Mt[3] @ 0.63% Nb_2O_5	[REE]		544±7 (K/Ar) 464±5 (K/Ar) 484±5 (K/Ar)	Carlson and Treves (2005)[5] Daigle (2012)

No.	Deposit, Country	Tonnage and Grade	Co-Products [potential]	Production Capacity	Age (method)	References
12	Iron Hill, United States (*HR*)	656 Mt[1] @ 0.057% Nb_2O_5	[TREO, 0.397%] [ThO_2, 0.0043%]		570 (K/Ar) 579±20 (Rb/Sr) 550 (fission track)	Olson et al. (1977) [5] Staatz et al. (1979) van Gosen (2009)
13	Mabounie, Gabon (*HR+W*)	401.2 Mt[1] @ 1.11% Nb_2O_5	[P_2O_5, 24%]		660±13 (K/Ar)	Reunion Mining PLC (1998) Oris and Chernoff (2002)
14	Montviel, Canada (*HR*)	183.9 Mt @ 0.126% Nb_2O_5 66.7 Mt[3] @ 0.14% Nb_2O_5	[TREO, 1.45%] [Y_2O_3, 0.007%]		1894.2±3.5 (Pb/Pb)	David et al. (2006) [5] Desharnais and Duplessis (2011)
15	Mount Weld (Crown Polymetallic Resource), Australia (*W*)	1.5 Mt @ 0.037% Ta_2O_5 1.4% Nb_2O_5 36.2 Mt[3] @ 0.024% Ta_2O_5 1.06% Nb_2O_5	[P_2O_5, 7.99%] [TiO_2, 4.01%] [Fe_2O_3, 42.8%] [Y_2O_3, 0.09%] [TREO, 1.16%]			Lynas Corporation (2008)
16	Mrima Hill, Kenya (*W*)	47.8 Mt @ 0.66% Nb_2O_5 94.4Mt @ 0.73% Nb_2O_5	[TREO, 3.85%]			Pacific Wildcat Resources Corp. (2013a)
17	Oka, S-60 Zone, Canada (*HR*)	10.63 Mt @ 0.68% Nb_2O_5 3.22[3] MT @ 0.61% Nb_2O_5			131±7 (U/Pb) 109 (Rb/Sr)	Wen et al. (1987) [5] Cox and Wilton (2006) [5] Lavoie and Caron (2011)
18	Panda Hill, Tanzania (*HR+W*)	82 Mt[3] @ 0.52% Nb_2O_5			113±6 (K/Ar)	Cradle Resource Limited (2013)
19	Prairie Lake, Canada (*HR*)	517 Mt[3] @ 0.0017% Ta_2O_5 0.091% Nb_2O_5	[P_2O_5, 3.0%] [LREO, 0.15%]		1023±74 (Rb/Sr)	Bell and Blenkinsop (1980) [5] Nuinsco Resources Limited (2014)
20	Seis Lagos, Brazil (*HR+W*)	239 Mt[1] @ 2.47% Nb_2O_5 2659[1] Mt @ 2.84% Nb_2O_5	[TiO_2] [REE]			Justo and Souza (1986) Jacobi (2009)
21	St Honoré, Canada (*HR*)	458 Mt @ 0.42% Nb_2O_5 336 Mt[3] @ 0.37% Nb_2O_5	[466.8 Mt @ 1.65% TREO]	4500 t/yr (Nb_2O_5)	~650 (K/Ar)	Vallée and Dubuc (1970) [5] Clow et al. (2011) Lafleur and Ayad (2012)
22	Sukulu, Uganda (*W*)	230.7 Mt[1] @ 0.24% Nb_2O_5	[P_2O_2]			Karagambe-Kaliiza (1989)

No.	Deposit, Country	Tonnage and Grade	Co-Products [potential]	Production Capacity	Age (method)	References
23	Upper Fir, Canada (*HR*)	51.78 Mt @ 0.0192% Ta_2O_5 0.149% Nb_2O_5 8.8 Mt[3] @ 0.0186% Ta_2O_5 0.186% Nb_2O_5			332.5±5.7 (U/Pb)	Gorham et al. (2009) [5] Chong et al. (2012)
	PEGMATITE-RELATED					
24	Kenticha, Ethiopia (*HR+W*)	100 Mt[1] @ 0.016% Ta_2O_5		Care and maintenance (120t/yr @ ~55% Ta_2O_5)	530±1.3 (U/Pb) 530±2.3 (U/Pb)	Küster et al. (2009) [5] Papp (2012)
25	Greenbushes, Australia (*HR+W*)	88.6 Mt[2] @ 0.0223% Ta_2O_5	Li_2O	Care and maintenance (550 t/yr Ta_2O_5)	2527±2 (Pb/Pb)	Partington et al. (1995) [5] Sons of Gwalia Ltd. (2002) Fetherston (2004)
26	Marropino, Mozambique (*HR*)	7.40Mt[3] @ 0.0223% Ta_2O_5		81.5 t/yr (Ta_2O_5)		Hains and Mounde (2010)
27	Mibra, Volte Grande, Brazil (*HR*)	6.32 Mt @ 0.0375% Ta_2O_5 19.2 Mt[3] @ 0.0377% Ta_2O_5, 0.0092% Nb_2O_5	SnO_2 (0.0517%) Li_2O (0.73%)	220 t/yr (Ta_2O_5)		Advanced Metallurgical Group (2013)
28	Morrua, Mozambique (*HR*)	4.65 Mt @ 0.051% Ta_2O_5 3.12 Mt[3] @ 0.039% Ta_2O_5	[Li_2O]			Hains and Mounde (2010)
29	Mt. Cattlin, Australia (*HR*)	12.8 Mt @ 0.0163% Ta_2O_5 4.35 Mt[3] @ 0.0132% Ta_2O_5	Li_2O, 1.09%	Care and maintenance (25 t/yr Ta_2O_5)		Galaxy Resources Limited(2011)
30	Muiane, Mozambique (*W*)	1.375 Mt[3] @ 0.025% Ta_2O_5	[Li_2O]			Pacific Wildcat Resources Corp. (2013b)
31	Rose, Canada (*HR*)	37.2 Mt[3] @ 0.0158% Ta_2O_5	[Li_2O, 0.94%] [Cs_2O,0.0092 %] [Rb_2O, 0.23%]			Richard and Pelletier (2011)
32	Tanco, Canada (*HR*)	1.879 Mt[1] @ 0.216% Ta_2O_5	7.3 Mt @ 2.76% Li_2O 0.92 Mt @ 0.2% BeO 0.35 Mt @ 23.3% Cs_2O	Care and maintenance (80 t/yr Ta_2O_5)	2641±3 (U/Pb) 2657±18 (Pb/Pb)	Černý (2005) Camacho et al. (2012)*
33	Wodgina, Australia (*HR+W*)	63.5 Mt[2] @ 0.037% Ta_2O_5	Sn_2O	Care and maintenance (250 t/yr Ta_2O_5)	2829±11 (Pb/Pb) 2803±115 (Pb/Pb)	Kennedy (1998) [5] Kinny (2000) [5] Sons of Gwalia Ltd (2002) Simandl (2002) Fetherston (2004)

No.	Deposit, Country	Tonnage and Grade	Co-Products [potential]	Production Capacity	Age (method)	References
	PERALKALINE COMPLEX-RELATED					
34	Aires prospect, Motzfeldt, Greenland (*HR*)	340 Mt[1] @ 0.012% Ta_2O_5, 0.185% Nb_2O_5	[REE] [ZrO_2]		1310±31 (Rb/Sr)	Blaxland et al. (1978) [5] Ram Resources (2013)
35	Ghurayyah, Saudi Arabia (*HR*)	400 Mt[3] @ 0.024% Ta_2O_5 0.28% Nb_2O_5				Tertiary Minerals Plc (2013)
36	Kanyika, Malawi (*HR*)	23 Mt @ 0.0149% Ta_2O_5 0.3274% Nb_2O_5 37 Mt[3] @ 0.013% Ta_2O_5 0.27% Nb_2O_5	[ZrO_2, 0.5%] [U_3O_8, 0.009%]			Globe Metals & Mining (2013)
37	Lovozero, Russia (*HR*)	>1000 Mt[1] @ 0.30% Nb_2O_5	ZrO_2 REE	11 500 t/yr loparite concentrate (~30% TREO, 16% Nb_2O_5)	370.4±6.7 (Rb/Sr) 347 (U/Pb)	Kramm and Kogarko (1994) [5] Richardson and Birkett (1995) Arzamastsev et al. (2007) [5] Zaitsev and Kogarko (2012)
38	Narraburra, Australia (*HR*)	73 Mt[1] @ 0.0126% Nb_2O_5	[ZrO_2, 0.12%] [Y_2O_3, 0.015%] [TREO, 0.033%]			Capital Mining Limited (2013)
39	Nechalacho, Canada (*HR*)	121.3 Mt @ 0.0309% Ta_2O_5 0.3453% Nb_2O_5 183.4 Mt[3] @ 0.02% Ta_2O_5 0.33% Nb_2O_5	[ZrO_2, 2.44%] [TREO+Y, 1.36%]		2094±10 (U/Pb)	Bowring et al. (1984) [5] Sinclair et al. (1994) [5] Ciuculescu et al. (2013)
40	Strange Lake, B-Zone, Canada (*HR*)	278 Mt @ 0.18% Nb_2O_5 214 Mt[3] @ 0.14% Nb_2O_5	[ZrO_2, 1.83%] [TREO+Y, 0.90%]		1240±2 (U/Pb)	Miller et al. (1997) [5] Gowans et al. (2013)
	PERALUMINOUS GRANITE-RELATED					
41	Abu Dabbab, Egypt (*HR*)	32.5 Mt @ 0.015% Ta_2O_5 12 Mt[3] @ 0.020% Ta_2O_5	[SnO_2, 0.09%]		600-450 (Rb/Sr, K/Ar)	Gippsland Ltd. (2013a)
42	Beauvoir, France (*HR*)	200 Mt[1] @ 0.012% Ta_2O_5	LiO_2, 1.3% SnO_2, 0.13%	Past Producer	208±2 (Ar/Ar)	Cheilletz et al. (1992) [5] Cuney et al. (1992)
43	Moolyella, Australia (*W*)	1.9 Mt[1] @ 0.143% Ta_2O_5	[SnO_2, 0.020%]			Lithex Resources Ltd. (2012)

No.	Deposit, Country	Tonnage and Grade	Co-Products [potential]	Production Capacity	Age (method)	References
44	Nuweibi, Egypt (*HR*)	48 Mt @ 0.0147% Ta_2O_5 50 Mt[3] @ 0.0138% Ta_2O_5			490±27 (Rb/Sr)	Hassanen and Harraz (1996) [5] Gippsland Ltd. (2013b)
45	Orlovka, Russia (*HR*)	28.5 Mt[1] @ 0.014% Ta_2O_5	LiO_2 (0.269%) Rb_2O (0.12%) Cs_2O (0.003%) SnO_2 (0.012%)	Past Producer	142.9±1.8 (Rb/Sr)	Reyf et al. (2000) Beskin et al. (1994) Dolgopoloca et al. (2004) Kovalenko et al. (1999) [5]
	OTHER					
46	Dubbo, Australia (*HR*)	35.9 Mt[2] @ 0.03% Ta_2O_5 0.46% Nb_2O_5	[ZrO_2, 1.93%] [Y_2O_3, 0.14%] [TREO, 0.74%] [HfO_2, 0.04%]			Alkane Resources Ltd. (2013)
47	Pitinga, Brazil (*HR+W*)	266.7 Mt[1] @ 0.027% Ta_2O_5 0.217% Nb_2O_5	SnO_2 (0.21%)	Active mine (production not known)	1834±6 (U/Pb) 1783±5 (Ar/Ar) 1794±19 (U/Pb)	Fuck et al. (1993) [5] Lenharo (1998) [5] Pareja (2011)

Resources reported are NI-43-101 or JORC compliant and combine measured and indicated categories, unless otherwise noted. The tonnage and grade column contains only Nb_2O_5 and Ta_2O_5 data. In column four, square brackets denote potential co-products. Depending on market conditions, for some deposits, the commodities in brackets may become the principal reason for development. In the case of Lovozero, Nb_2O_5 is a by-product of REE production (extrapolated from unpublished info from Roskill Information Services). Production capacities for ore deposits on "care and maintenance" are shown in parenthesis.

[1] Unconfirmed reserve estimates (non NI 43–101 or JORC compliant)
[2] Proven+probable
[3] Inferred
[4] Reserve and resource estimates
[5] Age date determinations reference. Ages are for emplacement of deposit-related intrusions and do not necessarily represent timing of mineralization
TREO; total rare earth oxides

HR hard rock ore, *W* weathered ore, *HR+W* both hard rock and weathered ore. In the case of Pitinga, alluvium is an important source of ore. The weathered crusts formed above the Greenbushes and Wodgina pegmatites have been mostly exhausted. Mining is now focused on hard rock reserves.

The LCT family of pegmatites show petrogenetic affinity to peraluminous and metaluminous S-type rare-element enriched granites (Černý, 1991a, b; Černý and Ercit, 2005; Martin, 2007). These pegmatites mainly occur in orogenic settings, are associated with crustal shortening (subduction or continental collision) and are located adjacent to granitic cupolas or aligned along deep faults (Moloshag, 1974; Anhaeusser, 1976; Černý, 1982; Trueman and Černý, 1982; Möller and Morteani, 1983). Many of these pegmatites display syn-kinematic textures (Hatcher and Clynick, 1990). Pegmatites that were historically, or are currently, mined for Ta (as well as Li, Cs, and Sn) belong to the LCT family. Highly fractionated pegmatites may contain hundreds of exotic accessory minerals consisting of Li, Rb, Cs, Ta, Nb, Be, Y, REEs, Mo with the presence of H_2O, F, B_2O_3, and P_2O_5 (Černý, 1991a). Rare-element content (specifically Li, Cs, Be, Ta, and Nb), Ta:Nb ratio and degree of albitization increase with distance from the source intrusion (Fig. 2.5). These pegmatites are characterised by the presence of muscovite, garnet, tourmaline, and aluminosilicates (Černý and Ercit, 2005).

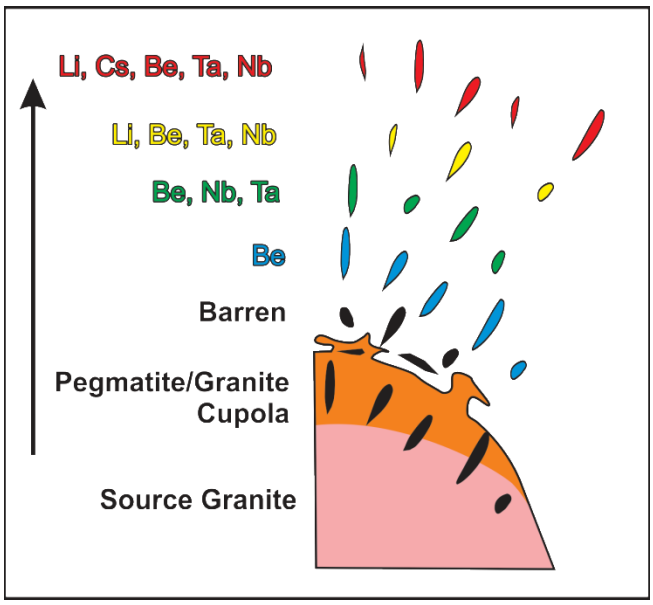

Figure 2.5 Schematic representations of granite-pegmatite relationship within a pegmatite field. Arrow denotes increasing complexity of zonation, extent of replacement (albitization) and increasing Ta/Nb ratio with distance from the source granite. Modified from Trueman and Černý (1982), Černý and Meintzer (1988), and Černý (1991b).

Common Ta-bearing minerals are columbite-tantalite, microlite, wodginite, and euxenite (Table 2.2; Hatcher and Bolitho, 1982; Trueman and Černý, 1982; Černý,

1991a; Hatcher and Clynick, 1990). LCT pegmatites have substantially higher Ta content (e.g. Tanco 0.2160 % Ta_2O_5) than rare element-enriched peraluminous granites (e.g. Orlovka, 0.0147 % Ta_2O_5; Beauvoir, 0.0120 % Ta_2O_5) or carbonatite hosted deposits (e.g. Upper Fir, 0.0191 % Ta_2O_5). Examples of economically significant Ta-bearing pegmatites are Wodgina and Greenbushes (Australia), Tanco (Canada), Volta Grande (Brazil), and Morrua (Mozambique). These can be further enriched by weathering (e.g. Greenbushes or Volta Grande).

The Wodgina pegmatite district within the Archean Wodgina greenstone belt, Western Australia, is one of the largest known Ta resources in the world (Sweetapple et al., 2001a, b; Sweetapple and Collins, 2002). Historic Ta mining in the Wodgina area focused on alluvial deposits and the Wodgina main-lode pegmatite which was mined out by 1994 (Fetherston, 2004). As mining progressed, the Wodgina North and South pits merged. The same occurred at the Mount Cassiterite and Mount Tinstone pits. Since 1998, the majority of mining activities have occurred at Mount Cassiterite which contains the majority of remaining reserves and resources in the area.

The pegmatites of the Wodgina district (LCT pegmatite group of Černý, 1991a) belong to beryl-columbite subtype (beryl-bearing albite-quartz-muscovite pegmatites), albite spodumene type (Mount Cassiterite), and albite type (Wodgina) and increase in degree of fractionation with distance north of the Numbana granite, located approximately 1–1.5 km southeast of the Wodgina and Mount Cassiterite pegmatites. The Wodgina albite type pegmatites trend north–south and cut metakomatiites (Fig. 2.6; Blewett et al., 2001; Sweetapple et al., 2001b; Sweetapple and Collins, 2002). The main pegmatite body is 5–40 m in thickness and dips gently east. Its northern portion has been dismembered by late faulting (Fig. 2.7; Sweetapple and Collins, 2002; Fetherston, 2004). Ta mineralization consists of primary tantalite-(Mn) as skeletal grains and cores in radial aggregates of cleavelandite with minor columbite-(Mn) and wodginite (Miles et al., 1945; Sweetapple and Collins, 1998; Sweetapple et al., 2001b; Sweetapple and Collins, 2002; Fetherston, 2004). Most Ta mineralization is hosted by the massive cleavelandite (white lamellar albite) unit, which is overprinted by fine-grained sugary texture albite and minor muscovite alteration. The aplitic albite-quartz-muscovite unit also contains microlite and

fersmite. An irregular body of massive grey quartz is observed in the centre of the northern portion of the pegmatite (Fig. 2.7).

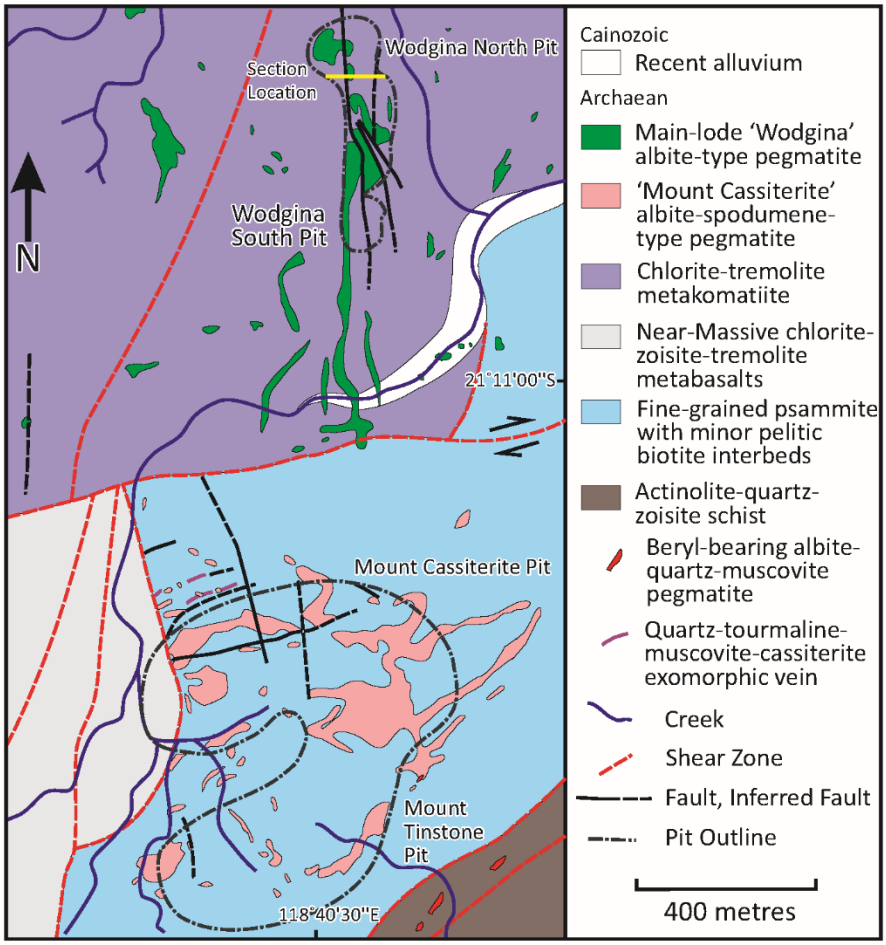

Figure 2.6 Lithologic map of the Wodgina and Mt. Cassiterite pegmatite groups, Western Australia. Only Li is currently extracted from the Mount Cassiterite and Tinstone pits. The Wodgina pit is essentially mined out. Modified from Sweetapple et al. (2001b), Sweetapple and Collins (2002), and Fetherston (2004).

The nearby Mount Cassiterite albite-spodumene-type pegmatites (located about 400 m south of the Wodgina main-lode pegmatite; Fig. 2.6) consist of stacked sheets averaging 5 to 12m (up to 100 m locally) in thickness, gently dipping west to southwest, hosted in psammitic and interbedded biotite pelite metasediments (Sweetapple et al., 2000a, 2001b; Sweetapple and Collins, 2002; Fetherston, 2004). The Mount Cassiterite pegmatite is much more homogenous than the Wodgina main lode and consists predominantly of albite, primary spodumene, with minor K-feldspar and muscovite. Fine-grained albite sporadically overprints the primary assemblage. Ta mineralisation consists of wodginite

and subordinate columbite-(Mn), tantalite-(Mn), Sn-bearing microlite, defect (high A-site vacancy) microlite, and fibrous calciotantite. Cassiterite, the main Sn mineral, contains 5 to 8 % Ta_2O_5 (Hall, 1994; Sweetapple et al., 2000b; Sweetapple and Collins, 2002). Beryl-bearing albite-quartz-muscovite pegmatites are not considered as major sources of Ta but at least one of these pegmatites contains columbite-(Mn) with fine grain microlite inclusions (Sweetapple et al., 2000b).

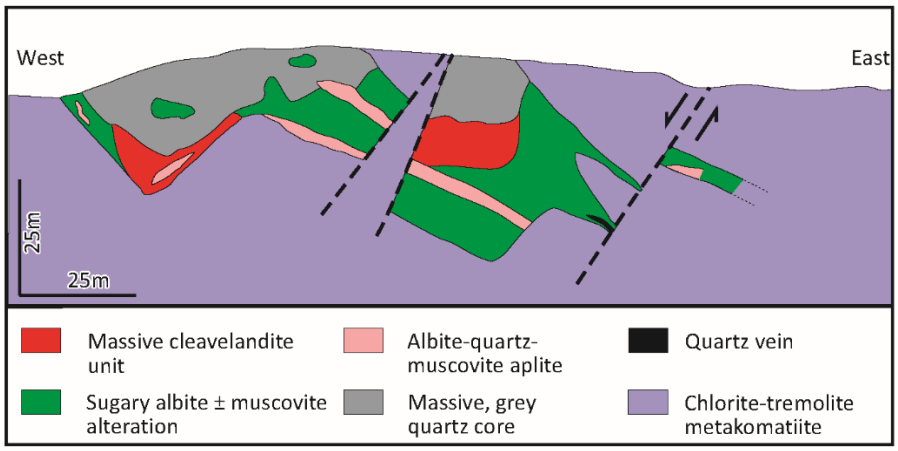

Figure 2.7 Cross section of the Wodgina pegmatite across the north end of the pit (area of highest Ta grades). Modified from Sweetapple et al. (2001b) and Fetherston (2004).

Niobium-Yttrium-Fluorine family pegmatites are found mainly in continental anorogenic settings and may have originated from the fractionation of metaluminous A- and I-type granites (Černý, 1991a; Černý and Ercit, 2005). They also share characteristics with pegmatitic phases of peralkaline and carbonatite complexes (Martin and De Vito, 2005; Martin, 2007) and can be mineralized (e.g. Lovozero, Russia, and Strange Lake, Canada).

2.2.2 Carbonatite-related Nb-Ta deposits

Carbonatite is defined as an igneous rock containing more than 50 % modal carbonate minerals and no more than 20 wt. % SiO_2 (Le Maitre, 2002) and is commonly subdivided based on proportions of CaO, MgO, and $FeO+Fe_2O_3+MnO$. More elaborate classifications involving mineralogical and genetic concepts were developed by Woolley (2003), Mitchell (2005a), and Woolley and Kjarsgaard (2008). The Mitchell (2005a) classification is rarely used by the exploration industry. Most carbonatite intrusions are

located within alkaline provinces in intracontinental extensional tectonic settings, less commonly at cratonic margins and rarely occur in oceanic settings (Woolley and Kjarsgaard, 2008). Most carbonatites are classified as magmatic (Woolley and Kjarsgaard, 2008). They form sills, dikes, plugs, or zoned carbonatite complexes such as Oka (Gold et al., 1967, 1986) and St. Honoré (Fig. 2.8; Thivierge et al., 1983; Lafleur and Ayad, 2012), but some form extrusive and pyroclastic occurrences. Carbonatites emplaced prior to regional tectonic/metamorphic events could be complexly deformed (e.g. the Nb- and Ta-bearing Upper Fir carbonatite, Canada; Chong et al., 2012).

Carbonatite composition can range from calcite-dolomite to magnesite, with local siderite and ankerite (Woolley, 2003; Mitchell, 2005a; Woolley and Kjarsgaard, 2008). Enrichment in incompatible elements (Sr, Ba, Nb, REEs, and especially light REE [LREE]) is common. Carbonatites are the main targets in exploration for Nb and LREEs, but they may also host economic concentrations of U, Th, Ba, P, Zr, F, V, Fe, and possibly Ta (Mariano, 1989a, b; Richardson and Birkett, 1995; Birkett and Simandl, 1999). Many carbonatite complexes, such as St. Honoré (Fig. 2.8; Thivierge et al., 1983; Lafleur and Ayad, 2012), have spatially associated silicate intrusive rocks (Woolley, 2003; Mitchell, 2005a; Woolley and Kjarsgaard, 2008). At least 113 of the 573 known carbonatites occurrences, including St. Honoré, are associated with nepheline syenite intrusions (Woolley, 2003; Mitchell, 2005a; Woolley and Kjarsgaard, 2008).

Regardless of mineralization, many carbonatite complexes are enveloped by zones of fenitization formed by alkali-rich fluids that penetrated into and reacted with the country rock (Heinrich, 1985; Le Bas, 2008). Fenitization is described as sodic or potassic and in some cases both varieties are linked to the same intrusion. The degree of fenitization varies concentrically outward, from rocks macroscopically indistinguishable from alkaline igneous varieties, through extensively reconstituted host rocks, to mildly brecciated or fractured rocks containing veinlets of K, Na, and/or Fe minerals. Recognition of the fenitization zones is important in exploration because it increases the size of the carbonatite target; however, in some cases fenite zones may have higher Nb content than the carbonatite intrusion itself (e.g. the Lonnie [Simandl et al., 2013] and Wicheeda complexes [Trofanenko et al., 2014]). Silicate rocks associated with undeformed carbonatites commonly form lunate intrusions, with the complex younging

progressively inwards (Fig. 2.8; Mitchell, 2005a; Woolley and Kjarsgaard, 2008). Late stage, carbothermal fluids may cause the formations of a central brecciated, REE-, Sr- and Ba-rich plug (Mitchell, 2005a; Woolley and Kjarsgaard, 2008). Nb mineralization associated with carbonatite complexes is commonly interpreted as magmatic. Economic enrichment of Ta and REEs may be related to magmatic hydrothermal solutions or redistribution of primary mineralogy by later hydrothermal fluids.

The St. Honoré carbonatite complex forms a semi-circular shape in plan view, and is about 4 km across (Lafleur and Ayad, 2012). The intrusive complex consists of concentric crosscutting feldspathoid-bearing silicate rocks with a core of carbonatite (Fig. 2.8; Fortin-Bélanger, 1977; Thivierge et al., 1983; Fournier, 1993; Lafleur and Ayad, 2012). The intrusive complex youngs progressively inwards with the carbonatite ranging in composition from calcite through dolomite with local ankerite found in the core (Fortin-Bélanger, 1977). Nb mineralization is concentrated in the carbonatites forming peripheral to the core of the complex while REE mineralization is concentrated in the central ankerite-bearing brecciated core (Fig. 2.8; Fournier, 1993; Lafleur and Ayad, 2012). Nb mineralization is predominantly pyrochlore ($[Ca,Na]_2[Nb,Ti,Ta]_2O_6[O,OH,F]$) with secondary columbite ($[Fe,Mn][Ta,Nb]_2O_6$; Table 2.2) and minor Nb-rutile ($[Ti,Nb,Fe]O_2$; Fournier, 1993; Lafleur and Ayad, 2012). The main REE minerals are bastnaesite ($Ce[CO_3]F$), parasite ($Ca[Ce,La]_2[CO_3]_3F_2$), and synchysite ($CaCe[CO_3]_2F$); REE bearing minerals of secondary importance include monazite ($[Ce,La,Nd,Th]PO_4$) and thorite ($[Th,U]SiO_4$; Fournier, 1993; Lafleur and Ayad, 2012). Pyrochlore is also known to contain up to 1 wt. % REEs in the carbonatite (Fournier, 1993).

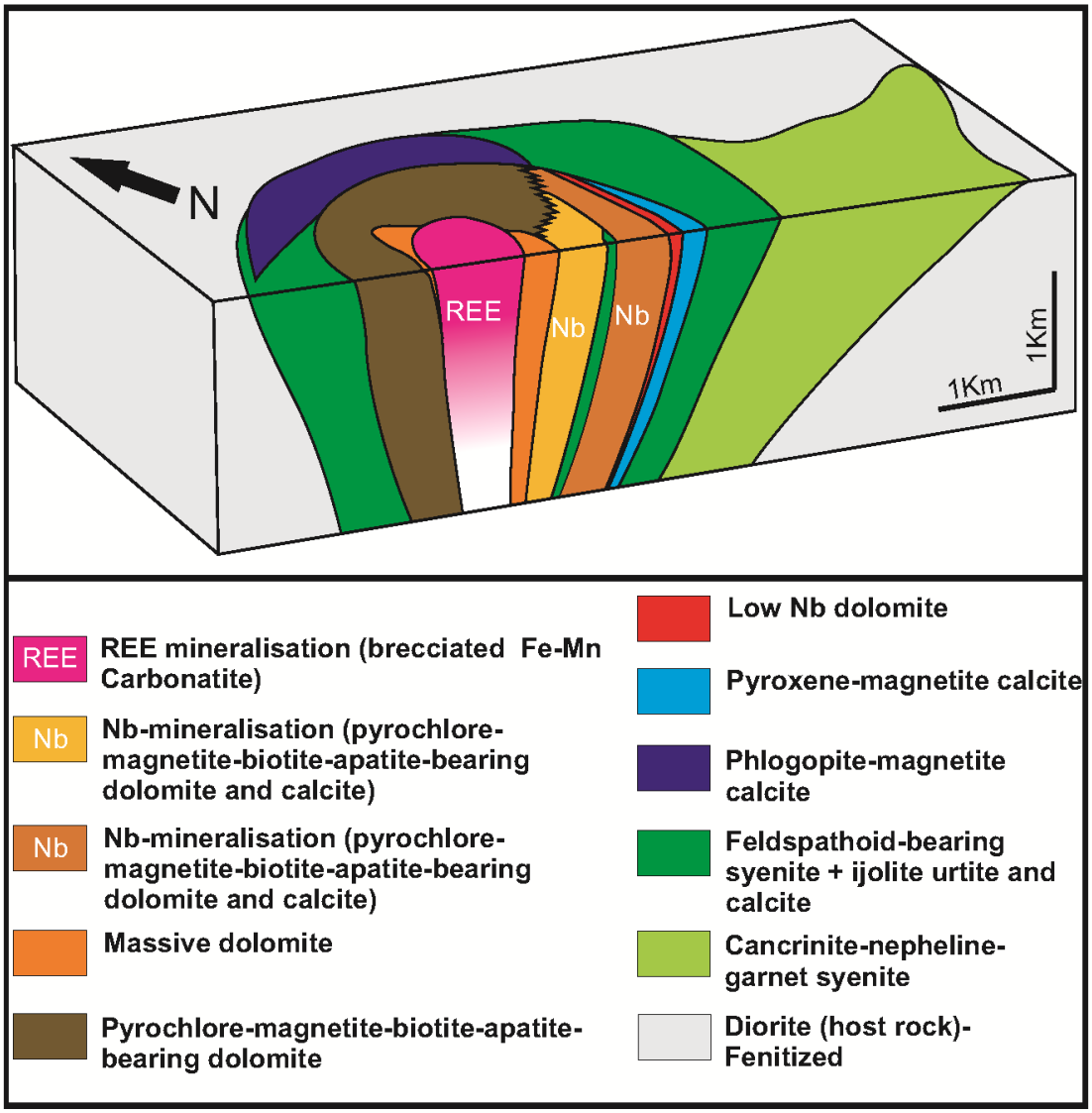

Figure 2.8 Block diagram of the St. Honoré carbonatite complex displaying conical, circular, or crescent shapes. The two units currently mined for niobium are denoted by "Nb." The REE mineralization is concentrated in the brecciated Fe–Mn carbonatite core. The diorite host rock is strongly fenitized in contact with the carbonatite and syenite intrusions. Modified from Lafleur and Ayad (2012).

The Araxá and Catalão complexes in Brazil are characterised by carbonatite-glimmerite association (Traversa et al., 2001). Secondary concentration of pyrochlore in laterites overlying these carbonatites has produced the largest exploited deposits of Nb (Tantalum-Niobium International Study Center, 2013b). The carbonatite-related Araxá deposit is hosted by one of the intrusions forming the Alta Paranaíba alkaline province in Brazil. The complex is a circular intrusion approximately 4.5 km in diameter with a core of dolomite carbonatite, calcite carbonatite, phoscorite (plutonic ultramafic rocks

composed predominatnly of magnetite, apatite, and at least one of olivine, augite, and/or phlogopite; Krasnova et al., 2004), and glimmerite (Fig. 2.9; Issa Filho et al., 1984; Traversa et al., 2001). It intrudes into Proterozoic biotite schist and quartzite (Traversa et al., 2001). Carbonatite emplacement produced a fenitized aureole containing arfvedsonite and aegirine up to 1 km wide in the quartzite and schist country rock (Fig. 2.9; Issa Filho et al., 1984; Nasraoui and Waerenborgh, 2001; Traversa et al., 2001).

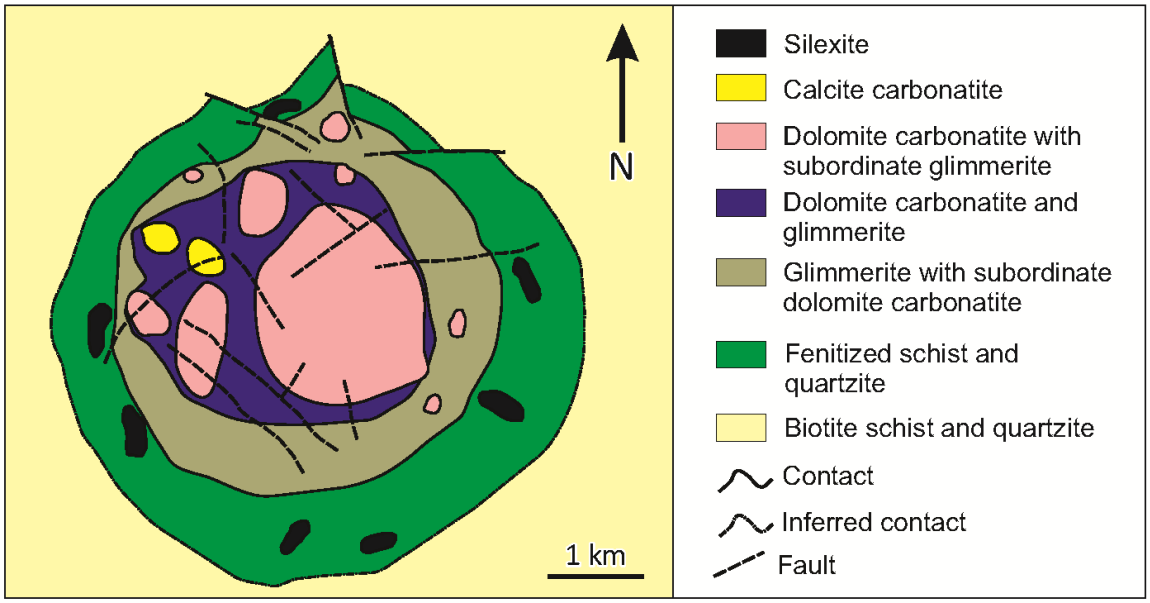

Figure 2.9 Schematic lithologic map of the Araxá Carbonatite (Barreiro), Brazil. Modified from Grozzi-Sad and Torres (1976), Issa Filho et al. (1984), and Traversa et al. (2001).

The average Nb_2O_5 content of the primary ore is 2.5 %, with a maximum grade of 8 % Nb_2O_5, (Issa Filho et al., 2001). A weathered crust has developed over the carbonatite core of the Araxá complex blanketing the intrusive core to an average thickness of 80 m, locally up to 230 m (Nasraoui and Waerenborgh, 2001; Traversa et al., 2001). Only the weathered crust developed above the carbonatite core is currently mined for Nb. Residual ore, currently mined by open pit, averages 2.3 % Nb_2O_5 (CBMM, 2014). It consists of bariopyrochlore (4 %), limonite/goethite (36 %) barite (20 %), magnetite with ilmenite exsolutions (16 %), gorceixite (6 %), monazite (4 %), ilmenite (5 %), quartz (4 %), and other minor constituents (Issa Filho et al., 2001). Weathered ore and waste do not require drilling and blasting during stripping and mining; processing is described by Issa Filho et al. (2001).

2.2.3 Peralkaline complex-hosted Nb-Ta-REE deposits

Peralkaline igneous rocks have an alumina saturation index wt% $(K_2O+Na_2O)/Al_2O_3>1$ (Shand, 1927) and are mainly emplaced during extensional activity within anorogenic continental settings (Pitcher, 1983, 1993; Barbarin, 1990); however, in some cases evidence of the original tectonic setting is not preserved. All peralkaline intrusions are enriched in HFSE; however, this is especially true for agpaitic varieties bearing complex Zr–Ti–REE silicates such as eudialyte, mosandrite, and rinkite (Gerasimovskii, 1956; Sørensen, 1960; 1968). These agpaitic intrusions can be broadly subdivided into two categories: (a) layered intrusions, such as Nechalacho (Canada), Lovozero (Russia), and Ilímaussaq (Greenland), characterised by rhythmic or microrhythmic layering as described in Sørensen (1968) and Bailey et al. (2006); or (b) more homogeneous intrusions such as Strange Lake (Canada), where HFSE are present mainly in pegmatitic/stockscheider facies of the pluton apex, related cupola(s) or nearby pegmatite/aplite dikes (Miller, 1986; Richardson and Birkett, 1995; Salvi and Williams-Jones, 1990). Both of these intrusion types are commonly affected by hydrothermal remobilization (Gysi and Williams-Jones, 2013). Peralkaline complexes commonly contain highly evolved pegmatitic phases with NYF affinity enriched in HFSE elements and magmatic mineralization, which may be remobilized during autometasomatism or late metasomatism (Martin, 2007). Nb mineralization in stock or pluton-type settings is concentrated in the latest, most fractionated portions of the intrusive complexes and often coincides with late hydrothermal alteration and REE mineralization (Boily and Williams-Jones, 1994; Linnen and Cuney, 2005; Salvi and Williams-Jones, 2005). Silicate mineralogy is characterised by sodic phases such as aegirine, reibeckite, arfvedsonite, and albite.

The Strange Lake rare-element deposit on the Quebec-Labrador border, Canada, is hosted within a small peralkaline complex, approximately 6 km in diameter (Fig. 2.10; Miller, 1986, 1990). The complex consists of aegirine-arfvedsonite granite. There are three main phases of intrusions, unaltered hypersolvus (single feldspar), unaltered subsolvus (two feldspars), and altered subsolvus granites (Fig. 2.10). The main mineralised zone, the B-zone, consists of pegmatites and aplites (Fig. 2.10). The main ore

minerals in the B-zone are pyrochlore (that may contain 3–6 % REE oxides; Table 2.2), monazite, bastnaesite, and possibly parisite, gadolinite ($Y_2FeBe_2Si_2O_{10}$), gerenite ($[Ca,Na]_2[Y,REE]_3Si_6O_{18}\cdot 2[H_2O]$), kainosite ($Ca_2[Y,Ce]_2Si_4O_{12}[CO_3]\cdot H_2O$), and other yet-unidentified calcium-yttrium-REE-bearing silicates (Gowans et al., 2013). Pyrochlore mineralization is hosted by an altered subsolvus granites and pegmatites (Boily and Gosselin, 2012).

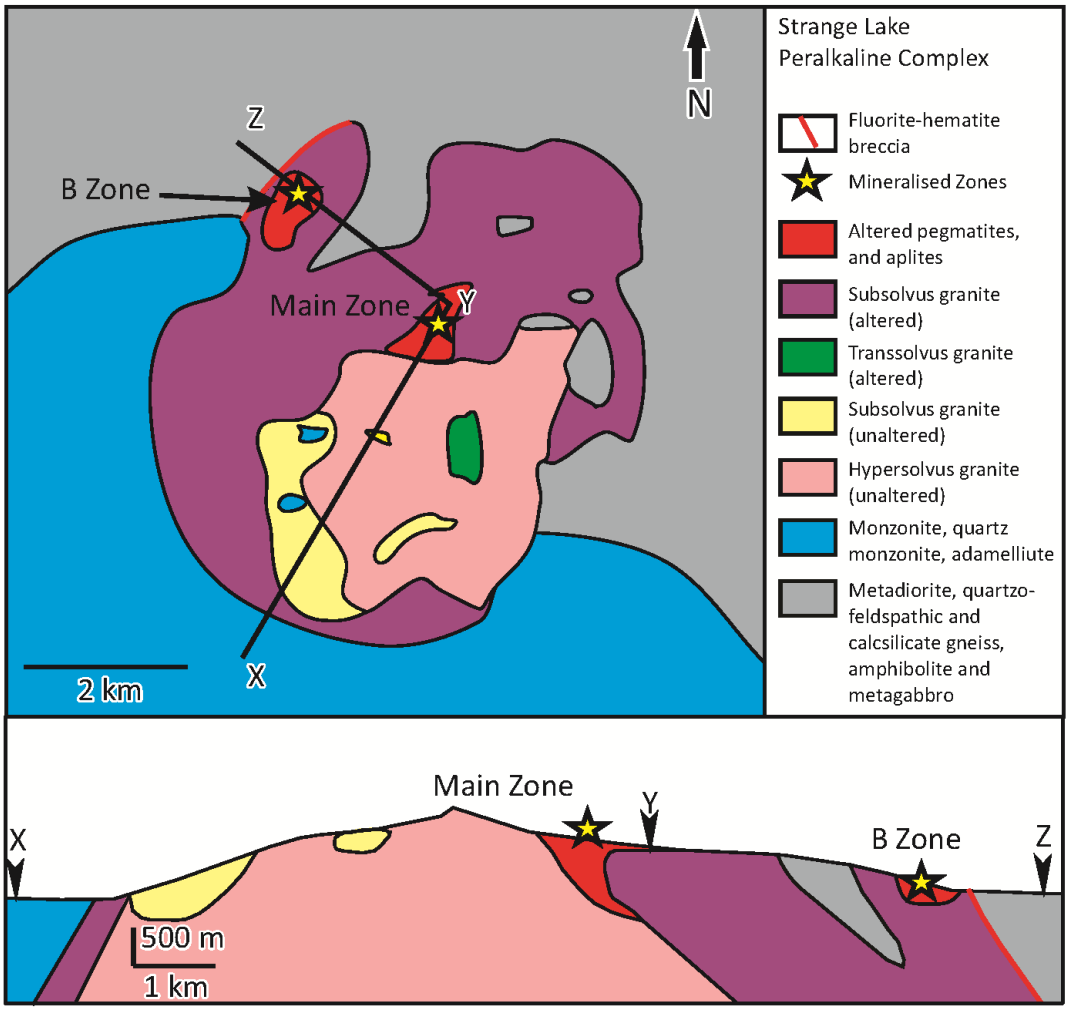

Figure 2.10 Lithologic map and schematic cross section of the Strange Lake peralkaline complex. The locations of strongest Zr–Y–Nb–REE mineralization are denoted by yellow stars. Modified From Miller (1986, 1990), Salvi and Williams-Jones (1990, 1996, 2006), Daigle et al. (2011) and Boily and Gosselin (2012).

The Lovozero peralkaline complex Kola Peninsula, Russia, is a large, 12×16 km, ring-shaped body topped by a 2-km thick laccolith with extensions down to 7 km (Kramm and Kogarko, 1994; Ermolaeva et al., 2007). It consists of a layered peralkaline intrusive

complex (miaskitic nepheline syenites) at its base to agpaitic nepheline syenites (eudialyte-lujavrites) at the top of the deposit (Kogarko, 1987; Kramm and Kogarko, 1994). The exposed sequence is cut by late agpaitic to hyperagpaitic nepheline syenite and is highly enriched in LREEs, Ba, Th, Nb, Ta, Hf, Zr, and F (Kramm and Kogarko, 1994). Over 390 minerals have been reported in this complex with a number of Nb, Ta, and/or REE-bearing varieties (Vlasov et al., 1966; Khomyakov, 1995; Pekov, 2000; Pekov et al., 2005). The main ore mineral is loparite ([Ce,La,Na,Ca,Sr][Ti,Nb]O_3; Table 2.2) characterised in detail by Kogarko et al. (2002). Lovozero is the only peralkaline complex currently producing Nb as a co-product of REE (Zaitsev and Kogarko, 2012). Metallurgical difficulties have prevented extraction of REE, Zr, and Nb contained in eudialyte (Gupta and Suri, 1994; Zakharov et al., 2011).

The Nechalacho deposit, Canada, is a layered peralkaline complex of silica-undersaturated intrusive rocks. The complex is inferred to form a domal structure more than 300 m thick, with a diameter exceeding 1.5 km (Fig. 2.11; Sheard et al., 2012). This layered complex consists of sodalite cumulates, coarse-grained to pegmatitic nepheline aegirine syenites (upper zone) and a basal zone composed of foyaitic syenite with altered eudialyte cumulates (Fig. 2.11). The degree of alkalinity increases with depth (Salvi and Williams-Jones, 2005; Sheard et al., 2012). Mineralization is associated with autometasomatic replacement of primary igneous minerals and consists of: LREE in allanite ($[Ce,Ca,Y]_2[Al,Fe]_3[SiO_4]_3[OH]$), monazite, bastnaesite, and synchysite; Nb in columbite-(Fe) (Table 2.2); HREEs, Nb, and Ta in fergusonite ($YNbO_4$; Table 2.2); HREE, Nb, Ta, and Zr in zircon ($ZrSiO_4$); and Ga in biotite, chlorite, and feldspar (Ciuculescu et al., 2013).

Measured and indicated resources estimates are: 54.59 Mt at 1.42 % total rare-earth oxide and Y (TREO+Y), 0.14 % heavy rare-earth oxide and Y (HREO+Y), 1.96 % ZrO_2, 0.28 % Nb_2O_5 and 0.02 % Ta_2O_5 for the upper zone; and 66.67 Mt at 1.57 % TREO+Y, 0.34 % HREO+Y, 3.05 % ZrO_2, 0.40 % Nb_2O_5 and 0.04 % Ta_2O_5 for the basal zone (Ciuculescu et al., 2013). Nb, Ta, and Zr content and the proportion of HREO relative to LREO increases downwards. This coincides with the increase in fergusonite and zircon content in the basal zone. Relative abundance of columbite-(Fe) decrease, indicating fergusonite as the main Nb- and Ta-bearing ore mineral in the basal zone (Sheard et al.,

2012; Ciuculescu et al., 2013). Monazite, allanite, and REE-bearing fluorocarbonate content decreases with depth, which is reflected in the higher HREE to LREE ratio in the basal zone. The deposit is currently considered a potential source of Zr, Nb, and REEs (Sheard et al., 2012; Ciuculescu et al., 2013).

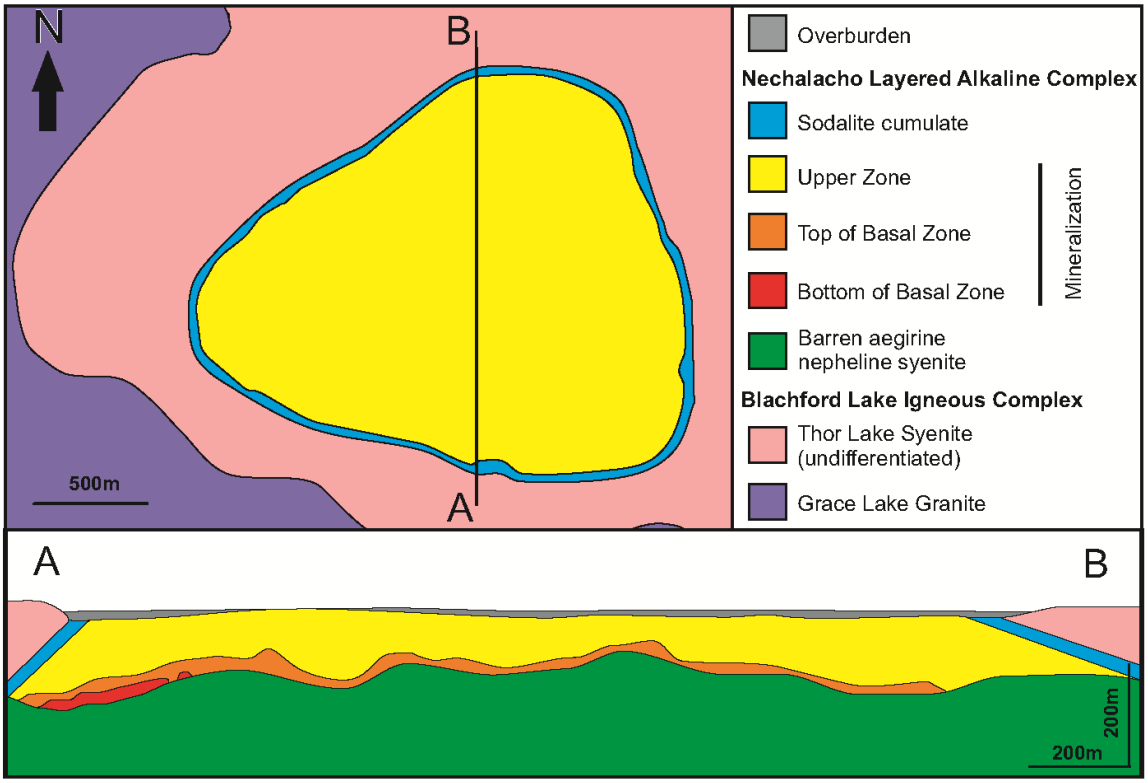

Figure 2.11 Geologic map and cross section of the Nechalacho (Thor Lake) deposit based on drill hole data. Location of the cross section is identified by the black line (A, B). The cross section depicts the domal layered igneous complex. The contact between the upper and basal zones is based on a sharp increase in HREE and total REE content. The basal zone-bottom has TREO >1 % and HREO >0.15 % with a HREE/LREE ratio of 0.25; the basal zone-top has TREO >1 % and HREO >0.15 % with HREE/LREE ration of 17 % (Ciuculescu et al., 2013). Modified from Möller and Williams-Jones (2013), Sheard et al. (2012), and Ciuculescu et al. (2013).

2.2.4 Peraluminous granite-related Ta±Nb deposits

Ta±Nb enrichment in granites is commonly associated with rare-element-enriched peraluminous to metaluminous intrusions. Granitic rocks are considered as peraluminous if they have a molar ratio $Al_2O_3/(CaO+Na_2O+K_2O)>l$ (Shand, 1927; Clarke, 1981). Rare-

element-enriched granites are found in post-orogenic and orogenic tectonic settings (Pitcher, 1983, 1993; Barbarin, 1990; Lin et al., 1995; Linnen and Cuney, 2005). Their rare-element content increases and Sr, Ba, Ti, and Zr decrease with increasing degree of fractionation (Černý and Meintzer, 1985; Breaks et al., 2003). The Mg:Li ratio in whole rock analysis is one of the best indicators of the degree of fractionation (Breaks et al., 2003). Rare-element-enriched granites consist of quartz, plagioclase, alkali feldspar, and one or more characteristic minerals such as biotite, muscovite, garnet, cordierite, staurolite, kyanite, andalusite, sillimanite, mullite, topaz, tourmaline, spinel, and corundum (Clarke, 1981). They are generally small, covering a surface area from 0.25 km^2 (Beauvoir granite; Raimbault et al., 1995) to about 2 km^2 (Orlovka; Reyf et al., 2000), and are vertically zoned. In some cases, these granites display stockscheider and/or greisenized cupola containing quartz, muscovite, lepidolite, topaz, and commonly tourmaline, fluorite, wolframite, cassiterite with possible accessory beryl or Ta- and Nb-bearing minerals (Černý and Meintzer, 1988; Lin et al., 1995; Linnen and Cuney, 2005). Examples of granites currently or historically mined for Ta include the Beauvoir granite in France (Raimbault et al., 1995), the Yichun granite in China (Lin et al., 1995), and the Orlovka granite in Russia (Seltmann et al., 2010).

The Beauvoir peraluminous granite is located in the Echassiéres massif, France. The areal extent of the Echassiéres massif is 40 km^2, with an average thickness of 3 to 4 km and extensions down to 6 km (Raimbault et al., 1995). The Beauvoir granite intruded into mica schist host rock and is 500×500 m in area with average thickness of 550 m, consisting predominantly of albite, quartz, and K-feldspar (Cuney et al., 1992). Lepidolite rich layers up to a metre thick are also observed. The majority of rare-element mineralization in the Beauvoir granite is related to magmatic assemblages with Ta and Nb concentrations increasing upwards in the intrusive body (Cuney et al., 1992). The Beauvoir granite has produced Sn and Ta in the past (Cuney et al., 1992; Laznicka, 2010) and kaolin and Li have been mined from the upper section of the cupola (Cuney et al., 1992; Simandl, 2002). Mineralization consists of lepidolite, cassiterite, and columbite-tantalite, but it is currently not economic (Cuney et al., 1992; Raimbault et al., 1995; Linnen and Cuney, 2005).

The Yichun granite is part of the Yashan batholith, China. The uppermost portion of the granite consists of a porphyritic topaz-lepidolite unit that is 200 to 350 m thick (Lin et al., 1995). A cupola-related stockscheider ranges in thickness from tens of centimetres to approximately 7 m and contains lepidolite, columbite-tantalite, Ta-rich cassiterite, and minor microlite (Lin et al., 1995).

Other Ta-bearing granite-hosted deposits such as Orlovka (in the Chita region of Siberia, Russia; Reyf et al., 2000) and Zinnwald-Cinovec (Germany-Czech Republic border; Rub et al., 1998) are also spatially associated with greisens. The Orlovka deposit is a past Ta-producing mine located within one of the cupolas of the composite Khangilay granitic pluton (Dolgopolova et al., 2004; Seltmann et al., 2010). The mineralized zone is approximately 1200 m long, 250 m wide, and 80–100 m thick, with an average Ta_2O_5 grade of 0.014 %. Mining from 1964 to 1993 exhausted the higher grade portion of this mineralized zone (Reyf et al., 2000; Seltmann et al., 2010). Orlovka is hosted by highly fractionated, subhorizontal or shallow dipping layered granitic rocks (Fig. 2.12). Ta mineralization is hosted in the following units: quartz-zinnwaldite-topaz body, quartz-amazonite-albitites pegmatoid, amazonite-albite granite with muscovite and Fe-lepidolite, amazonite albite granite with Fe-lepidolite, and amazonite-albite granite with zinnwaldite (Fig. 2.12). It occurs as fine grained disseminated columbite-tantalite and microlite (Reyf et al., 2000; Webster et al., 2004; Dolgopolova et al., 2004). Intense albitization and greisenization was accompanied by formation of amazonite, lepidolite, and zinnwaldite (Reyf et al., 2000). A lamprophyre dike cross cuts the mineralization (Fig. 2.12). Similar to Orlovka, the Zinnwald-Cinovec cupola displays zones with greisen-like characteristics and Ta enrichment (Johan and Johan, 1994; Webster et al., 2004; Johan et al., 2012); however, greisenization did not affect Ta content (Rub et al., 1998). Instead, Ta mineralization is related to albitization (Rub et al., 1998).

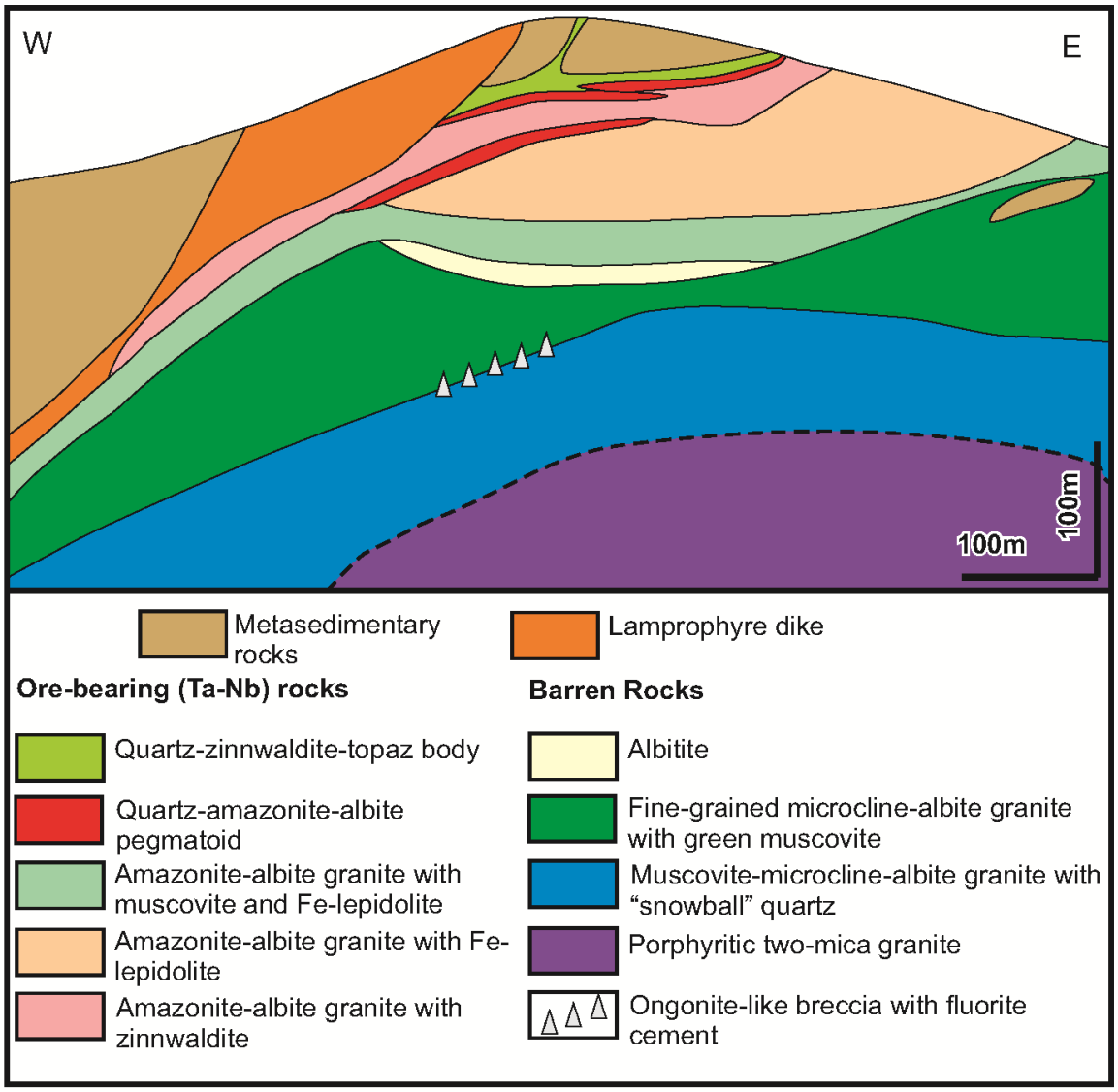

Figure 2.12 Vertical cross section of the Orlovka deposit. Tantalum mineralization is hosted in apical, highly differentiated units. Tantalum content increases upwards. Modified from Seltmann et al. (2010).

2.2.5 Secondary Ta sources

Secondary sources have historically accounted for up to 40 % of global Ta production (Schwartz et al., 1995). Cassiterite placer deposits in Thailand and Malaysia were mined for their Sn content; however, Ta_2O_5 derived from columbite-tantalite and Ta-Nb rutile (strüverite) was also recovered from these deposits (Hassan, 1994; Schwartz et al., 1995).

2.3 Grade and tonnage

Deposits hosting Ta (Fig. 2.13a) and Nb (Fig. 2.13b) range widely in grade and tonnage. The level of confidence for resource and reserve estimates from many deposits in South America and Africa is lower than well-defined deposits in North America and Australia (Table 2.3). Information is unavailable or incomplete for many deposits in China and Russia and such deposits are not shown. Chinese and Russian production is also predominantly consumed internally. Diagonal lines in Fig. 2.13 indicate isotonnage of contained metal oxides. For example, two deposits plotting along such lines, or on any parallel line in Fig. 2.13a, will have varying ore grades and tonnages, but will have the same mass of contained Ta_2O_5.

Overall, the highest Ta_2O_5 grades (Fig. 2.13a; Table 2.3) correspond to pegmatites (e.g. Tanco, Canada; Wodgina, Australia; and Morrua, Mozambique). Peralkaline complexes have the largest resource in terms of ore tonnage though in-depth investigation of some of these deposits has not been carried out (e.g. Ghurayyah, Saudi Arabia, and the Aires prospect, Motzfeldt, Greenland). The highest Nb_2O_5 grades and tonnages (Fig. 2.13b; Table 2.3) correspond to weathering-enriched carbonatite complexes (e.g. Araxá, Catalão I and II, and Seis Lagos, Brazil) followed by hard rock carbonatite-related deposits (e.g. Aley and St. Honoré, Canada). Peralkaline-related deposits also represent significant ore tonnages and contained Nb_2O_5 content (e.g. Lovozero, Russia, and Nechalacho, Canada).

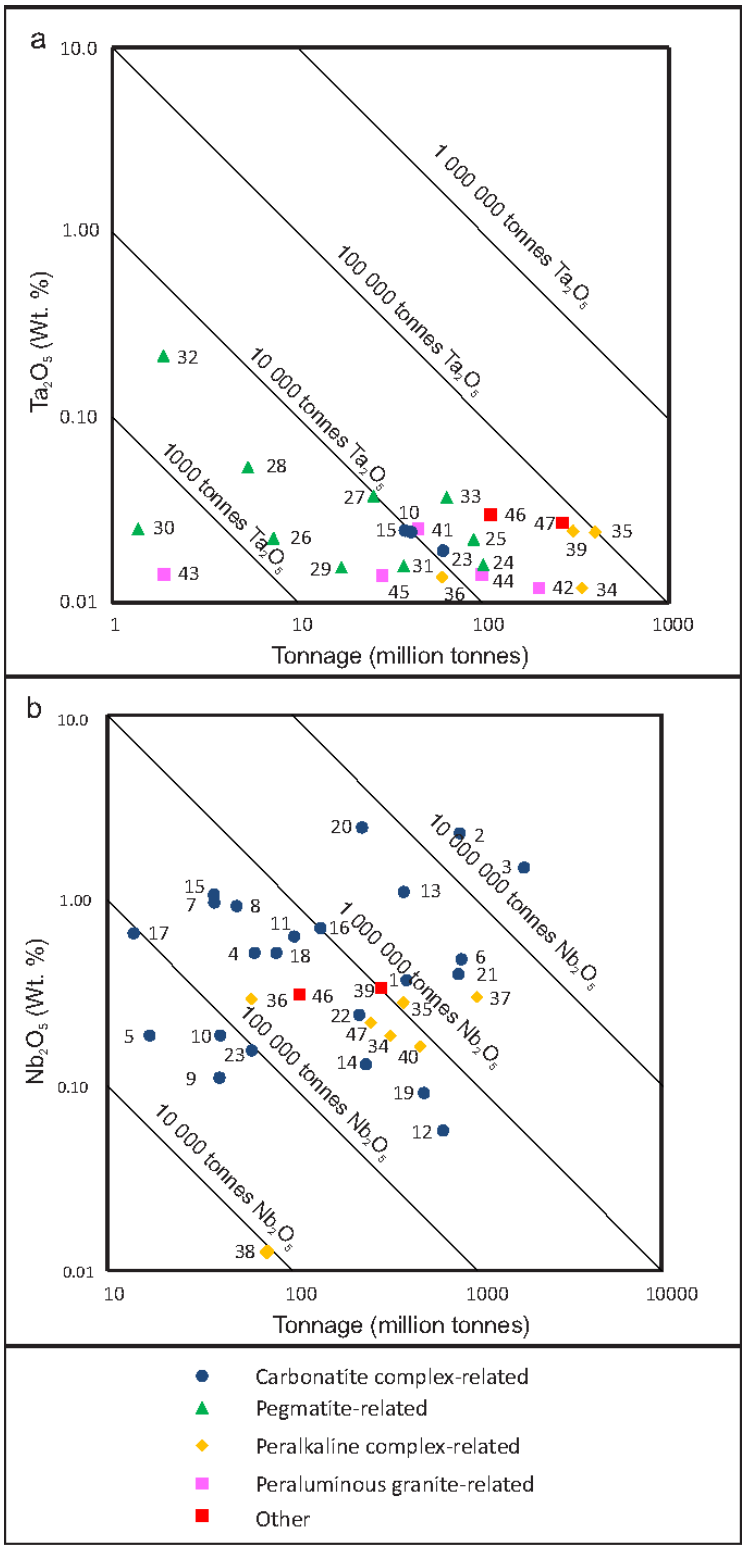

Figure 2.13 Grade and tonnage characteristics of (a) Ta and (b) Nb deposits associated with carbonatite complexes, pegmatites, peralkaline complexes and rare-element granites. Diagonal lines indicate tonnage of Ta_2O_5 and Nb_2O_5, respectively. Numbers correspond to deposits listed in Table 2.3.

2.4 Ta and Nb concentrate considerations

Nb-and Ta-bearing deposits are subject to the same evaluation methods as precious and base metal deposits; however, as with most specialty metals and high-value industrial minerals, the market is limited and prices of Ta and Nb concentrates are determined by negotiations between buyer and sellers.

According to the Tantalum-Niobium International Study Center (2013a), tantalite concentrates are expected to contain more than 30 % Ta_2O_5; however, concentrates with a minimum content of 20 % Ta_2O_5 are also of interest to processors. The value of Ta concentrate is based on Ta_2O_5 content and Nb_2O_5 is commonly ignored. The price for Nb concentrate with low Ta_2O_5 content is determined by summation of Nb_2O_5+Ta_2O_5 content and valuation is based on the price for Nb_2O_5. The difference between Nb_2O_5 and Ta_2O_5 prices is ignored (Tantalum-Niobium International Study Center, 2013a, b). The above valuation method is not applicable if the concentrate is sold for production of ferroniobium where Ta cannot be removed.

Furthermore, Ta and Nb minerals may contain significant levels of U and Th. Concentrations of these elements may be of concern during mining and transportation of the concentrate (Tantalum-Niobium International Study Center, 2013a, b). The Kenticha Ta deposit, Ethiopia, ceased production due to the high U–Th content of its concentrates and restrictive international transportation regulations for shipping radioactive materials (Stratton and Henderson 2013). Metallurgical aspects of Ta and Nb deposits are outside of the scope of this study. However, they are covered in detail in Shaw and Goodenough (2011) and Linnen et al. (2014). The potential for Nb recovery as a co-product of Zr and REE from peralkaline complexes is determined to a large extent by the mineralogy, texture and particle size and is deposit specific as illustrated by Nechalacho (Ciuculescu et al., 2013), Kipawa (Saucier et al., 2013), and Lovozero (Zaitsev et al., 1998).

2.5 Summary

Most (~40 %) of Ta is mined from primary pegmatites and their weathering-enriched equivalent that typically have higher Ta grades than peraluminous granite-hosted deposits. Historically, large-scale mechanised mining of pegmatite-hosted Ta-bearing deposits such as at Greenbushes and Wodgina (Australia) have been the main sources of Ta. These operations are currently on care-and-maintenance status. With increased resistance to the use of artisinally mined conflict minerals (Coltan), production from these traditional sources may resume. Placer deposits have historically provided up to 40 % of world Ta production and currently account for approximately 20 % of the supply chain. Recycling accounted for about 30 % of Ta produced in 2012.

Carbonatite complexes and their weathered equivalents remain the main sources of Nb, although peralkaline intrusion-hosted deposits may produce Nb and Ta as coproducts of REE and Zr mineralization. At present, more than 90% of Nb mine production comes from weathering-enriched residual materials overlying carbonatite complexes in Brazil with the balance from a fresh carbonatite deposit at St. Honoré (Canada) and loparite concentrate from Lovozero (Russia) and other minor sources. As much as 20 % of the total Nb supply is from recycling. Nb and Ta are economically important metals and are subject to high supply risk. Until 2014, both Nb and Ta were on the critical metals list of the report of the Ad hoc Working Group on defining critical raw materials (European Commission) for the European Union. Recently, the supply risk for Ta was downgraded. Relatively high economic importance and supply risk drive current exploration and re-evaluation of known Ta and Nb deposits.

3 Stream sediment orientation survey and QEMSCAN® study

3.1 Stream sediment orientation surveys

3.1.1 Aley carbonatite stream sediment orientation survey

Published as: Mackay, D.A.R. and Simandl, G.J. 2014. Portable X-ray fluorescence to optimize stream sediment chemistry and indicator mineral surveys, case 1: Carbonatite-hosted Nb deposits, Aley carbonatite, British Columbia, Canada. In: Geological Fieldwork 2013, British Columbia Ministry of Energy and Mines, British Columbia Geological Survey Paper 2014-1, pp. 183-194.

3.1.1.1 Introduction

Carbonatite, carbonatite complexes, and their weathered equivalents are the main sources of Nb and ferroniobium (Mariano, 1989a, b; Birkett and Simandl, 1999; Simandl et al. 2010, 2013a; Tantalum-Niobium International Study Center, 2013a). They are most common along rift zones and in intracratonic settings (Woolley and Kjarsgaard, 2008). The Aley carbonatite is one of a series of carbonatite complexes, syenite complexes, and other alkaline rocks that forms the British Columbia alkaline province (Fig. 3.1; Pell, 1994). Aley lies 135 kilometres north of Mackenzie, British Columbia and 20 kilometres northeast of the Ospika Arm of Williston Lake, east of the Rocky Mountain Trench, and was discovered following base metal exploration (Pride, 1983). It was the subject of further study and exploration over the next 30 years (Mäder, 1986, 1987; Pride, 1987a, b; Robert et al., 2005; Nethery, 2007; Chung and Crozier, 2008). The deposit has a measured resource of 113 million tonnes at 0.41% Nb_2O_5 and an indicated resource of 173 million tonnes at 0.35% Nb_2O_5 with a cut-off grade of 0.20% Nb_2O_5 (Jones et al. 2014).

The main objectives of this section are to: 1) determine if stream sediment geochemistry can be used effectively to explore for carbonatite-related Nb deposits like the Aley carbonatite; 2) establish the best stream sediment size fraction (based on pathfinder element content) for indicator minerals that might point to Nb-bearing carbonatite deposits; 3) characterize the geochemical gradient of potential pathfinder elements (Nb, Ta, REEs, P, Ba, Sr, U, and Th) in sediments downstream from the

deposit; and 4) evaluate the usefulness of portable X-Ray Fluorescence (pXRF) analyses for preliminary assessment of indicator mineral and stream sediment studies. The area has been glaciated, most recently during the last glacial maximum from about 30000-25000 to 11,000–10,500 ^{14}Cyr before present (Clauge and James, 2002). The carbonatite is located in a U-shaped glacial valley. Regional ice flow was generally from west to east. Glacial distribution of indicator minerals is possible but is outside of the scope of this thesis. Boreal forest coveres the area below ~1600m; the central portion of the deposit is dominated by alpine shrubs and grasses.

3.1.1.2 Geological setting

Carbonatite intrusions of the British Columbia alkaline province were emplaced during three main events: ~ 800-700 Ma (postulated breakup of Rodinia), ~ 500 Ma (extensional tectonism and attenuation of the continental margin), and ~ 360-340 Ma (renewed extensional tectonics; Pell, 1994; Millonig et al., 2012). Multiple phases of deformation and associated subgreenschist to amphibolite grade metamorphism overprinted the carbonatites between ~ 155 and 50 Ma (Read et al., 1991; Pell, 1994; Millonig et al., 2012).

The Aley carbonatite cuts Lower to Middle Paleozoic sedimentary rocks of the western Cordilleran foreland fold and thrust belt (Figs. 3.2). The regional geology of the area was originally mapped at the scale of 1:253 440 by Irish (1970). The carbonatite intrudes a platformal assemblage of siliciclastic and carbonate rocks that were deposited along the western margin of Laurentia (Mäder, 1986; Pell, 1994). The Kechika Formation (Cambrian to Early Ordovician) unconformably overlies the Rosella Formation (Lower Cambrian; Pyle and Barnes, 2001) and consists of argillaceous limestone, calcareous siltstone, and dolostone. The Skoki Formation (Lower to Middle Ordovician) is generally in fault contact with the Kechika Formation and consists of dolostone and volcanic rocks (Mäder, 1986). The Road River Group (Lower to Upper Ordovician-Silurian) caps the succession, locally unconformably overlies the Skoki Formation, and consists of cherty dolostone, shale, argillaceous limestone, and rare quartzite and quartz pebble

conglomerate (Mäder, 1986; Pyle and Barnes, 2001). Regional metamorphism reached lower greenschist facies (Mäder, 1986) and coincided with convergent tectonism and orogenesis between ~ 155 and 50 Ma (Pell, 1994; Millonig et al., 2012).

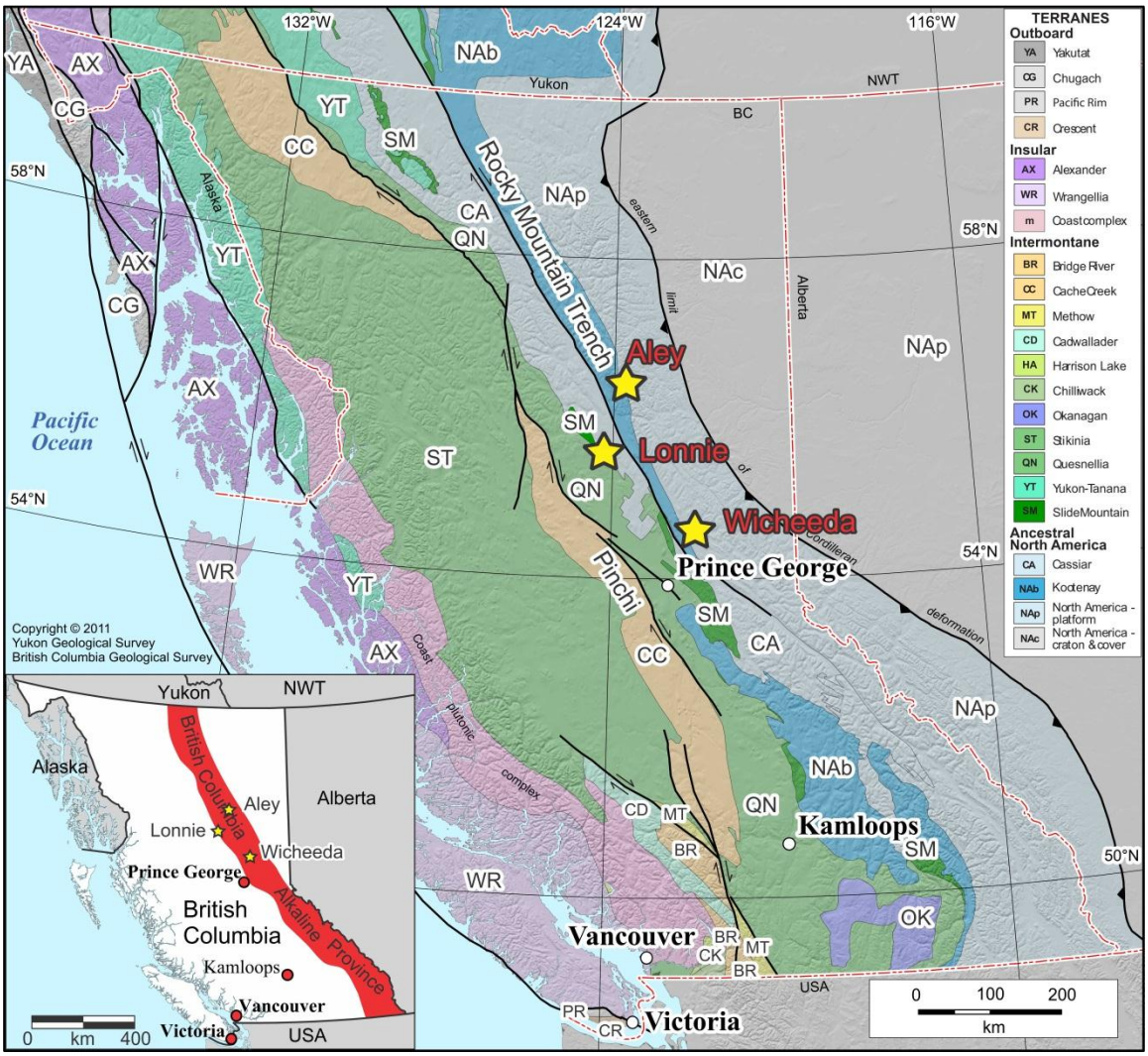

Figure 3.1 Location and tectonic setting of the Aley, Lonnie, and Wicheeda carbonatites (yellow stars). Modified from Colpron and Nelson (2011). British Columbia Alkaline Province (red in inset map) is based on Pell (1994).

The metasedimentary sequence was intruded by the Aley carbonatite, REE-bearing carbonatite dikes, the Ospika diatreme, and lamprophyre dikes (Fig. 3.2; Mäder, 1986; Pell, 1994; McLeish, 2013). Zircon from the dolomite carbonatite phase of the Aley carbonatite contains insufficient radiogenic Pb for U-Pb geochronology (Mäder, 1986; McLeish, 2013), but McLeish (2013) reported a U-Pb titanite age of 365.9 ± 2.1 Ma for

the Ospika diatreme. The Aley carbonatite displays an early phase of deformation lacking in the Ospika diatreme indicating that it is older than ~ 366 Ma (McLeish, 2013). The Road River Group, (Lower to Upper Ordovician-Silurian, based on conodont biostratigraphy; Mäder, 1986; Pyle and Barnes, 2001), is the youngest unit overprinted by this early deformation that is cut by lamprophyre dikes (considered related to the Aley carbonatite and Ospika diatreme) suggesting that the Aley carbonatite is older than 366 Ma and younger than the Road River Group (McLeish, 2013).

3.1.1.3 Geology of the Aley carbonatite complex

The Aley carbonatite outcrops intermittently over an area 3 to 3.5 km in diameter (Fig. 3.2; Mäder 1986) and intruded sedimentary host rocks as a sill which was subsequently folded within a recumbent nappe (McLeish et al., 2010; McLeish, 2013). The main phase of the carbonatite consists of layered or banded dolomite carbonatite surrounded by minor calcite carbonatite (Mäder, 1986). Kressal et al. (2010) observed that the dolomite carbonatite phase contains apatite, pyrite, calcite, and Nb-bearing minerals such as pyrochlore ($[Na,Ca]_2[Nb,Ti,Ta]_2O_6[O,OH,F]$), columbite-(Fe) ($[Fe,Mn][Ta,Nb]_2O_6$), fersmite ($[Ca,Ce,Na][Nb,Ta,Ti]_2[O,OH,F]_6$), and rare, fine-grained acicular aggregates of Nb-rich rutile ($[Ti,Nb,Fe]O_2$). Pods or lenses of magnetite (10s of centimetres to metres in size) are found throughout the dolomite carbonatite phase and contain apatite, phlogopite, Nb-bearing minerals, zircon, and interstitial carbonates (Kressall et al., 2010). The magnetite pods likely represent deformed and distended cumulate layers (Kressall et al., 2010). Monazite ($[Ce,La,Nd,Th]PO_4$) commonly co-exists with fersmite in pseudomorphs after primary columbite-(Fe) or pyrochlore (Mäder, 1986; Kressall et al., 2010).

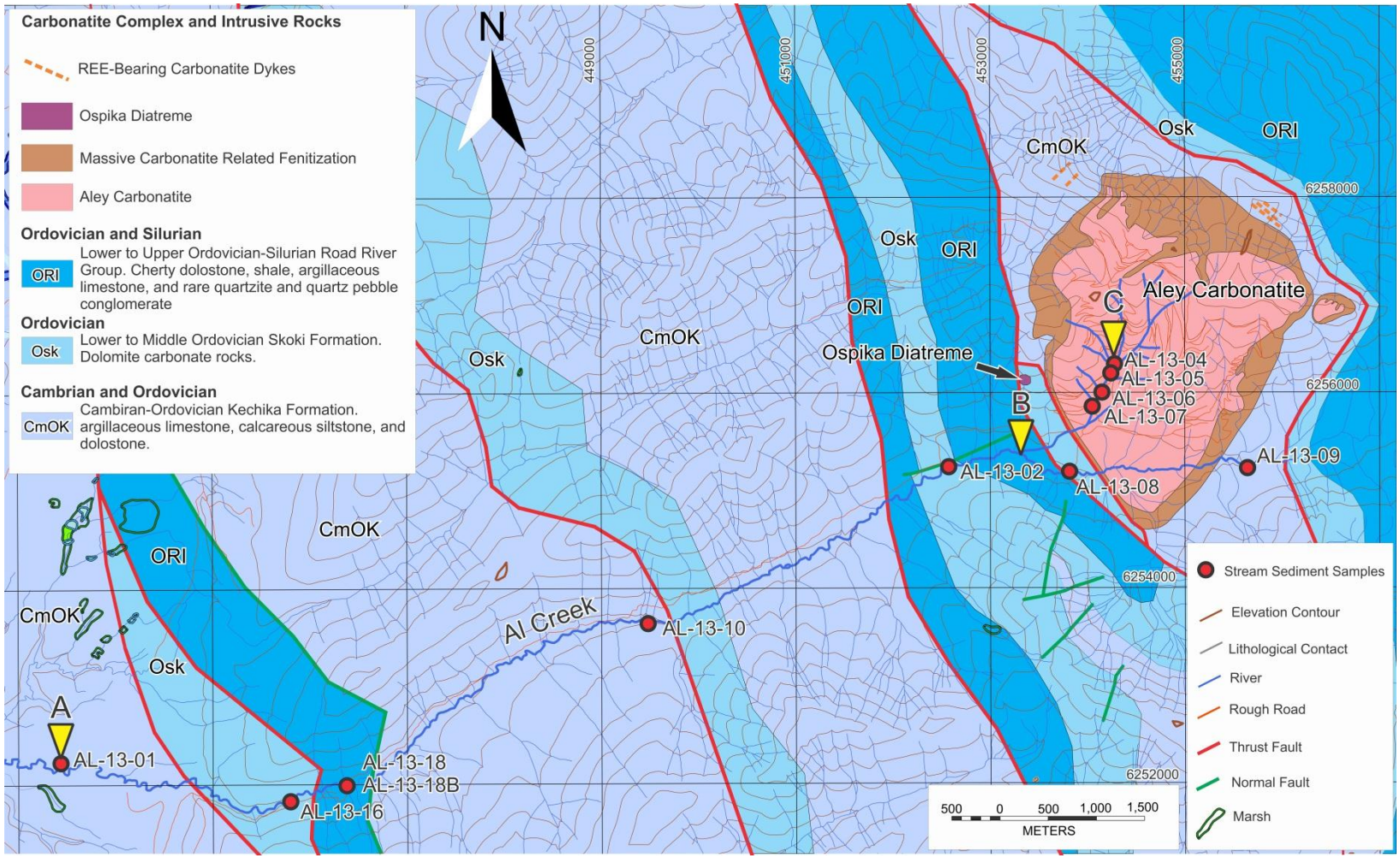

Figure 3.2 Geological setting of the Aley carbonatite and locations of stream sediment samples. Yellow markers (A-B-C) denote location of profile in Figure 3.6. Modified after Pride (1983), Mäder (1986), Massey et al. (2005), and McLeish (2013). UTM zone 10, NAD 83.

Massive fenite surrounds the carbonatite intrusion (Fig. 3.2), displaying a characteristic dark blue-green colour and contains abundant richterite, arfvedsonite, and aegirine (Mäder, 1986; Kressall et al., 2010). The fenite contains brecciated metasedimentary and feldspathic material. The feldspathic breccia clasts resemble altered syenite fragments; however, they are probably strongly fenitized and albitized fragments of the Kechika Formation.

Carbonatite dikes exposed on the northwest ridge above the main deposit (Fig. 3.2) contain significant concentrations of light rare earth elements (LREE; Mäder, 1986). The LREE mineralisation consists of REE-bearing carbonates and fluorocarbonates (Mäder, 1986). The dikes probably represent late differentiated phases of the Aley carbonatite melt (Mäder, 1986).

3.1.1.4 Methods

Twelve stream sediment samples were collected from a creek (“Al”) and its tributaries (Fig. 3.2) draining the Aley carbonatite area during the 2013 field season (Table 3.1). One sample was collected upstream of the deposit to assess background geochemistry. Four samples, spaced 200 to 300 m apart, were collected along the dry tributary of Al Creek directly over the deposit (Fig. 3.3). The remaining seven samples were collected along the creek, downstream from the deposit, 1.5 to 3 km apart as access allowed (Figs. 3.2, 3.4). The bed of the creek consists mainly of boulders, cobbles, and pebbles (Fig. 3.4). Sample sites included dry pools (Fig. 3.3), and the leeward areas of boulders and fallen trees, and bars (Table 3.1). Matrix material between cobbles and boulders, generally from an area < 1 m^2, was sampled (Fig. 3.4; Table 3.1). Organic material (conifer needles, leaves, and twigs) was scraped from the surface of samples sites. Not all of the organic material could be avoided during sample collection, and minor amounts were retained in the coarser fractions (+500 μm and coarser). Material was wet sieved through a + 8 mm screen, except where noted in Table 3.1. Weights for dried samples range from 4.1 to 21.8 kg. Sample AL-13-18B is a preconcentrate (washed by hand using a pan) of stream sediment close to sample AL-13-18.

Samples were dried in an oven at 40°C, weighed, and dry sieved into > 4 mm, 2 mm to 4 mm, 1 mm to 2 mm, 500 µm to 1 mm, 250 µm to 500 µm, 125 µm to 250 µm, 63 µm to 125 µm, and < 63 µm fractions. To shorten the text and simplify figures, the following notation was used throughout for the same grain size intervals; + 4 mm, + 2 mm, + 1 mm, + 500 µm, + 250 µm, + 125 µm, + 63 µm, and - 63 µm. Each size fraction was weighed individually. Selected size fractions were split using a riffle splitter with a portion being archived as a witness sample, a portion for magnetic separation, and a portion for XRF analyses.

Samples for XRF analyses were milled using ring and roller bowl tungsten carbide mills. Standard XRF sample pulp cups were then prepared and analysed by portable XRF. Analyses were carried out using a portable Thermo Fisher Scientific Niton FXL-950 instrument equipped with a Ag anode X-ray tube with a maximum voltage of 50 kV, current of 0.2 mA, and power of 4 W. The instrument was operated in "mining Hf/Ta mode" to obtain the highest resolution measurements for the elements of interest in carbonatite exploration. The detector temperature was allowed 10 minutes to stabilize at -25ºC before system checks. Five standards were analysed before and after stream sediment samples. Information about standards, limits of detections, and data quality control are in Appendix B.

The factory-calibrated pXRF data are internally consistent (see Appendix B and Luck and Simandl, 2014). For example, good accuracy is expected for La and Nb. Other elements (e.g. Sr) are underestimated. Remaining elements, including U and Th, are overestimated. Based on strong positive correlation between 11 U and 15 Th pXRF analysis and corresponding ICP-MS analyses of stream sediments from Aley, Lonnie, and Wicheeda (unpublished) processed in exactly the same manner as those in the present study, U and Th are overestimated of the order of 35% and 90% respectively. The pXRF is not a substitute for traditional laboratory methods where high accuracy and precision are required.

Figure 3.3 Al-13-05 sample site; dry pool below chute over fenite bedrock. Sampled material forms matrix between cobbles and boulders. Looking north up the dry stream bed valley toward the Aley Carbonatite. Shovel is 1 m long.

Figure 3.4 Al-13-08 sample site; Al creek, downstream of the Aley carbonatite. Sampled material constitutes matrix between cobbles and boulders, which form the predominant substrate. Stream is 3.5 m wide; looking east upstream.

3.1.1.5 Results

Samples AL-13-02, AL-13-18, and AL-13-18B, were chosen for systematic study of all size fractions. The particle size distributions for samples AL-13-02 and AL-13-18 are skewed toward coarser size fractions, whereas AL-13-18B displays a nearly normal distribution (Fig. 3.5).

In samples Al-13-18 and Al-13-18B, carbonatite pathfinder elements (Nb, Ta, Y, La, Ce, Pr, Nd, U, Th, and P) are enriched in the + 125 μm, and + 63 μm size fractions relative to other sizes (Fig. 3.5). Similar trends exist for Al-13-02, however, the + 250 μm, and + 500 μm fractions also contain relatively high Nb, Ta, Y, La, Ce, Pr, Nd, U, and Th concentrations. Phosphorus is detectable in the +125 μm fraction for AL-13-18 and AL-13-18B, but is below the limit of detection in the + 125 μm fraction for sample AL-13-02. High abundances of pathfinder elements (relative to other size fractions from the

same samples) are also observed in the + 125 μm and + 63 μm size fractions in sediments from the nearby Lonnie (Luck and Simandl, 2014) and Wicheeda (Section 3.1.2) carbonatite study areas. The +125 μm fraction was chosen for systematic study because of these higher abundances and because it is a suitable size for indicator mineral studies. The ranges in abundance of selected major oxides (Table 3.2) are: < 16.5 to 45.8 wt% SiO_2, < 1.8 to 7.0 wt% Al_2O_3, 1.3 to 15.2 wt% Fe_2O_3, 10.9 to 31.8 wt% CaO, < 0.1 to 0.3 wt% TiO_2, < 1.4 to 6.4 wt% MgO, and 0.2 to 2.6 wt% K_2O. Concentration ranges for trace elements (Table 3.2) are: 15 to 9988 ppm Nb, < 7 to 166 ppm Ta, 14 to 170 ppm Y, 70 to 2010 ppm La, 115 to 2977 ppm Ce, 147 to 1579 ppm Nd, 80 to 661 ppm Pr, 140 to 910 ppm Ba, 177 to 2018 ppm Sr, < 90 to 9412 ppm P, < 1 to 62 ppm U, and 9 to 570 ppm Th.

3.1.1.6 Discussion

High concentrations of Nb, Ta, La, Ce, Pr, Nd, U, and Th in the + 250 μm, + 125 μm, and + 63 μm fractions (Fig. 3.5) probably reflect the presence of carbonatite indicator minerals. The highest values typically coincide with the Aley carbonatite (samples AL-13-04, AL-13-05, AL-13-06; Figs. 3.6, 3.7). As expected, relative concentrations as high as 9988 ppm Nb, 133 ppm Ta, 2010 ppm La, 2977 ppm Ce, 171 ppm Y, 44 ppm U, 570 ppm Th, and 2018 ppm Sr occur over or directly downstream of the deposit and decrease with increasing distance downstream to between 3495 and 3311 ppm Nb, 79 and 73 ppm Ta, 596 and 561 ppm La, 936 and 866 ppm Ce, 72 and 71 ppm Y, 35 and 26 ppm U, 266 and 251 ppm Th, and 827 and 711 ppm Sr (Figs. 3.6, 3.7; Table 3.2). Barium does not follow this trend, suggesting barite input from dolostones and argillaceous limestones of the Skoki and Kechika formations.

Table 3.1 Characteristics of stream channel and sample sites. Sample AL-13-09 was collected upstream of the deposit. Samples Al-13-04, AL-13-05, AL-13-06, and AL-13-07 were collected directly over the deposit. Remaining samples are in order of increasing distance downstream of the deposit.

Sample	**Location**		**Elevation**	**Stream Character**			**Clast Size (cm)**		**Dry wt.**	**Sample Site Characteristics**
	Northing	Easting	(m)	Width (m)	Depth (m)	Flow	Average	Maximum	(kg)	
AL1309	6255259	455696	1406	2.5	0.2	moderate	2 to 5	30	14.2	Lee of fallen tree; clasts predominantly white dolomite, limestone, and slate.
AL1304	6256338	454355	1520	1.5	N/A	N/A	2 to 5	50	4.9	Exposed bedrock (partly covered by boulders); dry streambed; sampled from matrix between cobbles and boulders; not sieved in the field.
AL1305	6256192	454249	1479	3	N/A	N/A	5 to 10	40	6.7	Dry pool below chute in dry streambed (Fig. 3); exposed bedrock (partly covered by boulders); not sieved in the field.
AL1306	6256016	454132	1431	2	N/A	N/A	3 to 5	150	6.8	Fine-grained material in dry pools (<50 x 50cm) between fenite and carbonatite cobbles and boulders; not sieved.
AL1307	6255865	454059	1400	2	N/A	N/A	2 to 5	35	6.9	Dry pool below cobbles and boulders; no exposed bedrock in dry streambed; large scree slope upstream; not sieved.
AL1308	6255181	453823	1298	3.5	0.3	rapid	5 to 15	100	9.4	Sample from matrix between cobbles and boulders (Fig. 4); predominantly slate and limestone clasts; rare fenite breccia clasts.
AL1302	6255244	452580	1246	3.5	0.3	rapid	5 to 10	150	14.7	Sample from matrix between cobbles and boulders; rare fenite boulders
AL1310	6253666	449483	1082	4.5	0.4	rapid	5 to 10	200	14.8	Near stream bank in active channel; lee of boulders; upstream of several slides; slate, limestone, and rare fenite breccia clasts are predominant.
AL1318	6251991	446312	928	4	0.8	rapid	1 to 2	200	12.2	Bar (4 x 16m) downstream of fallen trees; sample from matrix between pebbles and cobbles; downstream of several slides; few subrounded to subangular fenite, carbonatite, and Ospika diatreme boulders a few m downstream of sample site.
AL1318B	6251991	446314	928	4	0.8	rapid	1 to 2	200	4.1	Same as above; preconcetrated (sieved to 8mm; washed in pan) close to AL-13-18.
AL1316	6251818	445779	891	3	0.4	rapid	2 to 5	40	14.4	5 x 10m area in lee of fallen trees; upstream of a landslide.
AL1301	6252228	443432	793	5	0.3	rapid	1 to 3	15	21.8	Lee of fallen trees.

Samples taken immediately below slides (greater than 200 m^2) and scree slopes (such as AL-13-07) show a decrease in the concentrations of Nb, Ta, La, Ce, Y, U, Th, and Sr relative to adjacent upstream (Al-13-06) and downstream samples (AL-13-02; Figs. 3.6, 3.7). This demonstrates the effect of dilution of pathfinder elements by incorporation of unmineralized material (unconsolidated overburden and slate and limestone scree). Sample AL-13-02, taken in an active stream channel, has higher concentrations of pathfinder elements relative to AL-13-07 (Fig. 3.6), possibly due to concentration of indicator minerals by winnowing. Sample AL-13-09, obtained upstream of the Aley carbonatite (Fig. 3.7), has low concentrations of carbonatite pathfinder elements relative to samples downstream of the deposit. Subrounded to subangular carbonatite, fenite, and diatreme boulders were found immediately downstream of AL-13-18 and AL-13-18B (Figs. 3.6, 3.7; Table 3.2). It is unclear if these boulders were derived from the Aley carbonatite or a different occurrence. Sample AL-13-16, downstream of this site, displays an increase in Nb, Ta, La, Ce, Y, U, Th, and Ba relative to Al-13-18 and AL-13-18B, which may be related to the boulders.

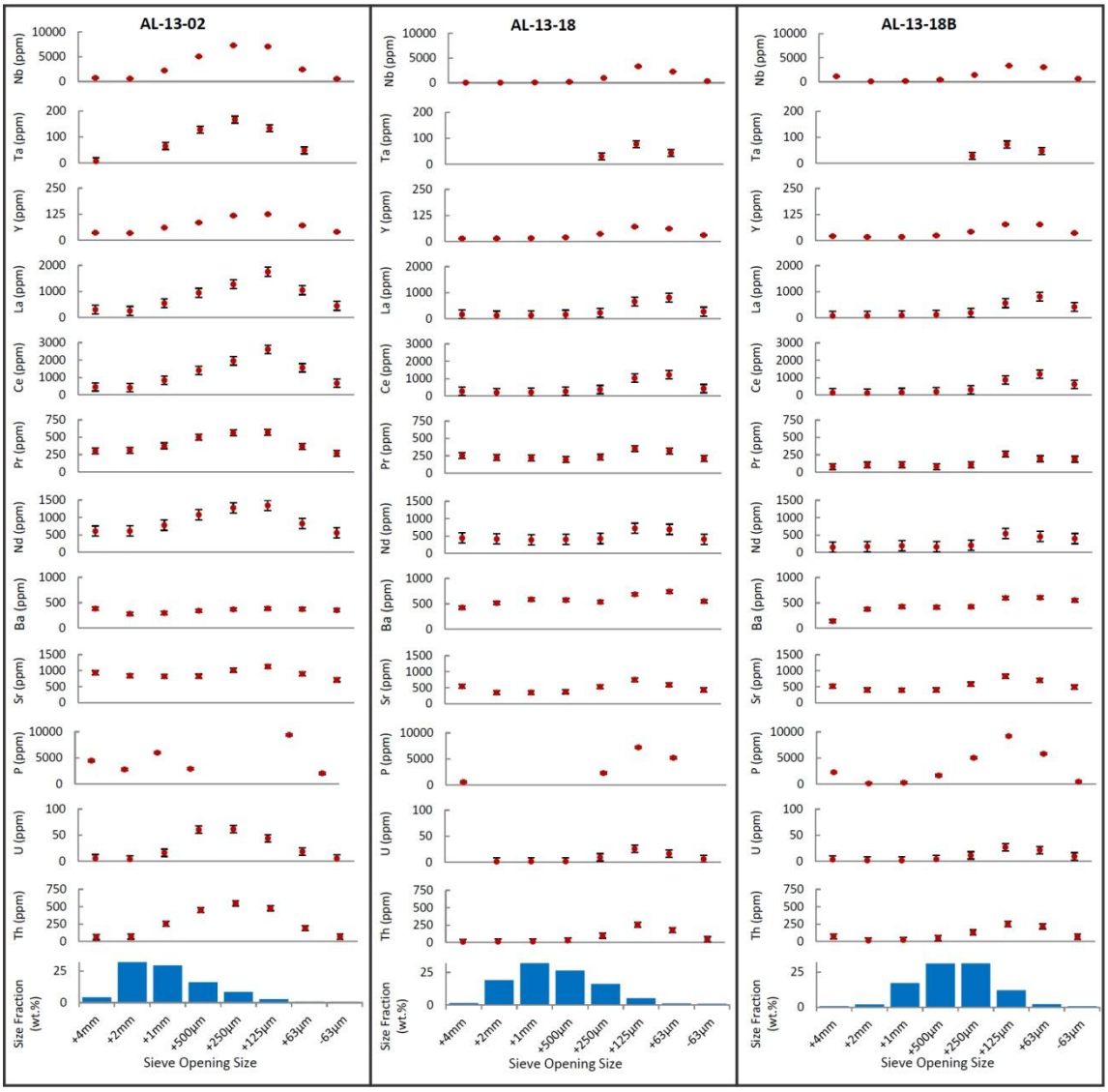

Figure 3.5 Portable XRF analyses for selected trace elements and grain size fraction distributions of samples AL-13-02, AL-13-18, and AL-13-18B. The + 250 µm, + 125 µm, and + 63 µm size fractions are enriched in Nb, Ta, Y, La, Ce, Pr, Nd, P, U, and Th relative to other size fractions. Analyses below detection limits are not shown. Error bars based on average 2σ values determined from multiple analyses of standards by pXRF (Appendix B).

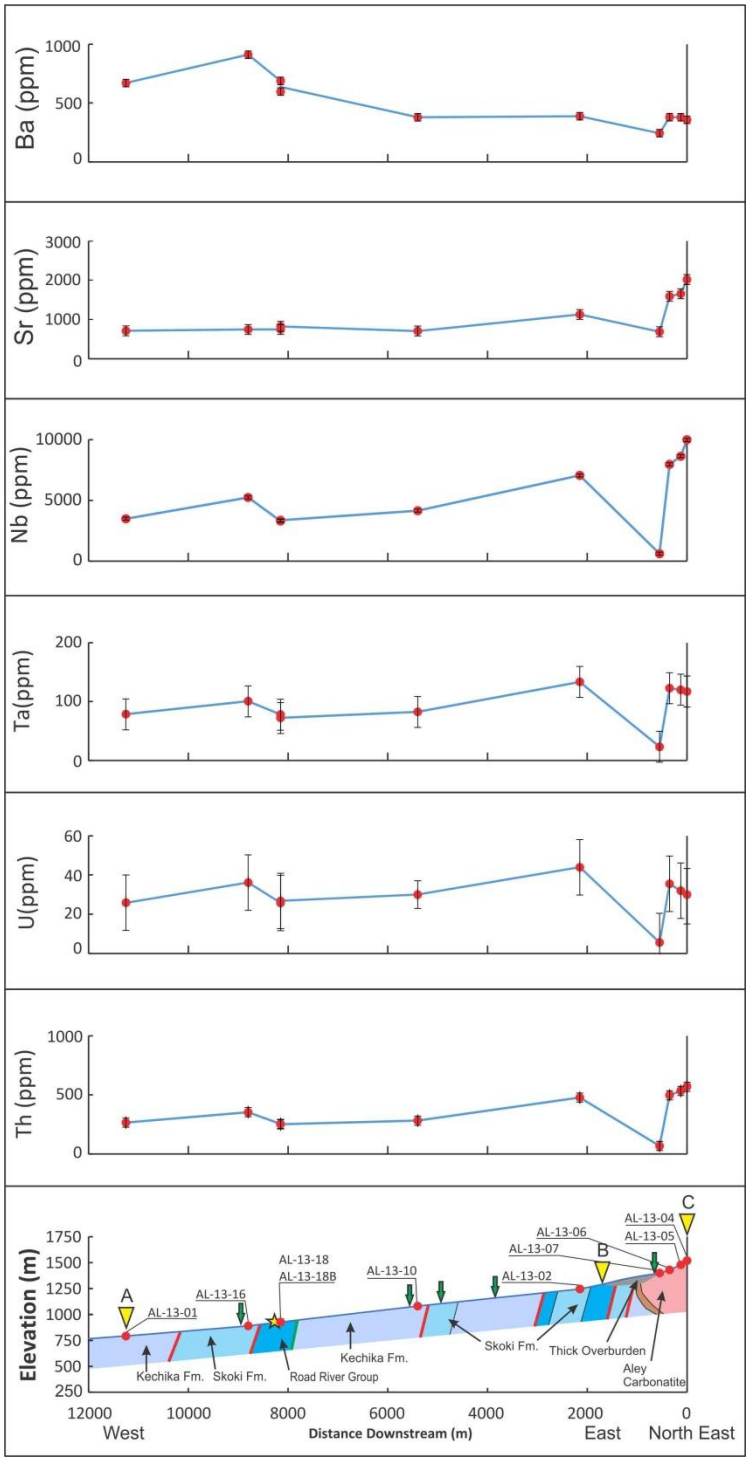

Figure 3.6 Downstream variation in carbonatite pathfinder elements concentrations (+ 125 μm size fraction) with increasing distance from the Aley carbonatite. Yellow star-fenite, carbonatite, and Ospika diatreme boulders. Green arrow-landslides. A thick layer of overburden is located downhill of the Aley carbonatite. Legend for geology is the same as in Figure 3.2. For location see yellow markers (A-B-C) on Figure 3.2. Error bars based on average 2σ values determined from multiple analyses of standards by pXRF (Appendix B).

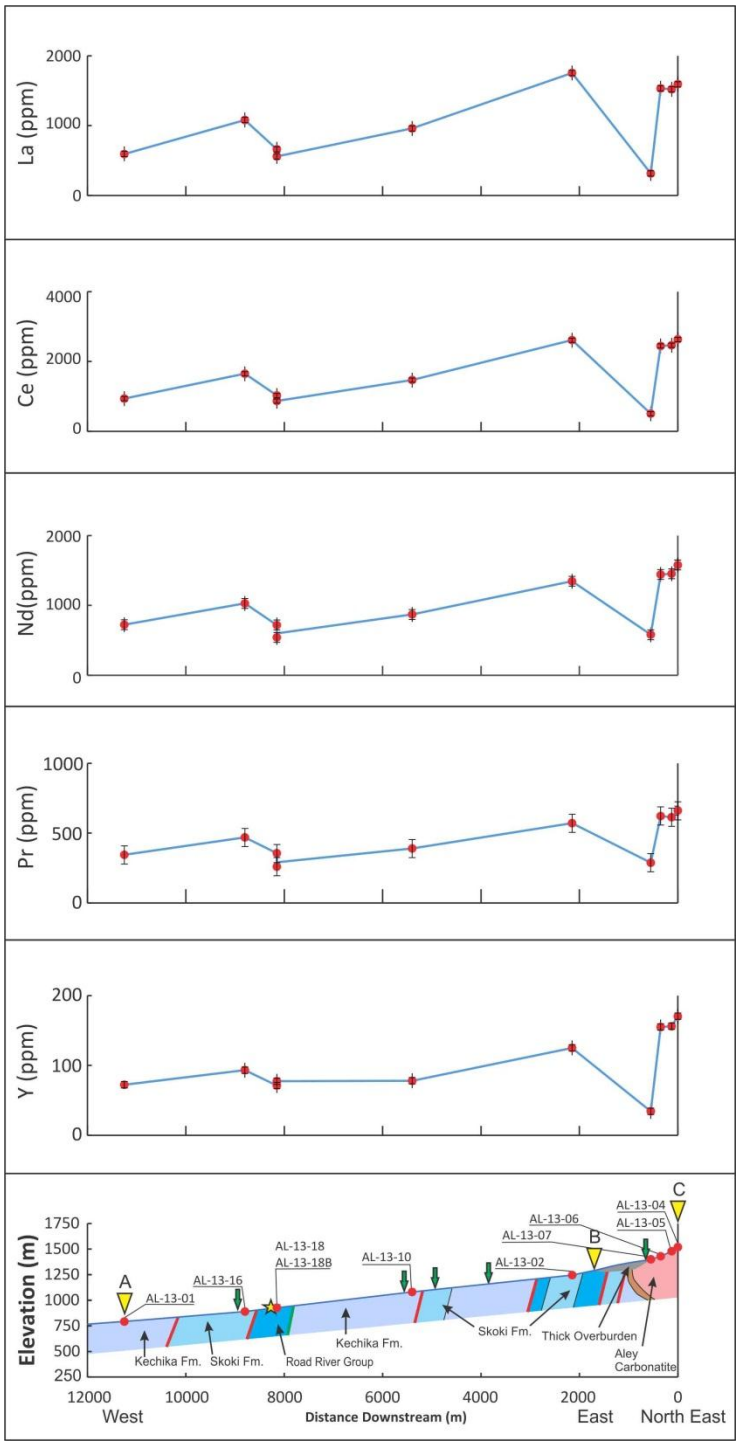

Figure 3.6 continued

Table 3.2 Relative concentrations of major and trace element analysed by factory-calibrated pXRF. Samples are listed in order of increasing distance downstream of the deposit. Concentrations in ppm excepted were otherwise indicated. The data are internally consistent but have not been recalibrated as described in Simandl et al. (2014) to improve accuracy by correcting for matrix effects and biases. Based on strong positive correlation between 11 U and 15 Th pXRF analysis and corresponding ICP-MS analyses of stream sediments from Aley, Lonnie, and Wicheeda (unpublished) processed in exactly the same manner as those in the present study, systematic overestimation of U and Th, of the order of 35% and 90% respectively, is expected. [a]Total Fe as ferric oxide (Fe_2O_3).

Sample	Size Fraction (mm)	Nb	Ta	Y	La	Ce	Nd	Pr	Ba	Sr	P	U	Th	% Fe_2O_3[a]	% CaO
AL-13-09	+0.125	444	28	29	184	288	351	188	324	177	1885	9	53	2.28	10.94
AL-13-04	+0.125	9988	117	171	1595	2634	1579	661	358	2018	<90	30	570	12.88	29.34
AL-13-05	+0.125	8647	120	156	1521	2466	1453	614	379	1655	<90	32	534	12.45	27.84
AL-13-06	+0.125	7977	123	155	1536	2447	1443	623	380	1591	<90	36	497	12.96	27.06
AL-13-07	+0.125	615	23	34	316	505	580	289	244	688	4215	6	68	3.2	26.06
AL-13-08	+0.125	6695	135	124	2010	2977	1421	599	421	1054	<90	40	461	11.39	22.43
AL-13-02	+4.00	728	7	36	304	451	607	303	385	934	4475	6	63	3.32	31.84
	+2.00	585	<7	34	252	410	608	311	282	842	2788	4	70	4.03	29.99
	+1.00	2205	65	60	545	833	777	377	297	822	5983	16	255	7.75	28.55
	+0.500	5056	128	85	946	1402	1078	498	342	826	2894	60	451	15.06	25.42
	+0.250	7283	167	118	1274	1949	1276	561	370	1016	<90	62	549	15.24	24.36
	+0.125	7056	133	125	1755	2610	1347	571	388	1127	<90	44	478	11.16	23.75
	+0.063	2429	48	71	1048	1552	827	368	374	900	9412	18	192	4.63	21.83
	-0.063	530	<7	40	446	659	557	270	353	710	2042	5	67	3.34	22.48
AL-13-10	+0.125	4157	82	78	960	1469	870	390	379	708	<90	30	282	7.06	17.36
AL-13-18	+4.00	15	<7	14	166	269	442	254	427	545	560	<1	9	1.6	28.42
	+2.00	24	<7	15	122	194	414	225	516	349	<90	1	12	1.68	25.33
	+1.00	55	<7	16	128	209	387	219	588	352	<90	2	12	1.89	23.22
	+0.500	184	<7	20	159	266	403	196	574	375	<90	2	28	2.13	22.39
	+0.250	971	30	36	232	370	425	230	538	531	2292	9	99	3.34	21.6
	+0.125	3311	78	71	662	1025	721	355	688	747	7221	26	255	6.13	21.56
	+0.063	2250	44	62	813	1220	691	319	743	589	5224	16	177	4.44	19.7
	-0.063	321	<7	30	273	429	408	212	552	433	<90	6	45	3.13	20.6
AL-13-18B	+4.00	1142	<7	21	71	129	147	81	141	519	2264	3	71	1.31	30.58
	+2.00	67	<7	17	73	115	167	103	377	402	104	2	13	1.86	27.86
	+1.00	142	<7	18	87	145	191	104	427	393	260	1	22	1.91	25.69
	+0.500	431	<7	24	117	185	156	81	416	401	1636	4	47	2.46	23.57
	+0.250	1412	28	42	194	302	205	108	426	583	5036	11	129	3.75	23.16
	+0.125	3361	73	77	561	866	542	259	598	827	9203	27	251	5.69	23.24
	+0.063	3047	48	77	813	1208	458	193	604	703	5800	21	217	4.7	22.26
	-0.063	633	<7	36	416	614	396	187	552	491	453	9	68	2.82	23.8
AL-13-16	+0.125	5246	101	93	1083	1648	1028	470	910	745	<90	36	355	8.55	20.98
AL-13-01	+0.125	3495	79	72	596	936	724	346	670	711	7117	26	266	5.84	21.97

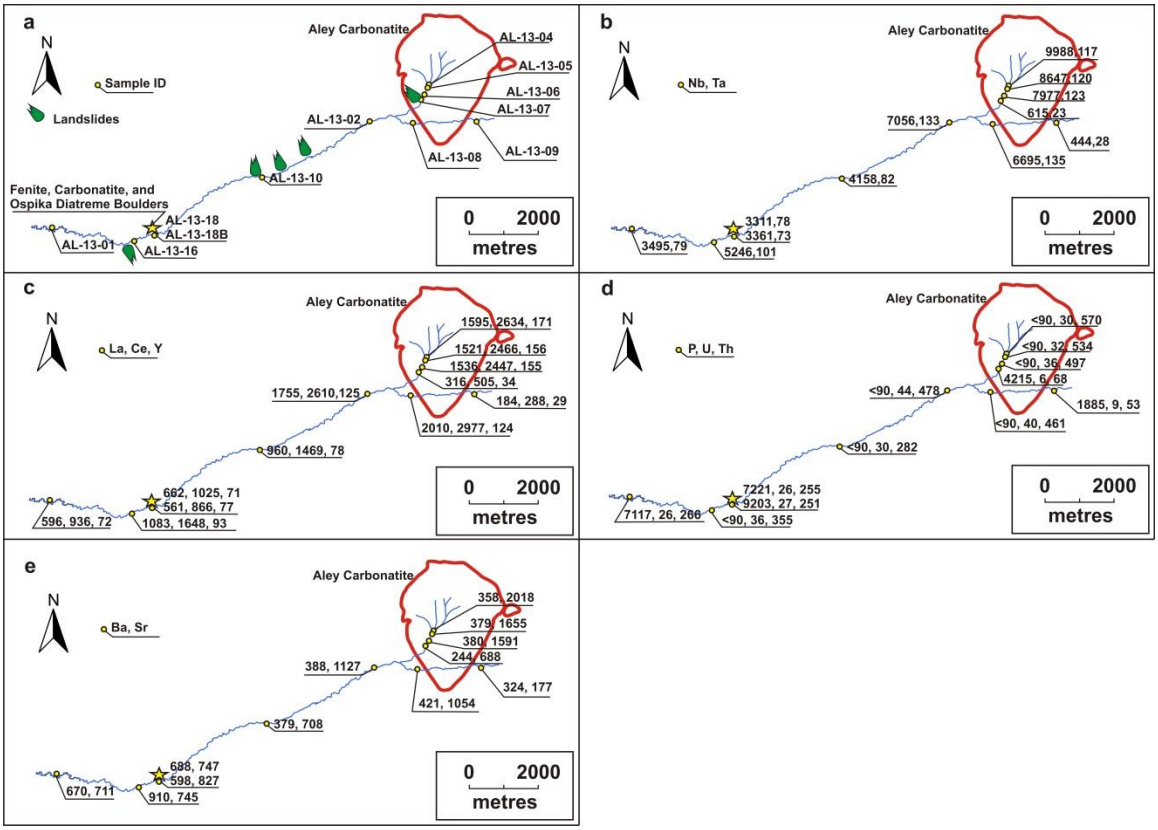

Figure 3.7 Carbonatite pathfinder elements in creeks draining the Aley carbonatite complex. a) Location of samples and landslides (greater than 200 m^2). b) Nb and Ta. c) La, Ce, and Y. d) P, U, and Th. e) Ba and Sr. All concentrations in ppm. Concentrations of Nb, Ta, La, Ce, Y, U, Th, and Sr show a decreasing trend with increasing distance downstream of the deposit. Sample AL-13-07 shows the effects of significant dilution of source detritus. Sample AL-13-09 (upstream of the deposit) shows the background concentrations of trace elements.

The coefficient of determination (R^2) represents the goodness of fit to a trend line. An R^2 of 1.0 and trend line with slope of 1 and y-intercept of 0 would indicate perfect agreement between the two analytical methods; an R^2 of 0.90 indicates that 90% of the variation is explained by this relationship. The strong linear dependence between Nb and FeO (R^2 = 0.97; Fig. 3.8a) likely represents the co-occurrence of Nb-bearing minerals and magnetite in the stream sediments. Niobium-bearing minerals commonly contain Fe (e.g. columbite-tantalite series minerals). Correlation between Nb and Ta (R^2 = 0.83; Fig. 3.8b) agrees with the expected presence of pyrochlore, columbite-(Fe), and/or fersmite in the stream sediments. The Nb:Ta ratio of pyrochlore and columbite-(Fe) from carbonatites is typically high and is reflected in the high (on average 50:1) Nb:Ta ratio of

the sediments (Table 3.2). Niobium and La (R^2 = 0.81; Fig. 3.8c) display a strong relationship which is likely the result of coincidence of Nb-bearing and REE-bearing minerals in the stream sediments. It remains unclear if most of the REEs are in the crystal structure of Nb-bearing minerals rather than REE-bearing carbonates, fluorocarbonates, and/or phosphates. Poor linear dependence between Nb and TiO_2 (R^2 = 0.20; Fig. 3.8d) is likely the result of low Ti concentrations expected in pyrochlore sourced from carbonatites and high uncertainty for TiO_2. The poor linear dependence may also indicate negligible concentrations of Nb-rutile in stream sediments, mirroring the low abundance of this mineral in the deposit reported by Kressal et al. (2010). Samples AL-13-04, AL-13-05, and AL-13-06 have the highest Nb contents (Fig. 3.7 a-d) and fail to plot directly on the best-fit line (Fig. 3.8a). These samples were taken from a dry tributary of Al creek; the higher Nb contents might reflect reduced levels of fluvial reworking in an intermittent stream. Alternatively, they might be the consequence of local variations in the concentration of fersmite, columbite, and pyrochlore in underlying mineralisation.

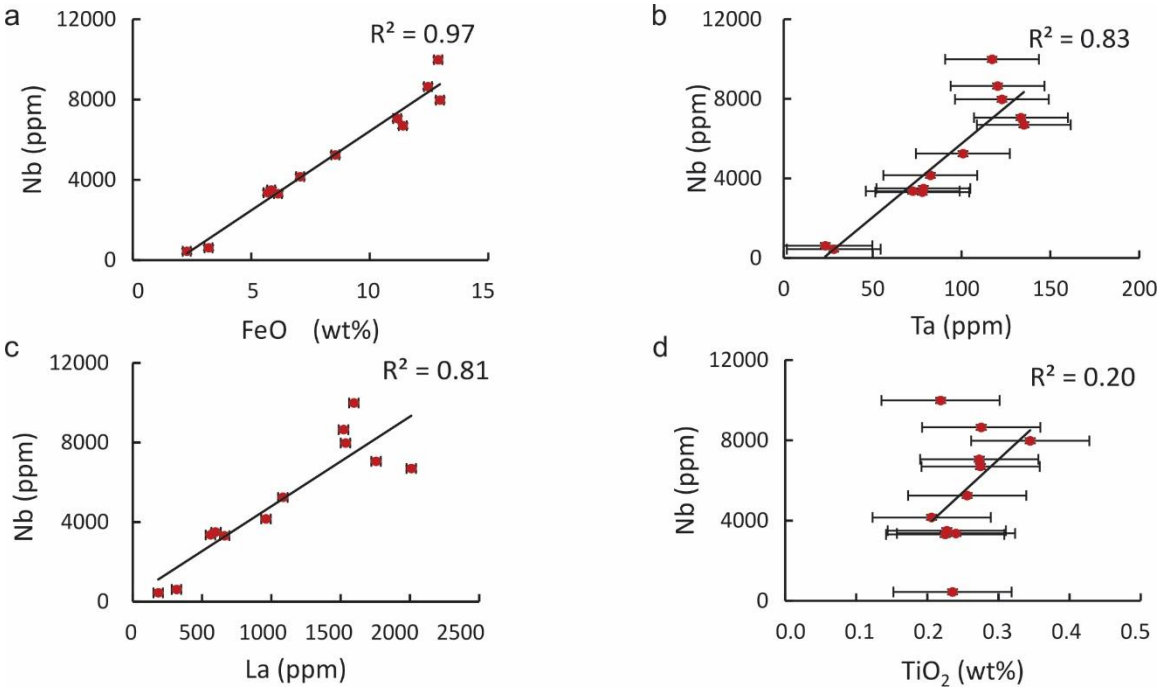

Figure 3.8 Correlations between concentrations of a) Nb and FeO. b) Nb and Ta. c) Nb and La. d) Nb and TiO_2. Error bars based on average 2σ values determined from multiple analyses of standards by pXRF (Appendix B).

Cerium correlates strongly with La (R^2 = 0.99) and well with Nd (R^2 = 0.95), Pr (R^2 = 0.94), and Y (R^2 = 0.85). This is expected as REEs have similar physical and chemical properties and commonly substitute for each other in monazite, REE-bearing carbonates and fluorocarbonates, and Nb-bearing minerals. Strong correlation between Ce and Th (R^2 = 0.90) may reflect accumulations of monazite. Zirconium correlates strongly with Ce (R^2 = 0.95), Nd (R^2 = 0.88), and Pr (R^2 = 0.87), La (R^2 = 0.86), and Y (R^2 = 0.82) and may relate to co-occurrence of zircon with REE-bearing minerals. As expected, a significant relationship exists between Th and U concentrations (R^2 = 0.70) likely caused by co-occurrence of heavy minerals containing these element (e.g. monazite, zircon, and possibly pyrochlore).

An unknown analytical error may explain < 90 ppm P values for samples collected from directly over the deposit (Figs. 3.6, 3.7), which contains local apatite (2-10%, Kressall et al., 2010). As P is a light element; it has to be present in high concentrations to be a useful pathfinder due to error induced by the matrix effects of Ca and Fe (Simandl et al. 2014).

Lack of linear dependence between Sr and Ba (R^2 = 0.06) suggest that these elements are not present as a uniform barite-celestite solid solution. Strontium is commonly a constituent of aragonite and minor constituent of calcite and is found in higher concentrations in REE-bearing carbonates, fluorocarbonates, and strontianite. Ba is also common in some REE-bearing carbonates, fluorocarbonates, and barite. All these minerals were reported by Mäder (1986) from Aley deposit and/or associated dikes; however, barite input from non-carbonatite sources such as dolostones of Kechika and Skoki Formations is an alternative explanation.

3.1.1.7 Conclusions

Stream sediment geochemistry represents a valid exploration method for Aley type carbonatite deposits. Niobium, Ta, La, Ce, Pr, Nd, Y, Th, U, and Sr in combination with each other, or alone, are good pathfinder elements in stream sediments. The Ba signature of the Aley deposit, if present, is masked by barite derived from dolostones. As P is a light element, it has to be present in higher concentrations than the above elements to be a

useful pathfinder. The + 125 (or 125-250) μm size fraction of the stream sediments is a useful geochemical sampling media and the most promising candidate for study of carbonatite related indicator minerals using QEMSCAN® methods. Based on this study and the mineralogy of the Aley deposit, pyrochlore, columbite-(Fe), and fersmite are expected to be useful indicators. Monazite, REE-bearing carbonates, and fluorocarbonates, and to some extent fersmite and apatite are also possible indicator minerals based on the mineralogy of the deposit and chemical composition of stream sediments. Factory calibrated pXRF is a cost effective method for determining relative concentrations of key pathfinder elements, such as Ni, Ta, La, Ce, Y, Th, U, and Sr in stream sediments; however, without recalibration, depending on the element, analyses can be strongly biased (e.g. Th or U). Additional mineralogical studies using modern laboratory methods such as electron microprobe, ICP-MS, and QEMSCAN®, are required to establish relative concentrations of indicator minerals in stream sediments with increasing distance from the carbonatite.

3.1.2 Wicheeda carbonatite stream sediment orientation survey

Published as: Mackay, D.A.R. and Simandl, G.J., 2014. Portable X-ray fluorescence to optimize stream sediment chemistry and indicator mineral surveys, case 2: Carbonatite-hosted REE deposits, Wicheeda Lake, British Columbia, Canada. In: Geological Fieldwork 2013, British Columbia Ministry of Energy and Mines, British Columbia Geological Survey Paper 2014-1, pp. 195-206.

3.1.2.1 Introduction

Increased use of REE in consumer and green technologies has spurred demand and made these elements a focus of economic and strategic mineral development in the past few years (Tse, 2011). With 95% of world production of REE in China, from deposits such as the carbonatite-related Bayan Obo, and recent export restrictions, western industrialised nations are faced with supply uncertainties (Tse, 2011). Hence, increased exploration for and development of REE mineral deposits is taking place outside of China.

The Wicheeda carbonatite complex and carbonatite and syenite dikes are 80 km northeast of Prince George, British Columbia (Fig. 3.1). The Wicheeda carbonatite complex was originally explored for its base metal potential. Between 1979 and 1987 the complex was the subject of 1:5000 scale geological mapping and trenching (Betmanis, 1987), soil sampling and stream silt sampling (Lovang and Meyer, 1987), and geophysical surveying (Bruland, 2011). Spectrum Mining Corporation (Spectrum) acquired the claims that cover the Wicheeda carbonatite complex and conducted diamond drilling in 2008 and 2009 (Graf et al., 2009; Lane, 2009).

The main objectives of this section are to determine the best size fraction in stream sediments for indicator mineral and geochemical exploration programs, and to characterize the geochemical gradients of Nb, Ta, REEs, Ba, Sr, and Th in sediments downstream of the Wicheeda carbonatite complex using pXRF. These will help assess geochemical and indicator minerals methods for Wicheeda-type carbonatite-hosted REE deposit exploration.

3.1.2.2 Geological setting

The Wicheeda carbonatite complex is part of the British Columbia alkaline province, which coincides with the approximate margin of the Laurentian craton (Fig 3.1; Pell, 1994). The regional geology was originally mapped at a scale of 1:253 440 by Armstrong et al. (1969). The Wicheeda Lake carbonatite intrudes Lower to Middle Paleozoic platformal successions deposited on the western margin of Laurentia. These rocks consist of limestone, argillite, and calcareous siltstone of the Kechika Formation (Cambrian to Early Ordovician; Fig. 3.9; Armstrong et al., 1969). The Kechika Formation is in fault contact with limestone, slate, siltstone, and argillite of the Gog Group (Neoproterozoic) and unassigned Devonian to Permian felsic volcanic rocks to the west, and unassigned Cambrian to Devonian carbonates, slates, and siltstones to the east (Armstrong et al., 1969; Lane, 2009). Lower greenschist grade regional metamorphism overprints the country rocks (Lane, 2009). Faulting in the area follows the major northwest-southeast trend of the Rocky Mountain Trench. Regional ice flow was from the southwest to northeast.

Dalsin (2013) reported a Sm-Nd whole rock isochron age of 316 ± 36 Ma for samples from the carbonatite dikes ~3 km southeast of the main Wicheeda carbonatite complex. The carbonatite and syenite dikes and the Wicheeda complex follow the same northwest-southeast structural trend and are assumed to be related.

3.1.2.3 Geology of the Wicheeda carbonatite complex

The shape of the Wicheeda carbonatite complex is not well defined. It is sub-circular in plan (< 500 m in diameter), based on previous mapping and a Th radiometric anomaly (Lovang and Meyer, 1988; Mäder and Greenwood, 1988; Lane, 2009; Bruland, 2011). Reconnaissance fieldwork suggests that its emplacement was controlled by the intersection of two faults (Fig. 3.9). Drilling in 2008 and 2009 intersected high-grade zones consisting of 3.55% total rare earth oxide (TREO) over, 48.6 m, 2.2% over 144 m, and 2.9% over 72 m; other high grade intersections are near the top of drill holes in weathered dolomite carbonatite zones (Graf et al., 2009; Lane, 2009). A series of

carbonatite dikes has been identified northwest of the main carbonatite complex near Wicheeda Lake; a larger syenite-carbonatite dike complex is ~ 3 km to the southeast (Fig. 3.9).

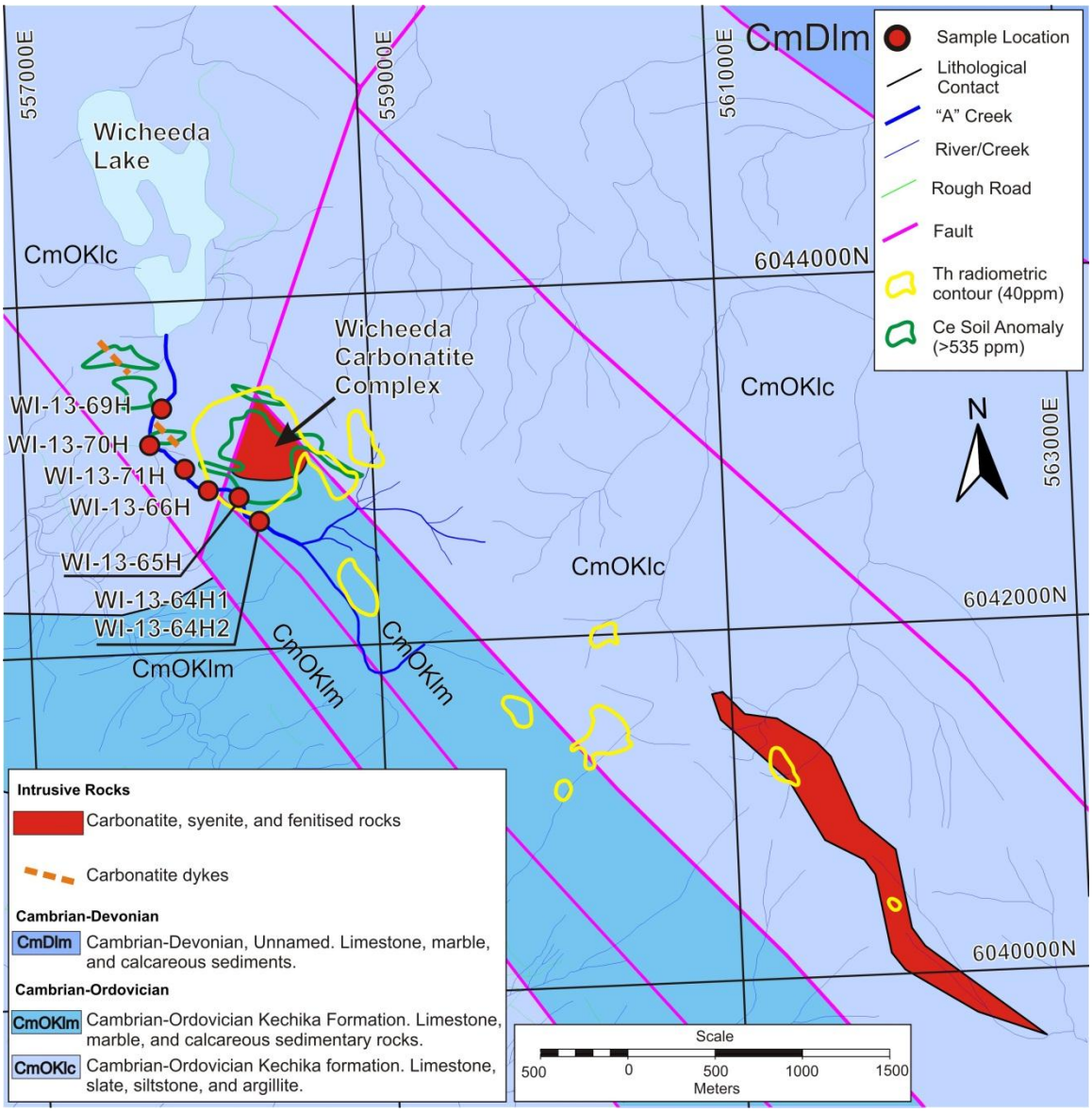

Figure 3.9 Geological setting of the Wicheeda carbonatite complex, associated dikes, and locations of stream sediment samples. Base map modified after Massey et al. (2005). Thorium radiometric anomalies from Bruland (2011) shown by yellow traces. Cerium soil anomaly from Lane (2009) shown by green traces. UTM zone 10, NAD 83.

The main carbonatite complex consists of two main units: dolomite carbonatite; and fenitized zones formerly referred to as syenite breccias. Based on the work of Le Couteur

(2008, 2009), Lane (2009), and observations from this study, the carbonatite consists mainly of dolomite (75-97%) ± ankerite. In general, calcite, plagioclase, potassium feldspar, biotite, muscovite/phlogopite, chlorite, and pyrite are minor constituents, and quartz, barite, strontianite, Fe-Ti oxides, molybdenite, galena, fluorite, apatite, and possibly powellite are present in trace amounts (Le Couteur, 2008, 2009; Lane, 2009). The main REE-bearing phases in the dolomite carbonatite are monazite and REE-bearing fluorocarbonates (such as bastnaesite, parisite, and/or synchysite) and carbonates (Le Couteur, 2008, 2009; Lane, 2009); however, it is expected some REEs form minor constituents in apatite, columbite, and possibly pyrochlore. The main Nb-bearing mineral is pyrochlore. Columbite-(Fe) and Nb-rutile may also be present. Calcite increases in abundance with depth. Le Couteur (2008, 2009) identified zones of predominantly calcite (85%), which contains biotite, strontianite, and magnetite.

The fenitized zones (albitized and potassic altered wall rock) observed in core contain abundant feldspar-rich (90%) xenoliths in a dolomite matrix. At the surface, patchy bluegreen, Na-amphibole (±pyroxene)-bearing fenite is in contact with dolomite carbonatite. By definition potassium feldspar, plagioclase, micas, amphiboles, and other silicates are more abundant in fenitized rocks than in carbonatites. The carbonatite is overlain by a characteristic red soil or regolith horizon, 5 cm to more than 50 cm thick. Outcrop exposure in the area is poor and the area. Boreal forest covers the area and vegetation is dense.

3.1.2.4 Methods

Seven stream sediment samples along “A” creek adjacent to the Wicheeda carbonatite complex were collected during the 2013 field season (Figs. 3.9, 3.10, Table 3.3). Sample sites are spaced 200-300 metres apart. There is more than 160 m elevation difference between sample WI-13-64H1 and WI-13-69H (Table 3.3). The streambed consists mainly of boulders, cobbles, and pebbles. Samples were collected in the lee of boulders and logs, and from inside stream bends, typically over areas < 1 m^2. Matrix material was wet sieved in the field through an 8 mm screen; only the < 8 mm fraction was retained. Samples were contained in permeable canvas bags and stored in plastic pails. The dried

samples weighed 1.1 to 5.4 kg (Table 3.3). Organic material (conifer needles, leaves, and twigs) was scraped from the surface of samples sites. Not all of the organic material could be avoided during sample collection, and minor amounts were retained in the coarser fractions (+ 500 µm and coarser). Sample prep and analytical methods (using a portable Thermo Fisher Scientific Niton FXL-950® instrument) are the same as in section 3.1.1. Error bars for figures in this study are based on 2σ values for standards analysed multiple times by pXRF (Appendix B).

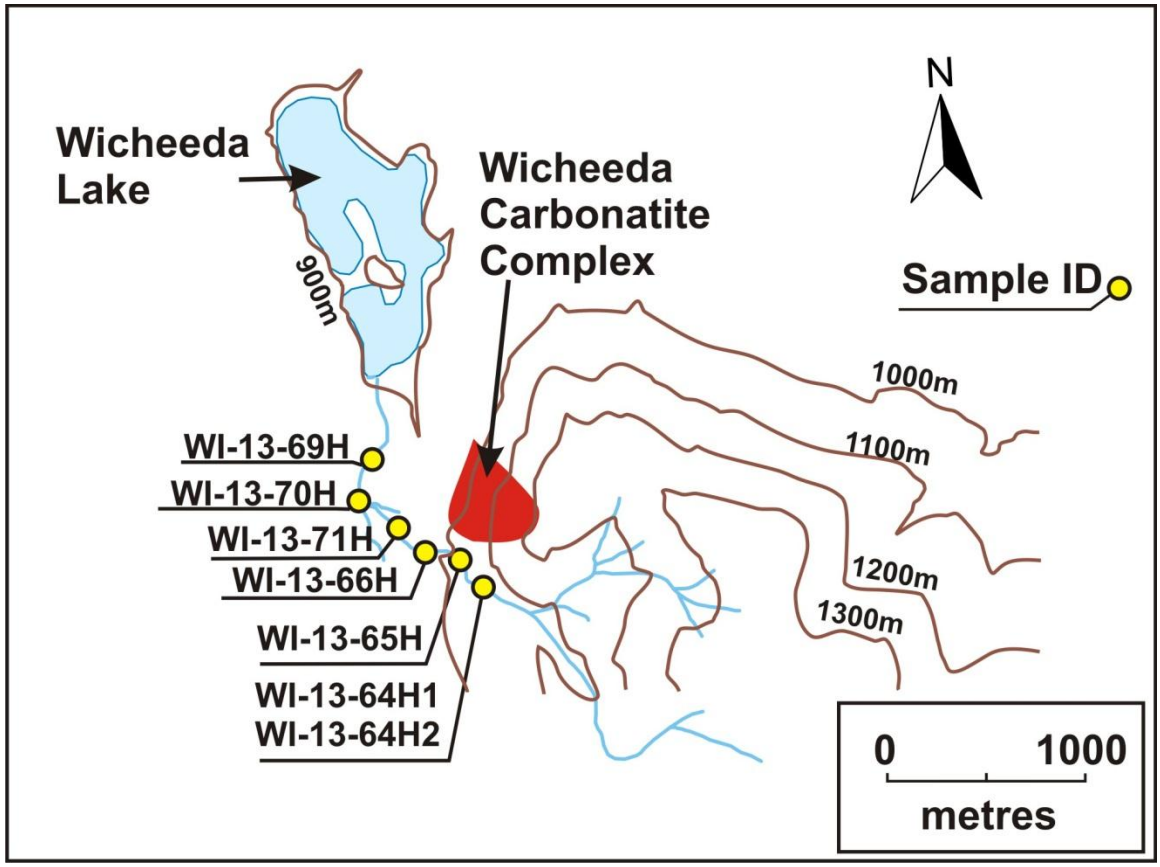

Figure 3.10 Location of stream sediment samples and local topography around the Wicheeda carbonatite complex. Samples are downhill of the Wicheeda carbonatite complex. Elevation contours denoted by brown lines (100 m contour interval). Modified after Massey et al. (2005).

3.1.2.5 Results

Two samples (WI-13-66H and WI-13-71H) were chosen for detailed study. Sample WI-13-66H was collected ~ 175 metres downslope from the deposit (Fig. 3.10); WI-13-71H was collected 220 metres downstream of sample WI-13-66H, where "A" creek enters a cut block in an area of low topographic relief. In both samples, the + 125 μm size fraction contains higher concentrations of pathfinder elements relative to other size fractions (Fig. 3.11). The + 250 μm and + 63 μm fractions are the next most enriched. These results are similar to those from stream sampling near the Lonnie carbonatite (Luck and Simandl, 2014) and the Aley carbonatite (Section 3.1.1). Based on these characteristics, the + 125 μm fractions of the remaining samples were analysed. Samples WI-13-66H and WI-13-71H show a grain-size distribution that is skewed toward coarse-grained material (Fig. 3.11).

Concentrations of major oxides in stream-sediment size fractions range from 42.8 to 57.9 wt% SiO_2, 16.3 to 23.4 wt% Al_2O_3, 4.5 to 7.0 wt% Fe_2O_3, 2.1 to 8.2 wt% CaO, 0.4 to 0.9 wt% TiO_2, 1.8 to 2.4 wt% MgO, and 4.5 to 6.9 wt% K_2O (Table 3.4). Trace element concentrations range from 57 to 283 ppm Nb, <22 to 34.7 ppm Ta, 19 to 46 ppm Y, 117 to 887 ppm La, 215 to 1301 ppm Ce, 167 to 482 ppm Nd, 97 to 225 ppm Pr, 806 to 1805 ppm Ba, 190 to 328 ppm Sr, < 5 to 7 ppm U (only 4 samples are above detection limits), and 24 to 141 ppm Th. All samples have P values of < 90 ppm.

Table 3.3 Characteristics of stream channel and sample sites. Samples are in order of increasing distance downstream of the Wicheeda carbonatite complex. UTM zone 10, NAD 83.

Sample ID	**Location**		**Elevation**	**Channel Characteristics**			**Clast Size (cm)**		**Dry wt. (<8 mm diameter)**	**Sample Site Characteristics**
	Northing	Easting	(m)	Width (m)	Depth (m)	Flow	Average	Max.	(kg)	
WI-13-64H1	6042772	558279	1077	1.5	0.10	rapid	0.5-1.5	5-7	1.7	Lee of fallen trees; steep-sided gully, upstream of trail; predominantly shale, siltstone, and carbonate clasts.
WI-13-64H2	6042772	558279	1077	1.5	0.10	rapid	0.5-1.5	5-7	1.1	2-3 m upstream of WI-13-64H1.
WI-13-65H	6042901	558198	1015	2.0	0.20	rapid	0.5-1.5	5-10	2.6	Inside of stream bend; steep-sided gully; grey slate clasts predominant.
WI-13-66H	6042929	558020	973	2.0	0.30	rapid	0.5-1.5	5-7	1.5	Pools below rapids (protected by fallen tree); steep sided gully; grey slate clasts predominant.
WI-13-71H	6043031	557916	935	1.5	0.15	slow	2-5	35	5.4	Lee of fallen tree; low relief topography; grey slate and limestone predominant.
WI-13-70H	6043178	557731	920	1.5	0.10	slow	1-2	10	2.6	Sample from matrix between cobbles; low relief topography; grey slate and limestone predominant; upstream of trail.
WI-13-69H	6043384	557792	911	1.0	0.15	moderate	0.2-0.5	5-7	2.8	Sample from matrix between cobbles; low relief topography; grey slate and limestone predominant; upstream of trail.

Table 3.4 Relative major oxide and trace element concentrations analysed by pXRF. This pXRF data has acceptable precision; however, it has not been recalibrated using results of standard laboratory analyses (as described in Simandl et al., 2014) to correct for matrix effects and analytical biases to improve accuracy. Portable XRF is not a substitute for conventional laboratory analyses. Eight size fractions reported for sample WI-13-71H. Six size fractions reported for WI-13-66H. The + 125 µm fraction is reported for all other samples. Results are in ppm except where otherwise noted. Samples are in order of increasing distance downstream of the Wicheeda carbonatite complex.

Sample	Size Fraction (mm)	Nb	Ta	Y	La	Ce	Nd	Pr	Ba	Sr	P	U	Th	% SiO_2	% CaO
WI-13-64H1	+0.125	144	<22	46	455	761	319	172	1707	305	<90	<5	100	47.68	6.27
WI-13-64H2	+0.125	140	<22	41	467	771	344	148	1805	328	<90	5	101	49.42	4.80
WI-13-65H	+0.125	253	<22	45	733	1176	442	192	1802	311	<90	<5	141	52.15	4.70
WI-13-66H	+2.00	87	<22	25	171	310	196	97	1363	243	<90	7	46	50.10	4.87
WI-13-66H	+1.00	85	24	27	151	315	216	119	1379	214	<90	<5	48	50.24	3.95
WI-13-66H	+0.500	85	<22	31	239	455	305	142	1501	216	<90	7	80	52.70	3.06
WI-13-66H	+0.250	119	<22	36	358	671	294	154	1690	253	<90	<5	86	52.60	3.41
WI-13-66H	+0.125	163	<22	40	482	819	361	172	1698	298	<90	<5	107	53.69	4.77
WI-13-66H	+0.063	119	<22	38	396	655	269	139	1463	277	<90	5	82	50.09	5.01
WI-13-71H	+4.00	62	23	19	135	244	300	178	806	257	<90	<5	24	47.78	8.20
WI-13-71H	+2.00	64	22	23	117	215	234	144	1216	190	<90	<5	30	51.49	4.10
WI-13-71H	+1.00	73	25	26	164	305	268	140	1291	192	<90	<5	42	51.88	3.74
WI-13-71H	+0.500	83	<22	30	214	444	282	160	1506	203	<90	<5	55	52.20	3.32
WI-13-71H	+0.250	108	<22	34	344	648	348	194	1661	244	<90	<5	80	52.87	3.66
WI-13-71H	+0.125	159	<22	40	480	806	378	184	1644	284	<90	<5	101	53.13	4.69
WI-13-71H	+0.063	100	<22	37	358	581	286	146	1391	255	<90	<5	69	51.56	4.65
WI-13-71H	-0.063	57	<22	38	193	341	167	97	1250	233	<90	<5	51	42.76	5.09
WI-13-70H	+0.125	251	26	46	886	1301	482	225	1329	231	<90	<5	129	55.86	3.06
WI-13-69H	+0.125	283	35	43	725	1119	424	191	1295	230	<90	<5	130	57.92	2.07

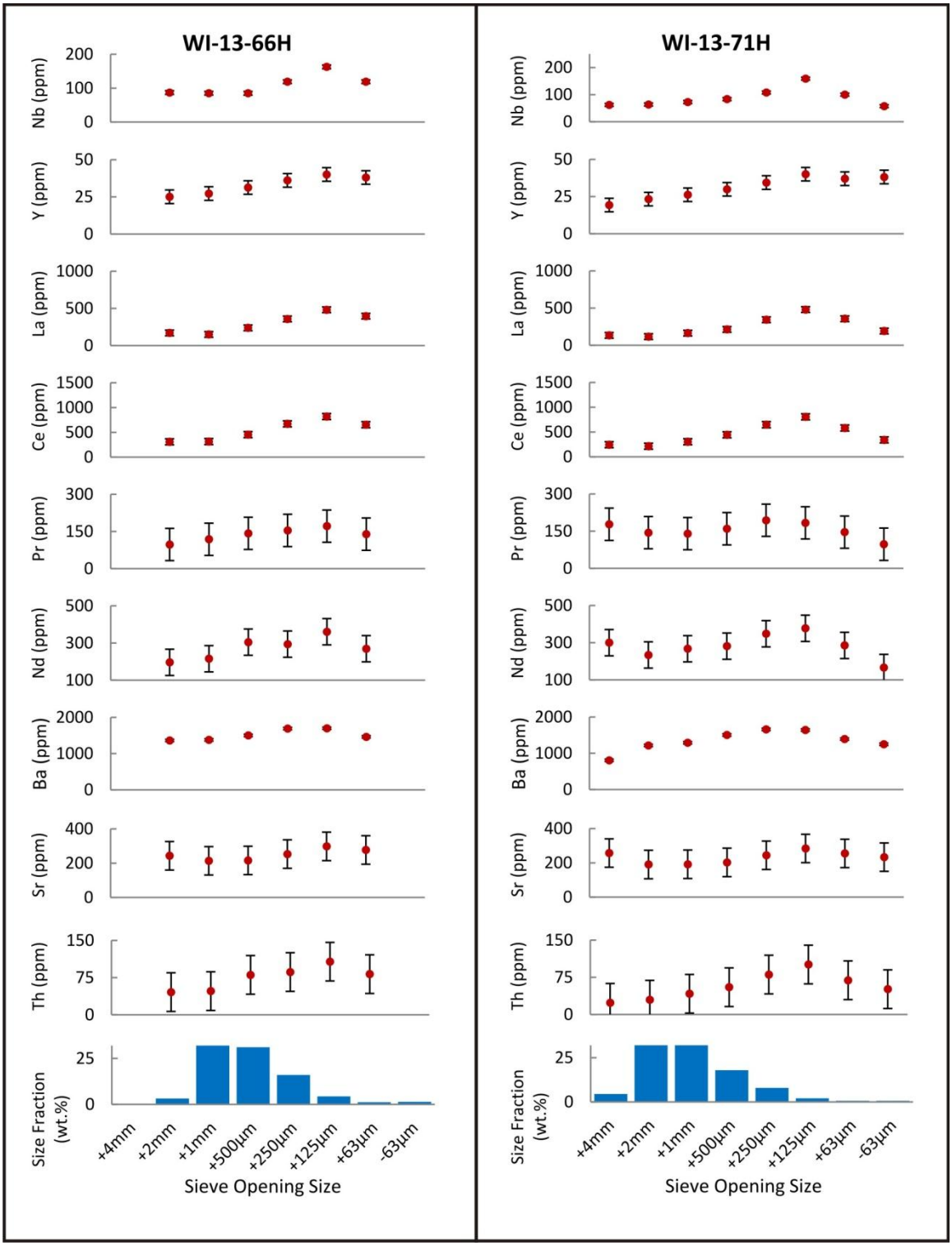

Figure 3.11 Portable XRF analyses for selected trace elements and grain size fraction distributions of samples WI-13-66H and WI-13-71H. The + 250 µm, + 125 µm, and + 63 µm size fractions are enriched in Nb, La, Ce, and Th relative to other size fractions.

3.1.2.6 Discussion

High concentrations of key pathfinder elements (Nb, Ta, REEs, Th, Ba, and Sr) suggest the presence of prospective indicator minerals in the +125 µm size fraction. Barium and to a lesser extent Sr concentrations decrease from southeast to northwest (Figs. 3.12, 3.13). Their source is probably upstream of the deposit. This may reflect input of material from other carbonatite-related showings in the area, or be related to sediment influx from limestones and marbles of the Kechika Formation. A slight decreasing trend in CaO with increasing distance downstream is observed, while the opposite is observed for SiO_2. This is probably due in part to a change in lithology across a fault from predominantly limestone and marble in the southeast to a predominantly pelitic assemblage in the northwest (Fig. 3.13).

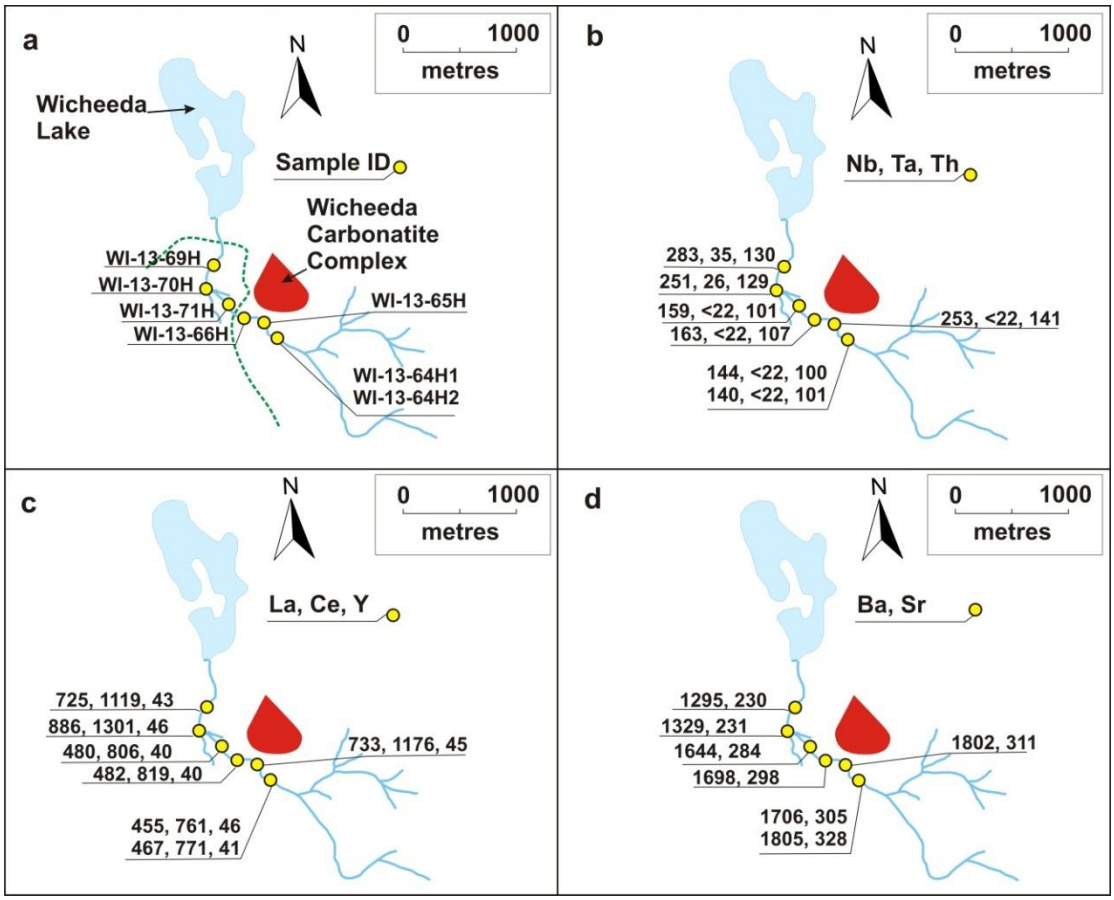

Figure 3.12 Selected trace element concentrations in stream sediment samples. a) Sample numbers. b) Nb, Ta, and Th. c) La, Ce, and Y. d) Ba and Sr concentrations in ppm. The edge of the cut block and the area of low topographic relief are denoted by the green dotted line.

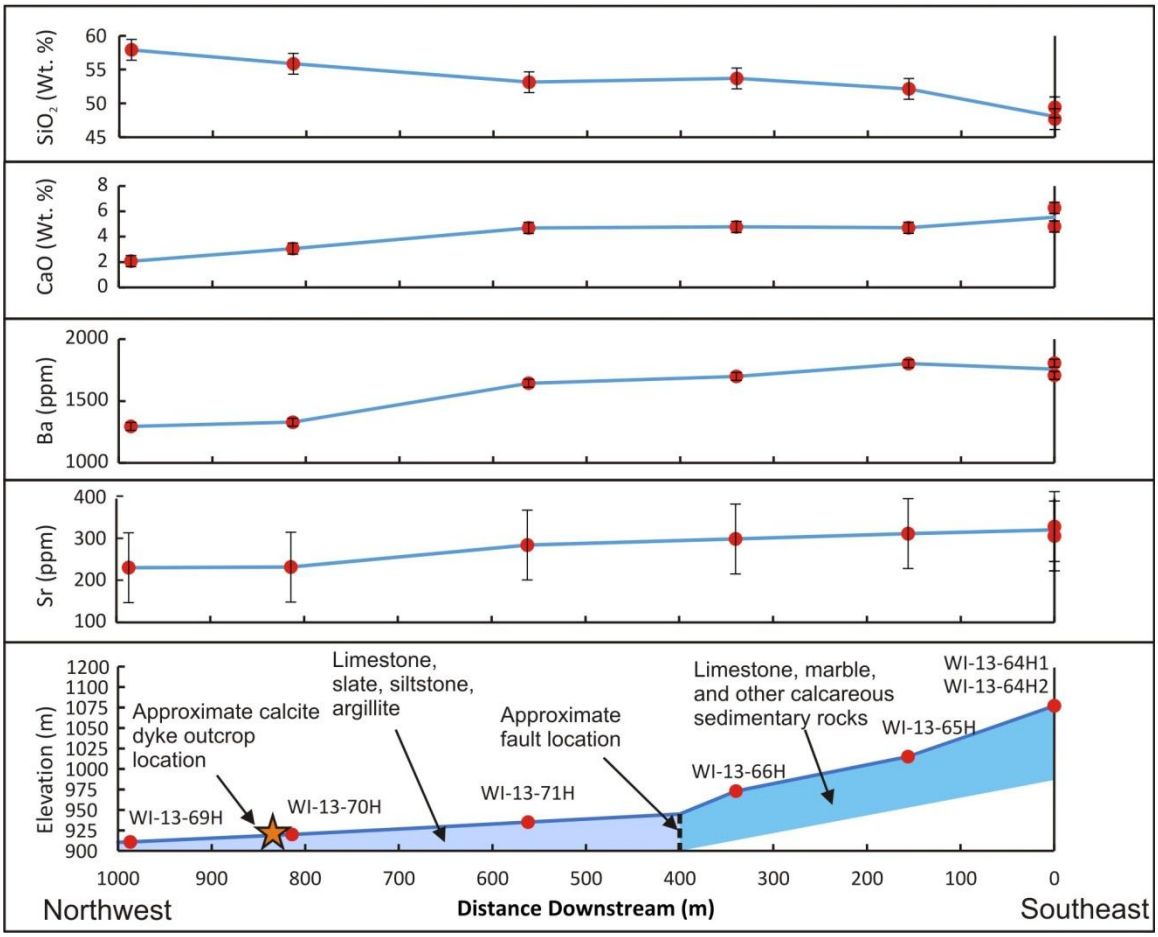

Figure 3.13 Profiles of SiO_2, CaO, Ba, and Sr concentrations in the + 125 µm size fraction; elevation (m above sea level). The approximate position of the calcite carbonatite dike outcrop is projected onto the profile.

Excluding Ba and Sr, samples WI-13-71H and WI-13-66H have consistently lower concentrations of pathfinder elements than the samples immediately upstream and downstream (WI-13-65H and WI-13-70H; Fig. 3.13). Calcite carbonatite dikes are reported by Lane (2009) northeast of the main carbonatite complex; during mapping in the summer of 2013, outcropping calcite carbonatite was observed near sample WI-13-70H (Fig. 3.9). Carbonatite boulders were also observed near the location of a dike reported by Lane (2009). Drilling in 2009 intersected one dike near sample WI-13-70H. These observations coincide with Ce soil and Th radiometric anomalies in the area (Fig. 3.9). Input of material from these occurrences probably contributes to increased pathfinder element concentrations in samples WI-13-69H and WI-13-70H (Fig. 3.14). Co-variation in pathfinder element concentrations between Nb, La, Ce, Nd, and Th (Fig.

3.14) is probably related to the presence of multiple indicator minerals in stream sediments. These minerals may have originated from multiple sources.

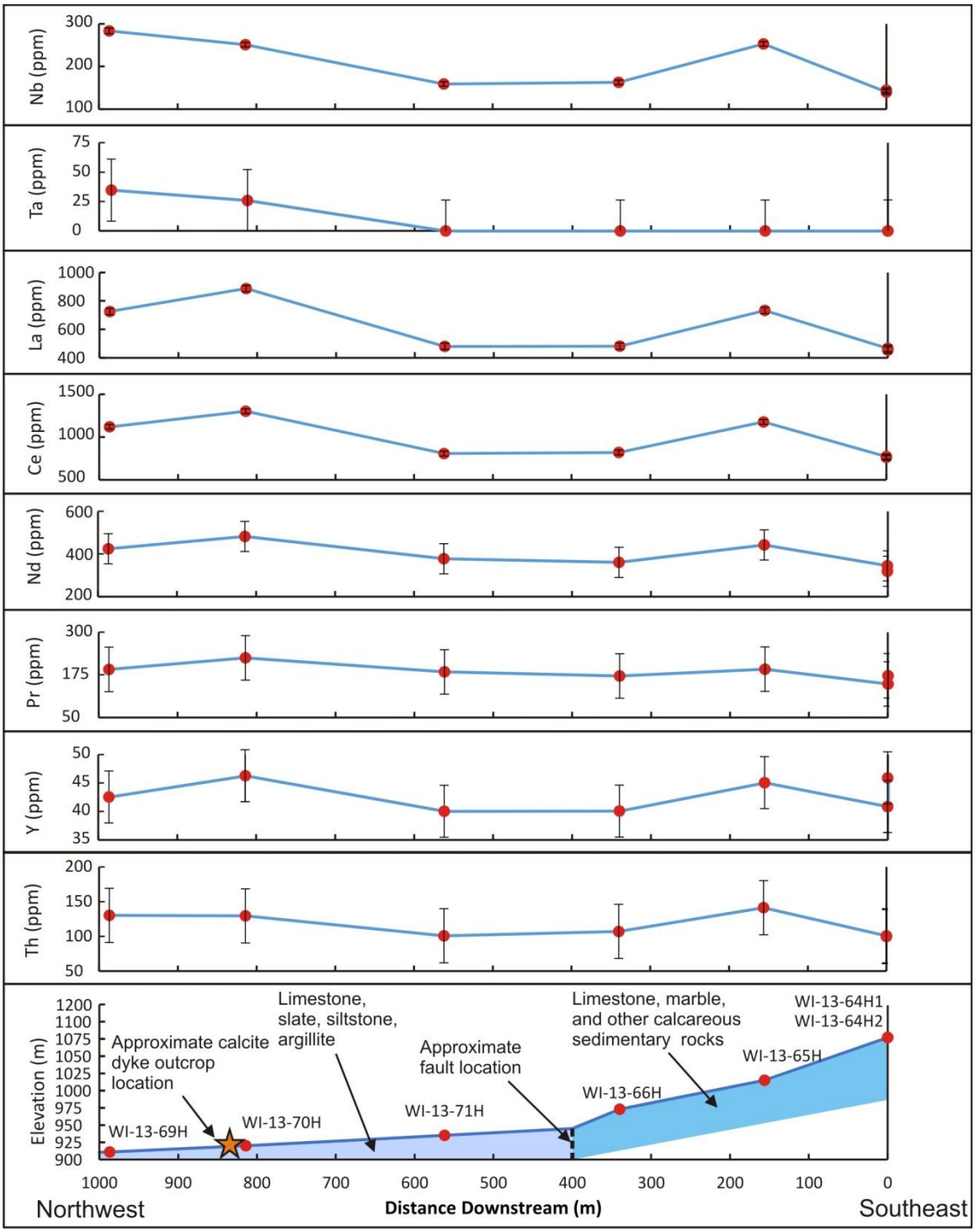

Figure 3.14 Profiles of key pathfinder elements concentration in the + 125 µm size fractions; and elevation (m above sea level). The approximate position of the calcite carbonatite dike outcrop is projected onto the profile.

High Ta concentrations (samples WI-13-69H and WI-13-70H) coincide with two of the highest Nb values (Fig. 3.14) and suggest the presence of Nb-Ta-bearing minerals such as pyrochlore or columbite-(Fe). Samples WI-13-69H and WI-13-70H are downstream of the inferred position of the calcite carbonatite dikes (Fig. 3.14). This may reflect a difference in mineralogy between the main carbonatite complex and carbonatite dikes near Wicheeda Lake. High Nb:Ta ratios are expected in carbonatites based on typical composition of Nb-bearing mineral phases.

Correlations of pathfinder elements observed in the +125 μm size fraction (Fig. 3.15) can be used to predict indicator minerals found in stream sediments. Strong correlations between Ce and La (R^2 = 0.99), Nd (R^2 = 0.94), and Pr (R^2 = 0.74) is expected due to ready substitution of these elements in the same minerals. Cerium and Th (R^2 = 0.87; Fig. 3.15a) linear dependency indicates that monazite-(Ce) is also a prospective indicator mineral. The co-variation of pathfinder elements is consistent with observed mineralogy for the Wicheeda carbonatite complex (Le Couteur 2008, 2009; Lane 2009); REE mineralisation in the main carbonatite is predominantly in monazite-(Ce) and REE-fluorocarbonates and carbonates. All P readings are below detection limits and pXRF does not measure F, hindering identification of these minerals in sediment samples. Phosphorus, a relatively light element (atomic weight 30.97), has to be present in higher concentrations than other pathfinder elements if it is to be detectible by pXRF.

Poor correlation between Ce and Y (R^2 = 0.34) reflects input of indicator minerals that are strongly enriched in light REEs relative to heavy rare earth elements including Y in the carbonatite complex. No meaningful relationship exists between Th and U.

Strong dependence between Nb-Ce (R^2 = 0.85; Fig. 3.15b) and Nb-La (R^2 = 0.82) probably indicates co-occurrence of Nb- and REE-bearing minerals. This is expected as REE-fluorocarbonates, monazite-(Ce), and pyrochlore have similar densities (4.0-5.0 g/cm^3, 4.5-5.5 g/cm^3, and 4.2-6.4 g/cm^3 respectively) and probably, settling velocities.

There is a strong linear dependence between Nb and TiO_2 (R^2= 0.98; Fig. 3.15c). This relationship may indicate that pyrochlore contains significant amounts of Ti, or the presence of Nb-rutile within stream sediments. The moderate correlation between Nb and FeO (R^2 = 0.73; Fig. 3.15d) indicates the coincidence of magnetite and Nb-bearing

mineral phases such as pyrochlore and Nb-rutile. Correlation between Nb and Ta is poor (R^2= 0.61; including below detection limit data).

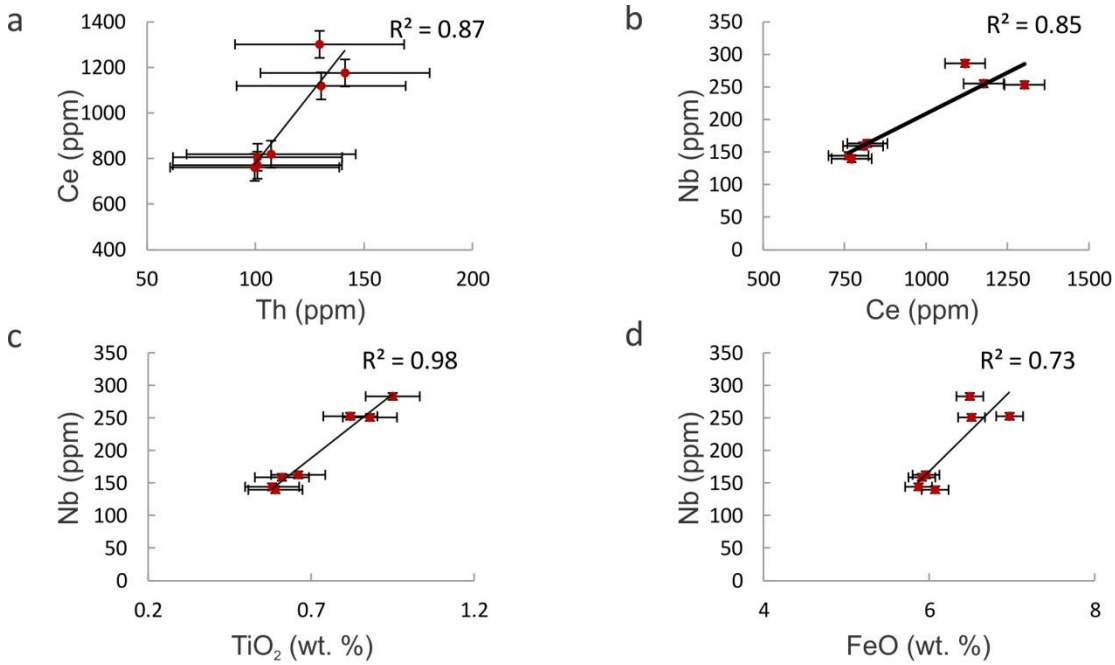

Figure 3.15 Correlations between the concentrations of selected elements in the + 125 µm size fraction of samples. a) Ce and Th. b) Nb and Ce. c) Nb and TiO_2. d) Nb and FeO.

Linear dependence between Ba and Sr (R^2 = 0.98) may reflect the presence of both elements in a common mineral phase such as REE-bearing fluorocarbonates and/or a consistent composition for barite-celestine solid solution minerals in the area. Input of Sr-Ba sulphates from limestones and marbles of the Kechika Formation cannot be ruled out as a possible source of Ba and Sr.

Further optical microscope and electron microprobe studies (Chapter 4) are required to identify and determine the chemical composition of indicator minerals. The use of QEMSCAN® (Section 3.2) reconciles stream sediment and indicator mineral chemistry. Pre-concentration of heavy minerals by gravity separation may be required. The economics and effectiveness of QEMSCAN® analyses relative to traditional indicator mineral methods involving hand-picking remains to be established. In combination with EMP and SEM analyses, QEMSCAN® will provide quantitative information on indicator minerals and establish mineralogical differences between calcite and dolomite carbonatites in the area. Further sampling of stream sediments downstream of other

mineralisation in the area and outside the influence of the Wicheeda carbonatite complex could strengthen the findings in this study.

3.1.2.7 Conclusions

Portable XRF concentrations of pathfinder elements (Nb, Ta, La, Ce, Pr, Nd, Y, and Th) in stream sediments collected near the Wicheeda carbonatite complex are preferentially enriched in the + 125 (or 125-250) μm size fraction relative to other sizes. Based on the mineralogy of the Wicheeda carbonatite complex and detectable concentrations of Nb, Ta, La, Ce, Pr, Nd, and Y, monazite, REE-fluorocarbonates and carbonates, and pyrochlore (± columbite-[Fe]) are prospective indicator minerals for Wicheeda carbonatite-type REE deposits. Stream sediment samples collected near the Wicheeda carbonatite complex do decrease in pathfinder element and indicator mineral concentrations downstream. The economics and effectiveness of QEMSCAN® analyses relative to traditional indicator mineral methods involving hand-picking, remains to be established.

3.2 Assessment of QEMSCAN® in specialty metal indicator mineral studies

Submitted to Journal of Geochemical Exploration: Mackay, D.A.R., Simandl, G.J., Ma, W., Redfearn, M., and Gravel, J., 2015. Indicator mineral-based exploration for carbonatites and related specialty metal deposits– A QEMSCAN® orientation survey, British Columbia, Canada.

3.2.1 Introduction

Traditional methodologies for kimberlite and metamorphosed or magmatic massive sulphide indicator mineral exploration studies are described by Averill (2001, 2014), McCurdy (2006, 2009), and McClenaghan (2011, 2014). These studies utilise the 0.25–2.0 mm size fraction of unconsolidated sediments. Samples are pre-concentrated (typically using a shaker table) before heavy liquid separation, isodynamic magnetic separation, and hand picking (McClenaghan, 2011). Following additional sieving, the 0.5-1 mm fraction is hand-picked for indicator minerals while the 0.25-0.5 mm fraction is subject to paramagnetic separation before hand-picking (Averill, 2001; McClenaghan, 2011). Traditional methodologies involving hand picking indicator minerals focus on monomineralic grains. Composite grains may not be recovered. Furthermore, texturally and mineralogically complex grains are difficult and time consuming to hand pick and characterise using optical and Scanning Electron Microscopy (SEM) methods. A single grain mount can take 6-12 hours to characterise (Layton-Matthews et al., 2014). This does not include the time required for complex processing and mineral separation required for traditional indicator mineral studies.

Detailed sample analysis using the QEMSCAN® Particle Mineral Analysis routine takes approximately 3.5-4.5 hours per sample. An additional 1-1.5 hours is required to change sample batches. This allows for 5-6 samples to be analysed per day. When only mineral identification and mineral concentrations are required, the much faster Bulk Mineral Analysis routine can be used instead. This reduces the QEMSCAN® analysis time from ~4 hours to ~30 minutes per sample (8 times faster). If transmitted light optical investigation is not required, polished pucks can be used. The sample holder for 30 mm

blocks may accommodate more samples (14) than the polished thin section holder (12 sections), slightly reducing turnaround time required to change batches.

3.2.1.1 Potential indicator minerals

Pyrochlore supergroup minerals (as defined by Atencio, 2010), columbite-tantalite series minerals (as defined by Černý and Ercit, 1985; Černý et al., 1992), rare earth element (REE)-bearing fluorocarbonates (such as bastnaesite and synchysite), monazite, and apatite (Belusova et al., 2002a) are ideal carbonatite indicator minerals because of their high density (Table 3.5) and high content of key pathfinder elements such as: Nb, Ta, LREE (for the purposes of this study LREE = ΣLa, Ce, Pr, and Nd), and P. Other potential indicator minerals occur as gangue and/or as constituents of fenitized (Na-K hydrothermal alteration) zones associated with carbonatites. These include, but are not limited to: magnetite, zircon (Belusova et al., 2002b), barite-celestine series minerals, Na-pyroxenes (e.g. aegirine), Na and K amphiboles (e.g. arfvedsonite and richterite), fluorite (Makin et al., 2014), Nb-rutile, baddeleyite, perovskite, and allanite.

3.2.1.2 Geological setting and characterization of carbonatite-related deposits

Three carbonatites in the British Columbia alkaline province were selected for indicator mineral studies. The Aley carbonatite (a large, high-grade Nb-deposit), is the most important Nb-deposit in the Canadian Cordillera (see Section 3.1.1). The Wicheeda carbonatite (a small, high-grade LREE deposit) is described by Graf et al. (2009), Lane (2009), Trofanenko et al. (2014), and in Sections 3.1.2.

The Lonnie carbonatite (a relatively small, low grade Nb showing) is located 220 km northwest of Prince George (Fig. 3.1) and occurs as an elongate 650 m by 50 m intrusive body dipping 60° to the southwest (Hankinson, 1958; Rowe, 1958). Trenching delineated a zone ~530 m long and ~17 m wide grading 0.21 wt. % Nb_2O_5 (Rowe, 1958; Chisholm, 1960). Geology is described by Simandl et al. (2013) and Luck and Simandl (2014).

Table 3.5 Potential indicator minerals for carbonatite-related deposits, their density, and corresponding pathfinder elements.

Mineral Name	Chemical Formula	Density (g/cm^3)	Main Pathfinder Elements (s)
Pyrochlore	$(Ca,Na)_2(Nb,Ti,Ta)_2O_6(O,OH,F)$	4.2–6.4	Nb
Columbite-(Fe)	$(Fe,Mn)(Ta,Nb)_2O_6$	5.3–7.3	Nb
Fersmite	$(Ca,Ce,Na)(Nb,Ta,Ti)_2(O,OH,F)_6$	4.69–4.79	Nb
Monazite	$(Ce,La,Nd,Th)PO_4$	4.8–5.5	LREE, Th, P
Zircon	$ZrSiO_4$	4.6–4.7	Zr, U
Bastnaesite	$Ce(CO_3)F$	4.95–5.00	LREE
Synchysite	$Ca(Ce,La)(CO_3)_2F$	3.90–4.15	LREE
Apatite	$Ca_5(PO_4)_3(OH,F,Cl)$	3.16–3.22	P
Barite	$BaSO_4$	4.48	Ba
Celestine	$SrSO_4$	3.9–4.0	Sr
Magnetite	Fe_3O_4	5.1–5.2	Fe
Arfvedsonite	$Na_3[(Fe,Mg)_4Fe]Si_8O_{22}(OH)_2$	3.44-3.45	n.a.
Richterite	$Na(Ca,Na)(Mg,Fe)_5(Si_8O_{22})(OH)_2$	3.09	n.a.
Aegirine	$NaFeSi_2O_6$	3.50–3.54	n.a.
Perovskite	$CaTiO_3$	3.98–4.26	Ti
Nb-rutile	$(Ti,Nb,Fe)O_2$	4.35–4.92	Ti, Nb
Allanite	$(Ce,Ca,Y)_2(Al,Fe)_3(SiO_4)_3(OH)$	3.3–4.2	n.a.

n.a. = not applicable; LREE = La, Ce, Pr, and Nd

3.2.1.3 Sampling, portable XRF analysis, and processing methodology

Sediments in streams draining the areas around the Aley, Lonnie, and Wicheeda deposits were sampled in the summer of 2013. Sample locations and sampling methodology are described in Sections 3.1.1 and 3.1.2 and by Luck and Simandl (2014). High concentrations of Nb, LREE, and P are detectable in stream sediments by pXRF (Luck and Simandl, 2014) and traditional chemical analyses. Within carbonatites, Nb is predominantly incorporated in pyrochlore and columbite-(Fe), LREE in REE-fluorocarbonates, LREE, P, Th, Y in monazite, and P in apatite (Table 3.5).

Distribution analyses of carbonatite pathfinder elements (Nb, Ta, LREE, Y, P, Ba, Sr, U, and Th) in stream sediments from the Aley, Lonnie, and Wicheeda carbonatites lead to selection of the 125-250 μm dry sieved fraction (herein referred to as ‘RAW’) as optimal for carbonatite indicator mineral studies in the British Columbia Alkaline Province (Luck and Simandl, 2014; Sections 3.1.1 and 3.1.2).

High pathfinder element concentrations (determined by pXRF) in stream sediments (Section 3.1.1) and extent of mineralization in the Aley deposit (Kressal et al. 2010; Jones et al. 2014) gave the expectation that indicator minerals would be detectable by QEMSCAN®. However, low content of pathfinder elements in sediments downstream from Lonnie and Wicheeda necessitated simple gravity concentration to increase the amounts of pyrochlore, columbite-(Fe), REE-fluorocarbonates, monazite, and apatite for QEMSCAN® analysis. Rigorous testing showed that both the Mozley C800 laboratory mineral separator and Wilfley #13 shaking table can consistently concentrate the pathfinder elements and, by extension, targeted indicator minerals (Appendix B and C). The Mozley C800 is more suitable for processing smaller samples. The optimized processing procedure for the Mozley C800 laboratory mineral separator is described in Appendix B.

3.2.2 Methodology

3.2.2.1 QEMSCAN® methodology

Approximately 2 g of RAW sample and/or corresponding Mozley C800 concentrate (CON) was mounted on polished smear sections (Fig 3.16). Smear sections were prepared by Vancouver Petrographics Ltd. and carefully polished to expose the cores of grains. Analysis was performed using an automated FEI Quanta Scanning Electron Microscope (SEM) with a tungsten filament operating at 10.00 nA and a maximum voltage of 25 keV. The QEMSCAN® procedure and IDiscover® software were used to collect and process data.

As part of the automated QEMSCAN® procedure (Particle Mineral Analysis routine), a Back Scatter Electron (BSE) image of each grain is acquired, with individual particle boundaries determined by contrast in brightness (Fig. 3.16). Energy Dispersive X-Ray Spectroscopy (EDS) analysis, performed on a grid (6.5 μm spacing in this study), provides chemical composition and identifies each mineral based on a customized Species Identification Protocol. Mineral abundance in weight percent (wt. %) is calculated using particle volume (based on surface area) and density of the identified

mineral. QEMSCAN® analysis output includes particle count, mineral wt. %, particle size distribution(s), chemistry, and proportion of monomineralic (or liberated) and composite grains with mineral associations (Fig. 3.16). QEMSCAN® bulk chemical composition is derived from chemical composition of mineral particles determined by EDS, volume measurements (which assume the polished smear section has representative mineral composition and each particle is uniform in shape), and idealized mineral densities.

3.2.2.2 Chemical analysis

To validate the pXRF analysis and determine the concentration of pathfinder elements not provided by pXRF (Table 3.2 and 3.4), a 3.5-10.5 g split of each RAW sample and corresponding Mozley concentrates was analysed using lithium borate fusion followed by ICP-MS for trace elements, Inductively Coupled Plasma Atomic Emission Spectroscopy (ICP-AES) for major elements (reported as their common oxides), and XRF for Nb (when in concentrations >2500 ppm Nb).

3.2.3 Results

3.2.3.1 QEMSCAN®

Mineral abundance by weight per cent (Table 3.6) and particle count (Table 3.7) for each polished smear section was determined using QEMSCAN® analysis. Concentrations of Fe_2O_3, Nb, and LREE (ΣLa, Ce, Pr, Nd) of each polished smear section from Aley were determined by QEMSCAN® analysis (Table 3.8).

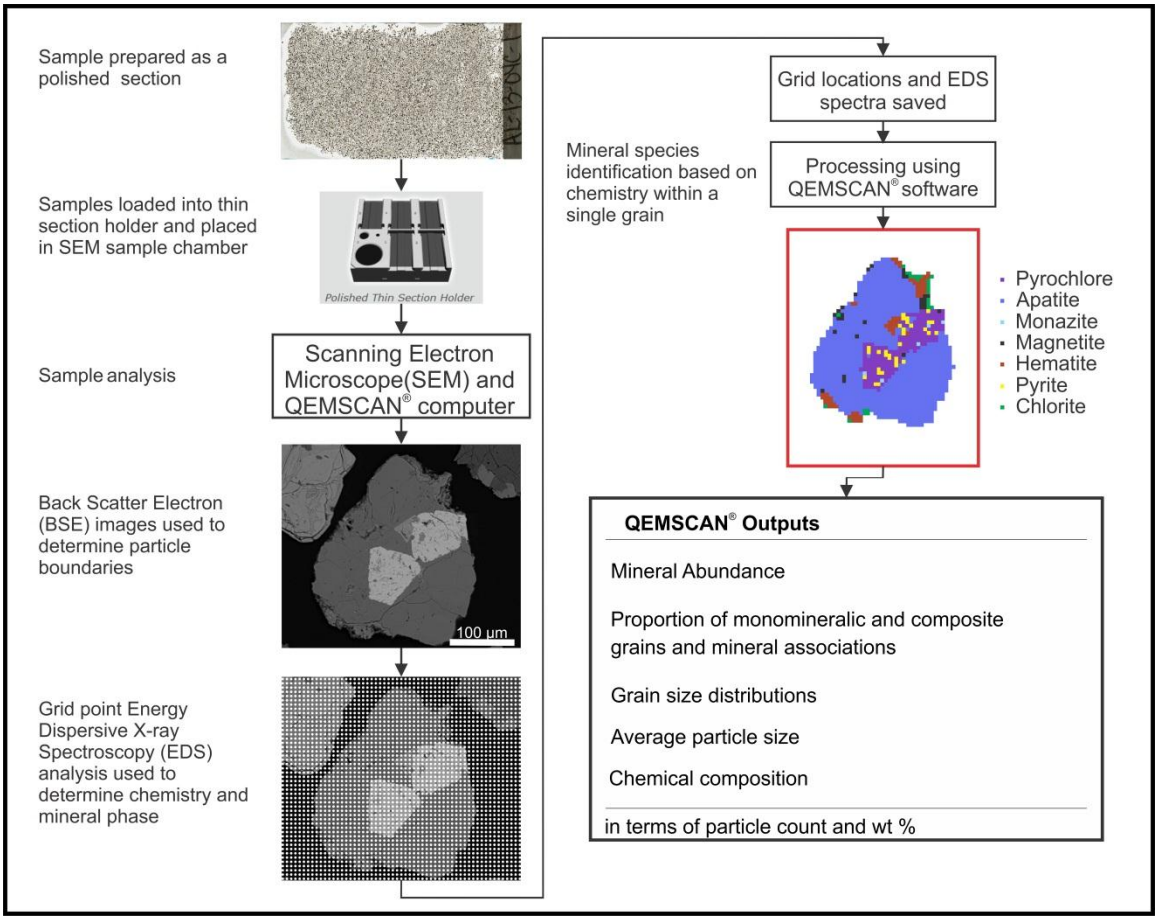

Figure 3.16 Flow chart for QEMSCAN® analysis. Based on QEMSCAN® software help file.

3.2.3.2 Geochemistry

Geochemical composition of the unprocessed 125-250 µm fraction of stream sediment samples and corresponding Mozley concentrates from the Aley (Table 3.9) and Lonnie (Table 3.10) carbonatite drainage were determined by ICP-MS, ICP-AES, and XRF analyses. These analysis are consistent with pXRF analysis of the same samples (Tables 3.2 and 3.4). Portable XRF results are consistently slightly lower than laboratory analysis. Carbonatite pathfinder elements associated with prospective indicator minerals (Table 3.5) are detected in all samples. Concentrations of Nb in RAW samples from the Aley drainage range from 3000-10000 ppm with an average of 5900 ppm. Concentrations in corresponding Mozley concentrates are substantially higher, ranging from 11900-25900 ppm Nb and averaging 17600 ppm Nb. Similarly, concentrations of Ta, Zr, LREE, U, Th, and P_2O_5 increased following Mozley processing. Relative to Aley, unprocessed samples

from Lonnie have very low pathfinder elements concentrations (Table 3.9 and 3.10). Niobium ranges from 39-70 ppm (53 ppm average). Mozley C800 processing substantially increased the concentrations of all pathfinder elements with the exception of Ba (Table 3.10). Insufficient material was retained for laboratory geochemical analysis following Mozley processing for samples from Wicheeda.

3.2.4 Discussion

This QEMSCAN® orientation survey focuses on samples from the Aley carbonatite drainage area for three reasons: 1) Aley has the largest number of samples; 2) Aley is the most important carbonatite-related deposit in the Canadian Cordillera; and 3) pre-concentration of samples from Aley is not required. Concentrations of pathfinder elements and indicator minerals are much lower in the Lonnie and Wicheeda areas (pre-concentration is required). Following pre-concentrations, the same QEMSCAN® methodology described for Aley can be applied to samples from Lonnie and Wicheeda.

3.2.4.1 Aley

3.2.4.1.1 Indicator mineral abundances

All carbonatite indicator minerals were detectable in RAW samples from the Aley carbonatite without additional processing (Table 3.6 and 3.7; Fig. 3.17). However, minimal processing by Mozley C800 table effectively concentrated heavy indicator minerals relative to RAW stream sediments (Fig. 3.17). Specifically, pyrochlore abundance increased on average by 12.9 x, columbite-(Fe) by 2.4 x, monazite by 3.2 x, REE-fluorocarbonates by 2.6 x, apatite by 1.7 x, magnetite by 5.8 x, and zircon by 3.2 x (Table 3.6). Comparable increases in pathfinder element concentrations were observed during other mineral concentrator optimization studies (Appendix B).

Table 3.6 Indicator and major rock forming mineral concentrations (wt. %) for the RAW stream sediment samples and corresponding CON from the Aley (AL), Lonnie (LO), and Wicheeda (WI) carbonatites. “Other” includes all other minor minerals and undefined minerals detected. Mineral abbreviations: pyrochlore (Pcl); columbite-(Fe) (Cmb); fersmite (Fer); REE-fluorocarbonates (REE-Fl); zircon (Zrc); apatite (Ap); magnetite (Mag); hematite (Hem); rutile (Rt); amphibole/pyroxene (Amp/Px); barite (Brt); calcite (Cal); dolomite (Dol); quartz (Qtz); feldspar (Fsp). n.d. = not detected

Sample ID	Pcl	Cmb	Fer	Mnz	REE-Fl	Zrc	Ap	Mag	Hem	Rt	Amp/Px	Brt	Cal	Dol	Qtz	Fsp	Other	Total
AL-13-01 RAW	0.64	0.32	0.01	0.63	0.07	0.14	6.22	2.03	5.18	0.14	1.49	0.16	10.33	40.07	19.10	5.97	7.50	100.00
AL-13-01 CON	1.42	1.36	0.04	1.45	0.32	0.36	13.10	3.76	12.73	0.24	1.42	0.26	6.49	41.03	9.65	1.57	4.80	100.00
AL-13-02 CON	1.82	2.07	0.05	3.38	0.47	0.54	17.47	3.67	22.14	0.19	1.00	0.01	3.67	33.33	4.23	1.07	4.89	100.00
AL-13-04 RAW	0.11	1.88	0.26	0.49	0.31	0.08	19.26	0.67	13.54	0.15	2.73	0.01	0.84	47.68	3.23	0.74	8.02	100.00
AL-13-04 CON	2.17	3.02	0.06	1.92	0.25	0.35	27.40	7.07	19.21	0.20	2.25	0.01	0.26	28.89	1.36	0.40	5.18	100.00
AL-13-10 CON	2.07	2.01	0.05	2.51	0.67	0.52	15.60	12.08	10.88	0.32	1.31	0.11	3.91	36.99	5.71	1.08	4.18	100.00
AL-13-16 RAW	0.06	0.87	0.35	0.47	0.17	0.17	6.42	1.29	8.51	0.13	1.12	0.14	9.52	38.24	18.43	6.15	7.96	100.00
AL-13-16 CON	1.02	1.12	0.04	1.61	0.38	0.41	10.66	6.16	6.68	0.18	1.69	0.06	5.57	44.87	11.83	2.46	5.26	100.00
LO-13-01 RAW	n.d.	0.01	0.00	0.11	0.01	0.08	0.46	0.03	0.35	0.47	3.30	0.00	0.05	0.01	53.31	30.55	11.26	100.00
LO-13-01 CON	0.01	0.06	0.00	0.21	0.04	0.27	1.23	0.17	0.66	1.25	6.09	0.00	0.01	0.03	47.42	27.21	15.34	100.00
LO-13-02 RAW	0.00	0.01	0.01	0.05	0.01	0.14	0.47	0.07	0.32	0.35	2.70	0.01	0.00	0.01	54.12	29.36	12.37	100.00
LO-13-02 CON	0.01	0.04	0.00	0.22	0.04	0.16	0.86	0.12	0.44	1.05	4.79	0.00	0.00	0.02	48.63	29.87	13.75	100.00
LO-13-25RAW	n.d.	0.00	0.00	0.05	n.d.	0.07	0.40	0.00	0.28	0.29	3.41	0.00	0.00	0.00	53.81	32.08	9.61	100.00
LO-13-25 CON	0.02	0.04	0.00	0.35	0.03	0.15	1.39	0.03	0.57	0.75	5.30	0.00	0.01	0.32	47.72	29.06	14.26	100.00
WI-13-64H2 RAW	0.00	0.00	0.02	0.25	0.12	0.04	0.23	0.06	2.70	0.42	2.52	0.02	7.59	0.11	33.17	32.58	20.17	100.00
WI-13-64H2 CON	0.01	0.02	0.05	2.01	1.56	0.20	0.70	0.79	15.13	2.77	2.00	0.11	7.34	0.55	32.75	13.51	20.50	100.00
WI-13-69H RAW	0.00	0.00	0.01	0.48	0.48	0.05	0.42	0.05	3.87	0.94	1.63	0.04	2.18	0.13	41.27	24.87	23.58	100.00
WI-13-69H CON	0.00	0.04	0.05	1.50	0.97	0.08	0.61	0.50	9.23	2.19	2.17	0.05	2.03	0.31	42.73	17.10	20.44	100.00
WI-13-70H RAW	0.00	0.04	0.02	0.43	0.58	0.08	0.35	0.05	3.23	0.76	1.53	0.06	3.88	0.33	39.61	25.54	23.51	100.00
WI-13-70H CON	0.01	0.09	0.07	2.74	1.37	0.17	0.57	1.48	10.65	2.45	1.72	0.05	3.90	0.50	40.03	13.96	20.24	100.00

Table 3.7 Indicator mineral concentrations (particle count) for the RAW stream sediment samples and corresponding CON from the Aley (AL), Lonnie (LO), and Wicheeda (WI) carbonatites. Proportion for each indicator minerals (%) of total grain count are shown in brackets. Mineral abbreviations same as Table 3.6.

Sample ID	Pcl	Cmb	Fer	Mnz	REE-Fl	Zrc	Ap	Mag	Hem	Rt	Amp/Px	Brt	Total
AL-13-01 RAW	121(0.605)	65(0.33)	130(0.65)	317(1.59)	88(0.44)	123(0.615)	2526(12.63)	309(1.55)	789(3.95)	1448(7.242)	6219(31.104)	24(0.12)	19994
AL-13-01 CON	353(2.58)	227(1.66)	327(2.39)	679(4.96)	157(1.15)	233(1.70)	4356(31.80)	851(6.21)	1717(12.53)	1233(9.000)	3635(26.533)	57(0.416)	13700
AL-13-02 CON	489(3.73)	375(2.86)	443(3.38)	1029(7.85)	224(1.71)	297(2.27)	5195(39.61)	891(6.79)	2298(17.52)	1110(8.464)	3053(23.28)	43(0.328)	13114
AL-13-04 RAW	177(0.914)	456(2.35)	323(1.67)	453(2.34)	145(0.748)	81(0.42)	5328(27.50)	348(1.80)	1951(10.07)	858(4.429)	3541(18.277)	32(0.165)	19374
AL-13-04 CON	707(4.18)	593(3.51)	654(3.87)	1178(6.97)	168(0.994)	305(1.80)	9910(58.61)	1096(6.482)	3342(19.77)	1188(7.026)	3769(22.291)	65(0.384)	16908
AL-13-10 CON	660(2.69)	478(1.95)	639(2.61)	1529(6.23)	560(2.28)	408(1.66)	6763(27.58)	2269(9.252)	2674(10.90)	1523(6.210)	4364(17.794)	75(0.306)	24525
AL-13-16 RAW	105(0.559)	222(1.18)	167(0.888)	271(1.44)	77(0.41)	119(0.633)	2605(13.86)	420(2.23)	1039(5.527)	1405(7.475)	5386(28.654)	26(0.138)	18797
AL-13-16 CON	335(1.77)	227(1.20)	323(1.71)	668(3.53)	162(0.857)	167(0.883)	4850(25.65)	795(4.20)	1563(8.265)	1043(5.515)	5961(31.52)	34(0.18)	18912
LO-13-01 RAW	0(0)	2(0.009)	8(0.036)	44(0.2)	6(0.027)	92(0.418)	356(1.617)	23(0.104)	190(0.863)	1116(5.069)	3606(16.378)	2(0.009)	22017
LO-13-01 CON	10(0.033)	9(0.029)	11(0.036)	73(0.237)	11(0.036)	146(0.475)	637(2.071)	69(0.224)	298(0.969)	2112(6.868)	4761(15.482)	5(0.016)	30752
LO-13-02 RAW	2(0.013)	6(0.038)	5(0.032)	27(0.173)	6(0.038)	80(0.513)	268(1.718)	26(0.167)	203(1.302)	847(5.431)	2631(16.87)	1(0.006)	15596
LO-13-02 CON	3(0.009)	1(0.003)	17(0.049)	62(0.179)	12(0.035)	103(0.298)	598(1.728)	53(0.153)	259(0.749)	1665(4.812)	4780(13.814)	33(0.095)	34602
LO-13-25RAW	0(0)	3(0.026)	9(0.078)	17(0.148)	0(0)	100(0.871)	160(1.393)	7(0.061)	141(1.228)	451(3.928)	1534(13.359)	2(0.017)	11483
LO-13-25 CON	10(0.047)	14(0.066)	10(0.047)	73(0.342)	9(0.042)	138(0.647)	553(2.592)	41(0.192)	176(0.825)	1119(5.244)	2675(12.537)	1(0.005)	21337
WI-13-64H2 RAW	4(0.009)	8(0.018)	59(0.131)	145(0.322)	37(0.082)	196(0.436)	952(2.12)	55(0.12)	815(1.81)	3504(7.788)	12009(26.69)	57(0.13)	44992
WI-13-64H2 CON	33(0.136)	37(0.152)	233(0.959)	488(2.009)	311(1.28)	181(0.745)	894(3.68)	544(2.24)	2262(9.31)	3902(16.06)	7414(30.52)	11(0.045)	24294
WI-13-69H RAW	11(0.057)	26(0.135)	51(0.265)	159(0.825)	59(0.306)	186(0.965)	912(4.73)	72(0.37)	728(3.78)	2972(15.42)	4828(25.05)	36(0.19)	19270
WI-13-69H CON	26(0.119)	29(0.133)	182(0.835)	324(1.486)	173(0.793)	180(0.825)	917(4.21)	321(1.47)	1257(5.765)	3681(16.88)	6013(27.58)	3(0.01)	21805
WI-13-70H RAW	5(0.025)	22(0.111)	45(0.227)	143(0.722)	60(0.303)	161(0.813)	924(4.67)	53(0.27)	652(3.29)	2806(14.17)	4862(24.55)	0(0)	19805
WI-13-70H CON	19(0.089)	57(0.267)	246(1.154)	469(2.2)	245(1.149)	187(0.877)	852(4.00)	523(2.45)	1556(7.300)	3459(16.23)	5911(27.73)	20(0.094)	21315

n.d.=not detected

Table 3.8 Concentration of Nb, LREE, and Fe_2O_3 in polished smear sections determined by QEMSCAN®.

Sample ID	Fe_2O_3 (wt. %)	Nb (ppm)	LREE (ppm)
AL-13-01 RAW	8.9	5189	2451
AL-13-04 RAW	17.5	11935	3305
AL-13-16 RAW	11.6	6503	3620
AL-13-01 CON	18.4	15106	4614
AL-13-02 CON	28.2	21141	13051
AL-13-04 CON	29.5	28214	10570
AL-13-10 CON	25.4	22139	11829
AL-13-16 CON	14.9	11696	10270

Table 3.9 Bulk chemical analysis of the RAW stream sediments and corresponding CON from the Aley carbonatite drainage.

Sample ID	**AL-13-01 RAW**	**AL-13-02 RAW**	**AL-13-04 RAW**	**AL-13-10 RAW**	**AL-13-16 RAW**	**AL-13-18 RAW**	**AL-13-01 CON**	**AL-13-02 CON**	**AL-13-04 CON**	**AL-13-10 CON**	**AL-13-16 CON**
Major Oxides (wt. %)											
SiO_2	30.00	23.60	7.30	25.90	28.90	30.10	14.90	6.35	3.85	8.04	14.00
Al_2O_3	3.68	3.10	1.04	3.47	3.61	3.85	1.67	0.76	0.55	0.90	1.50
Fe_2O_3	5.43	10.50	11.90	8.96	7.86	5.76	12.70	27.30	25.60	22.30	18.35
CaO	21.10	23.20	28.20	22.70	20.40	21.60	26.00	22.40	25.80	23.70	22.20
MgO	8.97	7.65	12.05	8.91	8.83	9.24	10.05	6.81	6.24	7.80	8.38
Na_2O	0.24	0.24	0.25	0.21	0.26	0.28	0.19	0.12	0.20	0.15	0.16
K_2O	1.11	1.16	0.19	1.17	1.15	1.24	0.42	0.26	0.16	0.28	0.44
TiO_2	0.32	0.39	0.40	0.38	0.38	0.33	0.53	0.70	0.73	0.64	0.61
MnO	0.14	0.21	0.48	0.19	0.16	0.16	0.19	0.24	0.32	0.23	0.18
P_2O_5	2.48	3.57	8.21	3.35	2.75	2.52	6.32	7.94	12.10	7.36	5.46
SrO	0.09	0.14	0.26	0.12	0.09	0.09	0.13	0.17	0.24	0.16	0.12
BaO	0.07	0.03	0.02	0.04	0.10	0.08	0.10	0.03	0.02	0.06	0.15
LOI	24.40	24.00	27.80	24.80	23.80	24.80	25.00	18.05	15.30	20.90	22.30
Trace Elements (ppm)											
Nb	3700	7400	10000	5800	5500	3000	11900	22400	25900	17700	15200
Ta	55	109	89	82	80	52	184	255	124	197	217
Ba	672	242	196	395	883	713	915	241	175	532	1400
Zr	424	912	849	765	680	459	1180	2800	2290	2100	1745
U	19	34	24	30	27	18	61	103	64	86	74
Th	137	267	324	206	189	134	450	786	723	615	522
La	576	1705	1430	1220	1015	658	1715	5150	3320	3560	2790
Ce	922	2650	2480	1900	1605	1065	2740	7880	5560	5560	4350
Pr	90	260	258	180	154	102	281	750	569	539	424
Nd	308	816	863	601	511	341	904	2470	1980	1805	1385
Sm	44	96	123	78	68	47	127	291	255	216	172
Eu	10	24	29	18	15	11	31	65	60	49	40
Gd	27	57	74	44	39	28	79	155	148	120	98
Tb	3	7	9	5	5	4	10	18	18	14	12
Dy	16	31	42	25	22	16	46	83	82	64	55
Ho	3	5	7	4	3	3	8	13	13	10	9
Er	7	12	16	10	8	6	18	31	31	24	21
Tm	1	1	2	1	1	1	2	4	3	3	2
Yb	4	8	10	6	5	4	11	19	18	14	13
Lu	1	1	1	1	1	0	1	2	2	2	2
Y	70	127	167	102	91	70	189	345	344	272	232
Rb	30	27	6	28	30	33	11	5	3	6	11
Sr	799	1275	2290	1075	839	857	1275	1630	2280	1535	1175
V	136	218	155	183	182	155	175	399	333	334	282
W	182	114	43	130	147	136	247	147	167	210	274
Cs	1	1	0	1	1	1	0	0	0	0	0
Total	**99.11**	**99.94**	**100.68**	**101.89**	**99.88**	**101.08**	**101.19**	**97.20**	**97.07**	**97.22**	**97.88**

Table 3.10 Bulk chemical analysis of the RAW stream sediments and corresponding CON from the Lonnie carbonatite drainage.

Sample ID	**LO-13-01 RAW**	**LO-13-02 RAW**	**LO-13-25 RAW**	**LO-13-01 CON**	**LO-13-02 CON**	**LO-13-25 CON**
Major Oxides (wt. %)						
SiO_2	80.20	77.10	79.70	71.40	72.90	73.10
Al_2O_3	9.78	10.25	9.71	9.89	10.10	10.50
Fe_2O_3	2.46	2.92	2.59	5.52	5.46	5.72
CaO	1.88	1.78	1.88	3.47	2.79	2.87
MgO	0.84	0.94	0.79	1.31	1.07	1.27
Na_2O	2.32	2.22	2.30	2.06	2.13	2.05
K_2O	1.48	1.60	1.47	1.02	1.11	1.30
TiO_2	0.55	0.59	0.50	1.95	1.72	1.37
MnO	0.08	0.11	0.15	0.32	0.37	0.46
P_2O_5	0.19	0.19	0.25	0.56	0.47	0.58
SrO	0.02	0.02	0.02	0.03	0.02	0.02
BaO	0.04	0.04	0.03	0.03	0.03	0.03
LOI	1.73	2.51	1.49	1.87	1.98	1.71
Trace Elements (ppm)						
Nb	50	70	39	235	290	192
Ta	2	3	2	7	10	7
Ba	332	345	280	285	267	263
Zr	155	195	230	531	576	553
Hf	4	5	6	12	13	13
U	3	4	7	12	15	19
Th	11	16	37	50	77	118
La	68	93	92	324	404	305
Ce	115	154	179	522	643	570
Pr	11	15	20	50	62	61
Nd	40	52	74	167	210	222
Sm	7	9	16	27	35	46
Eu	1	1	1	3	3	3
Gd	5	6	12	20	26	36
Tb	1	1	2	3	4	6
Dy	5	6	11	19	24	32
Ho	1	1	2	4	5	6
Er	3	4	7	12	15	19
Tm	0	1	1	2	2	3
Yb	3	4	6	12	14	18
Lu	0	0	1	2	2	3
Y	26	34	63	111	142	180
Rb	55	64	51	37	41	45
Sr	192	189	164	261	215	175
V	40	43	32	72	58	52
W	946	802	1150	2410	2400	2400
Cs	1	2	1	1	1	1
Total	**101.58**	**100.28**	**100.89**	**99.46**	**100.17**	**101.00**

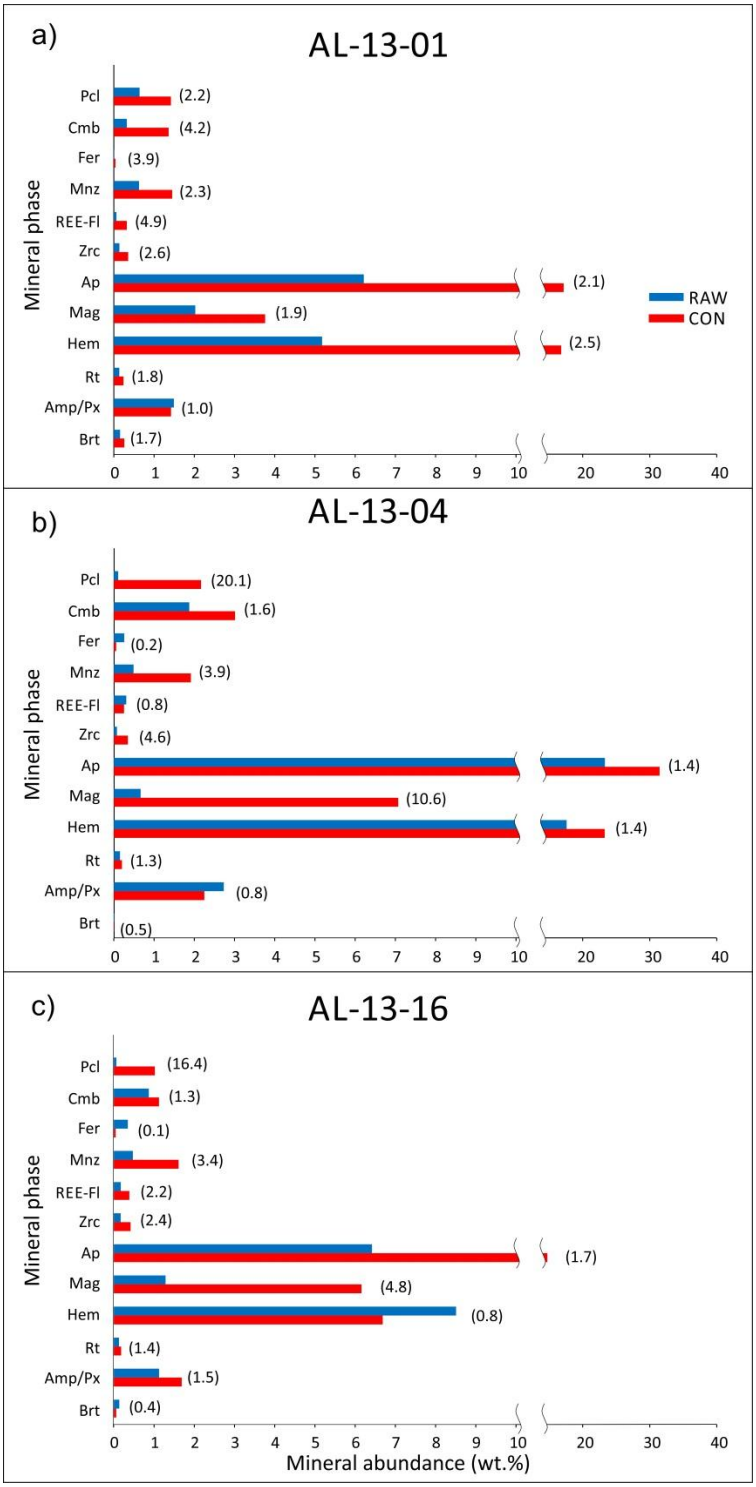

Figure 3.17 Mineral abundance (wt. %; determined by QEMSCAN®) for RAW and corresponding Mozley C800 concentrates (CON) for selected samples a) AL-13-01, b) AL-13-04, and c) AL-13-16. Concentration factors for CON relative to corresponding unprocessed (RAW) samples are shown in parentheses. Mineral abbreviations are the same as in Table 3.6.

3.2.4.1.2 Particle size distribution

QEMSCAN® provides particle size distributions for individual minerals in terms of particle count and weight percent in the 125-250 μm size fraction of RAW stream sediments and corresponding Mozley concentrates from the Aley drainage area. Indicator minerals are detectable by QEMSCAN® at particle sizes smaller than those used for hand picking (Fig. 3.18). Particle size distributions measured by particle count are skewed towards the smallest particle sizes (0-20 μm; Fig. 3.18a, c, e, g, and i). Monazite and REE-fluorocarbonates are heavily skewed towards small particle sizes, while pyrochlore and columbite-(Fe) occur more commonly as larger particles. This is most likely due to the presence of small inclusions within composite grains. The particle count for pyrochlore (Fig. 3.18a), columbite-(Fe) (Fig. 3.18c), monazite (Fig. 3.18g), and apatite (Fig. 3.18i) show an overall decreasing trend with increasing distance downstream of the Aley carbonatite (source). Particle size range in the RAW samples and Mozley C800 concentrates for pyrochlore, columbite-(Fe), and apatite (in terms of wt. %) show a comparatively normal size distribution (Fig. 3.18b, d, and j) while REE-fluorocarbonates and monazite show a broad, irregular distribution (Fig. 3.18f and h).

Lab analysis and QEMSCAN® comparison

The comparison of the chemical composition of samples derived from QEMSCAN® data (Table 3.8) with traditional laboratory analysis (Table 3.9) shows strong positive correlation (Fig. 3.19). Coefficients of determination between Nb (R^2=0.90; Fig. 3.19a), LREE (R^2=0.91; Fig. 3.19b), and Fe_2O_3 (R^2=0.87; Fig. 3.19c) determined by QEMSCAN® and laboratory chemical analysis indicates a predictable co-variation.

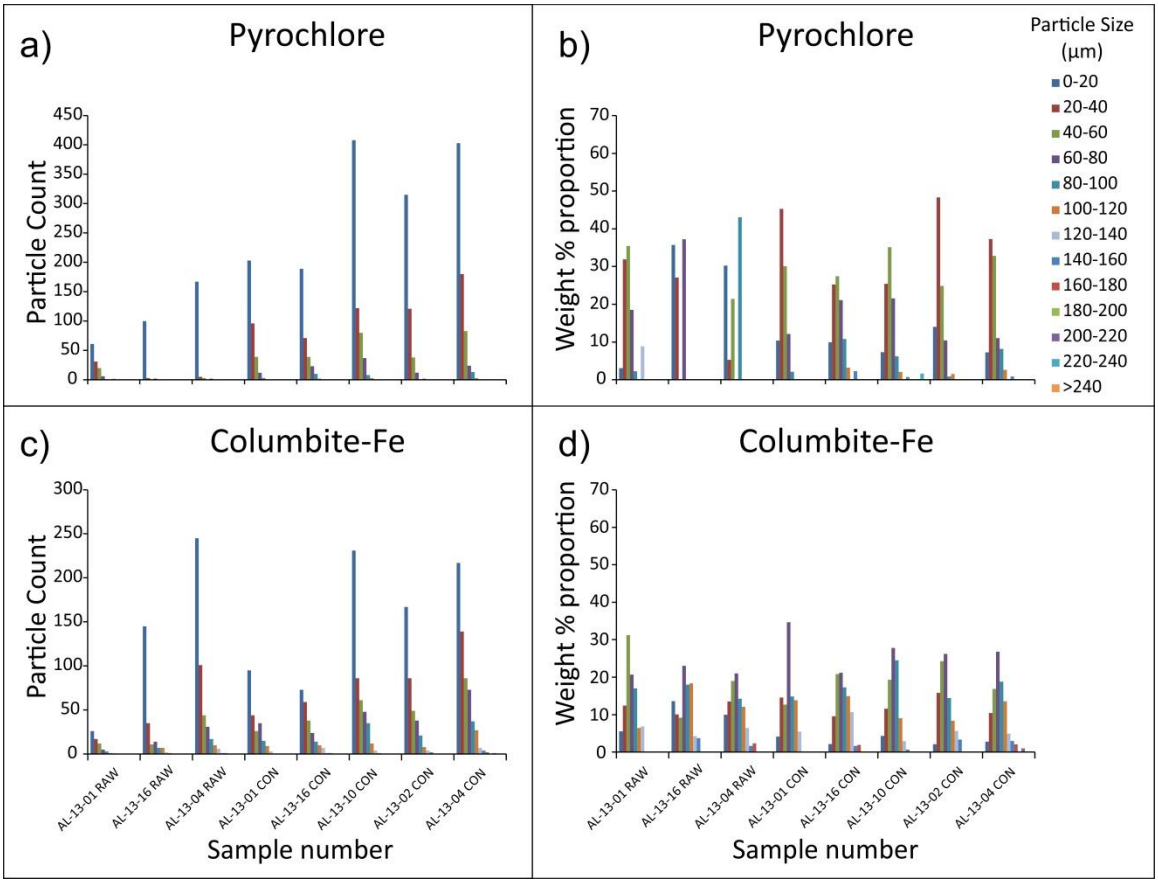

Figure 3.18 Particle size distribution in terms of particle count and wt. % for pyrochlore (a and b), columbite-(Fe) (c and d), REE-fluorocarbonates (e and f), monazite (g and h), and apatite (i and j). RAW samples and corresponding CON samples are each ordered from west (away from the deposit) to east (nearest the deposit). Particle sizes are in µm.

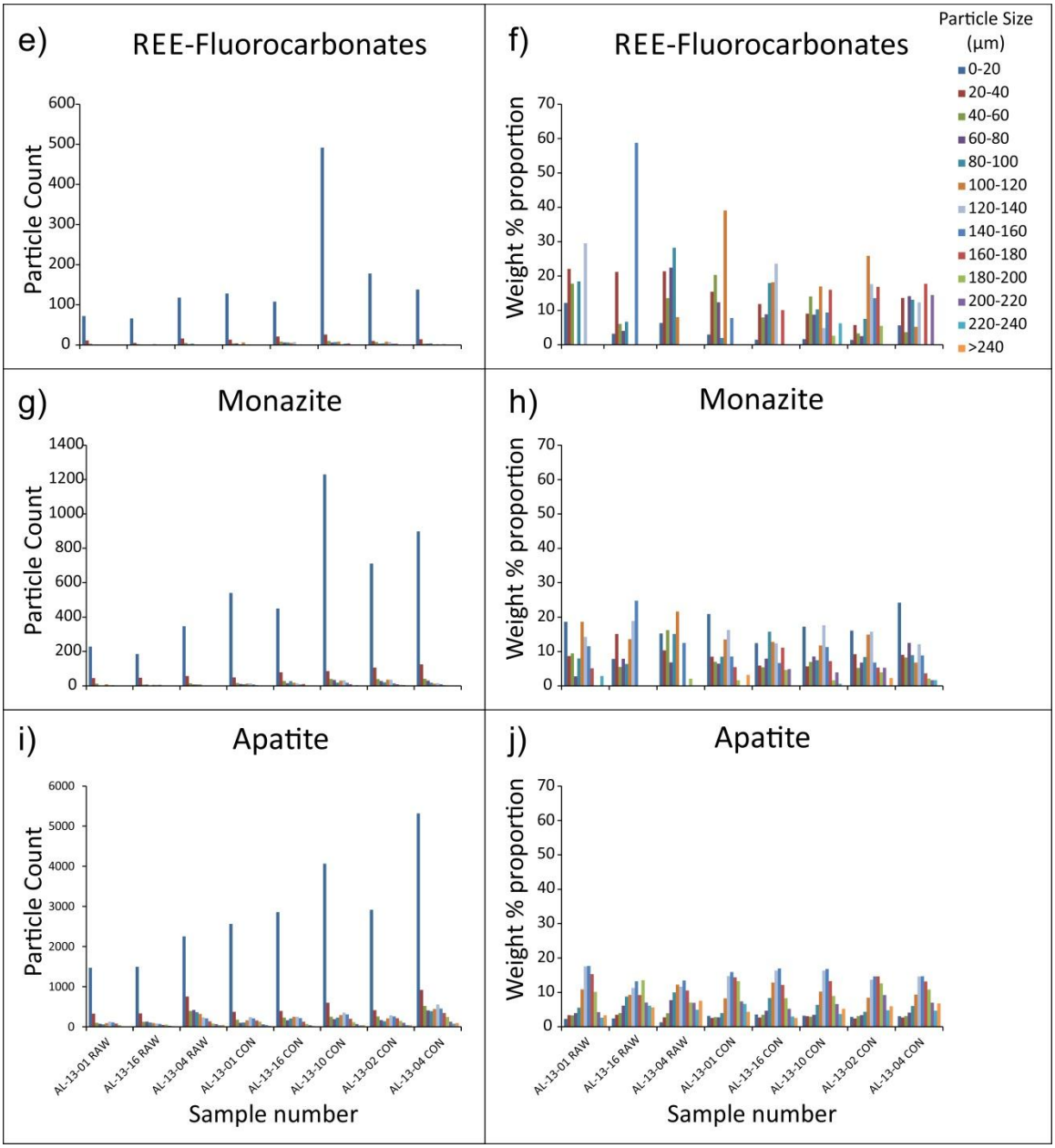

Figure 3.18 Continued.

3.2.4.1.3 Mineral abundance and pathfinder element concentration

There is a good fit between the concentration of carbonatite pathfinder elements (ppm or wt. %) determined for the 125-250 µm fraction using ICP-MS, ICP-AES, and XRF and abundance of carbonatite indicator minerals determined by QEMSCAN® expressed as particle count or wt. %. However, the highest coefficients of determination are

obtained when comparing bulk sample chemistry and indicator mineral concentration in terms of wt. %. Niobium content is related to pyrochlore (R^2=0.72; Fig 3.20a) and columbite-(Fe) (R^2=0.78; Fig 3.20b) concentrations; fersmite is a minor constituent (Fig 20c). Niobate (sum of pyrochlore, columbite-[Fe], and fersmite) concentration (R^2=0.90; Fig. 3.206d) shows the best fit with Nb content of samples. As fersmite is a minor Nb-bearing constituent, a low coefficient of determination between Nb content (XRF) and fersmite concentrations (QEMSCAN®) is expected. Surprisingly, R^2 for Nb content (XRF) and fersmite abundance (QEMSCAN®) in Mozley concentrates is very high (R^2=0.87; Fig 3.20c). High coefficient of determination (R^2= 0.98) between concentrations of columbite-(Fe) and fersmite may in part explain this relationship (Fig 3.21). These niobates commonly coexist in composite grains. The LREE content is strongly related to monazite concentration (R^2=0.91; Fig. 3.20e) and less strongly to REE-fluorocarbonate concentration (R^2=0.51; Fig. 3.20f). Concentration of P_2O_5 in RAW samples and corresponding Mozley C800 concentrates is strongly related to apatite concentration (R^2=0.98; Fig. 3.20g) and weakly to monazite content (R^2=0.25; Fig. 3.20h). Thus, overall indicator mineral abundance measured by wt. % is representative of bulk sample composition determined using ICP-MS, ICP-AES, and XRF. The above relationships between traditional laboratory analysis and QEMSCAN® analysis indicate that mineralogical information from QEMSCAN® analysis on selected samples can supplement relatively inexpensive and time efficient stream sediment geochemical surveys.

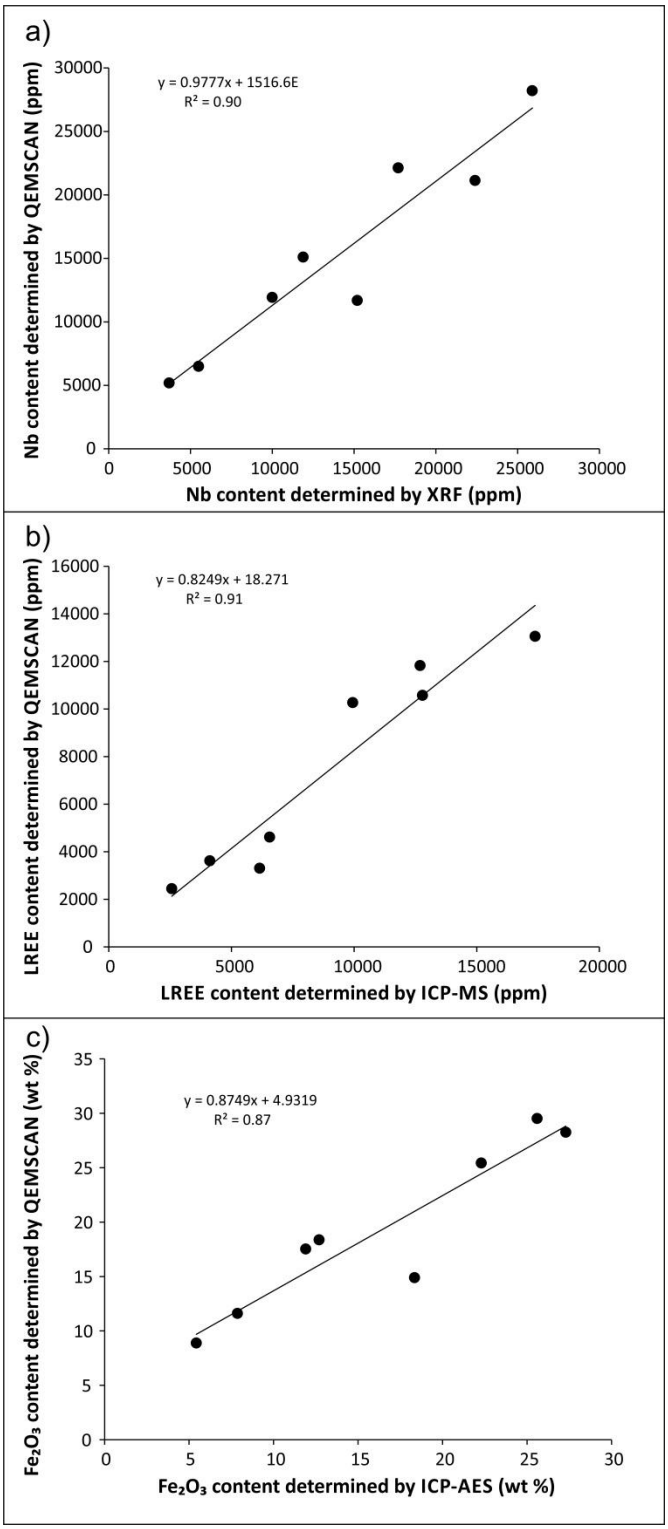

Figure 3.19 Comparison of a) Nb, b) LREE, and c) Fe_2O_3 content of stream sediments from the Aley drainage area, determined by QEMSCAN® and traditional chemical analysis.

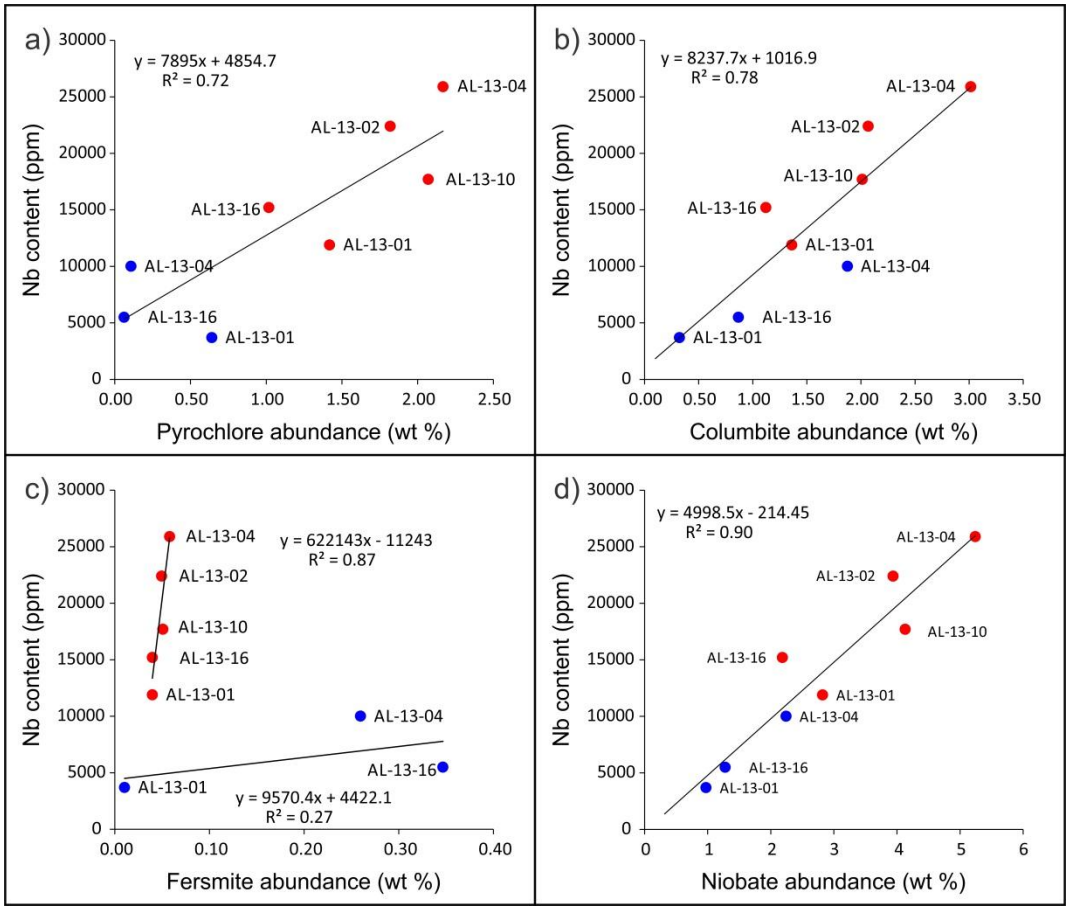

Figure 3.20 Relationship between indicator mineral concentrations (determined by QEMSCAN®) and corresponding pathfinder element content for: a) Nb vs. pyrochlore; b) Nb vs. columbite(Fe); c) Nb vs. fersmite; d) Nb vs. niobates (includes pyrochlore, columbite-(Fe), and fersmite); e) LREE vs. monazite; f) LREE vs. REE-fluorocarbonates; g) P_2O_5 vs. apatite; and h) P_2O_5 vs. monazite. Results are for unprocessed samples (blue circles) and Mozley C800 concentrates (red circles).

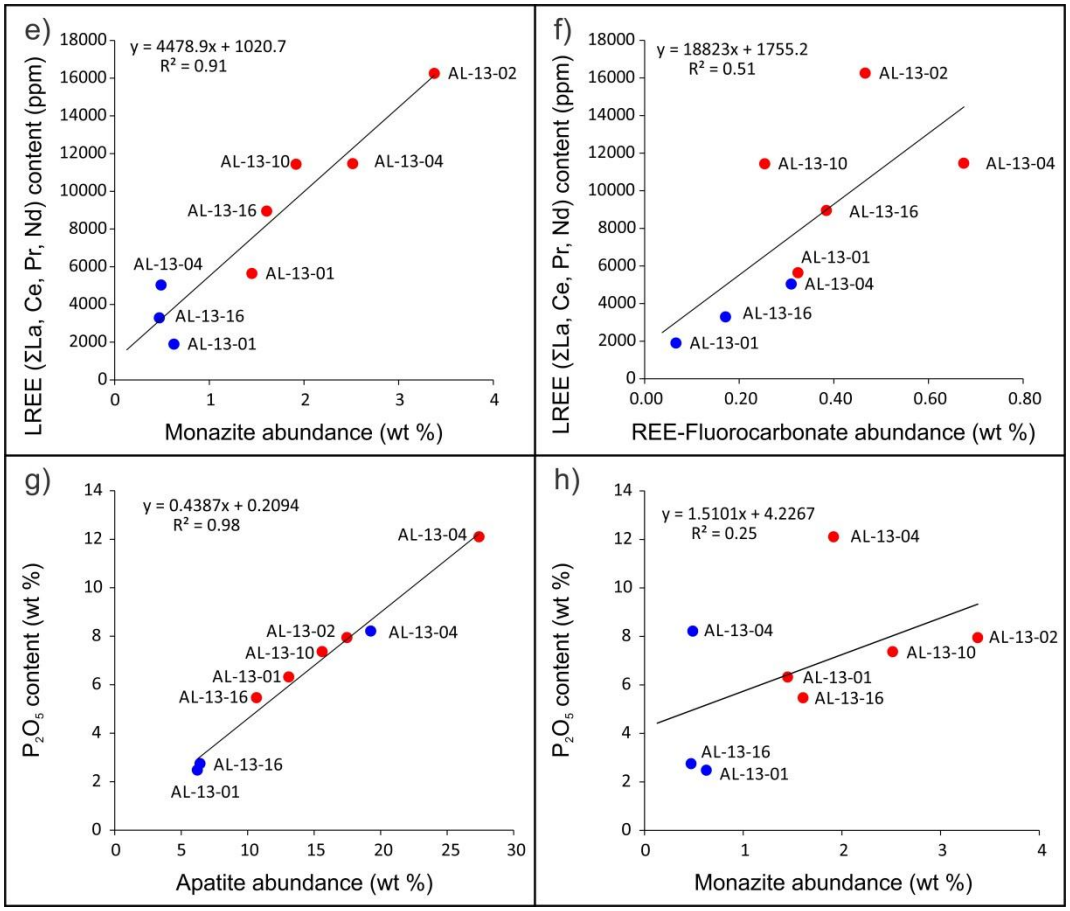

Figure 3.20 Continued.

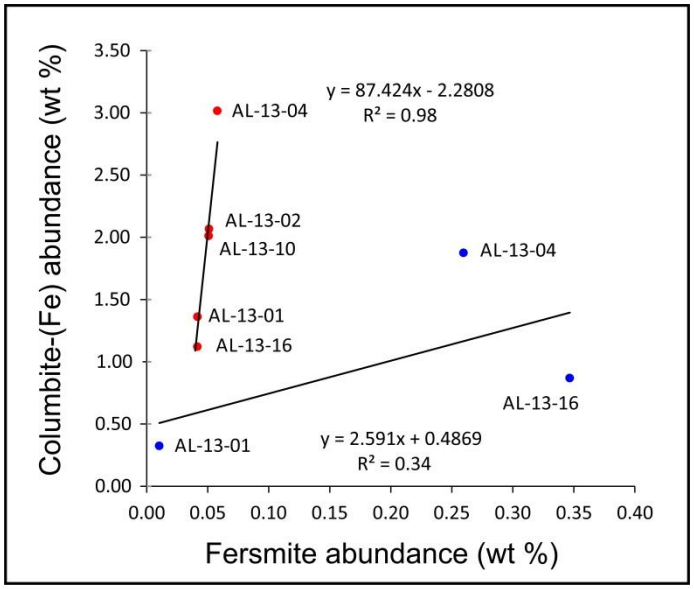

Figure 3.21 Comparison of columbite-(Fe) and pyrochlore concentrations (determined by QEMSCAN®) for RAW (blue circles) and corresponding Mozley C800 concentrate (red circles) samples.

3.2.4.1.4 Mineral association

QEMSCAN® determines the quantitative proportions of monomineralic (or liberated) grains and mineral associations in composite grains. Key selected mineral associations within composite grains and proportion of monomineralic grains are shown in Fig 3.22. Pyrochlore (wt. %) is predominantly contained in composite grains composed of minerals associated with carbonatite magmatism and alteration (columbite-[Fe], apatite, fersmite, ±monazite; Fig. 3.22a, b) while apatite (wt. %) is contained predominantly in monomineralic grains (Fig. 3.22j). Columbite-(Fe) (Fig. 3.22d), REE-fluorocarbonates (Fig. 3.22f), and monazite (Fig. 3.22h) fall in between these two extremes. Monazite (wt. %) in monomineralic grains or in association with pyrochlore, columbite-(Fe), fersmite, and apatite is inferred to be carbonatite mineralisation. However, monazite found in association with micas (chlorite, biotite, and muscovite), quartz, and other complex composite mineral grains ("Others" in Fig. 3.22) is likely metamorphic monazite sourced from detrital metasedimentary material.

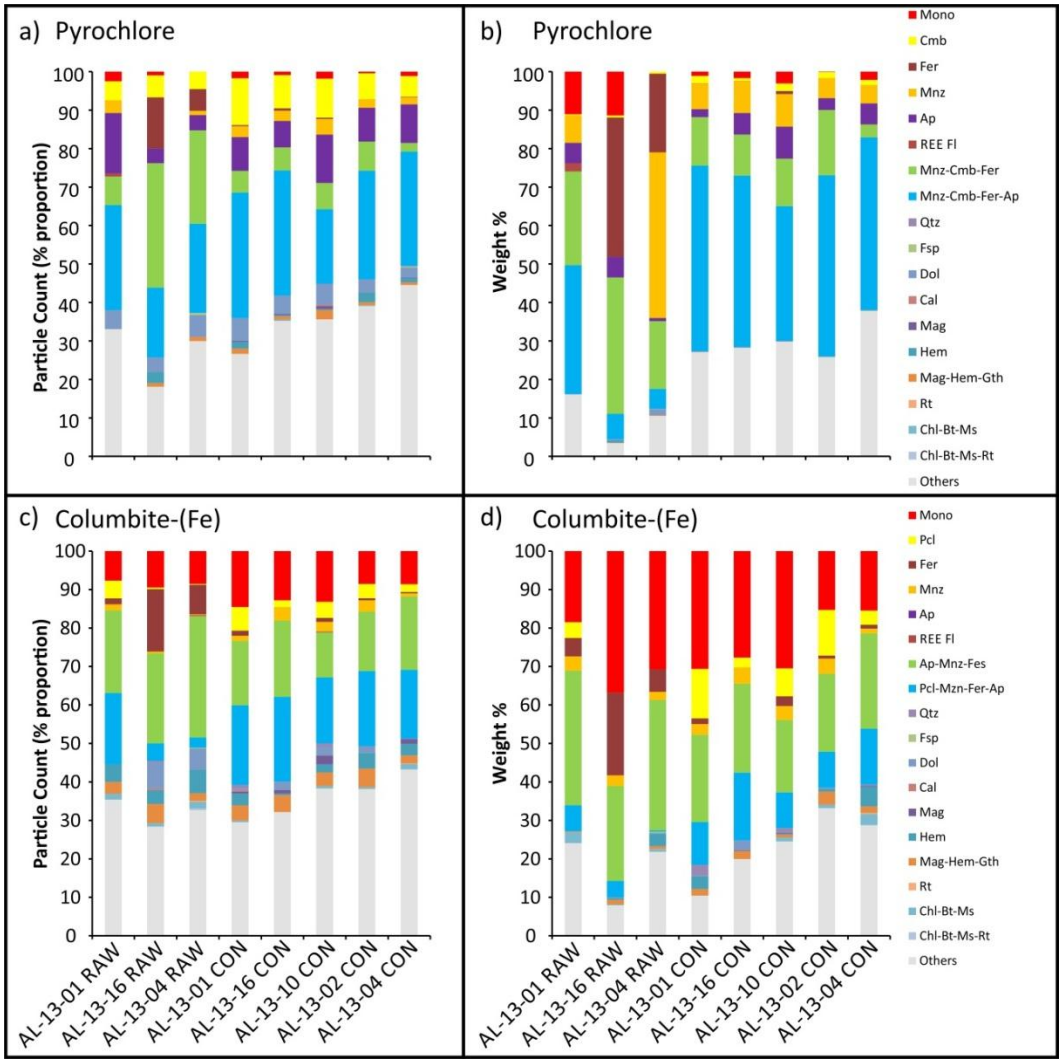

Figure 3.22 Proportions of monomineralic (Mono) and composite grains with predominant mineral associations (in terms of particle count and wt. %) for: a) and b) pyrochlore; c) and d) columbite-(Fe); e) and f) REE-fluorocarbonates; g) and h) monazite; i) and j) apatite. Results are for RAW samples and corresponding CON. Sample distance increases from directly over the deposit (AL-13-04) to 11.5 km downstream (AL-13-01). 'Others' refers to very complex composite grains, and those containing unidentified mineral phases. Abbreviations: pyrochlore (Pcl); columbite-(Fe) (Cmb); fersmite (Fer); REE-fluorocarbonates (REE-Fl); zircon (Zrc); apatite (Ap); magnetite (Mag); hematite (Hem); rutile (Rt); amphibole/pyroxene (Amp/Px); barite (Brt); quartz (Qtz); dolomite (Dol); calcite (Cal); feldspar (Fsp); hematite (Hem); goethite (Gth); chlorite (Chl); biotite (Bt); and muscovite (Ms).

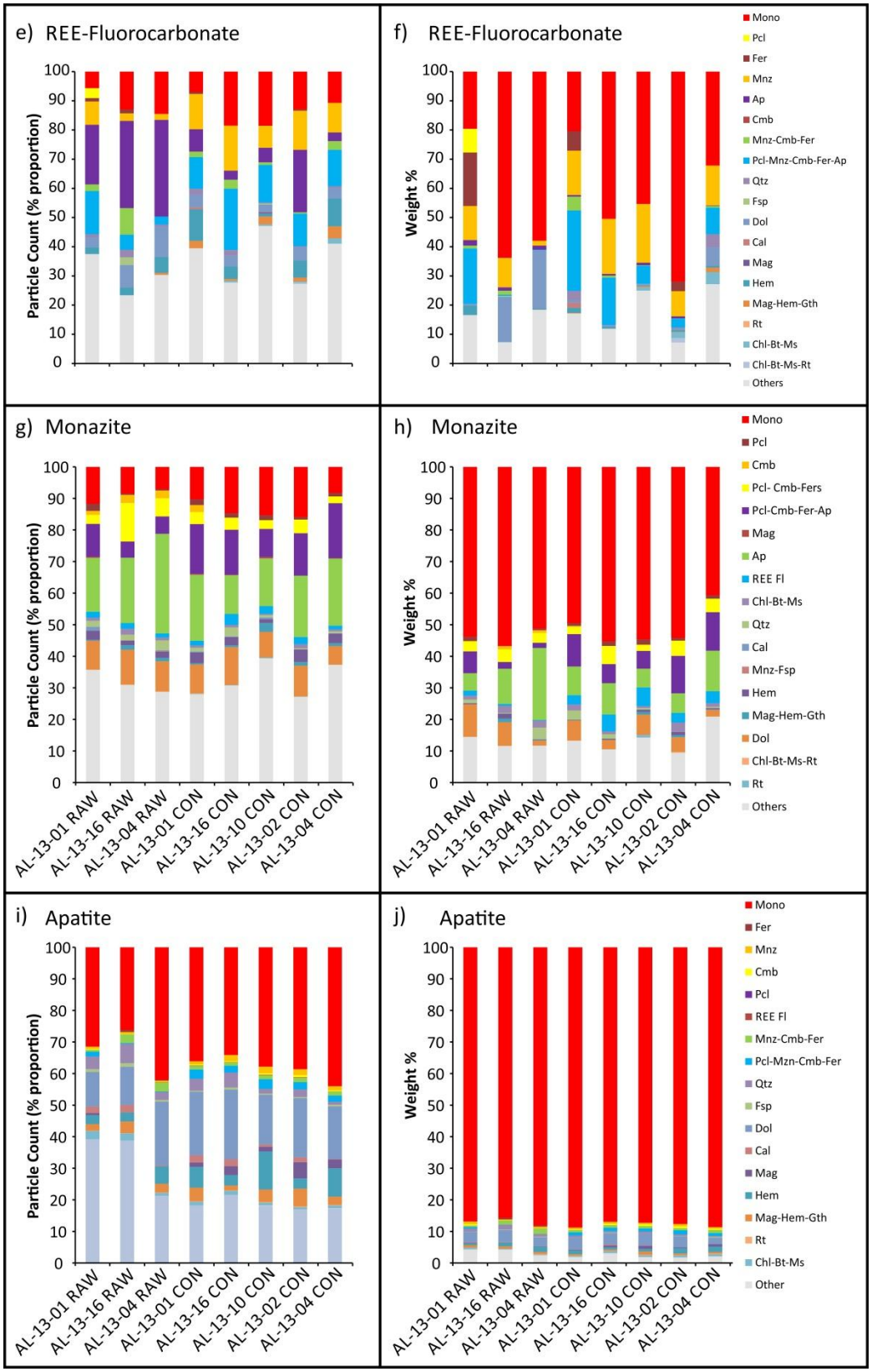

Figure 3.22 Continued.

3.2.4.2 Lonnie mineral abundances

All RAW stream sediment samples from Lonnie contain low concentrations of carbonatite pathfinder elements (Table 3.10). Columbite-(Fe) is detected in all RAW stream sediments samples by QEMSCAN® (Table 3.6 and 3.7). Pyrochlore is detected in only one out of three RAW samples (LO-13-02); however, it is detected in all samples following Mozley processing (Table 3.6 and 3.7). Mozley processing increases the concentration of indicator minerals in terms of wt. % (except fersmite and barite) for all Lonnie samples (Table 3.6). There is an increase in the average abundance of columbite-(Fe) by 41.2 x, monazite by 4.8 x, apatite by 2.7 x, magnetite by 8.2 x, zircon by 2.3 x, and rutile by 2.8 x in Mozley concentrates (Table 3.6). This demonstrates that when indicator mineral concentrations in stream sediments are low, minimal processing enables QEMSCAN® analysis to detect and characterise carbonatite indicators.

3.2.4.3 Wicheeda mineral Abundances

All carbonatite indicator minerals (except barite) were detected by QEMSCAN® in RAW samples from Wicheeda (Table 3.6 and 3.7). Pyrochlore, columbite-(Fe), fersmite, monazite, REE-fluorocarbonates, zircon, magnetite, hematite, apatite, and barite are successfully concentrated by Mozley C800 processing. Processing increased the average abundance of pyrochlore by 9.0 x, columbite-(Fe) by 10.7 x, monazite by 5.9 x, apatite by 2.0 x, magnetite by 17.4 x, zircon by 2.8 x, and rutile by 4.1 x (Table 3.6).

3.2.5 Conclusions

QEMSCAN® can detect indicator minerals in the dry sieved 125-250 μm size fraction without additional processing at the Aley, Lonnie, and Wicheeda carbonatites. If carbonatite pathfinder elements are in low concentration (e.g. samples from Lonnie), minimal processing using a Mozley C800 mineral separator can be used to increase the concentration of indicator minerals in a predictable way. QEMSCAN® can detect and characterise particle sizes too small for hand picking techniques and provides quantifiable

proportions of monomineralic grains and mineral associations within composite grains. QEMSCAN® can fully characterise a sample in 3.5-4.5 hours using the 'Particle Mineral Analysis' routine, much faster than the 6-12 hours required for traditional techniques to characterise a single sample with mineralogically complex grains. If the only mineral identification and their concentrations are needed, the Bulk Mineral Analysis routine can be used and analytical time is reduced to 30 minutes per sample.

4 Pyrochlore and columbite-tantalite discrimination diagrams

Published as: Mackay, D.A.R. and Simandl, G.J. 2015. Pyrochlore and columbite-tantalite as indicator minerals for specialty metal deposits. Geochemistry: Exploration, Environment, Analysis, published online first, doi:10.1144/geochem2014-289.

4.1 Introduction

Indicators minerals used in exploration and deposit targeting consist of ore, accessory, and alteration minerals in soil, lake, glacial, and stream sediments (McClenaghan, 2011). For the purpose of this thesis, indicator mineral-based deposit targeting is a procedure permitting the identification of a deposit type from which a specific indicator mineral was derived based on its chemical characteristics. The most versatile indicator minerals have physical properties that allow them to survive weathering and be transported away from the location of mineralisation, deposited, and readily separated from other sediments (owing to high densities, distinct magnetic properties, sizes between 0.063 and 2.0 mm, and diagnostic optical properties and/or chemical signatures). McClenaghan (2011) provides an in-depth discussion of indicator mineral separation techniques.

Pyrochlore supergroup minerals are a main ore constituent of Nb (±Ta) carbonatite complex-related deposits (including phoscorites) and are found in lower concentrations in specialty metal (Nb, Ta, Li, Cs, Zr, and rare earth elements [REEs+Y])-bearing deposits associated with peraluminous granites, Li-Cs-Ta enriched (LCT) pegmatites, and peralkaline complexes (Hogarth, 1961, 1977; Birkett and Simandl, 1999; Simandl et al., 2001; Simandl, 2002; Mitchell, 2005a, b; Pohl, 2012; Tantalum-Niobium International Study Center, 2013a, b; Linnen et al., 2014; Chakhmouradian et al., 2014). Pyrochlore are also found in the weathered crusts overlying these deposits (Nasraoui and Waerenborgh, 2001; Traversa et al., 2001). Columbite-tantalite series minerals are found in the same deposit-types as pyrochlore supergroup minerals and are the main constituent of Ta ore (Černy and Ercit, 1989; Pohl, 2012; Linnen et al., 2014; Chapter 2).

Discrimination diagrams based on quantifiable composition of pyrochlore supergroup and/or columbite-tantalite series minerals allow explorationists to relate indicator mineral

chemistry to established specialty metal deposit models. In this paper we develop two discrimination diagrams using a combination of new electron microprobe analyses of pyrochlore supergroup and columbite-tantalite series minerals from British Columbia and Quebec carbonatites, and data from the literature.

4.2 Pyrochlore supergroup

The pyrochlore supergroup is subdivided into the pyrochlore [$(Na,Ca)_2Nb_2O_6(OH,F)$], microlite [$(Na,Ca)_2Ta_2O_6(O,OH,F)$], and betafite [$(Ca,U)_2(Ti,Nb,Ta)_2O_6(OH)$] groups, as defined by the Commission on New Minerals, Nomenclature, and Classification of the International Mineralogical Association (CNMNC-IMA) approved classification of Atencio et al. (2010). These minerals are isometric and commonly display octahedral crystals, irregular masses, and rounded grains with subconcoidal to uneven and splintery fracture (Berry et al., 1983; Anthony et al., 2014). Pyrochlore have hardness 5 to 5 ½ and density ranging from 3.7 to 6.4 g/cm^3 (Berry et al., 1983; Anthony et al., 2014). These minerals are translucent to opaque and black to brown, chocolate-brown, honey-brown, reddish-brown, amber-orange, red-orange, pale yellow, greenish yellow, green, or colourless. They have brown to pale yellow streak, vitreous to resinous or adamantine lustre, and display weak anomalous anisotropism under reflected light. Pyrochlore supergroup minerals are often metamict due to their U and Th content (Berry et al., 1983; Anthony et al., 2014). Fersmite and columbite-tantalite series replacement is common (Lumpkin and Ewing, 1992, 1995).

The generalised chemical formula for the pyrochlore supergroup is $A_2B_2X_6Y_1 \cdot pH_2O$, where: the *A*-site hosts Na, Ca, U, Y, Ce, other REEs, Th, or H_2O; the B-site typically hosts Ta, Nb, and Ti; *X* is typically O, but can include OH and F; *Y* is an anion, vacancy, H_2O, or large monovalent cation. Weathered pyrochlore supergroup minerals are commonly hydrated and deficient in A-site cations (Nasraoui and Waerenborgh, 2001). Only the B-site lacks deficiencies (Atencio et al., 2010). The groups are divided based on the predominant valence of B-site ions (Atencio et al., 2010). Generally, however, Nb-rich pyrochlore belongs to the pyrochlore group; Ta-rich pyrochlore belongs to the

microlite group; and Ti-rich pyrochlore belongs to the betafite group. The two other groups (Sb-rich romeite and W-rich elsmoreite) are rare in nature and not discussed here.

4.3 Columbite-tantalite solid solution series

Columbite ([Fe,Mn]Nb_2O_6) and tantalite ([Fe,Mn]Ta_2O_6) form a solid solution series of orthorhombic minerals (Černy and Ercit, 1989; Černy et al., 1992). These minerals tend to form prismatic, massive, or granular grains, commonly with striae on crystal surfaces or cleavage faces, and have subconcoidal to uneven fracture (Berry et al., 1983; Anthony et al., 2014). Columbite-tantalite series minerals have hardness 6 to 6 ½ and densities ranging from 5.2 to 8.0 g/cm^3 (Berry et al., 1983; Anthony et al., 2014). Columbite-tantalite are opaque except on thin edges, and are iron-black (tantalite-[Fe]), black to brown-black (columbite-[Fe] and columbite-[Mn]), or pink to nearly colourless (tantalite-[Mn]). Lustre is submetallic to vitreous and streak is black to black-brown or, in the case of tantalite-(Mn), red. Columbite-tantalite minerals commonly have red to reddish brown internal reflections in reflected light (Berry et al., 1983; Anthony et al., 2014).

The generalised chemical formula for columbite-tantalite is AB_2O_6 where *A* is Fe or Mn and *B* is Nb or Ta (Černy et al., 1992; Anthony et al., 2014). Compositionally, following Černy and Ercit (1989), classification is determined by Ta/(Ta+Nb) and Mn/(Mn+Fe) molar ratios. The different classifications are columbite-(Fe), columbite-(Mn), tantalite-(Fe), tantalite-(Mn). The $FeNb_2O_6$, $MnNb_2O_6$, $FeTa_2O_6$, and $MnTa_2O_6$ end-members form the columbite-tantalite series quadrilateral. Compositions approaching the $FeTa_2O_6$ end-member are tetragonal and termed tapiolite-(Fe) (Černy and Ercit, 1989; Černy et al., 1992). There is an empirically derived miscibility gap between tantalite-(Fe) and tapiolite-(Fe) (Černy et al., 1992). A solid solution exists between tapiolite-(Fe) and tapiolite-(Mn); however, Mn has limited substitution for Fe, typically less than 2.0% MnO (Wise and Černy, 1996; Ercit, 2010).

4.4 Methodology

Polished thin sections of samples collected at the Aley, Roadside, Upper Fir, Mount Grace, Verity, and Wicheeda carbonatites and polished grain mounts of concentrate from the Oka and St. Honoré carbonatites, Quebec, (Fig. 4.1 inset) were examined optically using transmitted and reflected light. Twenty-four polished thin sections and two polished grain mounts containing pyrochlore supergroup and columbite-tantalite minerals were selected for detailed study. Pyrochlore supergroup and columbite-tantalite series minerals were analysed by wavelength-dispersive X-ray spectrometry on a fully automated CAMECA SX-50 electron microprobe at the University of British Columbia using the following operating conditions: 15-kV excitation voltage; 20-nA beam current; 20-s peak count time; 10-s background count-time; and 5-μm spot diameter. Data reduction was done using the 'PAP' $\phi(\rho Z)$ method (Pouchou and Pichoir, 1985).

For electron microprobe analysis of pyrochlore and columbite-tantalite, the following standards, X-ray lines, and detector types were used: topaz, FKα, TAP; albite, NaKα, TAP; diopside, MgKα, TAP; orthoclase, AlKα, TAP; diopside, CaKα, PET; rutile, TiKα, LIF; synthetic rhodonite, MnKα, LIF; synthetic fayalite, FeKα, LIF; YPO_4, YLα, PET; columbite, NbLα, PET; barite, BaLα, LIF; $CePO_4$, CeLα, LIF; microlite, TaLα, LIF; ThO_2 glass, ThMα, PET; UO_2 glass, UMα, PET. Additionally, Zr was analysed in pyrochlore using a zircon standard, ZrLα line, and PET detector.

4.5 Results

For pyrochlore supergroup minerals, we obtained 313 new electron microprobe analyses from British Columbia carbonatites, 18 from Oka, and 18 St. Honoré; for the columbite-tantalite series minerals we obtained 157 electron microprobe analyses from British Columbia carbonatites. Representative analyses of pyrochlore supergroup and columbite-tantalite series minerals from the Aley, Lonnie, Mount Grace, Roadside, Upper Fir, Verity, Wicheeda, Oka, and St. Honoré carbonatites are shown in Tables 4.1 and 4.2, respectively. Complete analyses are in supplementary material (see Appendix A). Analyses of pyrochlore supergroup and columbite-tantalite series minerals from Canadian carbonatites are restricted to small regions of a pyrochlore Nb-Ti-Ta ternary diagram (Fig. 4.1) and a columbite-tantalite series quadrilateral (Fig. 4.2).

Table 4.1 Representative electron microprobe analyses for pyrochlore supergroup minerals. Oxides are in wt. %.

Deposit	Mount Grace	Roadside	Roadside	Upper Fir	Upper Fir	Upper Fir	Upper Fir	Upper Fir	Verity	Verity	Verity
Sample	MG5-3-11	BR64B-2	BR64B-21	BR1-1	BR1-21	BR1-27	BR19-17	BR19-22	VER08A-1	VER07-5	VER07-12
Al_2O_3	0.02	bd	bd	0.01	0.00	0.00	0.00	bd	0.01	bd	0.01
$Fe_2O_3^T$	0.07	0.36	0.3	0.03	0.05	0.06	0.03	0.13	0.06	0.58	0.35
MnO	bd	0.07	0.03	bd	0.01	0.06	0.05	0.03	0.01	0.04	0.00
MgO	0.02	0.00	0.02	0.02	0.00	0.02	0.01	0.01	0.00	0.02	0.03
CaO	10.21	11.09	9.85	13.32	12.74	12.70	8.55	8.64	15.63	12.32	11.86
Na_2O	6.54	5.40	5.08	6.82	6.52	6.59	5.03	5.95	6.76	6.72	6.76
TiO_2	0.87	4.41	6.16	1.84	2.21	2.16	4.96	4.78	2.92	2.54	2.27
Y_2O_3	bd	bd	0.04	0.04	bd	bd	0.01	bd	bd	bd	0.07
Nb_2O_5	64.02	45.01	35.88	56.49	50	50.72	42.84	42.11	66.16	55.19	57.60
Ta_2O_5	6.10	16.26	22.71	14.02	21.61	21.77	16.99	18.86	1.72	12.12	10.54
Ce_2O_3	1.71	0.71	0.41	0.30	0.48	0.43	bd	0.22	0.38	0.48	0.60
BaO	bd	0.14	0.09	0.01	0.00	0.08	bd	0.07	0.12	0.16	bd
ZrO_2	bd	bd	bd	bd	bd	0.00	0.08	0.03	bd	0.07	bd
ThO_2	1.40	0.12	0.29	1.30	0.91	0.96	0.17	0.24	0.20	0.10	0.04
UO_2	3.12	12.99	16.26	0.48	1.39	1.46	17.00	16.33	bd	5.23	5.76
F	5.18	2.55	1.74	6.05	5.36	5.40	2.09	2.19	7.08	4.85	4.99
O=F	2.18	1.07	0.73	2.54	2.25	2.27	0.88	0.92	2.98	2.03	2.09
Total	97.07	98.00	98.08	98.19	99.03	100.15	96.92	98.65	98.06	98.32	98.75
A.p.f.u. based on 2 B-site cations											
Mn^{2+}	-	0.00	0.00	-	0.00	0.00	0.00	0.00	0.00	0.00	0.00
Mg^{2+}	0.00	0.00	0.00	0.00	0.00	0.00	0.00	0.00	0.00	0.00	0.00
Ca^{2+}	0.43	0.67	0.67	0.55	0.56	0.55	0.55	0.55	0.57	0.56	0.53
Na^{+}	0.49	0.59	0.62	0.51	0.52	0.52	0.59	0.69	0.44	0.56	0.55
Ba^{2+}	0.00	0.00	0.00	0.00	0.00	0.00	-	0.00	0.00	0.00	-
Ce^{3+}	0.02	0.01	0.01	0.00	0.01	0.01	-	0.00	0.00	0.01	0.01
Th^{4+}	0.01	0.00	0.00	0.01	0.01	0.01	0.00	0.00	0.00	0.00	0.00
U^{4+}	0.03	0.16	0.23	0.00	0.01	0.01	0.23	0.22	-	0.05	0.05
Y^{3+}	-	-	0.00	0.00	-	-	0.00	-	-	-	0.00
Σ A	0.98	1.46	1.54	1.07	1.11	1.1	1.37	1.47	1.02	1.18	1.15
Al^{3+}	0.00	-	-	0.00	0.00	0.00	0.00	-	0.00	-	0.00
Fe^{3+}	0.00	0.02	0.02	0.00	0.00	0.00	0.00	0.01	0.00	0.03	0.02
Nb^{5+}	1.85	1.43	1.19	1.66	1.5	1.5	1.39	1.37	1.83	1.63	1.68
Ta^{5+}	0.11	0.31	0.45	0.25	0.39	0.39	0.33	0.37	0.03	0.22	0.19
Ti^{4+}	0.04	0.23	0.34	0.09	0.11	0.11	0.27	0.26	0.13	0.12	0.11
Zr^{4+}	-	-	-	-	-	0.00	0.00	0.00	-	0.00	0.00
Σ B	2	2	2	2	2	2	2	2	2	2	2

Total Fe expressed as $Fe_2O_3^T$; bd = below detection

Table 4.1 continued.

Deposit Sample	Wicheeda WI53A-4	Wicheeda WI53A-17	Wicheeda WI53A-20	Lonnie LO24BB-1	Lonnie LO09X-27	Lonnie LO24B-3	Lonnie LO10A-19	Aley AL74-1	Aley AL74-24	Aley AL67-3	Aley AL67-18
Al_2O_3	0.01	0.02	0.01	0.01	0.00	0.03	0.00	0.00	0.02	bd	0.03
$Fe_2O_3^T$	0.16	0.20	0.73	0.04	0.26	bd	bd	0.07	1.08	0.95	0.95
MnO	0.06	0.03	0.06	0.05	0.03	0.03	0.00	0.02	0.05	bd	0.04
MgO	0.01	bd	0.01	0.02	0.00	0.02	0.00	0.02	0.07	0.00	0.05
CaO	15.24	15.39	10.48	12.31	11.17	13.87	13.26	15.17	15.94	14.34	13.10
Na_2O	6.20	5.98	3.74	6.79	6.88	5.40	7.68	7.22	0.03	6.29	5.53
TiO_2	7.13	6.68	10.09	3.01	4.73	4.64	1.56	3.32	3.34	0.56	1.37
Y_2O_3	bd	bd	bd	0.00	0.04	bd	0.06	bd	0.04	bd	bd
Nb_2O_5	58.16	58.61	55.94	65.04	59.24	63.52	70.20	66.81	72.88	64.20	61.61
Ta_2O_5	0.26	0.30	0.58	0.00	1.49	0.72	0.13	0.33	0.53	1.58	3.62
Ce_2O_3	0.88	1.01	1.28	2.80	3.82	1.29	1.42	0.24	0.62	0.92	0.66
BaO	bd	bd	0.59	0.00	0.06	0.07	bd	bd	0.03	bd	bd
ZrO_2	1.62	1.25	2.86	0.00	0.00	bd	bd	0.02	0.08	3.02	bd
ThO_2	2.38	3.46	2.48	0.57	4.69	0.26	0.30	0.75	0.17	3.07	2.22
UO_2	1.49	0.44	2.00	0.99	0.05	4.20	bd	0.08	0.11	0.01	0.03
F	6.36	6.39	3.64	6.06	5.18	3.95	4.75	4.49	0.56	4.01	3.39
O=F	2.67	2.68	1.53	2.54	2.18	1.66	1.99	1.89	0.24	1.68	1.42
Total	97.26	97.05	92.90	95.14	95.43	96.32	97.38	96.64	95.19	97.16	91.08
A.p.f.u. based on 2 B-site cations											
Mn^{2+}	0.00	0.00	0.00	0.00	0.00	0.00	0.00	0.00	0.00	-	0.00
Mg^{2+}	0.00	0.00	0.00	0.00	0.00	0.00	0.00	0.00	0.01	0.00	0.00
Ca^{2+}	0.58	0.59	0.37	0.49	0.49	0.66	0.60	0.70	0.82	0.68	0.66
Na^{+}	0.43	0.41	0.24	0.48	0.55	0.46	0.62	0.61	0.00	0.54	0.51
Ba^{2+}	-	-	0.01	0.00	0.00	0.00	-	-	0.00	-	-
Ce^{3+}	0.01	0.01	0.02	0.04	0.06	0.02	0.02	0.00	0.01	0.01	0.01
Th^{4+}	0.02	0.03	0.02	0.00	0.04	0.00	0.00	0.01	0.00	0.03	0.02
U^{4+}	0.01	0.00	0.01	0.01	0.00	0.04	-	0.00	0.00	0.00	0.00
Y^{3+}	-	-	-	0.00	0.00	-	0.00	-	0.00	-	-
Σ A	1.06	1.05	0.66	1.02	1.15	1.19	1.25	1.33	0.84	1.27	1.21
Al^{3+}	0.00	0.00	0.00	0.00	0.00	0.00	0.00	0.00	0.00	-	0.00
Fe^{3+}	0.01	0.01	0.03	0.00	0.01	0.00	0.00	0.00	0.04	0.04	0.05
Nb^{5+}	1.61	1.64	1.44	1.85	1.73	1.77	1.93	1.84	1.80	1.81	1.82
Ta^{5+}	0.00	0.01	0.01	0.00	0.03	0.01	0.00	0.01	0.01	0.03	0.06
Ti^{4+}	0.33	0.31	0.43	0.14	0.23	0.22	0.07	0.15	0.14	0.03	0.07
Zr^{4+}	0.05	0.04	0.08	0.00	0.00	-	-	0.00	0.00	0.09	-
Σ B	2	2	2	2	2	2	2	2	2	2	2

Total Fe expressed as $Fe_2O_3^T$; bd = below detection

Table 4.1 continued.

Deposit Sample	Oka OKA-10	Oka OKA-5	Oka OKA-8	St. Honoré NIOB-10	St. Honoré NIOB-2	St. Honoré NIOB-3
Al_2O_3	0.05	0.05	0.03	bd	0.01	bd
$Fe_2O_3^T$	1.51	1.65	2.64	0.10	0.60	1.58
MnO	0.25	0.24	0.19	0.04	0.32	0.35
MgO	0.00	0.04	0.12	0.00	0.02	bd
CaO	14.94	14.94	16.00	14.26	15.87	15.08
Na_2O	5.00	5.09	4.96	6.89	2.31	3.65
TiO_2	3.34	3.51	0.51	2.55	3.70	3.54
Y_2O_3	bd	bd	0.03	bd	bd	0.02
Nb_2O_5	60.38	59.36	63.26	64.16	62.78	66.20
Ta_2O_5	bd	0.06	0.11	bd	1.15	0.76
Ce_2O_3	6.66	7.36	5.25	0.71	0.75	0.39
BaO	0.01	0.04	0.17	0.13	0.54	0.06
ZrO_2	0.72	0.68	0.18	2.62	0.16	0.39
ThO_2	0.04	0.10	0.12	1.82	0.34	0.49
UO_2	bd	bd	bd	0.03	0.63	0.37
F	3.69	4.28	3.97	5.18	2.30	3.22
O=F	1.55	1.80	1.67	2.17	0.97	1.35
Total	96.44	97.23	97.26	98.47	91.44	95.94
A.p.f.u. based on 2 B-site cations						
Mn^{2+}	0.01	0.01	0.01	0.00	0.01	0.01
Mg^{2+}	0.00	0.00	0.01	0.00	0.00	-
Ca^{2+}	0.77	0.74	0.82	0.62	0.86	0.70
Na^{+}	0.47	0.46	0.46	0.55	0.23	0.30
Ba^{2+}	0.00	0.00	0.00	0.00	0.01	0.00
Ce^{3+}	0.12	0.12	0.09	0.01	0.01	0.01
Th^{4+}	0.00	0.00	0.00	0.02	0.00	0.00
U^{4+}	-	-	-	0.00	0.01	0.00
Y^{3+}	-	-	0.00	-	-	0.00
Σ A	1.36	1.33	1.39	1.20	1.13	1.03
Al^{3+}	0.00	0.00	0.00	-	0.00	-
Fe^{3+}	0.07	0.07	0.11	0.00	0.03	0.06
Nb^{5+}	1.75	1.73	1.84	1.80	1.77	1.76
Ta^{5+}	-	0.00	0.00	-	0.02	0.01
Ti^{4+}	0.16	0.17	0.02	0.12	0.17	0.16
Zr^{4+}	0.02	0.02	0.01	0.08	0.00	0.01
Σ B	2	2	2	2	2	2

Total Fe expressed as $Fe_2O_3^T$; bd = below detection

Table 4.2 Representative electron microprobe analyses for columbite-tantalite series minerals. Oxides are in wt. %.

Deposit	Roadside	Roadside	Roadside	Roadside	Upper Fir	Upper Fir	Upper Fir	Upper Fir
Sample#	BR64B-6	BR64B-9	BR64B-26	BR64B-30	BR43-20	BR1-8	BR1-16	BR02A-10
Al_2O_3	0.01	bd	bd	bd	0.01	0.01	0.00	0.00
FeO^T	14.10	14.12	14.22	13.06	12.83	15.62	15.19	14.40
MnO	0.61	0.68	0.63	0.87	1.25	1.38	1.30	1.31
MgO	3.65	3.55	3.29	3.61	3.87	2.21	2.26	2.08
CaO	0.01	0.07	0.05	0.00	0.07	0.08	0.03	0.07
Na_2O	bd	0.01	0.02	0.01	bd	bd	0.01	bd
TiO_2	2.17	2.19	2.32	1.44	1.58	1.18	1.15	1.39
Y_2O_3	0.01	bd	bd	bd	0.02	bd	bd	bd
Nb_2O_5	73.25	76.06	71.45	69.70	75.59	73.73	74.41	63.34
Ta_2O_5	6.38	4.83	8.15	11.79	4.82	5.70	6.10	17.76
Ce_2O_3	bd	0.18	bd	bd	bd	bd	0.01	bd
BaO	bd	0.07	0.12	bd	0.04	bd	bd	bd
ThO_2	bd	bd	bd	0.11	bd	0.07	bd	bd
UO_2	bd	bd	0.01	bd	0.10	0.05	bd	0.06
F	0.05	bd	0.05	0.04	bd	0.01	bd	0.11
O=F	0.02	0.00	0.02	0.02	0.00	0.01	0.00	0.05
Total	100.23	101.76	100.25	100.56	100.18	100.01	100.47	100.37
Al^{3+}	0.00	-	-	-	0.00	0.00	-	-
Fe^{2+}	0.65	0.64	0.66	0.62	0.59	0.73	0.71	0.71
Ca^{2+}	0.00	0.00	0.00	0.00	0.00	0.00	0.00	0.00
Na^{+}	-	0.00	0.00	0.00	-	-	0.00	-
Mn^{2+}	0.03	0.03	0.03	0.04	0.06	0.07	0.06	0.07
Mg^{2+}	0.30	0.29	0.27	0.30	0.32	0.18	0.19	0.18
Ce^{3+}	-	0.01	-	-	-	-	0.00	-
Th^{4+}	-	-	-	0.00	-	0.00	-	-
U^{4+}	-	-	0.00	-	0.00	0.00	-	-
Ba^{2+}	-	0.00	0.00	-	0.00	-	-	-
Y^{3+}	0.00	-	-	-	0.00	-	-	-
Nb^{5+}	9.18	9.34	9.03	8.91	9.42	9.37	9.41	8.40
Ta^{5+}	0.48	0.36	0.62	0.91	0.36	0.44	0.46	1.42
Ti^{4+}	0.18	0.18	0.20	0.12	0.13	0.10	0.10	0.12
Mn/(Mn+Fe)	0.042	0.046	0.043	0.063	0.090	0.082	0.080	0.084
Ta/(Ta+Nb)	0.050	0.037	0.064	0.092	0.037	0.044	0.047	0.144

Total Fe expressed as $Fe_2O_3^T$; bd = below detection

Table 4.2 Continued.

Deposit	Lonnie	Lonnie	Aley	Aley	Aley	Aley
Sample#	LO13-21	LO13-7	AL63-3	AL58-14	AL61-16	AL68-9
Al_2O_3	0.01	bd	0.01	0.01	bd	0.01
FeO^T	19.13	19.27	20.15	25.93	19.98	19.92
MnO	0.70	1.47	0.20	0.61	0.66	0.91
MgO	0.55	0.43	0.13	0.19	0.58	0.06
CaO	0.05	bd	0.65	0.05	1.58	0.52
Na_2O	0.02	0.00	0.05	0.01	0.03	0.01
TiO_2	2.05	1.97	0.70	0.97	5.12	4.16
Y_2O_3	0.15	bd	0.04	0.04	bd	bd
Nb_2O_5	78.39	78.40	72.74	69.47	61.79	69.35
Ta_2O_5	0.45	0.53	0.01	0.47	0.43	bd
Ce_2O_3	0.01	0.02	bd	0.06	2.73	0.21
BaO	bd	bd	0.13	0.01	0.03	bd
ThO_2	0.02	0.00	0.57	0.23	0.36	1.77
UO_2	bd	bd	0.05	0.02	0.01	0.15
F	0.07	bd	0.31	bd	0.77	0.21
O=F	0.03	0.00	0.13	0.00	0.32	0.09
Total	98.12	102.12	95.31	98.06	92.98	96.97
A.p.f.u based on 6 oxygen atoms						
Al^{3+}	0.00	-	0.00	0.00	-	0.00
Fe^{2+}	0.87	0.88	0.99	1.26	1.00	0.96
Ca^{2+}	0.00	-	0.04	0.00	0.10	0.03
Na^{+}	0.00	0.00	0.01	0.00	0.00	0.00
Mn^{2+}	0.03	0.07	0.01	0.03	0.03	0.04
Mg^{2+}	0.04	0.03	0.01	0.02	0.05	0.01
Ce^{3+}	0.00	0.00	-	0.00	0.18	0.01
Th^{4+}	0.00	0.00	0.02	0.01	0.01	0.05
U^{4+}	0.00	0.00	0.00	0.00	0.00	0.00
Ba^{2+}	-	-	0.00	0.00	0.00	-
Y^{3+}	0.00	-	0.00	0.00	-	-
Nb^{5+}	9.69	9.67	9.66	9.14	8.33	9.04
Ta^{5+}	0.03	0.04	0.00	0.04	0.03	-
Ti^{4+}	0.17	0.16	0.06	0.09	0.46	0.36
Mn/(Mn+Fe)	0.036	0.072	0.010	0.023	0.032	0.044
Ta/(Ta+Nb)	0.003	0.004	0.000	0.004	0.0047	0.00

Total Fe expressed as $Fe_2O_3^T$; bd = below detection

Pyrochlore supergroup minerals from the Upper Fir and Roadside carbonatites plot with >40% Nb, ≤35% Ti, and <40% Ta on a Nb-Ti-Ta ternary diagram (Fig. 4.1). Those from the Verity carbonatite plot with >75% Nb, <10% Ti, and <20% Ta. The analyses from the Wicheeda, Lonnie, Aley, Oka, and St. Honoré carbonatites plot with >70% Nb, <30% Ti, and <5% Ta, whereas pyrochlore from Mount Grace have <10% Ta. The analyses presented above fall within the pyrochlore group field, with some from Upper Fir approaching the microlite field.

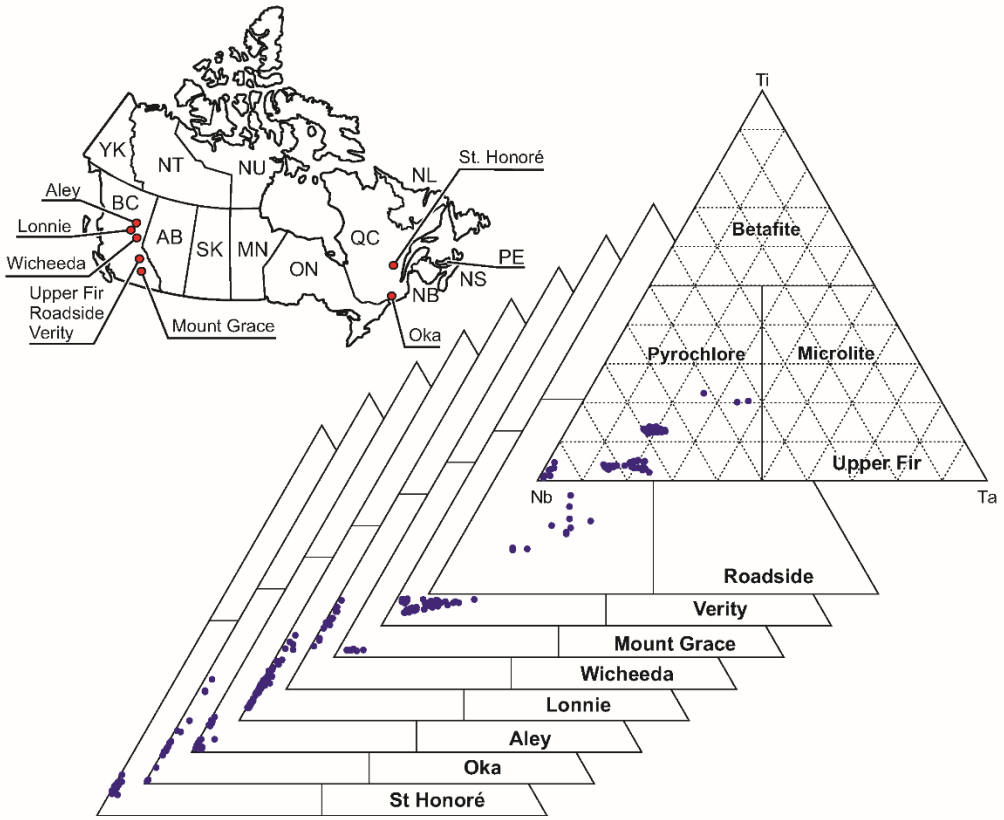

Figure 4.1 Chemical compositions of pyrochlore supergroup minerals from the Upper Fir, Roadside, Verity, Mount Grace, Wicheeda, Lonnie, Aley, Oka, and St. Honoré carbonatites plotted on Nb-Ti-Ta ternary diagrams. Solid lines bound the pyrochlore, betafite, and microlite fields as defined by Atencio et al. (2010). Inset map of Canada shows the location of carbonatite occurrences.

Columbite-tantalite series minerals from the Upper Fir carbonatite have Ta/(Ta+Nb) ratios ≤0.15 and Mn/(Mn+Fe) ratios <0.1125 (Fig. 4.2). Those from the Aley carbonatite

have Ta/(Ta+Nb) ratios of <0.0125 and Mn/(Mn+Fe) ratios of <0.15. Columbite-(Fe) from the Lonnie carbonatite have Ta/(Ta+Nb) ratios of <0.0125 and Mn/(Mn+Fe) ratios between 0.0375 and 0.075.

4.6 Discussion

We combine our new data with analyses from the world literature (Appendix A; supplementary material) to generate diagrams that discriminate between minerals from carbonatites (e.g. St. Honoré), peralkaline complexes (e.g. Lovozero), LCT pegmatites (e.g. Greenbushes), and peraluminous granites (e.g. Beauvoir granite) as defined in Chapter 2.

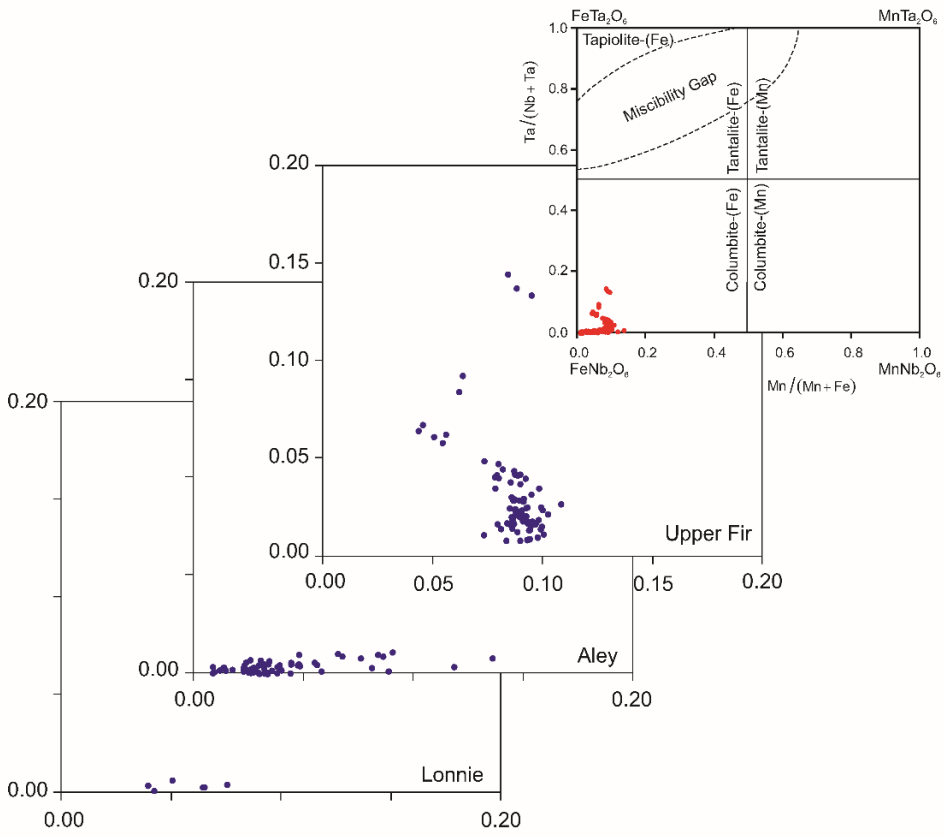

Figure 4.2 Chemical compositions of columbite-(Fe) from the Upper Fir, Aley, and Lonnie carbonatites. Inset shows the full columbite-tantalite series quadrilateral with all new analyses from Upper Fir, Aley, and Lonnie (red dots). Mineral classification is according to Černy and Ercit (1985) and Černy and Ercit (1989). The empirically derived tantalite-tapiolite miscibility gap is from Černy et al. (1992).

4.6.1 Pyrochlore supergroup Nb-Ti-Ta ternary diagrams

Analyses of pyrochlore supergroup minerals from British Columbia and Quebec (Fig. 4.1) were combined with data compiled from the literature (Appendix A) in ternary Nb-Ti-Ta diagrams (Fig. 4.3a-d). Carbonatite-hosted deposits contain predominantly pyrochlore group minerals (>35% Nb, <65% Ti, and <45% Ta; Fig. 4.3a). Only 2 out of 1007 analyses, one each from the Oka (Canada) and Amba Dongar (India) carbonatite complexes have betafite composition. The composition of pyrochlore from peralkaline complexes is constrained to a narrow zone paralleling the Nb-Ti join (>40% Nb, <60% Ti, and <10% Ta; Fig. 4.3b). Only 2 out of 92 analyses, one from the Lovozero (Russia) and the other from Mont Saint-Hilaire (Canada), plot in the betafite group field. Nb-Y-F (NYF) enriched pegmatites, as defined by Černy (1991a) and Černy and Ercit (2005), are grouped with peralkaline intrusions based on their spatial and genetic affinity.

Pyrochlore supergroup minerals from LCT pegmatites occupy the microlite field (<90% Nb, ≤40% Ti, and > 15% Ta; Fig. 4.3c) and are characterized by the highest Ta/Nb ratio (average of 15 for analyses in our database) for the major specialty metal deposit types. Two of the analyses from pegmatites lie near the Nb-apex (Fig. 4.3c). These highly atypical analyses come from the metasomatic zone of the Varutrask petalite-subtype granitic pegmatite, where pyrochlore is present as microscopic patches and veinlets reflecting the Ta/(Ta+Nb) ratio of columbite-tantalite series minerals from which they were derived (Černy et al. 2004). Six of the analyses from pegmatites are from the Tordal pegmatite (Norway), which is classified as a mixed LCT+NYF family pegmatite (Bergstol and Juve 1988; Černy and Ercit 2005). One analysis plots in the betafite field, while the rest broadly overlap with those from LCT pegmatites (Fig. 4.3c). Historically, using the traditional Hogarth (1977) classification, betafite group minerals were commonly reported from pegmatites and, less commonly, in carbonatite and peralkaline complexes. However, using the CNMNC-IMA approved pyrochlore supergroup classification of Atencio et al. (2010), betafite is extremely rare.

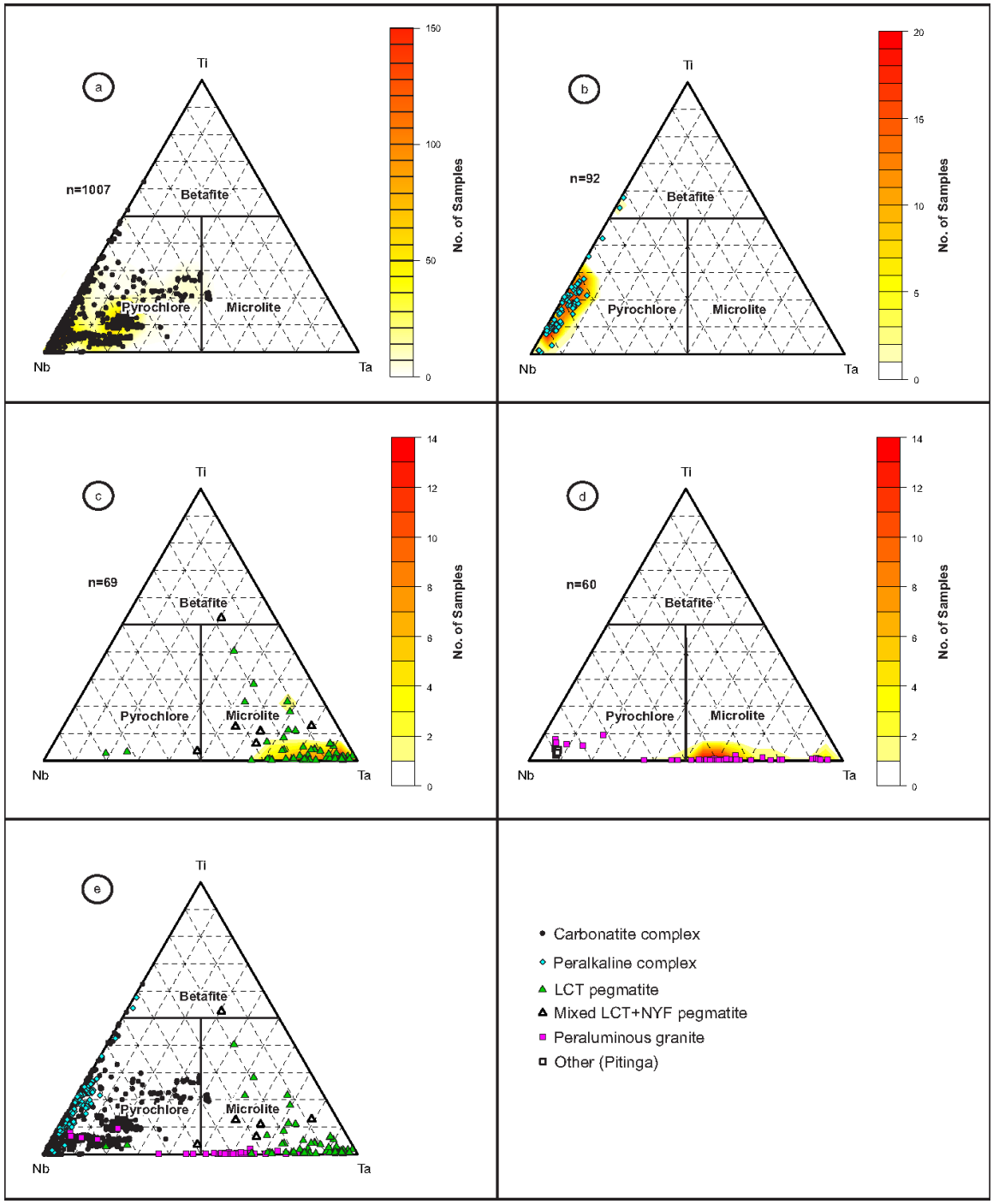

Figure 4.3 Chemical compositions of pyrochlore supergroup minerals from (a) British Columbia and Quebec carbonatites supplemented by those of pyrochlore supergroup minerals from other North and South American, African, European, and Asian carbonatite complexes; (b) peralkaline complexes; (c) LCT pegmatites; (d) peraluminous granites; and (e) a synthesis of all of the above data. Contour shading refers to number of data points per unit area. Sources for the worldwide data compilation are in Appendix A.

.

Pyrochlore from peraluminous granites occupy a narrow area of the microlite field along the Nb-Ta join and extend slightly into the pyrochlore field (<65% Nb, <10% Ti, and >35% Ta; Fig. 4.3d). Six pyrochlore analyses ('Other' in Fig. 4.3d) from the Pitinga deposit (Brazil) plot near the Nb-rich apex of the ternary diagram. These minerals are hosted by a peralkaline unit within a predominantly peraluminous granite complex (Nardi et al. 2012). Pyrochlore from the Cinovec-Zinnwald granite (Czech Republic-Germany) have high Nb content (>70%), and plot near the Nb-rich apex of the pyrochlore group field. These minerals are found as micro inclusions (<100 μm in diameter) in mica and contain up to 10.1 wt. % silica (Johan and Johan 1994). Because of their small size, these minerals are unlikely to be recovered as indicator minerals using traditional hand-picking.

4.6.2 Columbite-tantalite quadrilateral

New electron microprobe columbite-tantalite series analyses from British Columbia carbonatites (Fig. 4.2; Table 4.2) were combined with data from deposits listed in Appendix A and plotted on the columbite-tantalite series quadrilateral (Fig. 4.4). The columbite-tantalite series minerals from carbonatite-hosted deposits plot near the $FeNb_2O_6$ corner, with Mn/(Mn+Fe) and Ta/(Ta+Nb) ratios of ≤0.25 and ≤0.20, respectively. Columbite-tantalite minerals from peralkaline complexes plot along the $FeNb_2O_6$–$MnNb_2O_6$ join of the quadrilateral and have Mn/(Mn+Fe) ratios of ≤0.65. LCT pegmatites and peraluminous granites contain all varieties of columbite-tantalite as well as tapiolite-(Fe).

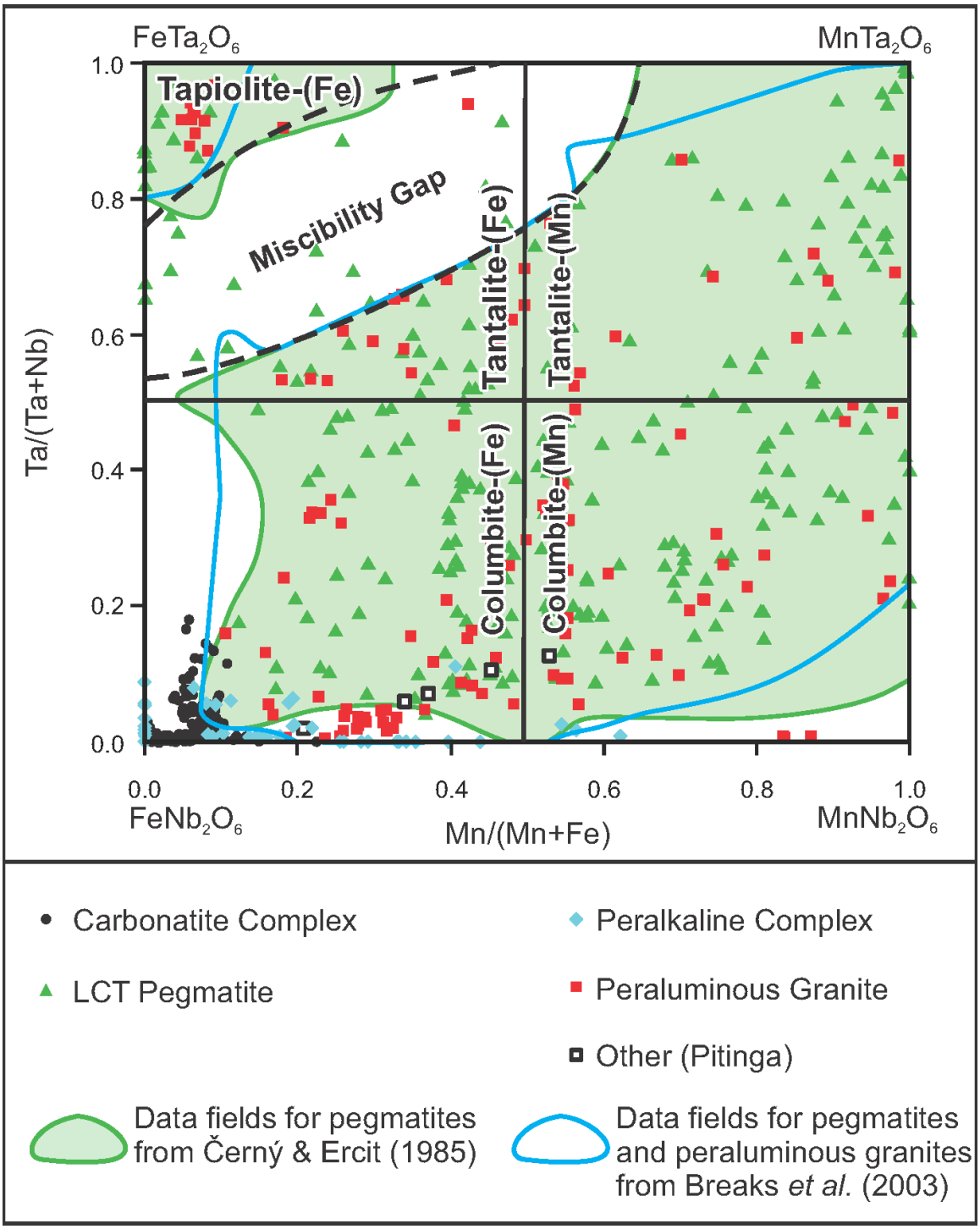

Figure 4.4 Chemical composition of columbite-tantalite minerals from British Columbia carbonatites supplemented by data available from other carbonatite complexes, LCT pegmatites, peralkaline complexes, and peraluminous granites. Sources for the worldwide data compilation are in Appendix A.

4.6.3 Discrimination diagrams

From the combined pyrochlore supergroup (Fig. 4.3) and columbite-tantalite series (Fig. 4.4) data-sets two discrimination diagrams were generated (Figs 4.5 and 4.6). The discrimination diagram for the pyrochlore supergroup shows minerals from carbonatite and peralkaline complexes plotting distinctly from LCT pegmatites and peraluminous granites (Fig. 4.5). The compositional overlap of pyrochlore from carbonatite and peralkaline complexes is expected because of the close association of carbonatite and peralkaline occurrences, which are commonly in the same intrusive complex. Similarly, overlap exists between the composition of microlite from LCT pegmatite and peraluminous granite (Fig. 4.5) as these intrusions are genetically related (Černy, 1991a, b; Černy and Ercit, 2005; Martin, 2007).

The columbite-tantalite series discrimination diagram (Fig. 4.6) shows overlap between compositions of columbite from peraluminous granites and LCT pegmatites; however, tapiolite-(Fe) is commonly found in pegmatites and is rare in peraluminous granites (Fig. 4.6). There is a minor overlap between the fields from carbonatites, peralkaline complexes, LCT pegmatites, and peraluminous granites near the FeNb2O6 corner of the quadrilateral. The compositional fields for columbite-tantalite series minerals from peraluminous granites and LCT pegmatites largely overlap.

These discrimination diagrams can be used individually. However, if a given sample contains both pyrochlore supergroup and columbite-tantalite series minerals, then the effect of the compositional overlaps can be mitigated by using both discrimination diagrams simultaneously. For example, a columbite-(Fe) grain plotting in the overlap between the LCT pegmatite and carbonatite-related fields (star in Fig. 4.6) does not provide a definitive answer regarding the deposit type it was sourced from. However, if the same sample contains a pyrochlore grain with a carbonatite signature (star in Fig. 4.5), then both minerals were probably derived from a carbonatite or carbonatite-related deposit.

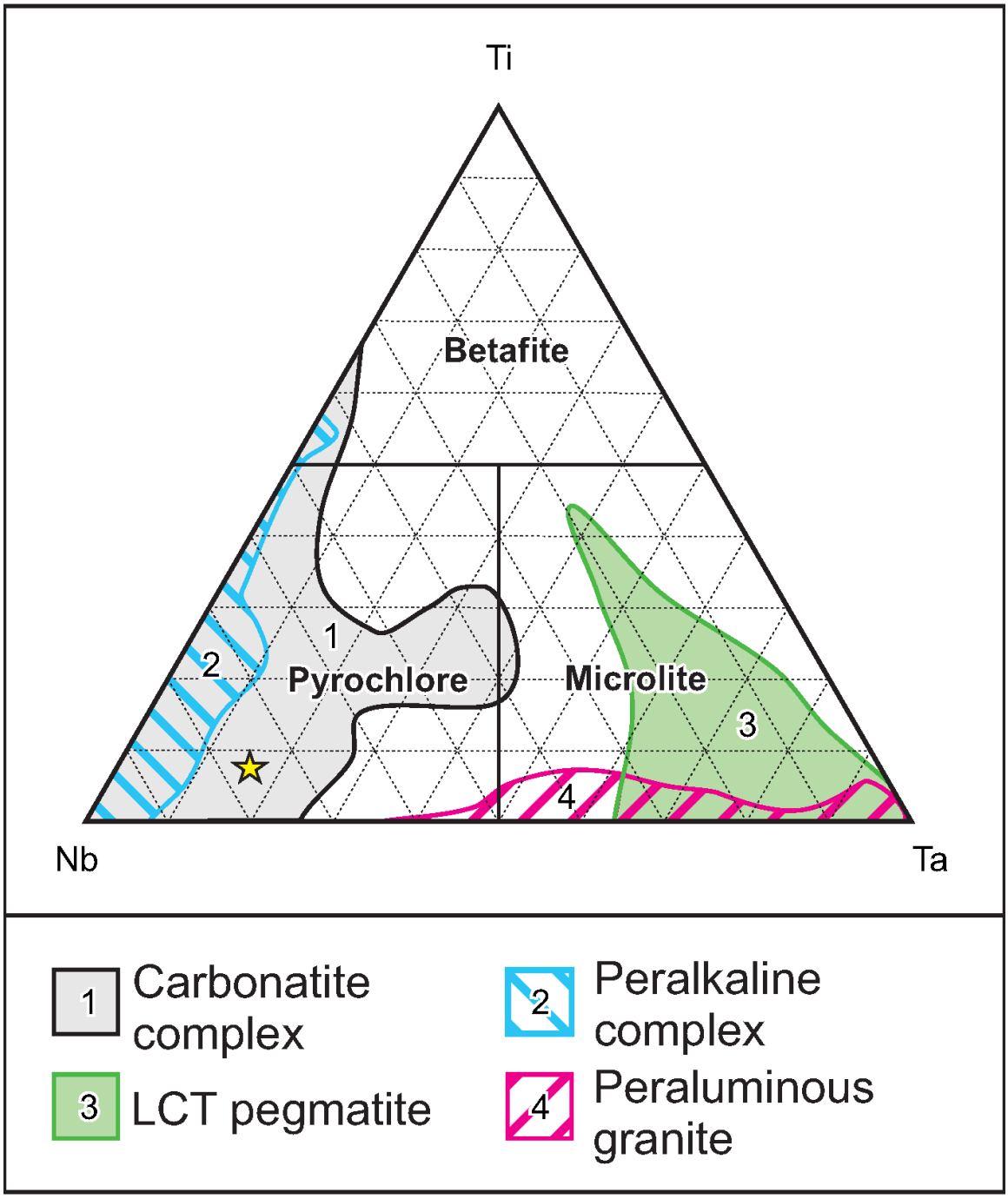

Figure 4.5 Discrimination diagram for the pyrochlore supergroup minerals from carbonatite complexes, peraluminous granites, LCT pegmatites, and peralkaline complexes. The yellow star denotes the composition of a pyrochlore grain from a hypothetical sample. A corresponding columbite-(Fe) grain from the same sample is denoted by a yellow star in Fig. 4.6.

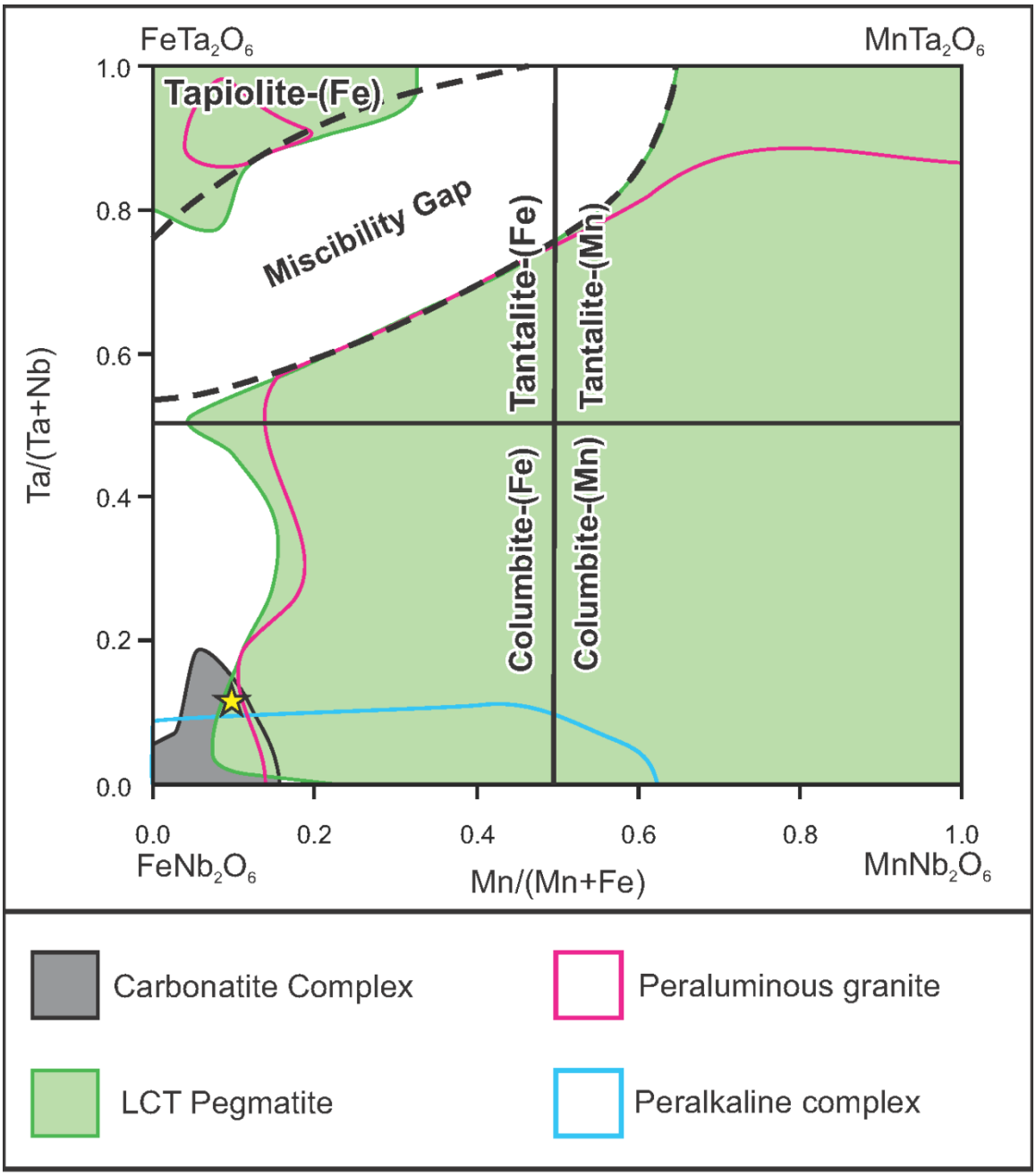

Figure 4.6 Discrimination diagram for minerals belonging to columbite-tantalite series from carbonatite complexes, peraluminous granites, LCT pegmatites, and peralkaline complexes.

4.7 Conclusions

Pyrochlore supergroup and columbite-tantalite series minerals can be used as indicators to explore for specialty metal deposits. Discrimination diagrams based the composition of these minerals can aid deposit targeting and vectoring towards mineralization. The compositional fields for pyrochlore supergroup minerals from carbonatite and peralkaline complexes partially overlap. The fields for LCT pegmatites and peraluminous granites also partially overlap but plot discretely from carbonatite and peralkaline complexes. The effectiveness of the discrimination diagrams increases if both pyrochlore supergroup and columbite-tantalite series minerals coexist in the same samples, reducing uncertainty related to overlaps between deposit-specific fields.

5 Conclusions

- Carbonatite complexes are the main sources of Nb and ferroniobium. At present, more than 90% of Nb mine production comes from Brazil, with the balance from the St. Honoré carbonatite (Canada) and loparite concentrate from the Lovozero peralkaline complex (Russia). Carbonatite related deposits are also the main source of REE and prospective Ta targets. For these reasons, carbonatites are highly sought after exploration and development targets.

- The use of pXRF in exploration for specialty metals permits identification of the ideal stream sediment size fraction and help select samples for detailed indicator mineral studies. Stream sediment orientation surveys at the Aley, Wicheeda, and Lonnie carbonatites determined that the 125-250 µm size fraction is ideal for carbonatite exploration. The 125-250 µm size fraction of stream sediments was selected based on elevated concentration of carbonatite pathfinder elements (Nb, Ta, LREE, Y, U, Th) determined by pXRF. This size fraction also contained enough material of an ideal grain size for further indicator mineral studies.

- QEMSCAN® provides quantitative results in indicator mineral weight percent and mineral count, mineral grain size distribution, proportions of mineral associations in compound grains, and proportions of monomineralic (liberated) grains to compound grains, with no additional processing. No quantitative information (with the exception of grain count) is provided by traditional indicator mineral methods. Where pXRF analysis of stream sediments suggests low concentrations of indicator minerals, processing using a Mozley C800 laboratory mineral separator prior to QEMSCAN® analysis is recommended.

- Indicator mineral surveys are an effective method to explore for covered and poorly exposed carbonatite-related deposits. Discrimination diagrams based on major element composition of pyrochlore supergroup (Nb, Ta, and Ti) and columbite-

tantalite series (Nb, Ta, Fe, and Mn) indicator minerals identify the deposit types from which these minerals are derived.

Pyrochlore supergroup minerals from carbonatites and related deposits occupy the pyrochlore field and extend slightly into the betafite and microlite fields (>35% Nb, <65% Ti, and <45% Ta). Those from peralkaline complexes define a narrow zone paralleling the Nb-Ti join (>40% Nb, <60% Ti, and <10% Ta). Pyrochlore supergroup minerals from LCT pegmatites occupy the microlite field (<90% Nb, ≤40% Ti, and >15% Ta) whereas those from peraluminous granites plot in the microlite field along the Nb-Ta join, extending slightly into the pyrochlore field (<65% Nb, <10% Ti, and >35% Ta) on the Nb-Ti-Ta ternary diagram. The compositional fields for pyrochlore supergroup minerals from carbonatite and peralkaline complexes partially overlap. The fields for LCT pegmatites and peraluminous granites also partially overlap but plot discretely from carbonatite and peralkaline complexes.

Columbite-tantalite series minerals from carbonatites and related deposits are Nb-rich, with Mn/(Mn+Fe) and Ta/(Ta+Nb) atomic ratios ≤0.25 and ≤0.20, respectively. Columbite from peralkaline complexes plot along the $FeNb_2O_6$–$MnNb_2O_6$ join of the quadrilateral and have Mn/(Mn+Fe) ratios of ≤0.65 and Ta/(Ta+Nb) ratios of ≤0.15. Fe-Nb-rich varieties within this zone slightly overlap with those from carbonatites. Columbite-tantalite series minerals from Li-Cs-Ta (LCT) pegmatites and peraluminous granites are not well constrained but do slightly overlap with columbite-(Fe) from carbonatites. A minor overlap exists between the fields from carbonatites, peralkaline complexes, LCT pegmatites, and peraluminous granites near the columbite-(Fe) corner of the quadrilateral.

Future work:

Further work on the trace element composition of pyrochlore supergroup and columbite-tantalite series minerals using laser ablation, ICP-MS analysis could further discriminate minerals from carbonatite complex-, peralkaline complex-, LCT pegmatite-, and peraluminous granite-related deposits. Extensive analysis would be required as complete trace element analysis is lacking for many deposits and deposit types in the literature.

Bibliography

Abdalla, H.M., Helba, H.A., and Mohamed, F.H., 1998. Chemistry of columbite-tantalite minerals in rare metal granitoids, Eastern Desert, Egypt. Mineralogical Magazine, 62, 821–836.

Advanced Metallurgical Group, 2013. AMG advanced metallurgical group N.V. announces tantalum mineral resources update at Volte Grande mine. http://www.amg-nv.com/Investors/Press-Releases/Press-Release-Details/2013/AMG-Advanced-Metallurgical-Group-NV-Announces-Tantalum-Mineral-Resources-Update-at-Volte-Grande-Mine/default.aspx. Accessed 11 Dec 2013.

Ali, M. A., 2013. Mineral Chemistry and genesis Of Zr, Th, U, Nb, Pb, P, Ce and F enriched peralkaline granites of El-Sibai shear zone, central Eastern Desert, Egypt. Geologija, 56, 107-128.

Alkane Resources Ltd., 2013. Dubbo project overview. http://www.alkane.com.au/index.php/projects/current-projects/dubbo. Accessed 11 Dec 2013.

Allsopp, H.L. and Hargraves, R.B., 1985. Rb–Sr ages and palaeomagnetic data for some Angolan alkaline intrusives. Transactions of the Geological Society of South Africa, 88:295–299.

ALS Limited 2015. Service Schedule. ALS Limited (Vancouver), Canada. www.alsglobal.com/~/media/Files/Divisions/Minerals/Geochemistry/Geochemistry%20Resources/Services%20Schedules/ALS-Geochemistry-Service-Schedule-2015-CAD.pdf. Accessed 15 Jan 2015.

Anglo American PLC, 2014. Annual report 2013. Anglo American PLC London, UK. http://www.angloamerican.com/%7E/media/Files/A/Anglo-American-Plc/reports/annual-report-2013/annualreport2013.pdf. Accessed 16 Jun 2014.

Anhaeusser, C.R., 1976. Archean metallogeney in Southern Africa. Economic Geology, 71, 16–45.

Anthony, J.W., Biduaex, R.A., Bladh, K.W., and Nichols, M.C., 2014. Handbook of mineralogy. Mineralogical Society of America, Chantilly, U.S.A, http://www.handbookofmineralogy.org/. Accessed December 29, 2014.

Armstrong, J.D., Tipper, H.W., and Hoadley, J.W., 1969. Geology of McLeod Lake, British Columbia. Geological Survey of Canada, Map 1204A; scale: 1:253 440.

Arzamastsev, A.A., Arzamastseva, L.V., Travin, A.V., Belyatsky, B.V., Shamatrina, A.M., Antonov, A.V., Larionov, A.N., Rodionov, N.V., and Sergeev, S.A., 2007.

Duration of formation of magmatic system of polyphase paleozoic alkaline complexes of the Central Kola: U–Pb, Rb–Sr, Ar–Ar data. Doklasy Earth Sciences, 413A, 432–436.

Atencio, D., Andrade, M.B., Christy, A.G., Gieré, R., and Kartashov, P.M., 2010. The pyrochlore supergroup of minerals: nomenclature. The Canadian Mineralogist, 48, 673-698.

Averill, S.A., 2001. The application of heavy indicator mineralogy in mineral exploration with emphasis on base metal indicators in glaciated metamorphic and plutonic terrains. In: McClenaghan, M.B., Bobrowsky, P.T., Hall, G.E.M., and Cook, S.J. (eds) 2001. Drift exploration in glaciated terrain. Geological Society, London, Special Publications, 185, 69-81.

Averill, S.A., 2014. Indicator mineral fingerprints in surficial sediments near Cu-Au deposits of the porphyry-epithermal-volcanogenic suite. In: McClenaghan, M.B., Plouffe, A., and Layton-Matthews, D., (eds) 2014. Application of indicator mineral methods to mineral exploration. Geological Survey of Canada, Open File 7553, 35-44.

Badanina, E.V., Sitnikova, M.A., Gordienko, V.V., Melcher, F., Gaber, H. –E., Lodziak, J.J., and Syritso, L.F., 2014. Mineral chemistry of columbite-tantalite from spodumene pegmatites of Lomozero, Kola Peninsula (Russia). Ore Geology Reviews, http://dx.doi.org/10.1016/j.oregeorev.2014.05.009

Bailey, J.C., Sørensen, H., Andersen, T., Kogarko, L.N., and Rose-Hansen, J., 2006. On the origin of microrhythmic layering in arfvedsonite lujavrite from the Ilímaussaq alkaline complex, South Greenland. Lithos, 91, 301–318.

Bambi, A.C.J.M., Costanzo, A., Goncalves, A.O., and Melgarejo, J.C., 2012. Tracing the chemical evolution of primary pyrochlore from plutonic to volcanic carbonatites: The role of fluorine. Mineralogical Magazine, 76, 377–392.

Barbarin, B., 1990. Granitoids: Main petrogenetic classification in relation to origin and tectonic setting. Geological Journal, 25, 227–238.

Bastos Neto, A.C., Pereira, V.P., Ronchi, L.H., de Lima, E.F., and Frant, J.C., 2009. The world-class Sn, Nb, Ta, F (Y, REE, Li) deposit and the massive cryolite associated with the albite-enriched facies of Madeira a-type granite, Pitinga mining district, Amazonas State, Brazil. Canadian Mineralogist, 47, 1329–1357.

Belkasmi, M., Cuney, M., Pollard, P.J., and Bastoul, A., 2000. Chemistry of the Ta-Nb-Sn-W oxide minerals from the Yichun rare metal granite (SE China): Genetic implications and comparison with Moroccan and French Hercynian examples. Mineralogical Magazine, 64, 507–523.

Bell, K. and Blenkinsop, J., 1980. Grant 42 ages and initial ^{87}Sr–^{86}Sr ratios from alkali complexes of Ontario. In: Pye (ed) Summary of research 1979–1980. Ontario Geological Survey, 93, 16–23.

Belousova, E.A., Griffin, W.L., O'Reilly, S.Y., and Fisher, N.I., 2002a. Apatite as an indicator mineral for mineral exploration: trace-element compositions and their relationship to host rock type. Journal of Geochemical Exploration, 76, 45-69.

Belousova, E.A., Griffin, W.L., O'Reilly, S.Y., and Fisher, N.I., 2002b. Igneous zircon: trace element composition as an indicator of source rock type. Contributions to Mineralogy and Petrology, 143, 602-622.

Bergstol, S., and Juve, G., 1988. Scandian Ixiolite, Pyrochlore and bazzite in granite pegmatites in Tordal, Telemark, Norway. A contribution to the mineralogy and geochemistry of scandium and tin. Mineralogy and Petrology, 38, 229–243.

Berry, L.G., Mason, B., and Dietrich, R.V., 1983. Mineralogy: Second edition. W.H. Freeman and Company, San Francisco.

Beskin, S.M., Grebennikov, A.M., and Matias, V.V., 1994. The Khangilai granite pluton and the related Orlovskoe tantalum deposit in the Transbaikal Region. Petrologiya, 2, 56–74.

Betmanis, A.I., 1987. Report on geological, geochemical, and magnetometer surveys on the Prince and George groups, Cariboo Mining Division, B.C. British Columbia Ministry of Energy, Mines, and Petroleum Resources, Assessment Report 15944, 86 p.

Birkett, T.C. and Simandl, G.J., 1999. Carbonatite-associated deposits. In: Simandl, G.J., Hora, Z.D., and Lefebure, D.V., (eds) Selected British Columbia mineral deposit profiles, vol. 3: industrial minerals and gemstones. British Columbia Ministry of Energy, Mines and Petroleum Resources, British Columbia Geological Survey, Open File 1999-10.

Blaxland, A.B., van Breemen, O., Emeleus, C.H., and Anderson, J.G., 1978. Age and origin of the major syenite centres in the Gardar Province of South Greenland: Rb–Sr studies. Geological Society of American Bulletin, 89, 231–244.

Blewett, R.S., Champion, D.C., Smithies, R.H., van Kranendonk, M.J., Farrel, T.R., and Thost, D., 2001. Geology of the Wodgina 1:100 000 sheet. North Pilbara National Geological Mapping Accord, Geological Survey of Western Australia.

Boily, M. and Gosselin, C., 2012. The main types of rare metal mineralisation (Y–Zr–Nb–Ta–Be–Li–REE) in Quebec. Géologie Quebéc Open Report ET-2012-01.

Boily, M. and Williams-Jones, A.E., 1994. The role of magmatic and hydrothermal processes in the chemical evolution of the Strange Lake plutonic complex, Québec-Labrador. Contributions to Mineral Petrology, 118, 33–47.

Bonazzi, P., Bindi, L., Zoppi, M., Capitani, G.C., and Olmi, F., 2006. Single-crystal diffraction and transmission electron microscopy studies of "silicified" pyrochlore from Narssarssuk, Julianehaad District, Greenland. American Mineralogist, 91, 794–801.

Bowring, S.A., van Schmus, W.R., and Hoffman, P.F., 1984. U–Pb zircon ages from Athapuscow Aulocogen, East Arm of Great Slave Lake, N.W.T., Canada. Canadian Journal of Earth Science, 21, 1315–1324.

Breaks, F.W., Selway, J.B., and Tindle, A.G., 2003. Fertile peraluminous granites and related rare-element mineralisation in pegmatites, Superior Province, Northwest and Northeast Ontario: Operation Treasure Hunt. Ontario Geological Survey, Open File Report 6099.

Brininstool, M. 2013. Copper. In: U.S. Geological survey, mineral commodity summaries 2014, pp 48–49.

Bruland, T., 2011. 2010 Helicopter-borne AreoTEM system electromagnetic, magnetic survey and radiometric survey. British Columbia Ministry of Energy, Mines, and Petroleum Resources, Assessment Report 32439, 57 p.

Brown, T.J., Walters, A.S., Idoine, N.E., Shaw, R.A., Wrighton, C.E., and Bide, T., 2012. World mineral production 2006–10. British Geological Survey, Keyworth, 78 p.

Camacho, A., Baadsgaard, H., Davis, D.W., and Černý, P., 2012. Radiogenic isotope systematic of the Tanco and Silverleaf granitic pegmatites, Winnipeg River Pegmatites District, Manitoba. Canadian Mineralogist 50, 1775–1792.

Camara, F., Williams, C.T., Della Tentura, G., Oberti, R., and Caprilli, E., 2004. Non-metamict betafite from Le Caracelle (Vico Volcanic Complex, Italy): Occurrence and crystal structure. Mineralogical Magazine, 68, 939–950.

Capital Mining Limited, 2013. Annual report 2013. http://www.capitalmining.com.au/Annual%20Reports/0001_CMY_Annual_Report_2013_FINAL-RELODGEMENT.pdf. Accessed 11 Dec 2013.

Carlson, M.P. and Treves, S.B., 2005. The Elk Creek carbonatite, southeast Nebraska—an overview. Natural Resources Research, 14, 39–45.

CBMM, 2014. Geology. http://www.cbmm.com/us/p/80/geology.aspx. Accessed 11 Jun 2014.

Černý, P., 1975. Pegmatite studies. Centre for Precambrian Studies, University of Manitoba, Annual Report, Part 2, 92–102.

Černý, P., 1982. The Tanco pegmatite, southeastern Manitoba. Am Mineral 67:183–183.

Černý, P., 1991a. Rare-element granitic pegmatites part I anatomy and internal evolution of pegmatite deposits. Geoscience Canada, 18, 49–67.

Černý, P., 1991b. Rare-element granitic pegmatites part II regional to global environments and petrogenesis. Geoscience Canada, 18, 68–81.

Černý, P., 2005. The Tanco rare-element pegmatite deposit, Manitoba: regional context, internal anatomy, and global comparison. In: Linnen, R.L. and Samson, I.M., (eds) Rare-element geochemistry and mineral deposits. Short Course Notes, Geological Association of Canada, special publication, 17, pp. 127–158.

Černý, P. and Ercit, T.S., 1985. Some recent advances in the mineralogy and geochemistry of Nb and Ta in rare-element granitic pegmatites. Bulletin de Minéralogie, 108, 499–532.

Černy, P. and Ercit, T.S., 1989. Mineralogy of niobium and tantalum: Crystal chemical relationships, paragenetic aspects and their economic implications. In: Moller, P., Černy, P., and Saupe, F. (eds) Lanthanides, Tantalum and Niobium. Springer-Verlag, Berlin, 27–79.

Černý, P. and Ercit, T.S., 2005. The classification of granitic pegmatites revisited. Canadian Mineralogist, 43, 2005–2026.

Černý, P. and Meintzer, R.E., 1988. Fertile granites in the Archean and Proterozoic fields of rare-element pegmatites, crustal environment, geochemistry and petrogenetic relationships. In: Taylor, R.P. and Strong, D.F., (eds) Recent advances in the geology of granite-related mineral deposits. Canadian Institute of Mining and Metallurgy, Special Volume, 39, 170-207.

Černy, P., Chapman, R., Ferreira, K., and Smeds, S.A., 2004. Geochemistry of oxide minerals of Nb, Ta, Sn, and Sb in the Varutrask granitic pegmatite, Sweden: The case of an “anomalous” columbite-tantalite trend. American Mineralogist, 89, 505–518.

Černy, P., Ercit, T.S., and Wise, M.A., 1992. The tantalite-tapiolite gap: natural assemblages versus experimental data. The Canadian Mineralogist, 30, 587–596.

Černy, P., Goad, B.E., Hawthorne, F.C., and Chapman, R., 1986. Fractionation trends of the Nb- and Ta-bearing oxide minerals in the Greer Lake pegmatitic granite and its pegmatites aureole, southeastern Manitoba. American Mineralogist, 71, 501–517.

Černý, P., Paul, B.J., Hawthorne, F.C., and Chapman, R., 1981. A niobian rutile disordered columbite intergrowth from the Huron Claim Pegmatite, Southeastern Manitoba. Canadian Mineralogist, 19, 541–548.

Chakhmouradian, A.R. and Mitchell, R.H., 1998. Lueshite, pyrochlore and monazite-(Ce) from apatite-dolomite carbonatites, Lesnaya Varaka Complex, Kola Peninsula, Russia. Mineralogical Magazine, 62, 769–782.

Chakhmouradian, A.R. and Mitchell, R.H., 2002. New data on pyrochlore- and perovskite-group minerals from the Lovozero Alkaline Complex, Russia. European Journal of Mineralogy, 14, 821–836.

Chakhmouradian, A.R. and Sitnikova, M.A., 1999. Radioactive minerals from murmanite-lorenzenite tinguaite at Mt. Selsurt, Lovozero Complex, Kola Peninsula. European Journal of Mineralogy, 11, 871–878.

Chakhmouradian, A.R. and Williams, C.T., 2004. Mineralogy of high-field-strength elements (Ti, Nb, Zr, Ta, Hf) in phoscoritic and carbonitic rocks of the Kola Peninsula, Russia. In: Wall, F., and Zaitsev, A.N. (eds) phoscorites and carbonatites from mantle to mine: The key examples of the Kola Alkaline Province. Mineralogical Society Series, 10, 293–340.

Chakhmouradian, A.R. and Zaitsev, A.N., 1999. Calcite-amphibole-clinopyroxene rock from the Afrikanda Complex, Kola Peninsula, Russia: Mineralogy and a possible link to carbonatites. I. Oxide minerals. The Canadian Mineralogist, 37, 177–198.

Chakhmouradian, A.R., Ekaterina, P.R., Kressall, R.D., Crozier, J., Pisiak, L.K., Sidhu, R., and Yang, P., 2014. Carbonatite-hosted niobium deposit at Aley, northern British Columbia (Canada): Mineralogy, geochemistry and petrogenesis. Ore Geology Reviews, 64, 642–666, URL http://dx.doi.org/10.1016/j.oregeorev.2014.04.020.

Cheilletz, A., Archibald, D.A., Cuney, M., and Charoy, B., 1992. Ages $^{40}Ar/^{39}Ar$ du leucogranite à topaze-lépidoldite de Beauvoir et des pegmatites sodolithiques Chédeville (Nord du Massi Central, France). Signification Pétrologique et Géodynamique. Comptes Rendus de l'Académie des Sciences, 315, 329–336.

Chisholm, E.O., 1960. Lonnie columbian deposit. British Columbia Ministry of Energy and Mines property file <http://propertyfile.gov.bc.ca/showDocument.aspx?&docid=138373> accessed November 2014.

Chong, A., Postolski, T., Mendoza, R.R., Lipiec, T., and Omidvar, B., 2012. Blue River tantalum-niobium project, (British Columbia, Canada). NI-43-101 Technical Report. Commerce Resource Corp. Vancouver, Canada, June 22, 2012. http://www.commerceresources.com/i/pdf/TechnicalReport-BlueRiverResourceUpdate.pdf. Accessed 11 Dec 2013.

Chudik, P., Uher, P., Gadas, P., Škoda, R., and Pršek, J.J., 2011. niobium-tantalum oxide minerals in the Jezuitske Lesy granitic pegmatite, Bratislava Massif, Slovakia: Ta to Nb and Fe to Mn evolutionary trends in a narrow Be, Cs-rich and Li, B-poor dike. Mineral Petrology, 102, 15–27.

Chudy, T.C., 2014. The petrogenesis of the ta-bearing Fir carbonatite system, east-central British Columbia, Canada. PhD thesis, University of British Columbia, Canada.

Chung, C.J. and Crozier, J., 2008. Assessment report on diamond drilling performed on the Aley carbonatite property. British Columbia Ministry of Energy, Mines, and Petroleum Resources, Assessment Report 30113, 194 p.

Ciuculescu, T., Foo, B., Gowans, R., Hawton, K., Jacobs, C., and Spooner, J., 2013. Technical report disclosing the results of the feasibility study on the Nechalacho rare earth elements project. Toronto, Ontario, Canada, Avalon Rare Metals Inc. http://avalonraremetals.com/_resources/projects/may_2013_ni43_report.pdf. Accessed 11 Dec 2013.

Clague, J.J. and James, T.S., 2002. History and isostatic effects on the last ice sheet in southern British Columbia. Quarternary Science Reviews, 21, 71-87.

Clarke, D.B., 1981. The mineralogy of peraluminous granites: a review. Canadian Mineralogist, 19, 1–17.

Clow, G.G., Salmon, B., Lavigne, M., Pelletier, P., and Vallières, D., 2011. Technical report on expansion options at the Niobec Mine, Québec. IAMGOLD Corporation, Toronto.

Colpron, M. and Nelson, J.L., 2011. A digital atlas of terranes for the northern Cordillera. British Columbia Ministry of Energy and Mines, British Columbia Geological Survey, GeoFile 2011-11.

Cordeiro, P.F.O., Brod, J.A., Palmieri, M., de Oliveira, C.G., Barbosa, E.S.R., Santos, R.V., Gaspar, J.C., and Assis, L.C., 2011. The Catalao I niobium deposit, central Brazil: Resources, geology and pyrochlore chemistry. Ore Geology Reviews, 41, 112–121.

Cox, R.A. and Wilton, D.H.C., 2006. U–Pb dating of perovskite by LA-ICP-MS: an example from the Oka carbonatite, Quebec, Canada. Chemical Geology, 235, 21–32.

Cradle Resources Limited, 2013. Panda Hill niobium project: Tanzania. http://www.cradleresources.com.au/_content/documents/CXX%20-%20PANDA%20HILL%20NIOBIUM%20PROJECT%20PRESENTATION.pdf. Accessed 5 Feb 2014.

Cummings, J.P. and Simonsen, S.H., 1970. The crystal structure of calcium niobate ($CaNb_2O_6$). American Mineralogist, 55, 90–97.

Cuney, M., Marignac, C., and Weisbrod, A., 1992. The Beauvoir topaz-lepidolite albite granite (Massif Central, France): the disseminated magmatic Sn–Li–Ta–Nb–Be mineralization. Economic Geolology, 87, 1766–1794.

Cunningham, L.D., 1996a. Tantalum. In: U.S. Geological Survey, Mineral Commodity Summaries 1996, pp 168–169.

Cunningham, L.D., 1996b. Niobium (columbium). In: U.S. Geological Survey, Mineral Commodity Summaries 1996, pp 48–49.

Cunningham, L.D., 1997a. Tantalum. In: U.S. Geological Survey, Mineral Commodity Summaries 1997, pp 170–171.

Cunningham, L.D., 1997b. Niobium (columbium). In: U.S. Geological Survey, Mineral Commodity Summaries 1997, pp 50–51.

Cunningham, L.D., 1999a. Tantalum. In: U.S. Geological Survey, Mineral Commodity Summaries 1999, pp 172–173.

Cunningham, L.D., 1999b. Niobium (columbium). In: U.S. Geological Survey, Mineral Commodity Summaries 1999, pp 54–55.

Cunningham, L.D., 2001a. Tantalum. In: U.S. Geological Survey, Mineral Commodity Summaries 2001, pp 164–165.

Cunningham, L.D., 2001b. Niobium (columbium). In: U.S. Geological Survey, Mineral Commodity Summaries 2001, pp 50–51.

Cunningham, L.D., 2003a. Tantalum. In: U.S. Geological Survey, Mineral Commodity Summaries 2003, pp 168–169.

Cunningham, L.D., 2003b. Niobium (columbium). In: U.S. Geological Survey, Mineral Commodity Summaries 2003, pp 54–55.

Cunningham, L.D., 2005a. Tantalum. In: U.S. Geological Survey, Mineral Commodity Summaries 2005, pp 166–167.

Cunningham, L.D., 2005b. Niobium (columbium). In: U.S. Geological Survey, Mineral Commodity Summaries 2005, pp 52–53.

Daigle, P., 2011. Technical report on the Clay-Howells Fe–REE project, Ontario, Canada. Canada Rare Earth Corporation. Toronto, Canada. http://www.canadarareearth.com/upload/documents/technicalreport-on-the-clay-howells.pdf. Accessed 11 Dec 2013.

Daigle, P., 2012. Elk Creek Nb project, Nebraska, US. Resource estimate update. Quantum Rare Earth Developments Corp. Toronto, Canada. http://www.quantumrareearth.com/images/files/ni-43-101-april-2012.pdf. Accessed 8 Jan 2014.

Daigle, P., Robinson, J., and Baughman, D., 2011. Strange Lake B zone resource model update. Quest Rare Minerals Ltd. Toronto, Canada. http://www.questrareminerals.com/pdfs/1155110100-REP-R0001-02%20FINAL%20(1).pdf. Accessed 25 Feb 2014.

Dalsin, M. L., 2013. The mineralogy, geochemistry and geochronology of the Wicheeda carbonatite complex, British Columbia. MSc, University of British Columbia, 265 p.

David, J., Dion, C., Goutier, J., Roy, P., Bandyayera, D., Legault, M., and Rhéaume, P., 2006. Datations U–Pb effectuées dans la sous-Province de l'Abitibi à la suite des ravaux de 2004–2005. Ressources Naturelles et Faune, Québec, RP 2006–04.

Desharnais, G. and Duplessis, C., 2011. Montviel core zone REE mineral resource estimate technical report, Quebec. Geomega Resources Inc., Saint-Lambert, Canada, 76p. http://ressourcesgeomega.com/wp-content/uploads/2013/04/4.-Montviel-initial-NI-43-101-resource-calculation.pdf. Accessed 11 Dec 2013.

Dolgopolova, A., Seltmann, R., Kober, B., Weiss, D., Stanely, C., and Dulski, P., 2004. Geochemical characteristics and lead isotope systematic of highly fractionated Li–F-enriched amazonite granites and related host rock of the Orlovka-Spokoinoe mining district, Eastern Transbaikalia (Russia). Applied Earth Science, 113, 83–99.

Duplessis, C. and Girard, R., 2010. Niobium and tantalum resource estimation update of the Crevier deposit—2010. MDN Inc. and Crevier Minerals Inc.

EICC, 2013. Electronic Industry Citizenship Coalition. http://www.eicc.info/CFSProgram.shtml. Accessed 14 Aug 2013.

Ercit, T.S., 2010. Hidden story of tapiolite. Mineralogical Magazine, 74, 715–729.

Ercit, T.S., Černý, P., and Hawthorne, F.C., 1992. The wodginite group: III. Classification and new species. Canadian Mineralogist, 30, 633–638.

Ermolaeva, V.N., Pekov, I.V., Chukanov, N.V., and Zadov, A.E., 2007. Thorium mineralization in hyperalkaline pegmatites and hydrothermalites of the Lovozero Pluton, Kola Peninsula. Geolology of Ore Deposits, 49, 758–775.

European Commission, 2011. Critical raw materials for the EU. http://ec.europa.eu/enterprise/policies/raw-materials/files/docs/report-b_en.pdf. Accessed 9 Dec 2013.

European Commission, 2014. Report on critical raw materials for the EU. http://ec.europa.eu/enterprise/policies/raw-materials/files/docs/crmreport-on-critical-raw-materials_en.pdf. Accessed 6 Jun 2014.

Ewing, R.C., 1976. A numerical approach toward the classification of complex, orthorhombic, rare-earth, AB_2O=-type Nb–Ta–Ti oxides. Canadian Mineralogist, 14, 111–119.

Ferguson, A.K., 1978. The occurrence of ramsayite, titan-låvenite and a fluorine-rich eucolite in a nepheline-syenite inclusion from Tenerife, Canary Islands. Contributions to Mineral Petrology, 66, 15–20.

Fetherston, J.M., 2004. Tantalum in Western Australia. Geological Survey of Western Australia, Mineral Resources Bulletin, 22.

Fleischer, M., 1960. New mineral names: leushite. American Mineralogist, 46, 1004.

Fletcher, W.K., 1997. Stream sediment geochemistry in today's exploration world. In A.G. Gubins, (ed), Proceeding of Exploration 97: Fourth Decennial International Conference on Mineral Exploration, Prospectors and Developers Association of Canada, Toronto, Canada, paper 32, p. 249–260.

Fortin-Bélanger, M., 1977. Le complexe annulaire à carbonatite de St. Honoré (P.Q., Canada) et sa minéralisation à niobium: Étude pétrographique et géochimique. PhD. Dissertation, Université Claude Bernard, Lyon, France.

Fournier, A., 1993. Magmatic and hydrothermal controls of LREE mineralization of the St-Honoré Carbonatite, Québec. MSc. Thesis, McGill University, Montreal, Canada .

Friske, P.W.B., Jackaman, W., Lett, R.E.W., and McCurdy, M.W. 2005. Regional stream sediment and water data, Bowser Lake and Spatsizi River, British Columbia. Geological Survey of Canada, Open File 5000/BC RGS 58. 73p.

Fuck, R.A., Pimentel, M.M., Macha do, N., and Daoud, W.E.K., 1993. U–Pb Age of the Madeira Granite, Pitinga (Amazonas state). In: 4th Brazilian Geochemical Congress (Brazilia), Extended Abstr., 246–249 (in Portuguese) .

Galaxy Resources Limited, 2011. 2011 Annual report. http://www.galaxyresources.com.au/documents/gxy_ar_31_dec_2011.pdf. Accessed 11 Dec 2013.

Gerasimovskii, V.I., 1956. Geochemistry and mineralogy of nepheline syenite intrusions. Geokhimya, 5, 494–511.

Ginsberg, A.I., 1984. The geological condition of the location and the formation of granitic pegmatites. Proceedings of the 27th International Geological Congress, 15, 245–260.

Gippsland Limited, 2013a. Abu Dabbab tantalum. http://www.gippslandltd.com/Projects/AbuDabbab.aspx.Accessed 11Dec 2013.

Gippsland Limited, 2013b. Nuweibi–tantalum, niobium, feldspar. http://www.gippslandltd.com/Projects/Nuweibi.aspx. Accessed 11 Dec 2013.

Globe Metals & Mining, 2013. Kanyika niobium project. http://www.globemetalsandmining.com.au/Projects/Kanyika-Niobium-Project.aspx%23.UqjTXdJDtyw. Accessed 11 Dec 2013.

Gold, D.P., Valleé, M., and Charette, J-P, 1967. Economic geology and geophysics of the Oka alkaline complex, Quebec. Canadian Mining and Metallurgy Bulletin 60, 1131–1144.

Gold, D.P., Eby, G.N., and Valleé, M., 1986. Carbonatites, diatremes and ultra alkaline rocks in the Oka area. Fieldtrip guidebook 21, GAC/MAC Meeting, Ottawa .

Gorham, J., Ulry, B., and Brown, J., 2009. 2008 diamond drilling and exploration at the blue river property, B.C. Technical report, British Columbia Ministry of Energy, Mines, and Petroleum Resources.

v. Gosen, B.S., 2009. The Iron Hill (Powderhorn) carbonatite complex, Gunnison County, Colorado: a potential source of several uncommon mineral resources. U.S. Geological Survey, Open-File Report 2009-1005.

Gowans, R.M., Hutchison, I., Lewis, W.J., Shoemaker, Jr. S., Spooner, J., and Zalnieriunas, R.V., 2013. NI 43–101 technical report on the prefeasibility study for the Strange Lake property, Quebec, Canada. Quest Rare Metals Ltd. Toronto, Canada. http://www.questrareminerals.com/pdfs/Strange%20Lake%20PFS%20Results%2043-101.pdf. Accessed 13 Dec 2013.

Graf, C., Lane, B., and Morrison, M., 2009. The Wicheeda carbonatite-syenite breccia intrusive complex hosted rare earth deposit. Conference Abstract, 5th Annual Minerals South Conference and Trade Show, Cranbrook, Canada. http://www.slideshare.net/RareMetalBelt/abstract-on-the-wicheeda-rare-earth-property#. Accessed December 13, 2013.

Graham, J. and Thornber, M.R., 1974. The crystal chemistry of complex niobium and tantalum oxides: I. Structural classification of MO_2 phases. American Mineralogist, 59, 1026–1039.

Grammatikopoulos, T., Mercer, W., and Gunning, C., 2013. Quantitative characterization of the REE minerals by QEMSCAN from the Nechalacho heavy rare earth deposit, Thor Lake project, NWT, Canada. SGS Minerals Services technical paper, 2011-07, http://www.sgs.com/~/media/Global/Documents/Technical%20Documents/Technical%20Bulletins/SGS%20MIN%202011%2007%20Quantitative%20characterization%20of%20REE%20minerals%20EN%2013%2009.pdf. Accessed 28 Feb, 2014.

Grossi-Sad, J.H. and Torres, N., 1976. Geology and mineral resources of the Barreiro Complex, Araxá, Brazil. In: Simpósio Internacional de Carbonatitos. Poços de Caldas, Brazil .

Gupta, C.K. and Suri, A.K., 1994. Extractive metallurgy of niobium. CRC Press, London.

Gysi, A.P. and Williams-Jones, A.E., 2013. Hydrothermal mobilization of pegmatite-hosted REE and Zr at Strange Lake, Canada: A reaction path model. Geochimica et Cosmochimica Acta, 122, 324–352.

Hains, D.H. and Mounde, M., 2010. Technical report on the Marropino project and associated properties, Zambezia Province, Mozambique. Noventa Limited, St. Helier, 252p.

Hall, S.J., 1994. Wodgina M45/50, M45/351 annual report year ending 4 July 1994. Perth, W.A., Pan West Tantalum Pty. Ltd., Unpublished report M1028/1, 6p.

Hankinson, J.D., 1958. The Lonnie group columbium deposit, Unpublished B.Sc. thesis, University of British Columbia, 32 p.

Harrisson, R., 1981. Geochronology, petrography and geochemistry of a section of the Crevier alkaline igneous complex. In: The St. Honoré and Crevier niobium–tantalum deposits and related alkaline complexes. Canadian Institute of Mining and Metallurgy, Excursion Guidebook: 40.

Hassan, W.F., 1994. Geochemistry and mineralogy of Ta–Nb rutile from Peninsular Malaysia. Journal of Southeast Asian Earth Science, 10, 11–23.

Hassanen, M,A, and Harraz, H.Z., 1996. Geochemistry and Sr- and Nd-isotopic study on rare-metal-bearing granitic rocks, Central Eastern Desert, Egypt. Precambrian Research, 80, 1–22.

Hasui, Y. and Cordani, U.G., 1968. Idades potássio-argônio de rochas eruptivas Mesozóicas do Oeste Mineiro e Sul de Goiás. In: XXII Congresso Brasileiro de Geologia. Belo Horizonte, 22, 139–143.

Hatcher, M.I. and Bolitho, B.C., 1982. The Greenbushes pegmatite, South-West Western Australia. In: Černý, P., (ed) Granitic pegmatites in science and industry. Mineralogical Association of Canada Short Course, 513–525.

Hatcher, M.I. and Clynick, G., 1990. Greenbushes tin–tantalum–lithium deposit. In: Hughes, F.E., (ed) Geology of the mineral deposits of Australia and Papua New Guinea. The Australas Institute of Mining and Metallurgy, Parkville, pp 599–603.

Hawkes, H.E., 1976. The downstream dilution of stream sediment anomalies. Journal of Geochemical Exploration, v. 6, p. 345–358.

Heinrich, E.W., 1985. Infinite variations on fenite theme. Indian Mineral, Sukheswala, volume 151–162.

Hirtopanu, P., Jakab, G., Andersen, C.J., and Fairhurst, J.R., 2013. Thorite, thorogummite and xenotime-(Y) occurrence in Ditrau alkaline intrusive massif, east Carpathians, Romania. Proceeding of the Romanian Academy, Series B, 15, 111–131.

Hodgson, N.A. and Le Bas, M.J., 1992. The Geochemistry and cryptic zonation of pyrochlore from San Vicente, Cape Verde Islands. Mineralogical Magazine, 56, 201–214.

Hogarth, D.D., 1961. A study of pyrochlore and betafite. The Canadian Mineralogist, 6, 610–633.

Hogarth, D.D., 1977. Classification and nomenclature of the pyrochlore group. American Mineralogist, 62, 403–410.

Hogarth, D.D. and Horne, J.E.T., 1989. Non-metamict uranoan pyrochlore and uranpyrochlore from tuff near Ndale, Fort Portal area, Uganda. Mineralogical Magazine, 53, 257–262.

Hogarth, D.D., Williams, C.T., and Jones, P., 2000. Primary zoning in pyrochlore group minerals from carbonatites. Mineralogical Magazine, 64, 683–697.

Hora, Z.D., Langrová, A., and Žák. K., 2010. Niobium-thorium-strontium-rare earth element mineralogy and preliminary sulphur isotope geochemistry of the Eaglet property, east-central British Columbia (NTS 093A/10W). In: Geological Fieldwork 2009, British Columbia Ministry of Energy and Mines, British Columbia Geological Survey Paper, 2010-1, 1-4.

Horbe, M.A., Horbe, A.C., Costi, H.T., and Teixeira, J.T., 1991. Geochemical characteristics of cryolite-tin-bearing granites from the Pitinga Mine, northwestern Brazil - A review. Journal of Geochemical Exploration, 40, 227–249.

Irish, E. J.W., 1970. Geology of the Halfway River map area, British Columbia. Geological Survey of Canada, Paper 69-11, 154 p.

Issa Filho, A., Lima dos Santos, P.R.A., and Souza, O.M., 1984. Aspects of the geology of the Barreiro carbonatitic complex, Araxá, MG, Brazil. In: Carbonatitic complexes of Brazil: Geology. Companhia Brasileira de Metalurgia e Mineração, São Paulo, p 19–44.

Issa Filho, A., Riffel, B.F., and de Faria Sousa, C.A., 2001. Some aspects of the mineralogy of CBMM niobium deposit and mining pyrochlore ore processing—Araxá, MG—Brazil. http://www.cbmm.com.br/Repositorio/Media/site/internas/operations/minerologyaspectsniobiumdeposit.pdf?. Accessed 11 Dec 2013.

Jacobi, P., 2009. Seis Lagos the largest niobium reserve in the world is still waiting to be developed. www.geologo.com.br/seislagos.asp. Accessed 5 Feb 2014.

Jahns, R.H., 1955. The study of pegmatites. Division of the Geological Sciences, California Institute of Technology, Pasadena, 106p.

Jambor, J.L. and Vanko, D.A., 1989. New mineral names. American Mineralogist, 74, 946–951.

Johan, V. and Johan, Z., 1994. Accessory minerals of the Cínovec (Zinnwald) granite cupola, Czech Republic. Mineralogy and Petrology, 51, 333–343.

Johan, Z., Strnad, L., and Johan, V., 2012. Evolution of the Cínovec (Zinnwald) granite cupola, Czech Republic: Composition of feldspars and micas, a clue to the origin of W, Sn mineralization. Canadian Mineralogist, 50, 1131–1148.

Jones, S., Merriam, K., Yelland, G., Rotzinger, R., and Simpson, R.G. 2014. Technical report on mineral reserves at the Aley project, British Columbia, Canada. Taseko Mines Limited, 291 p. <www.sedar.com> accessed February 3, 2015.

Justo, L.J.E.C. and Souza, M.M., 1986. Jazida de nióbio do morro dos Seis Lagos, Amazonas. In: Schobbenhaus, C., (ed) Principais depósitos minerais do Brasil, 2. BRASIL. Ministério das Minas e Energia. Departamento Nacional da Produção Minera, 463–468.

Kamitani, M. and Hirano, H., 1990. Important carbonatite-alkaline/alkaline complexes and related mineral resources in the world. Bulletin of the Geological Survey of Japan, 41, 631–640 .

Karagambe-Kaliiza, F.A., 1989. The Sukulu phosphate deposits, south- eastern Uganda. In: Bell, K., (ed) Carbonatites genesis and evolution. Unwin Hyman, London, pp 184–186 .

Kennedy, A.K., 1998. SHRIMP ages of apatites from Pilbara tin-bearing pegmatites. Geological Society of Australia Abstracts, 49, 242.

Khomyakov, A.P., 1995. Mineralogy of hyperagpaitic alkaline rocks. Clarendon Press, Oxford, ISBN 0-19-854836-2.

Kinny, P.D., 2000. U–Pb dating of rare metal (Sn–Ta–Li) mineralised pegmatites in Western Australia by SIMS analysis of tin and tantalum bearing ore minerals. New Frontiers in Isotope Geology Conference, Lorne, Victoria, February 2000, Proceedings pp 113–116.

Kogarko, L.N., 1987. Alkaline rocks of the eastern part of the Baltic shield (Kola Peninsula). Geological Society of London Special Publication, 30, 531–544.

Kogarko, L.N., Sorokhtina, N.V., Zaitsev, V.A., and Senin, V.G., 2009. Rare Metal Mineralization of Calcite Carbonatites from the Cape Verde Archipelago. Geochemistry International, 47, 531–549.

Kogarko, L.N., Williams, C.T., and Woolley, A.R., 2002. Chemical evolution and petrogenetic implications of Loparite in the layered, agpaitic Lovozero complex, Kola Peninsula, Russia. Mineralogy and Petrology, 74, 1–24.

Kovalenko ,V.I., Kostitsyn, Y.A., Yarmolyuk, V.V., Budnikov, S.V., Kovach, V.P., Kotov, A.B., Sal'nikova, E.B., and Antipin, V.S., 1999. Magma sources and the isotopic (Sr and Nd) evolution of Li–F rare-metal granites. Petrology, 7, 383–409.

Kramm, U. and Kogarko, L.N., 1994. Nd and Sr isotope signatures of the Khibina and Lovozero agpaitic centres, Kola alkaline province, Russia. Lithos, 32, 225–242.

Krasnova, N.I., Petrov, T.G., Balaganskaya, E.G., Garcia, D., Moutte, J., Zaitsev, A.N., and Wall, F. 2004. Introduction to phoscorites: occurrence, composition, nomenclature and petrogenesis. In: Wall, F. and Zaitsev, A.N. (eds). Phoscorites and Carbonatites from Mantle to Mine: the key example of the Kola Alkaline Province. Mineralogical Society of Great Britain & Ireland, London, pp 45-74.

Kravchenko, S.M. and Pokrovsky, B.G., 1995. The Tomtor alkaline ultrabasic massif and related REE-Nb deposits, northern Siberia. Economic Geology, 90, 676–689.

Kressall, R., McLeish, D.F., and Crozier, J., 2010. The Aley carbonatite complex – Part II petrogenesis of a Cordilleran niobium deposit. In: Simandl, G.J., and Lefebure, D.V. (Eds.), International workshop on the geology of rare metals, November 9-10, 2010, Victoria, Canada. Extended Abstracts Volume. British Columbia Ministry of Energy and Mines, British Columbia Geological Survey, Open File 2010-10, pp. 25-26.

Küster, D., Romer, R.L., Tolessa, D., Zerihun, D., Bheemalingeswara, K., Melcher, F., and Oberthür, T., 2009. The Kenticha rare-element pegmatite, Ethiopia: Internal differentiation, U–Pb age and Ta mineralization. Minerlium Deposita, 44, 723–750.

Lafleur, P.J. and Ayad, M.A.B., 2012. NI 43–101 technical report to present the mineral resources of the rare earth elements zone Niobec mine. IAMGOLD Corporation, Toronto, Canada. 145 p. http://www.iamgold.com/files/REE%2043-101%20Technical%20Report%20March%202012.pdf. Accessed 12 Dec 2013.

Lahti, S.I.. 2000. Compositional variation in columbite-group minerals from different types of granitic pegmatites of the Erajarvi District, south Finland. Journal of the Czech Geological Society, 45, 107–118.

Lane, B., 2009. diamond drilling report on the Wicheeda property, Cariboo Mining Division. British Columbia Ministry of Energy, Mines, and Petroleum Resources, Assessment Report 30873, 196 p.

Lavoie, S. and Caron, J-C., 2011. Modèle géologique et estimation des ressources de niobium de la Zone S-60. Niocan Inc, Oka.

Layton-Matthews, D., Hamilton, C., and McClenaghan, M.B., 2014. Mineral chemistry: modern techniques and applications to exploration. In: McClenaghan, M.B., Plouffe, A., and Layton-Matthews, D., (eds) 2014. Application of indicator mineral methods to mineral exploration. Geological Survey of Canada, Open File 7553, 9-18.

Laznicka, P., 2010. Giant metallic deposits: future sources of industrial metals, 2nd edn. Springer-Verlag, Berlin, 949p.

Le Bas, M.J., 2008. Fenites associated with carbonatites. Canadian Mineralogist, 46, 915–932.

Le Couteur, P.C., 2008. Petrographic report on four samples from the Wicheeda Property; unpublished company report, Spectrum Mining Corporation, 36 p.

Le Couteur, P.C., 2009. Petrographic report on four samples from the Wicheeda Property; unpublished company report, Spectrum Mining Corporation, 28 p.

Le Maitre, R.W., (ed) 2002. Igneous rocks: a classification and glossary of terms; recommendations of the International Union of Geological Sciences Subcommission on the systematics of igneous rocks. Cambridge University Press, Cambridge.

Lee, M.J., Lee, J.I., Garcia, D., Moutte, J., Williams, C.T., Wall, F., and Kim, Y., 2006. Pyrochlore chemistry from the Sokli phoscorite-carbonatite complex, Finland: Implications for the genesis of phoscorite and carbonatite association. Geochemical Journal, 40, 1–13.

Lenharo, S.L.R., 1998. Magmatic evolution and metallogenetic model of the mineralized granites from the Pitinga Region, Amazonas State, Brazil. Dissertation University of São Paulo, Brazil .

Lett, R., 2007. Workshop notes: drainage geochemical surveys–stream sediments, lake sediments, moss mats, heavy minerals. British Columbia Ministry of Energy and Mines, British Columbia Geological Survey, Geofile 2007-6, 63 p.

Levinson, A.A., 1974. Introduction to exploration geochemistry (second edition). Applied Publishing Ltd., Wilmette, Illinois, 924 p.

v. Lichtervelde, M., Salvi, S., Beziat, D., and Linnen, R.L., 2007. Textural features and chemical evolution in tantalum oxides: Magmatic versus hydrothermal origins for ta mineralization in the Tanco lower pegmatite, Manitoba, Canada. Economic Geology, 102, 257–276.

Lide, D.R., (ed) 2008. CRC handbook of chemistry and physics, 89th edn. CRC Press, Boca Raton .

Lin, Y., Pollard, P.J., Hu, S., and Taylor, R.G., 1995. Geological and geochemical characteristics of the Yichun Ta–Nb–Li deposit, Jiangxi Province, south China. Economic Geology, 90, 577–585.

Linnen, R.L. and Cuney, M., 2005. Granite-related rare-element deposits and experimental constraints on Ta–Nb–W–Sn–Zr–Hf mineralization. In: Linnen, R.L. and Samson, I.M., (eds) Rare-element geochemistry and mineral deposits, short course notes, Geological Association of Canada, Special Publication, 17, 45–68.

Linnen, R.L., Samson, I.M., Williams-Jones, A.E., and Chakhmouradian, A.R., 2014. Geochemistry of the rare-earth element, Nb, Ta, Hf, and Zr deposits. In: Holland, H. and Turekian, K. (eds) 2014. Treatise on geochemistry (second edition), 13, 543–568.

Linnen, R.L., Trueman, D.L., and Burt, R., 2014. Tantalum and niobium. In: Gunn, G., (ed) Critical metals handbook, 1st edn. John Wiley and Sons, Ltd, West Sussex, pp 361–384.

Lithex Resources Ltd., 2012. Maiden inferred mineral resource Moolyella project: Perth, Western Australia, Australia, March 12, 2 p. http://www.asx.com.au/asxpdf/20120301/pdf/424rgh8d3hr81q.pdf. Accessed 11 Dec 2013.

Lottermoser, B.G. and England, B.M., 1988. Compositional variation in pyrochlores from the Mt Weld carbonatite laterite, Western Australia. Mineralogy and Petrology, 38, 37–51.

Lovang, G., and Meyer, W., 1987. Report on trenching, stream silt concentrate and soil sampling on the George Group, Cariboo Mining Division. British Columbia Ministry of Energy, Mines, and Petroleum Resources, Assessment Report 16246, 18 p.

Luck, P. and Simandl, G.J., 2014. Portable X-ray fluorescence in stream sediment chemistry and indicator mineral surveys, Lonnie carbonatite complex, Canada. In: Geological Fieldwork 2013, British Columbia Ministry of Energy and Mines, British Columbia Geological Survey Paper 2014-1, pp. 169-182.

Lumpkin, G.R. and Ewing, R.C., 1992. Geochemical alteration of pyrochlore group minerals: Microlite subgroup. American Mineralogist, 77, 179–188.

Lumpkin, G.R. and Ewing, R.C., 1995. Geochemical alteration of pyrochlore group minerals: Pyrochlore subgroup. American Mineralogist, 80, 732–743.

Lynas Corporation, 2008. Diggers and dealers presentation. http://www.lynascorp.com/Presentations/2008/Diggers_and_Dealers_Presentation_August_2008_FINAL.pdf. Accessed 8 Jan 2014.

Mackay, D.A.R. and Simandl, G.J., 2014a. Geology, market and supply chain of niobium and tantalum–a review. Mineralium Deposita, 49, 1025-1047.

Mackay, D.A.R., and Simandl, G.J., 2014b. Portable X-ray fluorescence to optimize stream sediment chemistry and indicator mineral surveys, case 1: Carbonatite-hosted Nb deposits, Aley carbonatite, British Columbia, Canada. In: Geological Fieldwork 2013, British Columbia Ministry of Energy and Mines, British Columbia Geological Survey, Paper 2014-1, pp. 183-194.

Mackay, D.A.R. and Simandl, G.J., 2014c. Portable X-ray fluorescence to optimize stream sediment chemistry and indicator mineral surveys, case 2: Carbonatite-hosted REE deposits, Wicheeda Lake, British Columbia, Canada. In: Geological Fieldwork 2013, British Columbia Ministry of Energy and Mines, British Columbia Geological Survey, Paper 2014-1, 195-206.

Mackay, D.A.R., and Simandl, G.J., 2015. Pyrochlore and columbite-tantalite as indicator minerals for specialty metal deposits. Geochemistry: Exploration, Environment, Analysis, In Press.

Mackay, D.A.R., Simandl, G.J., Ma, W., and Redfearn, M., (In Review). QEMSCAN® in indicator mineral-based exploration for carbonatites and related specialty metal deposits, British Columbia, Canada.

Mäder, U. K., 1986. The Aley carbonatite complex. Master of Science thesis, University of British Columbia, 176 p.

Mäder, U. K., 1987. The Aley carbonatite complex, northern Rocky Mountains (94B/5), British Columbia. In: Geological Fieldwork 1986, British Columbia Ministry of Energy, Mines and Petroleum Resources, British Columbia Geological Survey Paper 1987-1, pp. 283-288.

Mäder, U.K., and Greenwood, H.J., 1988. Carbonatites and related rocks of the Prince and George claims, northern Rocky Mountains (93J, 93I): Geological Fieldwork 1987. British Columbia Ministry of Energy, Mines and Petroleum Resources, British Columbia Geological Survey Paper 1988-1, pp. 375-380.

Magyar, M.J., 2007a. Tantalum. In: U.S. Geological Survey, Mineral Commodity Summaries 2007, pp 165–166.

Magyar, M.J., 2007b. Niobium (columbium). In: U.S. Geological Survey, Mineral Commodity Summaries 2007, pp 50–51.

Maithani, P.B. and Singh, Y., 2011. Studies on tapiolite from Arehalli pegmatite, Hassan District, Karnataka. Journal Geological Society of India, 78, 349–354.

Makin, S.A., Simandl, G.J., and Marshall, D., 2014. Fluorite and its potential as an indicator mineral for carbonatite related rare earth element deposits. In: Geological Fieldwork 2013, British Columbia Ministry of Energy and Mines, British Columbia Geological Survey Paper 2014-1, 207-212.

Manser, R.J., Barley, R.W., and Wills, B.A., 1991. The shaking table concentrator – the influence of operating conditions and table parameters on mineral separation – the development of a mathematical model for normal operating conditions. Minerals Engineering, 4, 369-381.

Mariano, A.N., 1989a. Nature of economic mineralization in carbonatites and related rocks. In: Bell K (ed) Carbonatites: genesis and evolution. Chapman and Hall, London, pp 149–176.

Mariano, A.N., 1989b. Economic geology of rare earth minerals. In: Lipman, B.R. and McKay, G.A., (eds) Geochemistry and mineralogy of rare earth elements. Reviews in Mineralogy, 21, 309–338.

Martin, R.F., 2007. The importance of tectonic setting in understanding granitic pegmatites. Granitic pegmatites: the State of the Art—International Symposium. May 2007, Porto, Portugal.

Martin, R.F. and De Vito, C., 2005. The patterns of enrichment in felsic pegmatites ultimately depend on tectonic setting. Canadian Mineralogist, 43, 2027–2048.

Massey, N.W.D., McIntyre, D.G., Dejardins, P.J., and Cooney, R.T., 2005. Digital geology map of British Columbia. British Columbia Ministry of Energy, Mines and Petroleum Resources, British Columbia Geological Survey Open File 2005-2, DVD.

May, W.E. and Rumble, J. Jr, 2003. Certificate of analysis – standard reference material 2780. National Institute of Standards and Technology, Gaithersburg, USA, 4 p.

McClenaghan, M.B., 2011. Overview of common processing methods for recovery of indicator minerals from sediments and bedrock in mineral exploration. Geochemistry: Exploration, Environment, Analysis, 11, 265-278.

McClenaghan, M.B., 2014. Overview of indicator mineral recovery methods for sediments and bedrock: 2013 update. In: McClenaghan, M.B., Plouffe, A., and Layton-Matthews, D., (eds) 2014. Application of indicator mineral methods to mineral exploration. Geological Survey of Canada, Open File 7553, 1-7.

McCreath, J.A., Finch, A.A., Herd, D.A., and Armour-Brown, A.A., 2013. Geochemistry of pyrochlore minerals from the Motzfeldt center, south Greenland: The Mineralogy of a syenite-hosted Ta, Nb deposit. American Mineralogist, 98, 426–438.

McCurdy, M.W, Kjarsgaard, I.M., Day, S.J.A., McNeil, R.J., Friske, P.W.B., and Plouffe, A., 2009. Indicator mineral content and geochemistry of stream sediments and waters from northeast British Columbia (NTS 94A, 94B, 94G, 94H, 94I, 94K, 94N, 94O, 94P). British Columbia Ministry of Energy and Mines, Geological Survey of British Columbia, Report 2009-2 and Geological Survey of Canada, Open File 6311, 19 p.

McCurdy, M.W., Prior, G.J., Friske, P.W.B., McNeil, R.J., Day, S.J.A., and Nicholl, T.J., 2006. Geochemical, mineralogical and kimberlites indicator mineral electron microprobe data from silts, heavy mineral concentrates and water from a national geochemical reconnaissance stream sediment and water survey in northern and

southwestern Buffalo Head Hills, northern Alberta (parts of 84B, 84C, 84F, and 84G): Alberta Energy and Utilities Board, Alberta Geological Survey, Special Report 76 and Geological Survey of Canada Open File 5057, 11 p.

McLeish, D.F., 2013. Structure, stratigraphy, and U–Pb zircon-titanite geochronology of the Aley carbonatite complex, northeast British Columbia: evidence for Antler-aged orogenesis in the foreland belt of the Canadian Cordillera. MSc. Thesis. University of British Columbia, Vancouver, Canada.

McLeish, D.F., Kressall, R., and Crozier, J., 2010. The Aley carbonatite complex – Part I structural evolution of a Cordilleran niobium deposit mine. In: Simandl, G.J., and Lefebure, D.V., (eds), International Workshop on the Geology of Rare Metals, November 9-10, 2010, Victoria, Canada. Extended Abstracts Volume. British Columbia Ministry of Energy and Mines, British Columbia Geological Survey, Open File 2010-10, pp. 21-24.

Melcher, F., Graupner, T., Gabler, H-E., Sitnikova, M., Henjes-Kunst, F., Oberthür, T., Gerdes, A., and Dewaele, S., 2013. Tantalum-(niobium-tin) mineralisation in African pegmatites and rare metal granites: Constrains from Ta-Nb oxide mineralogy, geochemistry and U-Pb geochronology. Ore Geology Reviews, 2013, http://dx.doi.org/10.1016/j.oregeorev.2013.09.003

Melgarejo, J.C., Constanzo, A., Bambi, A.C.J.M., Goncalves, A.O., and Neto, A.B., 2012. Subsolidus processes as a key factor on the distribution of Nb species in plutonic carbonatites: The Tchivira case, Angola. Lithos, 152, 187–201.

Mikulski, S.Z. and Wierchowiec, J., 2013. Placer scheelite and gold from alluvial sediments as indicators of primary mineralization - examples from SW Poland. Geological Quarterly, 57, 503–514.

Miles, K.R., Carroll, D., and Rowledge, H.P., 1945. Tantalum and niobium: Perth, Department of Mines, Mineral Resources of Western Australia Bulletin 3, 150p.

Miller, R.R., 1986. Geology of the Strange Lake alkalic complex and the associated Zr–Y–Nb–Be–REE mineralization. In: Current Research, Newfoundland Department of Mines and Energy, Mineral Development Division; Report 86–1, pp 11–19.

Miller, R.R., 1990. The Strange Lake pegmatite-aplite-hosted rare-metal deposit, Labrador. In: Current Research, Newfoundland Department of Mines and Energy, Mineral Development Division; Report 90–1, pp 171–182.

Miller, R.R., Heaman, L.M., and Birkett, T.C., 1997. U–Pb zircon age of the Strange Lake peralkaline complex: implications for Mesoproterozoic peralkaline magmatism in North-Central Labrador. Precambrian Research, 81, 67–92.

Millonig, L.J., Gerdes, A., and Groat, L.A., 2012. U-Th-Pb geochronology of meta-carbonatites and meta-alkaline rocks in the southern Canadian Cordillera: A geodynamic perspective. Lithos, 152, 202-217.

Mitchell, R.H., 2005a. Carbonatites and carbonatites and carbonatites. The Canadian Mineralogist, 43, 2049–2068.

Mitchell, R.H., 2005b. Mineralogical and experimental constraints on origins of niobium mineralisation in carbonatites. In: Linnen, R.L., and Samson, I.M. (eds) Rare-Element Geochemistry and Mineral Deposits. Geological Association of Canada Short Course Notes 17, 201–213.

Möller, P. and Morteani, G., 1983. On the geochemical fractionation of rare earth elements during the formation of Ca-minerals and its application to problems of the genesis of ore deposits. In: Augusthitis, S.S. (ed) The significance of trace elements in solving petrogenetic problems and controversies. Theophrastus Publications, Athens, pp 747–791.

Möller, V. and Williams-Jones, A.E., 2013. Magmatic controls on the formation of the Nechalacho rare metal deposit. Society of Economic Geologists, ePosters, Whistler, Canada, 638–644.

Moloshag, V.P., 1974. On the geochemistry of the rare elements in one of the rare-metal pegmatites shields of Siberia. Moscow University Geology Bulletin, 29, 87–89.

Mongolia Central Geological Laboratory, 2006. Certified Reference Material “TRLK” Rare Earth Ore “CGL 124” Certificate of Analysis. Ulaanbaatar, Mongolia, 6 p.

Mozley Inc., (undated). Installation, operation and maintenance manual: C800 laboratory mineral separator. Mozley Inc., Gloucester, United Kingdom, 26 p.

Nakai, S., Masuda, A., Shimizu, H., and Qi, L., 1989. La–Ba dating and Nd and Sr isotope studies on the Baiyun Obo rare earth element ore deposits, Inner Mongolia, China. Economic Geology, 84, 2296–2299.

Nardi, L.V.S., Milton, L.L., Jarvis, K., Oliveira, L., Bastos Neto, A.C., and Fontana, E., 2012. REE, Y, Nb, U, and Th contents and tetrad effects in zircon from a magmatic-hydrothermal F-rich system of Sn-rare metal-cryolite mineralized granites from the Pitinga Mine, Amazonia, Brazil. Journal of South American Earth Science, 33, 34–42.

Nasraoui, M. and Bilal, E., 2000. Pyrochlores from the Lueshe carbonatites complex (Democratic Republic of Congo): A geochemical record of different alteration stages. Journal of Asian Earth Sciences, 18, 237–251.

Nasraoui, M. and Waerenborgh, J.C., 2001. Fe speciation in weathered pyrochlore-group minerals from the Lueshe and Araxá (Barreiro) carbonatites by ^{57}Fe Mössbauer spectroscopy. Canadian Mineralogist, 39, 1073–1080.

Nedosekova, I.L., 2007. New Data on Carbonatites of the Il’mensky-Vishnevogorsky alkaline complex, the southern Urals, Russia. Geology of Ore Deposits, 49, 129–146.

Nethery, B.T., 2007. Report of technical exploration and development – 2006 evaluation and exploration planning on the Aley Carbonatite property, Ospika River, BC (Omineca Mining District). British Columbia Ministry of Energy, Mines, and Petroleum Resources, Assessment Report 28733, 410 p.

Nowak, I. and Ziolek, M., 1999. Niobium compounds: preparation, characterization, and application in heterogeneous catalysis. Chemical Review, 99, 3603–3624.

Nuinsco Resources Limited, 2014. Prairie lake (Canada) project information. http://www.nuinsco.ca/projects/prairie-lake/. Accessed 5 Feb 2014.

Ohnenstetter, D. and Piantone, P., 1992. Pyrochlore-group minerals in the Beauvoir peraluminous leucogranite, Massif Central, France. The Canadian Mineralogist, 30, 771–784.

Olson, J.C., Marvin, R.F., Parker, R.L., and Mehnert, H.H., 1977. Age and tectonic setting of lower Paleozoic alkalic and mafic rocks, carbonatites, and thorium veins in south-central Colorado. Journal of Research of the US Geological Survey, 5, 673–687.

Orris, G.J. and Chernoff, C.B., 2002. Data set of world phosphate mines, deposits, and occurrences—part B. Location and mineral economic data. U.S. Geological Survey, Open-File Report 02-156-B, 328p.

Pacific Wildcat Resources Corp., 2013a. Mrima hill deposit. http://www.pacificwildcat.com/mrimahill.html. Accessed 11 Dec 2013.

Pacific Wildcat Resources Corp., 2013b. Muiane tantalum mine. http://www.pacificwildcat.com/muiane.html. Accessed 11 Dec 2013.

Pal, D.C., Mishra, B. and Bernhardt, H.-J., 2007. Mineralogy and geochemistry of pegmatites-hosted Sn-, Ta-Nb-, and Zr-Hf-bearing minerals from the southeastern part of the Bastar-Malkangiri pegmatites belt, central India. Ore Geology Reviews, 30, 30–50.

Papp, J.F., 2009a. Tantalum. In: U.S. Geological Survey, Mineral Commodity Summaries 2009, pp 164–165.

Papp, J.F., 2009b. Niobium (columbium). In: U.S. Geological Survey, Mineral Commodity Summaries 2009, pp 110–111.

Papp, J.F., 2011a. Tantalum. In: U.S. Geological Survey, Mineral Commodity Summaries 2011, pp 162–163.

Papp, J.F., 2011b. Niobium (columbium). In: U.S. Geological Survey, Mineral Commodity Summaries 2011, pp 110–111.

Papp, J.F., 2012. Niobium and tantalum (advanced release). In: U.S. Geological Survey 2011 Minerals Yearbook. http://minerals.usgs.gov/minerals/pubs/commodity/niobium/myb1-2011-niobi.pdf. Accessed 17 Jul 2013.

Papp, J.F., 2013a. Tantalum. In: U.S. Geological Survey, Mineral Commodity Summaries 2013, pp 162–163.

Papp, J.F., 2013b. Niobium (columbium). In: U.S. Geological Survey, Mineral Commodity Summaries 2013, pp 110–111.

Pareja, L., 2011. Minsur-investing in tin seminar. ITRI investing in tin seminar, December 5, 2011. https://www.itri.co.uk/index.php?option=com_mtree&task=att_download&link_id=49887&cf_id=24. Accessed 11 Dec 2013.

Partington, G.A., McNaughton, N.J., and Williams, I.S., 1995. A review of the geology, mineralization, and geochronology of the Greenbushes pegmatite, Western Australia. Economic Geology, 90, 616–635.

Pekov, I.V., 2000. Lovozero Massif: History, pegmatites, minerals. Ocean Pictures Ltd, Moscow.

Pekov, I.V., Agakhanoc, A.A., Boldyreva, M.M., and Grishin, V.G., 2005. Pautovite, $CsFe_2S_3$, a new mineral species from the Lovozero alkaline complex, Kola Peninsula, Russia. Canadian Mineralogist, 43, 965–972.

Pell, J., 1994. Carbonatites, nepheline syenites, kimberlites and related rocks in British Columbia. British Columbia Ministry of Energy, Mines and Petroleum Resources, British Columbia Geological Survey, Bulletin 88, 136 p.

Pena, F.E., 1989. Perfil Analitico do Piroclore (niobio). DNPM, Brasilia, 59p.

Petrella, L.L., 2012. The nature and origin of REE mineralization in the Misery syenitic intrusions, northern Québec, Canada. MSc thesis, McGill University.

Petruk, W. and Ownes, D.R., 1975. Electron microprobe analyses for pyrochlores from Oka, Quebec. The Canadian Mineralogist, 13, 282–285.

Pinckston, D.R. and Smith, D.G.W., 1995. Mineralogy of the Lake Zone, Thor Lake rare-metals deposit, N.W.T., Canada. Canadian Journal of Earth Science, 32, 516–532.

Pitcher, W.S., 1983. Granite type and tectonic environment. In: Hsü, K.J., (ed) Mountain building processes. Academic Press, London.

Pitcher, W.S., 1993. The Nature and origin of granite. Blackie, London.

Pohl, W.L., 2012. Sample chapter: niobium and tantalum (updated December 18, 2012). In: Pohl, W.L., (ed) Economic geology, principles and practice: metals, minerals, coal and hydrocarbons—an introduction to formation and sustainable exploitation of mineral deposits. Wiley-Blackwell, West Sussex, pp 261–265.

Pouchou, J.L. and Pichoir, F., 1985. PAP $\phi(\rho Z)$ procedure for improved quantitative microanalysis. Microbeam Analysis, 1985, 104–106.

Pride, K.R., 1983. Geological survey on the Aley claims. British Columbia Ministry of Energy, Mines, and Petroleum Resources, Assessment Report 12018, 16 p.

Pride, K.R., 1987a. 1986. Year end report on the Aley property: British Columbia Ministry of Energy, Mines, and Petroleum Resources, Assessment Report 15721, 69 p.

Pride, K.R., 1987b. 1986. Diamond drilling assessment report: British Columbia Ministry of Energy, Mines, and Petroleum Resources, Assessment Report 16484, 59 p.

Pyle, L.J. and Barnes, C.R., 2001. Conodonts from the Kechika Formation and Road River Group (Lower to Upper Ordovician) of the Cassiar Terrane, northern British Columbia: Canadian Journal of Earth Sciences, 38, 1387–1401.

Raimbault, L., Cuney, M., Azencott, C., Duthou, J.L., and Joron, J.L., 1995. Geochemical evidence for a multistage magmatic genesis of Ta, Sn, Li mineralization in the granite at Beauvoir, French Massif Central. Economic Geology, 90, 548–576.

Ram Resources Limited, 2013. Motzfeldt project. http://www.ramresources.com.au/greenland.html. Accessed 18 Dec 2013.

Razali, R. and Veasey, T.J., 1990. Statistical modelling of a shaking table separator – part one. Minerals Engineering, 3, 287-294.

Read, P.B., Woodsworth, G.J., Greenwood, H.J., Ghent, E.D. and Evenchick, C.A., 1991. Metamorphic map of the Canadian Cordillera. Geological Survey of Canada, Map 1714A, scale 1:2 000 000.

Rene, M. and Škoda, R., 2011. Nb-Ta-Ti oxides fractionation in rare-metal granites: Krasno-Morni Slavkov Ore District, Czech Republic. Mineral Petrology, 103, 37–48.

Reunion Mining PLC, 1998. Reunion Mining PLC Press Release. http://www.infomine.com/index/pr/Pa009223.PDF. Accessed 6 Feb 2014.

Reyf, F.G., Seltmann, R., and Zaraisky, G.P., 2000. The role of magmatic processes in the formation of banded Li, F-enriched granites from the Orlovka tantalum deposit, Transbaikalia, Russia: Microthermometric evidence. Canadian Mineralogist, 38, 915–936.

Richard, P.L. and Pelletier, C., 2011. 43–101 technical report and resource estimate on the Pivert-Rose property. Critical Elements Corporation, Montreal, Canada, 141p. http://www.cecorp.ca/documents/en/43-101_cecorp_pivertRose2011_sedar.pdf. Accessed 11 Dec 2013.

Richardson, D.G. and Birkett, T.C., 1995. Peralkaline rock-associated rare metals. In: Eckstrand, O.R., Sinclair, W.D., and Thorpe, R.I. (eds) Geology of Canadian mineral deposits types, No. 8. Geological Survey of Canada, pp 523–540.

Robert, M., Lyons, E.M., Hardy, J.L., and Nethery, B.T., 2005. Report of technical exploration and development – trenching, sampling, metallurgical testing and evaluation on the Aley carbonatite property, Ospika River, BC (Omineca Mining District): British Columbia Ministry of Energy, Mines, and Petroleum Resources, Assessment Report 27991, 60 p.

Rose, A.W., Herbert, H.E. and Webb, J.S., 1979. Geochemistry in Mineral Exploration (second edition). Academic Press, London, United Kingdom, 657 p.

Roskill, 2013a. Tantalum: market outlook to 2016. http://www.roskill.com/reports/minor-and-light-metals/tantalum. Accessed 27 Jul 2013.

Roskill, 2013b. Niobium: market outlook to 2017, 12th edn. http://www.roskill.com/reports/steel-alloys/niobium/?searchterm=niobium. Accessed 27 Jul 2013.

Rowe, R.B., 1958. Niobium (columbium) deposits of Canada. Geological Survey of Canada, Economic Geology Series 18, 103 p.

Rub, A.K., Štemprok, M., and Rub, M.G., 1998. Tantalum mineralization in the apical part of the Cínovec (Zinnwald) granite stock. Mineralogy and Petrology, 63, 199–222.

Sage, R.P., 1988. Geology of carbonatite-alkalic rock complexes in Ontario: Argor carbonatite complex, District of Cochrane. Ontario Geological Survey Study 41.

Salvi, S. and Williams-Jones, A.E., 1990. The role of hydrothermal processes in the granite hosted Zr, Y, REE deposit at Strange Lake, Quebec/Labrador: Evidence from fluid inclusions. Geochimica et Cosmochimica Acta, 54, 2403–2418.

Salvi, S. and Williams-Jones, A.E. 1996. The role of hydrothermal processes in concentrating HFSE in the Strange Lake peralkaline complex, northeastern Canada. Geochimica et Cosmochimica Acta, 60, 1917–1932.

Salvi, S. and Williams-Jones, A.E., 2005. Alkaline granite-syenite deposits. In: Linnen, R.L. and Samson, I.M., (eds) Rare-element geochemistry and mineral deposits. Short Course Notes, Geological Association of Canada, special publication, 17, 315–341.

Salvi, S. and Williams-Jones, A.E., 2006. Alteration, HFSE mineralization and hydrocarbon formation in peralkaline igneous systems: Insights from the Strange Lake Pluton, Canada. Lithos, 91, 19–34

Saucier, G., Noreau, C., Casgrain, P., Côté, P., Larochelle, E., Bilodeau, M., Hayden, A., Poirier, E., Garon, M., Bertrand, V., Kissiova, M., Malloux, M., Rouger, M., Camus, Y., and Gagnon, G., 2013. NI-43-101 report-feasibility study for the Kipawa project Temiscamingue area, Québec, Canada. Matamec Explorations Inc., Montréal.

Schwartz, M.O., Rajah, S.S., Askury, A.K., Putthapiban, P., and Djaswadi, S., 1995. The Southeast Asian tin belt. Earth Science Review, 38, 95–293.

Scott, P.W., Pascoe, R.D., and Hart, F.W., 1998. Columbite-tantalite, rutile and other accessory minerals from the St Austell topaz granite, Cornwall. Geoscience in South-West England, 9, 165–170.

Seltmann, R., Soloviev, S., Shatov, V., Pirajno, F., Naumov, E., and Cherkasov, S., 2010. Metallogeny of Siberia: Tectonic, geologic and metallogenic settings of selected significant deposits. Australian Journal of Earth Science, 57, 655–706.

Shand, S.J., 1927. Eruptive rocks, 1st edition. Wiley, New York.

Shaw, R. and Goodenough, K., 2011. Niobium–tantalum. British Geological Survey, Keyworth.

Sheard, E.R., 2010. Behaviour of zirconium, niobium, yttrium and the rare earth elements in the Thor Lake rare-metal deposit, Northwest Territories, Canada. MSc thesis, McGill University, Canada.

Sheard, E.R., Williams-Jones, A.E., Heiligmann, M., Pederson, C., and Trueman, D.L., 2012. Controls on the concentration of zirconium, niobium, and the rare earth elements in the Thor Lake rare metal deposit, Northwest Territories, Canada. Economic Geology, 107, 81–104.

Shimazaki, H., Yang, Z., Myawaki, R., and Shigeoka, M., 2012. Scandium-bearing minerals in the Bayan Obo Nb-REE-Fe deposit, Inner Mongolia, China. Resource Geology, 58, 80–86.

Simandl, G.J., 2002. Tantalum market and resources: an overview. In: Geological Field Work 2001. British Columbia Ministry of Energy and Mines, Geological Survey of British Columbia Paper 2002–1, pp 313–318.

Simandl, G.J., 2014. Geology and market-dependent significance of rare earth element resources. Mineralium Deposita, 49, 889-904.

Simandl, G.J., Jones, P.C., and Rotella, M., 2001. Blue river carbonatites, British Columbia-primary exploration targets for tantalum. Exploration and Mining in British Columbia – 2001.

Simandl, G.J., Reid, H.M., and Ferri, F., 2013. Geological setting of the Lonnie niobium deposit, British Columbia, Canada. In: Geological Fieldwork 2012. British Columbia Ministry of Energy, Mines and Natural Gas, British Columbia Geological Survey paper 2013–1, pp 127–138.

Simandl, G. J., Paradis, S., Stone, R. S., Fajber, R., Kressall, R., Grattan, K., Crozier, J., and Simandl, L.J., 2014a. Applicability of handheld X-ray fluorescence spectrometry in the exploration and development of carbonatite-related niobium deposits: a case study of the Aley carbonatite, British Columbia, Canada. Geochemistry: Exploration, Environment, Analysis, 14, 211-221.

Simandl, G.J., Prussin, E.A., and Brown, N., 2012. Specialty metals in Canada. British Columbia Ministry of Energy and Mines, British Columbia Geological Survey, Open File 2012-7, 48 p.

Simandl, G.J., Fajber, R., and Paradis, S., 2014. Portable X-ray fluorescence in the assessment of rare earth element-enriched sedimentary phosphate deposits. Geochemistry: Exploration, Environment, Analysis, 14, 166-169.

Simpson, R.G., 2012. Technical report—Aley carbonatite niobium project, Omenica Mining District, British Columbia, Canada. Taseko Mines Limited, Vancouver.

Sinclair, W.D., Hunt, P.A., and Birkett, T.C., 1994. U–Pb zircon and monazite ages of the Grace Lake granite, Blatchford Lake intrusive suite, Slave Province, Northwest Territories. In: Geological Survey of Canada, Current Research 1994-F, Report 8: 15–20.

Sivamohan, R. and Forssberg, E., 1985. Principles of tabling. International Journal of Mineral Processing, 15, 281-295.

Slater, J.C., 1964. Atomic radii in crystals. Journal of Chemical Physics, 41, 3199–3205.

Smith, M. and Spratt, J., 2012. The chemistry of niobium mineralisation at Bayan Obo, Inner Mongolia, China: Constraints on the hydrothermal precipitation and alteration of Nb-minerals. Acta Geologica Sinica, 86: ISSN 0001–5717.

Sonoki, I.K. and Garda, G.M., 1988. Idades K–Ar de rochas alcalinas do Brasil Meridional e Paraguai Oriental: Compilação e Adaptação as Novas Constants de Decaimento. Bol IG-USP 19, 63–85.

Sons of Gwalia Ltd., 2002. Sons of Gwalia Ltd. Annual Report 2001.

Sørensen, H., 1960. On the agpaitic rocks. Rep 21st International Geological Congress, Norden 13, 319–327.

Sørensen, H., 1968. Rhythmic igneous layering in peralkaline intrusions. An essay review on Ilimaussaq (Greenland) and Lovozero (Kola, USSR). Lithos, 2, 261–283.

Staatz, M.H., Armbrustmacher, T.J., Olson, J.C., Brownfield, I.K., Brock, M.R., Lemons, J.F. Jr, Coppa, L.V., and Clingan, B.V., 1979. Principal thorium resources in the United States. US Geological Survey Circular, 805.

Steger, H.F. and Bowman, W.S., 1981. OKA-1: a certified niobium reference ore. CANMET Report 81-1E, Canada Centre for Mineral and Energy Technology, Ottawa, Canada, 16 p.

Stewart, R., 1986. Routine heavy mineral analysis using a concentrating table. Journal of Sedimentary Research, 56, 555-556.

Stockford, H.R., 1972. The James Bay pyrochlore deposit. Canadian Institute of Mining and Metallurgy Bulletin, June; 61–69.

v. Straaten, P., 2002. Rocks for crops: Agrominerals of Sub-Saharan Africa. ICRAF, Nairobi.

Stratton, P. and Henderson, D., 2013. Tantalum market overview. Minor metals trace association. http://www.mmta.co.uk/tantalum-marketoverview. Accessed 18 Feb 2014.

Sugitani, Y., Suzuki, Y., and Nagashima, K., 1985. Polymorphism of samarskite and its relationship to other structurally related Nb–Ta oxides with the α-PbO_2 structure. American Mineralogist, 70, 856–866.

Sunde, O., 2013. Mineralogy and petrology of the amazonite pegmatite at Bakstevalåsen, øvre Eiker. MSc thesis, University of Oslo, Norway.

Sweetapple, M.T. and Collins, P.L.F., 1998. Tantalum–tin mineralized pegmatites at Wodgina and Mount Cassiterite, Pilbara Craton, Western Australia: geological society of Australia, 14th Australian Geological Convention, Townsville, Queensland, 1998, Abstracts no. 43, 435.

Sweetapple, M.T. and Collins, L.F., 2002. Genetic framework for the classification and distribution of Archean rare metal pegmatites in the north Pilbara Craton, Western Australia. Economic Geology, 97, 872–895.

Sweetapple, M.T., Collins, P.L.F., and Hickey, R.J., 2001a. Classification, distribution and petrogenetic affiliation of the Archaean rare metal pegmatites, Pilbara Craton, W.A. Australian Geological Survey Organisation-Geoscience Australia International Archaean Symposium, 4th, Perth, Western Australia, Proceedings: pp 475–477.

Sweetapple, M.T., Cornelius, H., and Collins, P.L.F., 2001b. Tantalum mineralisation of the Wodgina pegmatite district: The Wodgina and Mt. Cassiterite pegmatite

orebodies. In: Huston, D.L., Blewett, R.S., Sweetapple, M., Brauhart, C., Cornelius, H., and Collins, P.L.F., (eds) 2001. Metallogenesis of the North Pilbara granite-greenstones, Western Australia—a field guide. Geologic Survey of Western Australia Report, 2001/11:41–58.

Sweetapple, M.T., Hickey, R.J., and Collins, P.L.F., 2000a. Controls on regional distribution of rare metal pegmatites in the Archaean Pilbara Craton, Western Australia. Geological Society of Australia Abstract, 59, 425.

Sweetapple, M.T., Lumpkin, G.R., and Collins, P.L.F., 2000b. Characteristics of tantalum–niobium–tin oxide minerals from the Wodgina and Mt. Cassiterite Pegmatites, Pilbara Craton, Western Australia. Geological Society of Australia Abstract, 59, 426.

Tadesse, S. and Zerihun, D., 1996. Composition, Fractionation Trend and Zoning Accretion of the Columbite-Tantalite Group of Minerals in the Kenticha Rare-Metal Field (Adola, Southern Ethiopia). Journal of African Earth Sciences, 23, 411–431.

Tantalum-Niobium International Study Center, 2013a. Tantalum–raw materials and processing. http://tanb.org/tantalum. Accessed 17 Jul 2013.

Tantalum-Niobium International Study Center, 2013b. Niobium–raw materials and processing. http://tanb.org/niobium. Accessed 17 Jul 2013.

Tertiary Minerals PLC, 2013. Ghurayyah tantalum–niobium–rare-earth project, Saudi Arabia. http://www.tertiaryminerals.com/ghurayyah.html. Accessed 11 Dec 2013.

Thivierge, S., Roy, O.W., Chown, E.H., and Gauthier, A., 1983. Évolution du complexe alcalin de St. Honoré (Québec) Après sa Mise en Place. Mineralium Deposita, 18, 267–283.

Tindle, A.G. and Breaks, F.W., 1998. Oxide minerals of the Separation Rapids rare-element granitic pegmatites group, northwestern Ontario. The Canadian Mineralogist, 36, 609–635.

Tindle, A.G. and Breaks, F.W., 2000. Columbite-tantalite mineral chemistry from rare-element granitic pegmatites: Separation Lake area, N.W. Ontario, Canada. Mineralogy and Petrology, 70, 165–198.

Torro, L., Villanova, C., Castillo, M., Campeny, M., Goncalves, A.O., and Melgarejo, J.C., 2012. Niobium and rare earth minerals from the Virulundo carbonatite, Namibe, Angola. Mineralogical Magazine, 76, 393–409.

Traversa, G., Gomes, C.B., Brotzu, P., Buraglini, N., Morbidelli, L., Principato, M.S., Ronca, S., and Ruberti, E., 2001. Petrography and mineral chemistry of carbonatites and mica-rich rocks from the Araxa Complex (Alto Paranaiba Province, Brazil). Anais da Academia Brasileira de Ciencias, 73, 71–98.

Trofanenko, J., Williams-Jones, A.E., and Simandl, G.J., 2014. The nature and origin of the carbonatite-hosted Wicheeda rare earth elements deposit, British Columbia. In: Geological fieldwork 2013. British Columbia Ministry of Energy and Mines, British Columbia Geological Survey Paper 2014–1, pp 213–225.

Trueman, D.L. and Černý, P., 1982. Exploration for rare-element granitic pegmatites. In: Černý, P., (ed) Granitic pegmatites in science and industry. Mineral Association of Canada Short Course, Volume 8, Winnipeg, Canada, pp 463–493.

Tse, P.K., 2011. China's rare-earth industry. United States Geological Survey, Open-File Report 2011-1042, 11 p.

Tuck, C.A., 2013. Iron ore. In: U.S. Geological Survey, Mineral Commodity Summaries 2003, 84–85.

Tukiainen, T.T., 1988. Niobium-tantalum mineralisation in the Motzfeldt centre of the Igaliko nepheline syenite complex, south Greenland. In: Boissonnas, J., and Omenetto, P. (eds) Mineral deposits within the European Community. Springer, Berlin, 230–246.

Vallée, M. and Dubuc, F., 1970. St-Honoré carbonatite complex, Quebec. Canadian Mining and Metallurgical Bulletin, 63, 1384–1394.

Varlamoff, N., 1972. Central and West African rare-metal granitic pegmatites, related aplites, quartz veins and mineral deposits. Mineralium Deposita, 7, 202–216.

Viladkar, S.G. and Bismayer, U., 2010. Compositional variation in pyrochlore of Amba Dongar carbonatites complex, Gujarat. Journal Geological Society of India, 76, 495–502.

Vlasov, K.A., Kuzmenko, M.Z., Eskova, E.M., 1966. The Lovozero alkali massif. Translated by Fry DG, Sayers K. Oliver and Boyd, Edinburgh and London. Geological Journal, 5 xviii. doi:10.1002/gj.3350050219.Wall, F., Williams, C.T., Woolley, A.R., and Nasraoui, M., 1996. Pyrochlore from weathered carbonatite at Lueshe, Zaire. Mineralogical Magazine, 60, 731–750.

Wang, R.C., Fontan, F., Xu, S.J., Chen, X.M., and Monchoux, P., 1996. Hafnian zircon from the apical part of the Suzhou granite, China. The Canadian Mineralogist, 34, 1001–1010.

Wang, R.C., Fontan, F., Xu, S.J., Chen, X.M., and Monchoux, P., 1997. The association of columbite, tantalite and tapiolite in the Suzhour granite, China. The Canadian Mineralogist, 35, 699–706.

Webster, J., Thomas, R., Förster, H.J., Seltmann, R., and Tappen, C., 2004. Geochemical evolution of halogen-enriched granite magmas and mineralising fluids of the Zinnwald tin-tungsten mining district, Erzgebirge, Germany. Mineralium Deposita, 39, 452–472.

Wen, J., Bell, K., and Blenkinsop, J., 1987. Nd and Sr isotope systematics of the Oka Complex, Quebec, and their bearing on the evolution of the sub-continental upper mantle. Contributions to Mineralogy and Petrology, 97, 433–437.

Welkner, D., Godoy, E., and Bernhardt, H.H-J., 2002. Peralkaline rocks in the Late Cretaceous Del Salto pluton, eastern Patagonia Andes, Aisen, Chile. Revista geológica de Chile, 29, 3–15.

Wenger, M., Armbruster, T., and Geiger, C.A., 1991. Cation distribution in partially ordered columbite from the Kings Mountain pegmatite, North Carolina. American Mineralogist, 76, 1897–1904.

Wetzel, F., Schmitt, A.K., Kronz, A., and Worner, G., 2010. In situ ^{238}U-^{230}Th disequilibrium dating of pyrochlore at sub-millennial precision. American Mineralogist, 95, 1353–1356. Supplementary information, AM-10-037. http://dx.doi.org/10.2138/am.2010.3441

Williams, C.T., 1996. The occurrence of niobian zirconolite, pyrochlore and baddeleyite in the Kovdor carbonatite complex, Kola Peninsula, Russia. Mineralogical Magazine, 60, 639–646.

Williams, C.T., Wall, F., Woolley, A.R., and Phillipo, S., 1997. Compositional variation in pyrochlore from the Bingo carbonatite, Zaire. Journal of African Earth Sciences, 25, 137–145.

Winter, M., 2011. WebElements: the periodic table on the web: home of the periodic table. WebElements, The University of Sheffield and Web Elements Ltd., UK. www.webelements.com. Accessed 14 Feb 2014.

Wise, M.A. and Černy, P., 1996. The crystal chemistry of the Tapiolite series. The Canadian Mineralogist, 34, 631–647.

Woolley, A.R., 2003. Igneous silicate rocks associated with carbonatites: their diversity, relative abundances and implications for carbonatite genesis. Periód Mineral, 72, 9–17.

Woolley, A.R. and Kjarsgaard, B.A., 2008. Paragenetic types of carbonatite as indicated by the diversity and relative abundances of associated silicate rocks: evidence from a global database. Canadian Mineralogist, 46, 741–752.

Woolley, A.R. and Platt, R.G., 1988. The peralkaline nepheline syenites of the Junguni intrusions, Chilwa Province, Malawi. Mineralogical Magazine, 52, 425–433.

Yakovleva, O.S., Pekov, I.V., Horvath, L., Bryzgalov, I.A., Yapaskurt, V.O., and Guzeva, E.V., 2010. Mineralogy, geochemistry, and genesis of high-alumina fenites of the Mont Saint-Hilaire alkaline pluton, Quebec, Canada. Geology of Ore Deposits, 52, 725–735.

Yuan, Z., Bai, G., Wu, C., Zhang, Z., and Ye, X., 1992. Geological features and genesis of the Bayan Obo REE ore deposit, Inner Mongolia, China. Applied Geochemistry, 7, 429–442.

Zaitsev, V. and Kogarko, L., 2012. Sources and perspectives of REE in the Lovozero Massif (Kola Peninsula, Russia). European Mineralogical Conference, 1: EMC2012–EMC2290.

Zaitsev, A.N., Wall, F., and Le Bas, M.J., 1998. REE–Sr–Ba minerals from the Khibina carbonatites, Kola Peninsula, Russia: Their mineralogy, paragenesis and evolution. Mineralogical Magazine, 62, 225–250.

Zaitsev, A.N. A., Williams, C.T., Wall, F., and Zolotarev, A.A., 2012. Evolution of chemical composition of pyrochlore group minerals from phoscorites and carbonatites of the Khibina Alkaline Massif. Geology of Ore Deposits, 54, 503–515.

Zakharov, V.I., Maiorov, D.V., Alishkin, A.R., and Matveev, V.A., 2011. Causes of insufficient recovery of zirconium during acidic processing of Lovozero eudialyte concentrate. Russian Journal of Nonferrous Metals, 52, 423–428.

Zurevinski, S. and Mitchell, R.H., 2004. Extreme compositional variation of pyrochlore-group minerals at the Oka carbonatite complex, Quebec: Evidence of magma mixing? The Canadian Mineralogist, 42, 1159–1168.

Appendix A
Pyrochlore supergroup and columbite-tantalite series minerals

New electron microprobe analysis and data compiled from the literature for pyrochlore supergroup and columbite-tantalite series minerals are presented in the supplementary data file. Deposit name, locations, minerals, and sources are given in table A.1.

Table A.1 Mineral chemistry database sources

Deposit Name	Location	Minerals	Data Source
CARBONATITE COMPLEX			
Aley	British Columbia, Canada	Pyrochlore Columbite-(Fe)	Chakhmouradian et al. 2015
Afrikanada Complex	Murmansk Oblast, Russia	Pyrochlore	Chakhmouradian and Zaitsev 1999
Amba Dongar	Gujarat, India	Pyrochlore Betafite	Viladkar and Bismayer, 2010
Argor	Ontario, Canada	Pyrochlore	Hogarth et al. 2000
Bayan Obo	Inner Mongolia, China	Columbite-(Fe)	Shimazaki et al. 2012
Bingo	North Kivu, Democratic Republic of Congo	Pyrochlore	Williams et al. 1997
Bonga	Huila, Angola	Pyrochlore	Bambi et al. 2014
Buldym Massif	Chelyabinsk Oblast, Russia	Pyrochlore	Nedosekova 2007
Carillon Dam	Ontario-Québec, Canada	Pyrochlore	Hogarth et al. 2000
Catalão I	Goiás, Brazil	Pyrochlore	Cordeiro et al. 2011
Chilwa Island	Zomba, Malawi	Pyrochlore	Hogarth et al. 2000
Khibina	Murmansk Oblast, Russia	Pyrochlore	Zaitsev et al. 2012
Kovdor	Murmansk Oblast, Russia	Pyrochlore	Williams 1996 Chakhmouradian and Williams 2004
Fen	Telemark, Norway	Pyrochlore	Hogarth et al. 2000
Fogo Island	Cape Verde Archipelago, Central Atlantic Ocean	Pyrochlore	Kogarko et al. 2009
Laacher See	Rhineland-Palatinate, Germany	Pyrochlore	Wetzel et al. 2010
Lesnaya Varaka	Murmansk Oblast, Russia	Pyrochlore	Chakhmouradian and Mitchell 1998
Lueshe	North Kivu, Democratic Republic of Congo	Pyrochlore Columbite-(Fe)	Wall et al. 1996 Nasraoui and Bilal 2000 Hogarth et al. 2000

Deposit Name	Location	Minerals	Data Source
Meech Lake	Québec, Canada	Pyrochlore	Hogarth et al. 2000
Mount Weld	Western Australia, Australia	Pyrochlore	Lottermoser and England 1988
Ndale Tuff	Western Region, Uganda	Pyrochlore	Hogarth and Horne 1989
Oka	Québec, Canada	Pyrochlore Betafite	Hogarth et al. 2000 Zurevinski and Mitchell 2004 Petruk and Owens 1975
Panda Hill	Mbeya, Tanzania	Pyrochlore	Hogarth et al. 2000
St. Honoré	Québec, Canada	Pyrochlore Columbite-(Fe)	Clow et al. 2011
San Vicente Island	Cape Verde Archipelago, Central Atlantic Ocean	Pyrochlore	Hodgson and Le Bas 1992
Sokli	Lapland, Finland	Pyrochlore	Chakhmouradian and Williams 2004 Lee et al. 2006
Tomtor	Sakha Republic, Russia	Pyrochlore	Kravchenko and Pokrovsky 1995
Tchivira	Huila, Angola	Pyrochlore	Melgarejo et al. 2012
Upper Fir	British Columbia, Canada	Pyrochlore Microlite Columbite-(Fe)	Simandl et al. 2001 Chudy 2014
Verity	British Columbia, Canada	Pyrochlore Columbite-(Fe)	Simandl et al. 2001
Virulundo	Namibi, Angola	Pyrochlore	Torró et al. 2012
Vuoriyarvi	Murmansk Oblast, Russia	Pyrochlore	Chakhmouradian and Williams 2004
PERALKALINE COMPLEX			
Amis	Erongo, Namibia	Pyrochlore	Wetzel et al. 2010
Bakriya	Eastern Desert, Egypt	Columbite-(Fe) Columbite-(Mn)	Abdalla et al. 1998
Bakstevalåsen Ovre Eiker	Oslo, Norway	Columbite-(Fe)	Sunde 2013
Del Salto Pluton	Capitán Prat Province, Chile	Pyrochlore	Welkner et al. 2002
Ditrau Alkaline Massif	Harghita, Romania	Columbite-(Fe)	Hirtopanu et al. 2013
Eaglet	British Columbia, Canada	Pyrochlore	Hora et al. 2009
El-Sibai	Eastern Desert, Egypt	Columbite-(Fe)	Ali 2013
Jungjuni	Chilwa, Malawi	Pyrochlore	Woolley and Platt 1988
Lovozero	Murmansk Oblast, Russia	Pyrochlore	Chakhmouradian and Sitnikova 1999 Chakhmouradian and Mitchell 2002
Misery	Québec, Canada	Columbite-(Fe)	Petrella 2012
Mont Saint-Hilaire	Québec, Canada	Pyrochlore Columbite-(Fe) Columbite-(Mn)	Chakhmouradian and Mitchell 2002 Yakovleva et al. 2010

Deposit Name	Location	Minerals	Data Source
Motzfeldt Center	Kujalleq, Greenland	Pyrochlore	McCreath et al. 2013 Tukiainen 1988 Bonazzi et al. 2006
Nechalacho	Northwest Territories, Canada	Pyrochlore Columbite-(Fe)	Pinckston and Smith 1995 Grammatikopoulos et al. 2011 Sheard 2010
Vico Volcanic Complex	Latium, Italy	Pyrochlore	Cámara et al. 2004
Vysoký Kámen Stock	Karlovy Vary Region, Czech Republic	Columbite-(Fe)	René and Škoda 2011
LCT PEGMATITE			
Arehalli	Karnataka, India	Tapiolite-(Fe)	Maithani and Singh 2011
Bastar-Malkanriri pegmatite belt	Chhattisgarh State, India	Pyrochlore Microlite Columbite-(Fe) Tantalite-(Fe) Tantalite-(Mn)	Pal et al. 2007
Bikita	Masvingo, Zimbabwe	Columbite-(Fe)	Melcher et al. 2013
Bupo I and II	Adola Woredas, Ethiopia	Columbite-(Fe) Columbite-(Mn) Tantalite-(Mn)	Tadesse and Zerihun 1996
Dermi Dama	Adola Woredas, Ethiopia	Columbite-(Mn) Tantalite-(Mn)	Tadesse and Zerihun 1996
Eräjärvi District	Pirkanmaa Region, Finland	Columbite-(Fe) Columbite-(Mn) Tantalite-(Fe) Tantalite-(Mn) Tapiolite-(Fe)	Lahti 2000
Greer Lake	Manitoba, Canada	Microlite	Černý et al. 1986
Homestead	!Karas, Namibia	Tanatlite-(Mn)	Melcher et al. 2013
Jezuitské Lesy	Bratislava Region, Slovakia	Microlite Columbite-(Fe) Columbite-(Mn) Tantalite-(Fe) Tantalite-(Mn)	Chudik et al. 2011
Kenticha	Adola Woredas, Ethiopia	Columbite-(Fe) Tantalite-(Fe) Columbite-(Mn) Tantalite-(Mn)	Tadesse and Zerihun 1996 Melcher et al. 2013
Shuni Hill	Adola Woredas, Ethiopia	Columbite-(Fe)	Melcher et al. 2013
Kilkile I, II, and III	Adola Woredas, Ethiopia	Columbite-(Fe) Columbite-(Mn) Tantalite-(Mn)	Tadesse and Zerihun 1996
Kolmozero Pegmatites	Murmansk Oblask, Russia	Columbite-(Fe) Columbite-(Mn) Tantalite-(Mn)	Badanina et al. 2014
Marropino	Zambezia, Mozambique	Tantalite-(Mn)	Melcher et al. 2013

Deposit Name	Location	Minerals	Data Source
Morrua	Mozambique	Tantalite-(Mn)	Melcher et al. 2013
Rubikon	Erongo, Namibia	Columbite-(Mn)	Melcher et al. 2013
Separation Rapids Pegmatites	Ontario, Canada	Pyrochlore Microlite Columbite-(Fe) Tantalite-(Fe) Columbite-(Mn) Tantalite-(Mn)	Tindle and Breaks 1998 Tindle and Breaks 2000
Tanco	Manitoba, Canada	Microlite Tapiolite-(Fe)	v. Lichtervelde et al. 2007 Wise and Černý 2001
Varuträsk	Västerbotten, Sweden	Columbite-(Mn) Columbite-(Fe) Tantalite-(Mn) Tapiolite-(Fe)	Černý et al. 2004
Volta Grande	Minas Gerais, Brazil	Microlite	Lumpkin and Ewing 1992
PERALUMINOUS GRANITE			
Abu Dabbab	Eastern Desert, Egypt	Columbite-(Mn)	Melcher et al. 2013
Abu Rusheid	Eastern Desert, Egypt	Columbite-(Fe) Columbite-(Mn)	Abdalla et al. 1998
Beauvoir	Allier, France	Pyrochlore Microlite	Ohnenstetter and Piantone 1992
Hub stock	Karlovy Vary Region, Czech Republic	Columbite-(Fe) Columbite- (Mn) Tantalite-(Fe) Tantalite-(Mn) Tapiolite-(Fe)	René and Škoda 2011
Kenticha Alaskitic Granite	Adola Woredas, Ethiopia	Columbite-(Fe) Columbite-(Mn) Tantalite-(Fe) Tantalite-(Mn)	Tadesse and Zerihun 1996
Mueilha	Eastern Desert, Egypt	Columbite-(Fe)	Abdalla et al. 1998
Nuweibi	Eastern Desert, Egypt	Columbite-(Mn) Tantalite-(Mn)	Abdalla et al. 1998 Melcher et al. 2013
Saint Austel	Cornwall, United Kingdom	Columbite-(Fe) Columbite-(Mn)	Scott et al. 1998
Separation Rapids Pluton	Ontario, Canada	Columbite-(Fe)	Tindle and Breaks 1998
Suzhou Granite	Jiangsu Province, China	Columbite-(Fe) Columbite-(Mn) Tantalite-(Fe) Tantalite-(Mn) Tapiolite-(Fe)	Wang et al. 1996 Wang et al. 1997
Um Ara	Eastern Desert, Egypt	Columbite-(Mn)	Abdalla et al. 1998
Um Naggat	Eastern Desert, Egypt	Columbite-(Fe)	Abdalla et al. 1998
Yichun	Jiangxi Province, China	Pyrochlore Columbite-(Mn) Tantalite-(Mn)	Belkasmi et al. 2000

Deposit Name	Location	Minerals	Data Source
OTHER			
Pitinga	Amazonas State, Brazil	Pyrochlore	Bastos Neto et al. 2009
MIXED LCT+NYF PEGMATITE			
Tørdal	Telemark, Norway	Pyrochlore Microlite Betafite	Bergstøl and Juve 1988

Appendix B
Standards and data quality

B.1 Portable X-ray fluorescence data quality

Data quality for pXRF analysis and standards used are discussed by Luck and Simandl (2014) and presented in part with permission of the British Columbia Geological Survey:

"Standards included a 99.995% SiO_2 blank, Standard Reference Material NIST 2780 (May and Rumble, 2004), Certified Reference Material 'TRLK' Rare Earth Ore 'CGL 124' (Registration Number: USZ 42-2006; Mongolia Central Geological Laboratory, 2006), and Reference Niobium Ore OKA-1 (Steger and Bowman, 1981)."

"The accuracy and precision of the pXRF data can be assessed by considering the results of repeated analyses on standard reference materials of known composition (Tables B.1, B.2, and B.3). Accuracy is evaluated by percent difference:

$$\%diff = \frac{measured\ value - refermce\ valute}{reference\ value} \text{ x } 100\%$$

Precision was assessed as relative standard deviation expressed in percent (%RSD) and as defined by:

$$\%RSD = \frac{stanard\ deviation}{mean} \text{ x } 100\%$$

Error bars on diagrams for results herein reflect the precision (2σ) established by multiple analyses of standards. Of the elements for which abundances are reported here, only Ce had results above the detection limit on blank analyses. For n=38 an average of 119 ± 28 (2 σ) Ce was detected. For this reason, results for Ce should be considered

higher than true values. Analyses of the standard reference material NIST 2780 (Table B.1) resulted in %diff less than 10% for Ca, Sr, Th, and Zr; less than 20% diff for Fe, Ti, and Ba; and 50% diff for S. Uranium, La, and Ce were over 100% diff and Nd was over 1000% diff. Certified values for NIST 2780 to compare with elemental abundances determined in this work for Ta, Y, and Pr are unavailable. The %RSD of Fe, Ca, Ti, Ba, S, Sr, Zr, and Y were less than 5%; Ce, Nd, and Pr were less than 10%. Thorium, U, and La had %RSDs of 26.4, 29.7, and 12.5%, respectively. No measurements above detection limits were made on P, Nb, or Ta.

Repeated determinations of elemental abundances by pXRF on the Mongolian rare earth ore TRLK CGL 124 resulted in %diff of 10% or less for Sr, La, Ce, Nd, and Pr (Table B.2). For the elements Fe, Ca, Th, U, Nb, Zr, and Y it was between 10 and 46%, for Ba and S it was 160 and 170%. No determination of accuracy could be made for Ta, as certified values are unavailable. The precision was better than 5 %RSD for Fe, Ca, Ba, S, Sr, Th, Y, La, Ce, Nd, and Pr and better than 10% for U. Niobium, Ta, and Zr had %RSD of 11.8, 23.9, and 13.3% respectively.

The Nb Ore OKA-1 was evaluated for accuracy with reference to the CANMET certified values. For elements where no such value was available (indicated in Table B.3) the average of three Li-borate fusion ICP-MS analyses carried out by ASL Limited (Vancouver) were used instead. The %diff of Fe, Ba, Sr, Nb, and Zr were less than 10%. Those of Ca, Ti, S, Y, La, and Ce, were less than 25%. For P, Th, U, Nd, and Pr the %diff ranged from 49 to 270%. The %RSD of Fe, Ca, P, Ti, Ba, S, Sr, Nb, Y, La, Ce, Nd, and Pr were less than 5%. Thorium, U, and Zr, had %RSDs of 23.8, 16.1, and 15.4.”

Table B.1 Results of repeated analyses on the NIST Standard Reference Material 2780. From Luck and Simandl (2014).

		Certified Values		pXRF Values				
		ppm	+/-	n	Average	Std Dev	%diff	%RSD
Major Elements	Fe	27800	800	38	31400	345	13	1.1
	Ca	1950	200	38	1870	82	4	4.4
	P[a]	427	40	-	-	-	-	-
	Ti[a]	6990	190	38	6200	249	11	4.0
	Ba[a]	993	71	38	840	16	15	1.9
	S	12600	420	38	18800	327	50	1.7
Trace Elements	Sr[a]	217	18	38	232	4	7	1.5
	Th	12	12	38	13	3	7	26.4
	U	4		26	13	4	227	29.7
Specialty Metals	Nb	18	-	-	-	-	-	-
	Ta	-	-	-	-	-	-	-
	Zr	176	-	38	193	2	9	1.1
REE	Y	2570	160	38	168	3	93	1.8
	La	38	38	38	90	12	156	12.5
	Ce	64	-	38	180	15	176	8.6
	Nd	28	-	38	330	29	1064	8.9
	Pr	-	-	38	180	13	-	7.2

The number of readings above the LOD is denoted as “n”, standard deviation (1σ) as Std Dev. See text for details of %diff and %RSD.

[a] Non certified values supplied by Thermo Scientific.

Table B.2 Repeated analyses on the Certified Reference Material "TRLK" rare earth ore CGL 124. From Luck and Simandl (2014).

		Certified Values			pXRF Values			
		ppm	+/-	n	Average	Std Dev	%diff	%RSD
Major Elements	Fe[a]	39938.36	594.53	38	45400	588	14	1.3
	Ca[a]	233562.6	2858.78	38	259000	1103	11	0.4
	P[b]	688.24	15.64	-	-	-	-	-
	Ti[a]	1198.7	71.92	-	-	-	-	-
	Ba	307	10	38	800	23	160	2.9
	S[a]	560.65	-	38	1510	62	170	4.1
Trace Elements	Sr	4900	400	38	4450	40	9	0.9
	Th	946	51	38	1180	19	25	1.6
	U	51.4	-	38	75	4	46	5.6
Specialty Metals	Nb	31	4.54	38	23	3	27	11.8
	Ta	-	-	30	60	13	-	23.9
	Zr	136	-	38	80	11	40	13.3
REE	Y	167	20	38	209	2	25	1.1
	La	21100	1100	38	20700	169	2	0.8
	Ce	27600	500	38	27400	234	1	0.9
	Nd	6500	300	38	5900	150	10	2.6
	Pr	2300	300	38	2160	41	6	1.9

The abbreviations are identical to those in Table B.1.

[a] Have been converted to ppm from the oxide weight percent reported from the Mongolia Central Geological Laboratory.

Table B.3 Statistical assessment of repeated analyses of the reference material OKA-1. From Luck and Simandl (2014).

		Certified or Laboratory Values		pXRF Values				
		ppm	+/-	n	Average	Std Dev	%diff	%RSD
Major Elements	Fe	28000	-	37	30600	494	9	1.6
	Ca	313000	-	37	354000	1592	13	0.4
	P	11000	-	37	4300	203	60	4.6
	Ti[c]	1358	40	2	1530	41	13	2.7
	Ba[a]	2887	117	37	3070	32	6	1.0
	S	6000	-	37	4900	157	18	3.2
Trace Elements	Sr[a]	13501	56	37	12400	63	8	0.5
	Th[a]	57	4	37	150	37	169	23.8
	U[a]	29	5	37	43	7	49	16.1
Specialty Metals	Nb	3700	0.01	37	3390	64	8	1.9
	Ta[a]	36	8	-	-	-	-	-
	Zr[a]	112	5	37	120	18	6	15.4
REE	Y[a]	61	1	37	74	2	20	2.4
	La[a]	1107	43	37	1360	20	23	1.4
	Ce[a]	2045	75	37	2310	32	13	1.4
	Nd[a]	535	13	37	1400	39	162	2.7
	Pr[a]	182	4	37	670	32	270	4.8

The abbreviations are identical to those in Table B.1. Unless otherwise noted values are from the CANMET reported of Steger and Bowman (1981).

[a] Average of three analyses by Li meta borate fusion inductively coupled plasma mass spectrometry (ICP-MS). The error bracket corresponds to the absolute difference of the most extreme outlying value from the average.

Portable XRF detection limits for Nb, Ta, La, Ce, Pr, Nd, Y, Ba, Sr, and P are given in Table B.4, as described by Luck and Simandl (2014).

Table B.4 Portable XRF limits of detection (LOD) for elements pertinent to carbonatite exploration. From Luck and Simandl (2014).

	Matrix	
Element	SiO2 (ppm)	Natural Sample or SiO2+Fe+Ca (ppm)
Nb	2	2
Ta	NA	NA
Y[a]	1.5	4
La[a]	34	43
Ce[a]	40	47
Pr[a]	46	57
Nd[a]	75	93
Ba	28	33
Sr	2	2
P	80	90
U	NA	NA
Th	NA	NA
S	50	60

For elements denoted with ([a]) LODs were derived from a Thermo Fisher Scientific Niton XL3t Ultra. Thermo Fisher Scientific Niton FXL-950 is expected to have lower LODs.

"Statistical assessments of pXRF results for standard reference materials (Tables B.1, B.2, and B.36) indicate that the method is precise but prone to bias. Elements with the highest accuracy (less than 30%diff) in concentration ranges observed at Lonnie are Nb, Y, Sr, Th, FeO, CaO, and TiO_2. Lanthanum, Ce, Nd, Ba, and U have %diff exceeding 100%. The % diff values for Ta, Pr, and P are unavailable.

Recommended values for standard reference materials are reported as a mean of results from several different techniques, making comparison with results from pXRF complicated. From a practical point of view pXRF analyses presented in this paper should be viewed as internally consistent but relative. Recalibration using results of standard laboratory analyses (as described in Simandl et al., 2014) to correct for matrix effects and analytical biases to improve accuracy has not been performed."

B.2 Laboratory chemical analysis

Laboratory analysis was performed at ASL Limited (Vancouver). Analytical techniques used are ICP-MS for trace elements, ICP-AES for major elements (reported as their common oxides), and XRF for Nb (when in concentrations >2500 ppm Nb). Analytical codes ME-MS81d and XRF10 Nb were used. Lower and upper limits of detection provided by ALS Limited (Table B.5).

Table B.5 Lower and upper limits of detection for analytical methods from ALS Limited. From ALS Limited (2015).

Element	Lower limit of detection (ppm)	Upper limit of detection (ppm)	Analytical method	Analytical code
Ba	0.5	10000		
Ce	0.5	10000		
Cr	10	10000		
Cs	0.01	10000		
Dy	0.05	1000		
Er	0.03	1000		
Eu	0.03	1000		
Ga	0.1	1000		
Gd	0.05	1000		
Hf	0.2	10000		
Ho	0.01	1000		
La	0.5	10000		
Lu	0.01	1000		
Nb	0.2	2500		
Nd	0.1	10000	ICP-MS	ME-MS81d
Pr	0.03	1000		
Rb	0.2	10000		
Sm	0.03	1000		
Sn	1	10000		
Sr	0.1	10000		
Ta	0.1	2500		
Tb	0.01	1000		
Th	0.01	1000		
Tm	0.05	1000		
U	0.05	1000		
V	5	10000		
W	1	10000		
Y	0.5	10000		
Yb	0.03	1000		
Zr	2	10000		

Table B.5 continued.

Element	Lower limit of detection (%)	Upper limit of detection (%)	Analytical method	Analytical code
Al_2O_3	0.01	100		
BaO	0.01	100		
CaO	0.01	100		
Cr_2O_3	0.01	100		
Fe_2O_3	0.01	100		
K_2O	0.01	100		
MgO	0.01	100	ICP-AES	ME-MS81d
MnO	0.01	100		
Na_2O	0.01	100		
P_2O_5	0.01	100		
SiO_2	0.01	100		
SrO	0.01	100		
TiO_2	0.01	100		
LOI	0.01	100		
Nb	0.01	10	XRF	XRF10 Nb

Appendix C
Heavy mineral processing by Mozley C800 mineral separator

Published as: Mackay, D.A.R., Simandl, G.J., Grcic, B., Li, C., Luck, P., Redfearn, M., and Gravel, J. 2015. Evaluation of Mozley C800 Laboratory Mineral Separator for Heavy Mineral Concentration of Stream Sediments in Exploration for Carbonatite-Hosted Specialty Metal Deposits: Case Study at the Aley Carbonatite, Northeastern British Columbia (NTS 094B). In: Geoscience BC Summary of Activities 2014, Geoscience BC, Report 2015-1, p. 111-122.

C.1 Introduction

Finding tools to explore for overburden-covered or poorly exposed ore deposits is one objective of Natural Resources Canada's Targeted Geoscience Initiative 4 (TGI-4). Indicator minerals and geochemical studies are particularly effective tools. General principles about stream sediment surveys are given by Levinson (1974), Hawkes (1976), Rose et al. (1979), and Fletcher (1997). Lett (2007), Friske (2005) and McCurdy et al. (2006, 2009) provided guidelines for regional geochemical surveys. Methods for regional indicator mineral studies at the regional scale are also well established (McCurdy et al., 2006, 2009; McClenaghan, 2011). Indicator mineral studies generally require large samples (≥ 10 kg; McClenaghan, 2011) that need to be treated by heavy liquid separation, isodynamic magnetic separation, optical identification, and hand picking. The limited budgets of exploration companies targeting specific deposit types or commodities, or following up on regional geochemical or indicator mineral surveys, necessitates a more focused, customized approach. This orientation survey focuses on the 125-250 μm fraction of stream sediments from the Aley carbonatite (see Section 3.1.1).

C.2 Assessment of the Mozley C800 laboratory mineral separator procedure

The Mozley C800 laboratory mineral separator is a light and compact alternative to the shaker tables and gravity concentrators that are commonly used by metallurgists. The v-profile tray, best suited for coarse grain sizes (100 μm–2 mm), was used for this study instead of a flat tray, traditionally used for finer grain sizes (~100 μm or less). The Mozley C800 set up parameters were: 1.75° longitudinal slope; 70 rpm table speed; 6.35

cm amplitude (throw or stroke); and 1.6 L/min water flow rate. Specifications and detailed operating procedures for the Mozley C800 are described in the instrument manual (Mozley Inc., undated). Optimal operating conditions are determined by running synthetic standards.

C.3 Processing procedure

The operating procedure is relatively simple once optimal conditions for sample processing are identified. Dry sieved (125–250 μm size fraction) samples weighing ~75 g are gradually poured from a beaker onto the table and thoroughly wetted at the wash water pipe (Fig. C.1). A spray bottle is used to remove all material from the beaker. Tailings (low density material) separate first, moving longitudinally down the trough in the direction of water flow. The tailings are collected at the end of the table. Once the selected time interval is reached, the table and water are turned off. Tailings, middlings, and concentrate are separated and carefully washed into separate containers. The concentrate consists of the highest density material in the sample. The middlings are a transition zone between the tailings and concentrate. They contain medium-density material and a mixture of low- and high-density minerals. The division of sediment into concentrate, middlings, and tailings is visually discernable by shape and, to a lesser extent, colour (which in this study reflects the proportion of heavy minerals; Fig. C.2).

Following a sample run, suspended particles are allowed to settle, excess water is decanted from the concentrate, middlings, and tailings containers and the fractions are dried overnight at 90°C then weighed for quality control and bagged separately. This procedure allows for samples to be reconstituted and reprocessed if needed. The same procedure was used to process all synthetic samples (standards) and multiple splits of a natural stream sediment sample collected in the field to determine optimal operating conditions and run time. Once the optimal operating conditions were determined, table speed, slope, water flow rate, throw amplitude and size of the samples were kept constant. A portion (~75 g) of the 125–250 μm fraction of each stream sediment sample

was split and processed on the Mozley C800. After processing, concentrate, middlings and tailings were analyzed by pXRF.

Figure C.1 A sample being poured onto a Mozley C800 laboratory mineral separator. Water is supplied to the v-profile tray by the wash water pipe (copper tube) and the irrigation pipes (two white plastic tubes with water outlets at regular intervals). The direction of water flow is denoted by black arrows.

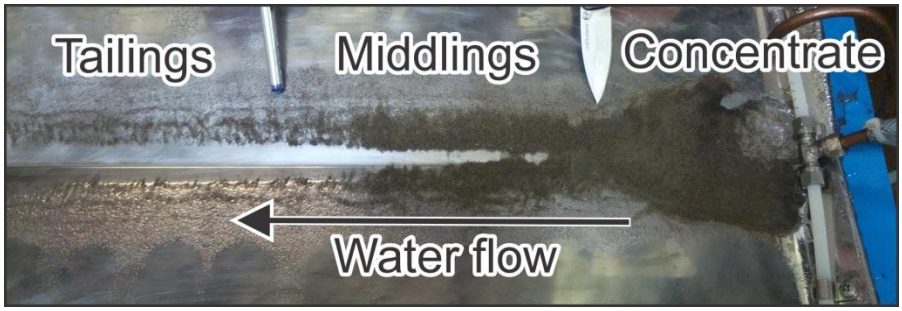

Figure C.2 View of the surface of the Mozley C800 laboratory mineral separator table and sample material after a completed run. Concentrate, middlings, and tailings are separated based on pattern and colour of the material stream.

C.4 Optimizing operating conditions based on synthetic and natural samples

Testing and optimizing operating conditions for the Mozley C800 were performed using synthetic standards and a quintet of subsamples split from the natural sample AL-13-16. Synthetic standards contained 75 g of material made up of magnetite (0.33–10 wt. %), garnet (0.33–10 wt. %), fluorite (0.33–10 wt. %), and quartz (remaining portion of the standard sample). All constituents of the synthetic standards were milled and sieved to the 125–250 μm size fraction (compatible with the size fraction identified previously for testing). Magnetite in Mozley C800 concentrates increased by 5.5 to 228.2 times relative to unprocessed synthetic standards. The strong correlation (R^2=0.98) between magnetite contained in unprocessed standard samples and Mozley C800 concentrates indicates consistent and predictable concentration of standards (Fig. C.3).

One of the larger natural samples (AL-13-16) was split using a riffle splitter into five identical subsamples (~75 g) and these subsamples were processed for 5, 10, 15, 20, and 25 minutes (Fig. C.4). The proportion of retained concentrate decreases with increasing processing time when all other parameters are kept constant (Fig. C.4). Reproducibility of the Mozley C800 was tested on three subsamples (~77 g each) of AL-13-16 processed for 25 minutes. The retained concentrate fraction varied only slightly with observed weights representing 12, 9.4, and 9.9% of the initial sample weights. Based on these tests, a processing time of 15 minutes was selected for processing stream samples from the Aley carbonatite. The 15-minute run time is a compromise that ensures adequate concentration of heavy minerals (magnetite) and minimal loss to tailings.

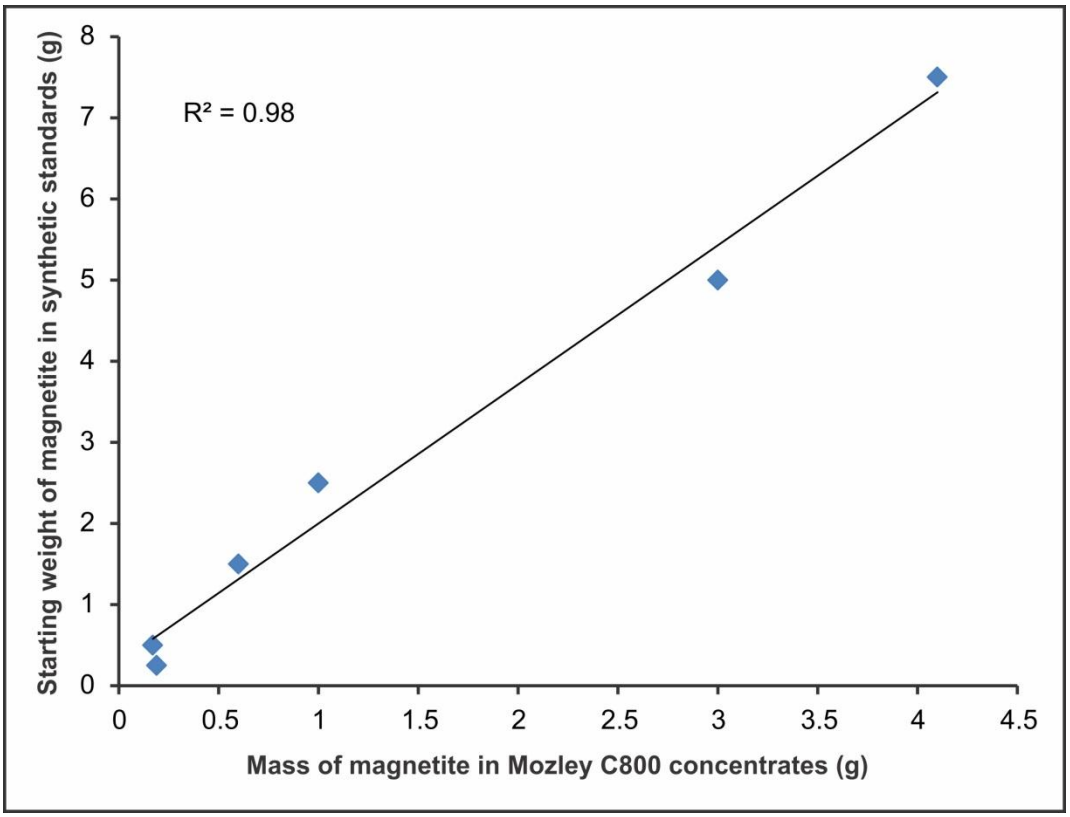

Figure C.3 Comparison of the weight of magnetite contained in unprocessed synthetic standards with corresponding weight of magnetite in Mozley C800 laboratory mineral separator concentrates.

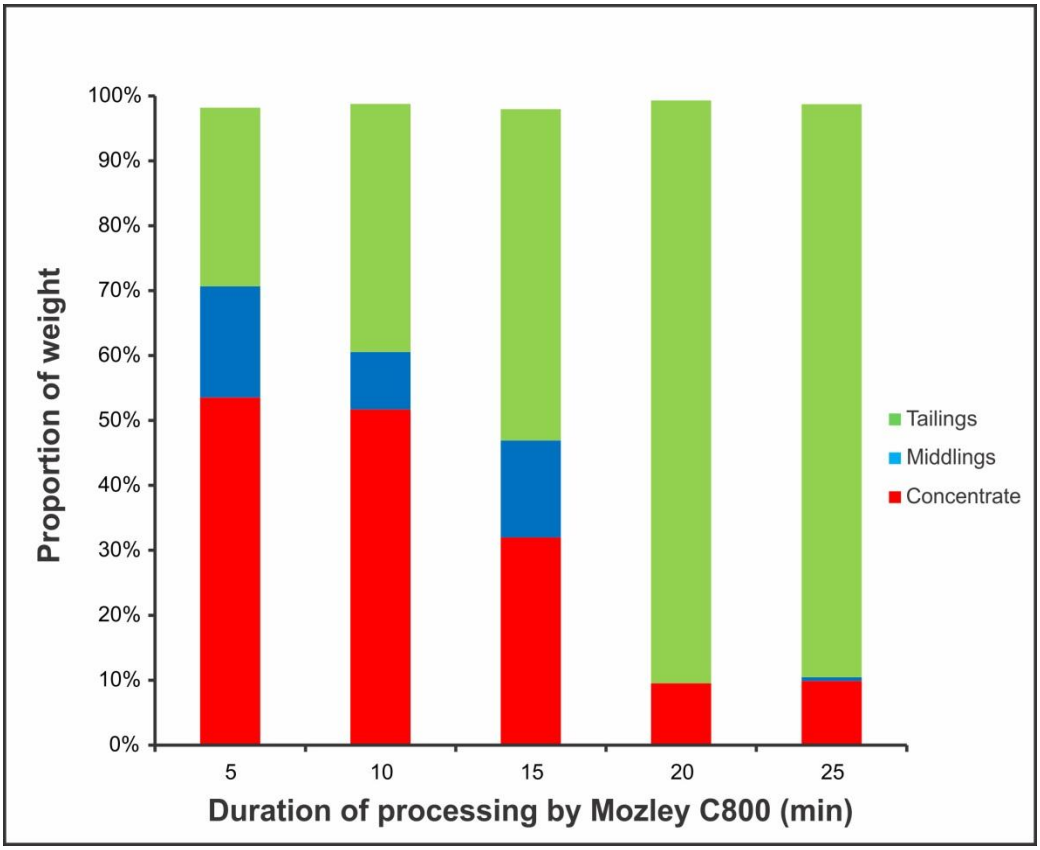

Figure C.4 Proportions of concentrate, middlings, and tailings in five subsamples of AL-13-16 (Fig. 3.2) after processing on the Mozley C800 laboratory mineral separator for 5, 10, 15, 20, and 25 minutes.

C.5 Mozley C800 laboratory mineral separator and geochemical analysis results

Separation by Mozley C800 of the 125–250 μm fraction of stream sediment samples from the Aley carbonatite drainage area produced a range in proportions of concentrate (3.8–32.0%), middlings (0–17.1%), and tailings (51.0–94.1%). Ten out of twelve samples show 24.7 to 32.0% of material retained in concentrate, consistent with the desired proportion of material retained in concentrate for the sample (AL-13-16) used to test the separation procedure (Fig. C.5). Only sample AL-13-09 shows noticeably lower proportions of retained concentrate (3.8%).

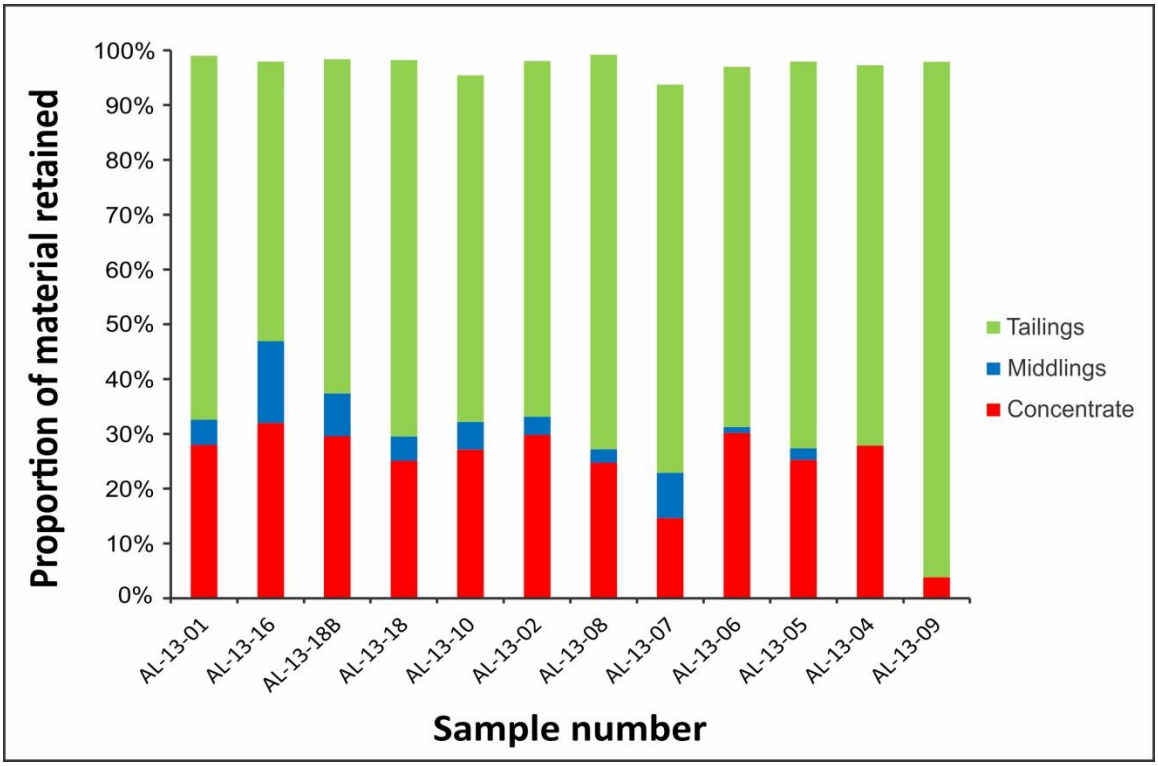

Figure C.5 Proportions of Mozley C800 laboratory mineral separator concentrates, middlings, and tailings for stream sediment samples from the Aley carbonatite drainage area, northeastern British Columbia. Samples were processed for 15 minutes. Samples appear in order of their geographic location from west to east (see Fig. 3.2 for sample locations).

Raw samples (Table 3.2) and Mozley C800 concentrates (Table C.1) from the Aley carbonatite drainage area were analyzed by pXRF following the procedure described by Luck and Simandl (2014) and in section 3.1.1.4. Abundances of Nb in Mozley C800 concentrates increased by a factor of 2.7 to 17.2 (average of 4.3) relative to the raw samples (Fig. C.6a). For samples with available analyses, concentration of Nb is 2.4 to 9.9 times higher in concentrates relative to middlings (Table C.1). The Mozley C800 concentrates also show large increases in the concentration of Ta (factor of 1.5 to 11.7; average of 3.1) and LREE (factor of 2.6 to 12.6; average of 3.9) relative to raw samples (Fig. C.6b, c).

C.6 Discussion

Processing samples using a Mozley C800 permits separation of dense indicator minerals (Table 3.5). Pyrochlore, columbite-(Fe), fersmite, monazite, and REE-fluorocarbonates such as bastnaesite and synchysite, have been identified in mineralogical studies of the Aley carbonatite (Mäder, 1986; Kressall et al., 2010; Chakhmouradian et al., 2014) and targeted as indicator minerals for carbonatite-hosted specialty metal deposits in this study. These minerals have similar or greater densities than magnetite (5.1–5.2 g/cm^3) in the synthetic standards used herein (Table 3.5). Based on the consistent and effective concentration of magnetite from the synthetic standards, the targeted heavy mineral fraction should be retained effectively in Mozley C800 concentrates.

Comparison of the results of the pXRF analyses of raw samples and Mozley C800 concentrates, middlings, and tailings shows that the concentration of Nb-, Ta-, and LREE-bearing heavy minerals was successful. A high concentration of Nb (average increase by a factor of 4.3) in Mozley C800 concentrates relative to tailings and corresponding raw samples (Fig. C.6a) indicate that most of the Nb-bearing minerals (pyrochlore, columbite-[Fe], and fersmite) were successfully concentrated by the Mozley C800. The correlation (R^2=0.94) between Nb in raw samples and Mozley C800 concentrates (Fig. C.7a) indicates that the procedure consistently and efficiently concentrates pyrochlore, columbite-(Fe), and fersmite in all samples in the range of 2000 to 30 000 ppm Nb. The correlation (R^2=0.86) between Fe in raw samples and concentrates indicates magnetite was successfully concentrated.

Table C.1 Relative concentrations (in ppm) of major and minor elements associated with carbonatite from Mozley C800 laboratory mineral separator concentrates, middlings, and tailings from stream sediment samples, analyzed by portable X-ray fluorescence spectrometer. Samples are listed from upstream of, to directly over, and with increasing distance downstream of the Aley carbonatite, northeastern British Columbia. See Fig. 3.2 for sample locations. Error propagation and elemental concentrations near the limit of detection greatly reduce the reliability of calculated values.

Sample	Nb	Ta	La	Ce	Pr	Nd	Y	Ba	Sr	P	U	Th	Fe	Ca
CONCENTRATE														
AL-13-09*	7635	327	1725	2688	1222	2210	223	976	842	34659	109	791	80156	162926
AL-13-04	26514	193	3857	6347	1061	2853	343	364	2076	n.d.	73	788	194756	193214
AL-13-05*	26389	325	4130	6593	1295	3235	365	664	2030	n.d.	87	1516	213404	222021
AL-13-06	21571	217	3785	6031	1029	2730	319	407	1779	n.d.	76	785	185251	190196
AL-13-07	2262	48	694	1076	354	762	72	218	987	10791	14	164	37475	223300
AL-13-08	23076	292	7325	11001	1373	3832	339	501	1275	n.d.	120	987	233457	150235
AL-13-02	21400	335	5541	8420	1153	3198	327	459	1464	n.d.	133	961	210258	175782
AL-13-10	17271	279	4047	6154	963	2611	277	773	1383	n.d.	111	942	169748	185713
AL-13-18	11923	176	2341	3600	734	1804	203	1225	1184	n.d.	84	573	114173	191843
AL-13-18B	10227	182	1869	2906	640	1534	184	1084	1204	n.d.	80	591	88135	194940
AL-13-16	14603	290	3023	4605	798	2006	229	1595	1059	n.d.	95	874	139688	172378
AL-13-01	11481	183	1795	2808	616	1486	189	1018	1112	n.d.	78	700	95421	189733
MIDDLINGS														
AL-13-07	939	27	325	502	184	359	46	158	874	6941	7	87	23952	213935
AL-13-18B	1547	23	327	529	163	362	60	335	996	11701	13	126	25994	190527
AL-13-16	1483	27	413	672	280	553	57	410	957	10436	13	124	26276	188037

*calculated values; n.d. = not detected

Table C.1 Continued.

Sample	Nb	Ta	La	Ce	Pr	Nd	Y	Ba	Sr	P	U	Th	Fe	Ca
TAILINGS														
AL-13-09	163	17	126	197	150	283	22	305	154	597	5	24	13718	76492
AL-13-04	3704	55	792	1356	476	1026	110	298	2027	21556	15	273	52382	215621
AL-13-05	2804	54	676	1134	406	901	91	299	1619	15708	14	214	47007	202470
AL-13-06	2487	47	689	1133	425	904	86	310	1524	13871	15	196	48808	194605
AL-13-07	279	n.d.	231	370	257	500	25	244	640	1686	6	39	18900	178263
AL-13-08	612	33	275	450	243	489	34	296	948	3624	10	62	21832	156680
AL-13-02	741	38	307	478	257	516	37	296	947	3959	11	74	22482	157974
AL-13-10	298	n.d.	190	330	220	426	27	318	744	2388	7	41	19832	151534
AL-13-18	320	17	164	282	192	354	26	501	590	1865	6	36	18935	140844
AL-13-18B	239	n.d.	180	294	211	412	25	473	625	2255	5	37	17959	149069
AL-13-16	242	22	171	265	199	352	23	552	529	<90	6	35	19601	124735
AL-13-01	284	28	157	271	190	347	24	496	528	1845	7	34	17322	137060

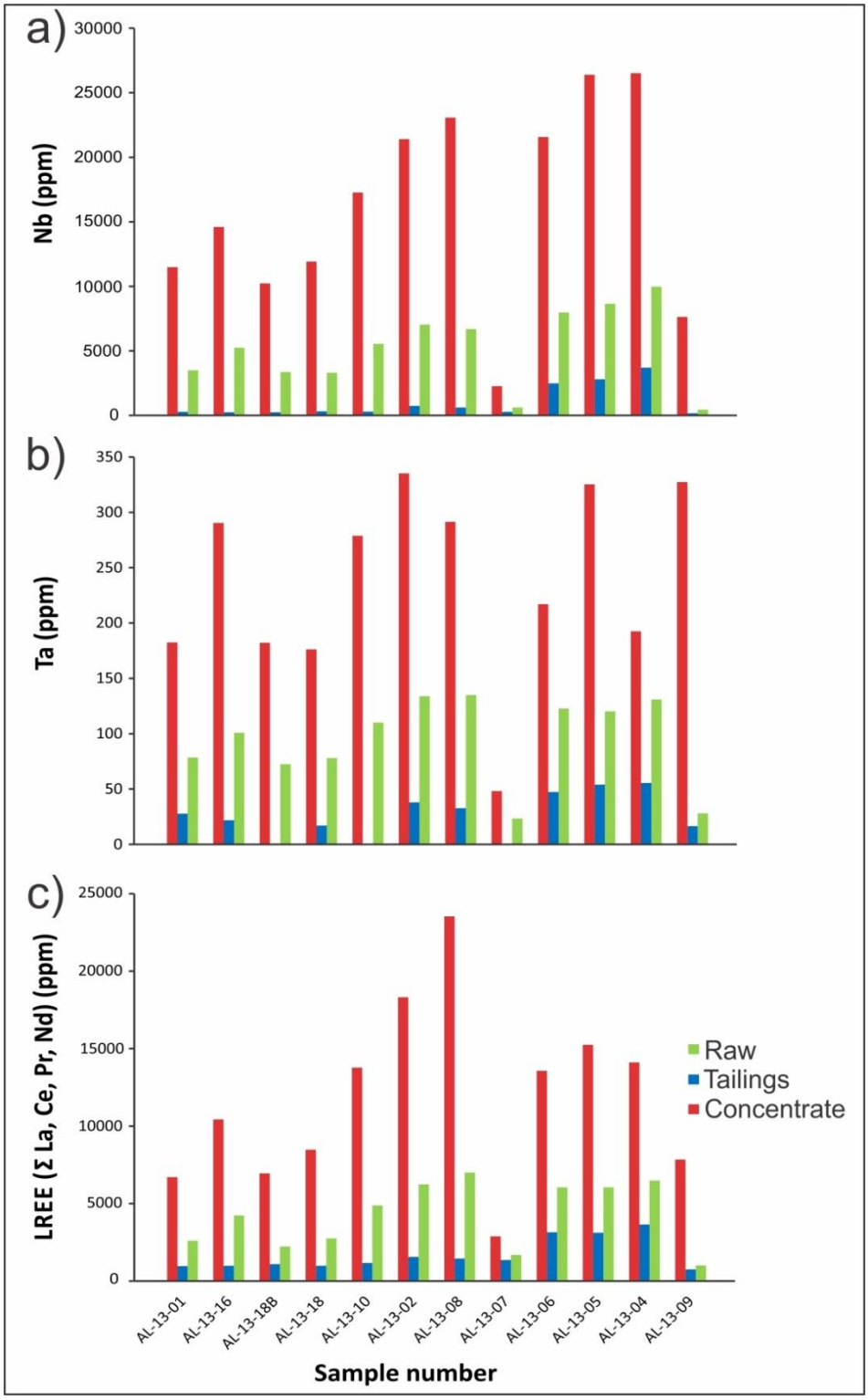

Figure C.6 Comparison of a) Nb, b) Ta, and c) LREE (ΣLa, Ce, Nd, Pr) concentrations in Mozley C800 laboratory mineral separator concentrates, tailings, and corresponding raw samples. Samples appear in order of their geographic location from west to east (see Fig. 3.2 for sample locations).

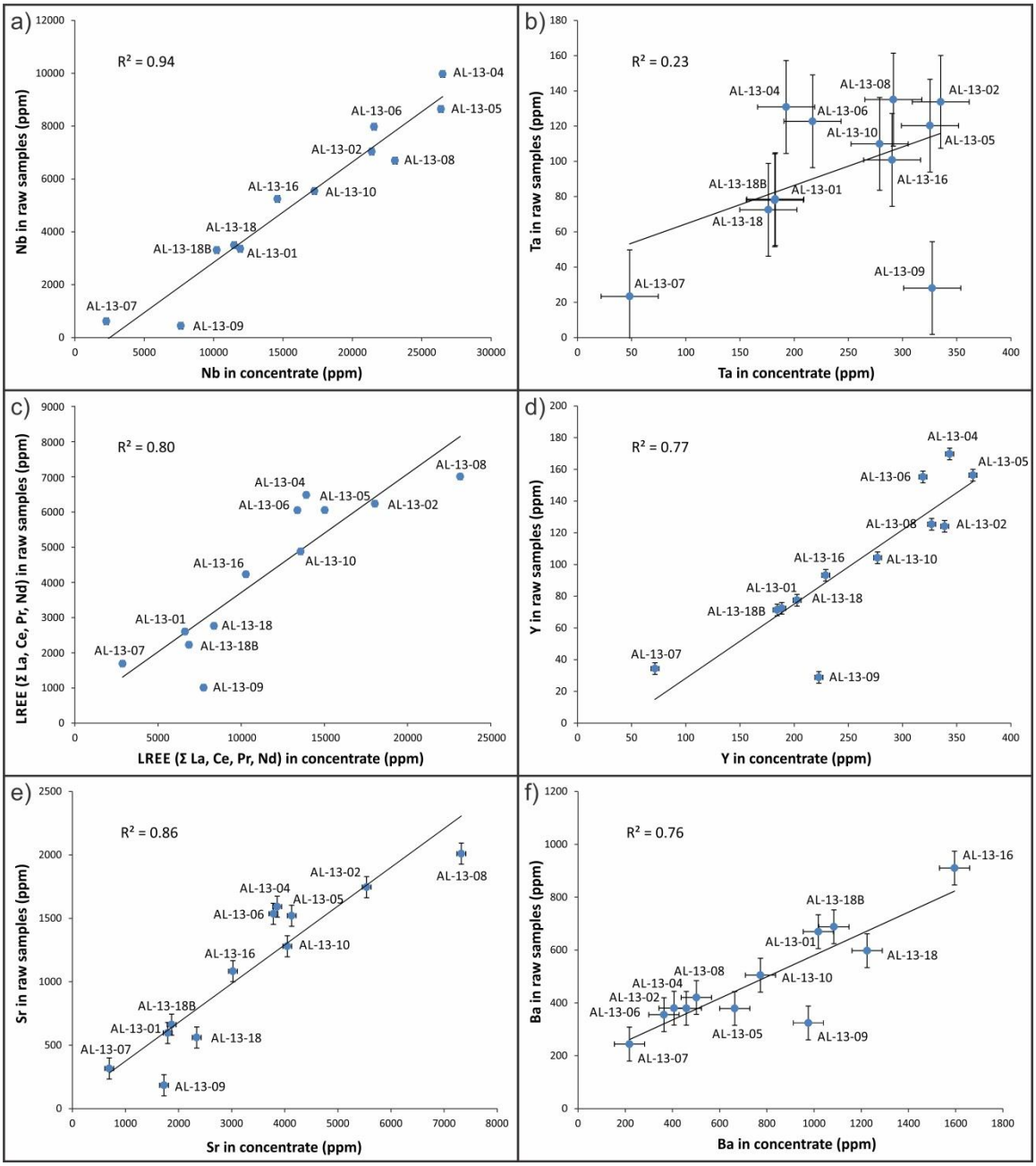

Figure C.7 Comparison of the concentrations of a) Nb, b) Ta, c) light rare earth elements (LREE), d) Y, e) Sr, and f) Ba in Mozley C800 laboratory mineral separator concentrates versus raw samples (from Aley carbonatite drainage area, northeastern British Columbia). Error bars (2σ) are based on repeated portable X-ray fluorescence analyses of standards as described in Appendix B.

High Ta contents (average increase by a factor of 3.1) in Mozley C800 concentrates relative to tailings and raw samples (Fig. C.6b) are likely due to pyrochlore and

columbite-(Fe); however the Ta:Nb ratio for these minerals in carbonatites is typically very low. The lack of correlation between Ta concentrations in raw samples and concentrate (R^2=0.23; Fig. C.7b) is likely due to low (near detection limit) contents. Also, the elemental concentration for two concentrates (AL-13-09 and AL-13-05) had to be calculated because the amount of material retained following Mozley separation was insufficient for chemical analyses (Table C.1). In these cases, elemental concentration can be calculated based on initial concentrations measured in raw samples and analyses of tailings and middlings (normalized to wt. % of retained material). Error propagation from analyses near detection limits combined with error in weights of raw samples, concentrates, middlings, and tailings makes calculated concentrations unreliable. Despite this, the calculated elemental concentrations for AL-13-05 do not appear to dramatically affect the results. Sample AL-13-09 was collected upstream of the Aley carbonatite and is unique in the sample set (Fig. 3.2). It shows a different grain size distribution relative to the other samples (Fig. C.8), and lower proportions of retained concentrate (3.8%; Fig. C.5). Elemental concentrations of Nb, Ta and LREE in raw samples are also much lower than in other samples (Fig. C.6). This may reflect background levels of heavy minerals in the Aley carbonatite area, and the different flow characteristics of the creek (meandering reach) upstream of the deposit.

Concentrations of LREE are also high (average increase by a factor of 3.9) in Mozley C800 concentrates relative to tailings and raw samples (Fig. C.7c). Combined with correlations for LREE (R^2=0.90; Fig. C.7c) and Y (R^2=0.77; Fig. C.7d), this indicates that heavy minerals, such as monazite and REE-bearing fluorocarbonates (e.g., bastnaesite and synchysite), were concentrated during Mozley separation in the range of 3000–40 000 ppm LREE. Correlation for Sr (R^2=0.86; Fig. C.7e) and Ba (R^2=0.76; Fig. C.7f) in raw samples and Mozley C800 concentrate indicate that the carbonatite signature in stream sediments is preserved following Mozley C800 concentration. The low coefficients of determination for Th (R^2=0.44) and U (R^2=0.43) are due to low concentrations (near detection limits) in samples AL-13-09 and AL-13-07 and the error propagation issue described for Ta.

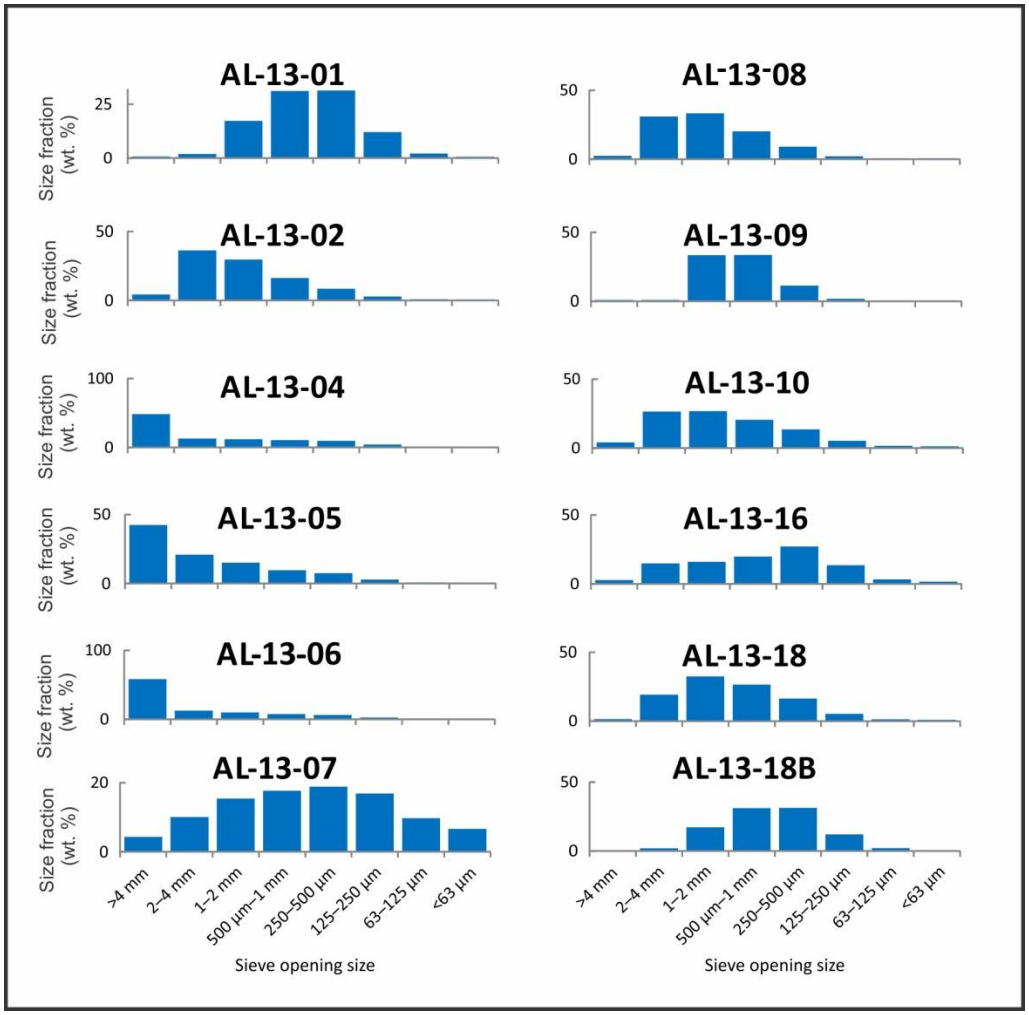

Figure C.8 Weight percent distribution of material for different size fractions in dry sieved stream sediment samples from the Aley carbonatite drainage area, northeastern British Columbia.

C.7 Conclusions

The Mozley C800 laboratory mineral separator is a compact, simple to operate instrument that can be transported and optimized for specific drainages, deposits or commodities. After selecting the most favourable size fraction (125–250 µm, dry sieved, in this study), the MSS was used to increase the heavy mineral content of the stream sediment samples from the drainage area surrounding the Aley carbonatite-hosted specialty metal deposit. This is substantiated by increased concentrations of Nb (average

factor of 4.3), Ta (average factor of 3.1), and LREE (average factor of 3.9) in Mozley C800 concentrates relative to corresponding raw samples. Correlations between Nb, LREE, and Y concentrations in the raw stream sediment samples and corresponding concentrates indicate that Nb- and LREE-bearing minerals (such as pyrochlore, columbite-(Fe), and REE-bearing fluorocarbonates) were consistently concentrated, and that a predictable relationship between indicator mineral counts in raw stream sediments samples and concentrates should be expected.

Appendix D
Heavy mineral processing by Wilfley shaking table

Published as: Mackay, D.A.R., Simandl, G.J., Luck, P., Grcic, B., Li, C., Redfearn, M., and Gravel, J., 2015. Concentration of carbonatite indicator minerals using a Wilfley gravity shaking table: A case history from the Aley carbonatite, British Columbia, Canada. In: Geological Fieldwork 2014, British Columbia Ministry of Energy and Mines, British Columbia Geological Survey Paper 2015-1, pp. 189-195.

D.1 Introduction

Indicator minerals are effective tools to explore for covered or poorly exposed ore deposits, and methods for their use in regional studies are well established (McCurdy et al., 2006, 2009; McClenaghan, 2011). The 250 µm–2.0 mm size fraction is commonly examined, and Wilfley-type tables are used to preconcentrate minerals before heavy liquid separation, isodynamic magnetic separation, and hand picking (McClenaghan, 2011). Indicator minerals for carbonatite-related specialty metal deposits are: Nb-bearing minerals (pyrochlore, columbite-[Fe], and fersmite), monazite, zircon, REE-fluorocarbonates (bastnaesite and synchysite), apatite, sulphates (barite-celestine) and potentially, magnetite, Na-K amphiboles, Na-pyroxenes, and allanite (Table 3.5). Herein we use sediment samples from streams draining the Aley carbonatite (Fig. 3.2) to determine if Wilfley tables can effectively concentrate carbonatite indicator minerals to a degree that additional processing is unnecessary before using QEMSCAN® to establish quantitative mineralogy. This orientation survey focuses on the 125-250 µm fraction of stream sediments from the Aley carbonatite (see Section 3.1.1).

D.2 Assessment of Wilfley mineral separator

Wilfley shaking tables separate silt and sand sized material based on mineral density (e.g., Sivamohan and Forssberg, 1985; Stewart, 1986; McClenaghan, 2011). Testing and optimization of operating conditions for the Mine and Smelter Supply Co. Wilfley shaking table (#13 table, 457 x 1016 mm) was performed using a synthetic standard, which contained 500 g of material made up of magnetite (40 g), garnet (30 g), fluorite (60

g), and quartz (370 g). Magnetite was selected as a proxy for heavy minerals targeted as carbonatite indicators. Synthetic standard components were milled to the same grain size range (125–250μm) as identified previously for testing (Luck and Simandl, 2014; Sections 3.1.1 and 3.1.2). Several runs with synthetic standards were performed, and operating parameters were optimized based on magnetite concentrations (a magnet was used to recover magnetite from concentrate). The main operating parameters for a Wilfley shaking table are: table inclination and slope, wash-water flow rate, material feed rate, table speed, and stroke amplitude (Razali and Veasey, 1990; Manser et al., 1991). Separation of material is also affected by feed grade and feed density. The table was set with an 8° incline, 3° slope, 10 mm stroke, and table speed of 250 rpm for all samples. Water flow was kept constant for all samples at 18 L/min based on optimization using synthetic standards. Water was not recycled. Optimized parameters increased the magnetite yield by 3.7 times.

D.3 Processing procedure

Dry sieved (125–250μm size fraction) stream-sediment samples varying from 380.4–938.4 g (Table D.1) were mixed into a slurry with water and gradually washed from a container into the sample feeder (Fig. D.1) using a water hose. Material moves in the direction of shaking across the table surface and diagonally down the table slope. Denser material (concentrate) is carried farthest left along the table ridges, while the least dense material is washed off the bottom of the table (Fig. D.2). Launder trays were positioned to collect the concentrate, middlings, and tailings. Suspended particles were allowed to settle and excess water was decanted from concentrates, middlings, and tailings. Samples were dried overnight at 90°C then weighed for quality control, allowing samples to be reconstituted and reprocessed if needed. After processing, concentrate, middlings, and tailings were analysed by pXRF using the method described by Luck and Simandl (2014) and in Section 3.1.1.

D.4 Results of Wilfley table separation and geochemical analysis

Wilfley table separation of the 125-250μm size fraction of stream-sediment samples from the Aley carbonatite drainage produced a range in proportions of concentrates (10.0-18.3 wt. %), middlings (48.8-68.8 wt. %), and tailings (11.0-38.2 wt. %; Fig. D.3). Due to minor loss of material during processing, the proportion of concentrate, middlings, and tailings do not total 100%. Relative to raw samples (Table D.1), the Nb content of Wilfley concentrates increased by 3.9-5.6 times (average of 4.8; Fig. D.4a). Similarly, Ta increased by 2.3-4.9 times (average of 3.6; Fig. D.4b) and LREE content increased by 1.8-5.1 times (average of 3.9; Fig. D.4c). The pXRF used in this study reports phosphorous values above 10000 ppm as below detection limit, hence P was determined by lithium borate fusion followed by ICP-AES (Tables D.1 and D.2). Phosphorous content of Wilfley concentrations increased by 1.8-2.4 times (average of 2.2) relative to raw samples.

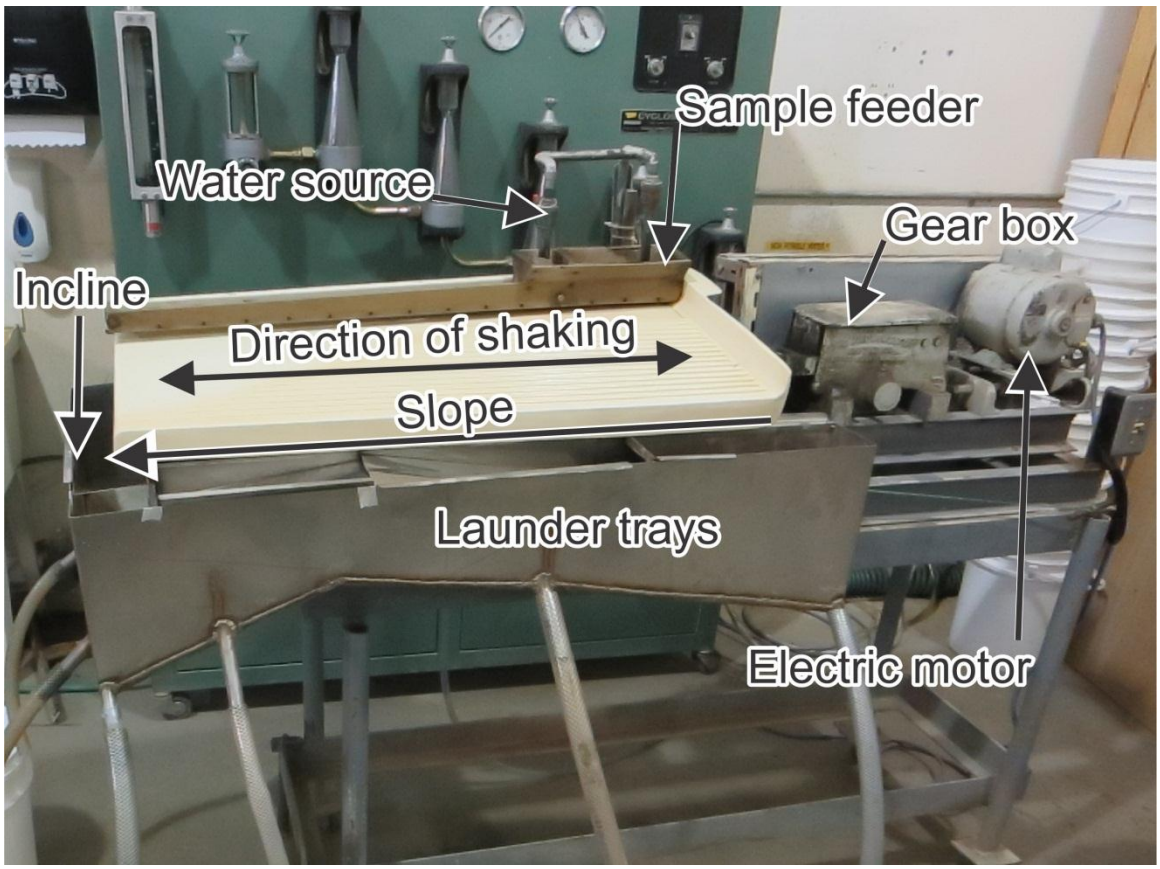

Figure D.1 Wilfley shaking table with adjustable launder trays. Slope and incline axes (angle from horizontal) are shown.

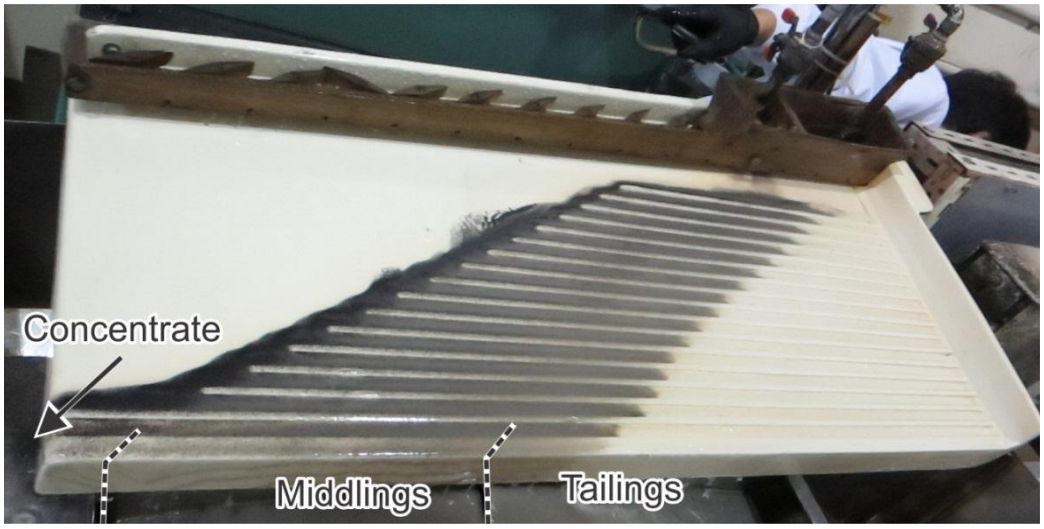

Figure D.2 Close-up of the Wilfley table. Heavy minerals (black) are separated from middlings and tailings as material moves from the top-right to bottom-left.

D.5 Discussion of Wilfley table heavy mineral separation

Relatively high coefficients of determination in raw samples versus Wilfley table concentrates for Nb (R^2=0.96; Fig. D.5a) and Ta (R^2=0.85; Fig. D.5b) suggest consistent concentration of Nb (±Ta)-bearing minerals (pyrochlore, columbite-(Fe), and fersmite). Similarly, high coefficients of determination for LREE (R^2=0.96; Fig. D.5c) and Y (R^2=0.94; Fig. D.5d) suggest that REE-fluorocarbonates, monazite, and other REE-bearing minerals were successfully concentrated by the Wilfley table treatment. High coefficient of determination (R^2=0.98) between Zr and LREE content of Wilfley table concentrates indicates zircon is a possible LREE-bearing indicator mineral for carbonatite exploration. Iron also shows a high coefficient of determination (R^2=0.97) suggesting the effective concentration of magnetite, hematite, and columbite-(Fe). The low coefficient of determination (R^2=0.01; Fig. D.5e) for Sr content in concentrates and raw samples and a low concentration factor (average of 1.2) from Wilfley table processing indicate that Sr in stream sediments was not concentrated in a predictable way. Coefficients for Ba (R^2=0.93; Fig. D.5f), Th (R^2= 0.95), and U (R^2=0.95) in raw samples and Wilfley table

concentrates indicate that the carbonatite signature in stream sediments is preserved following Wilfley table concentration.

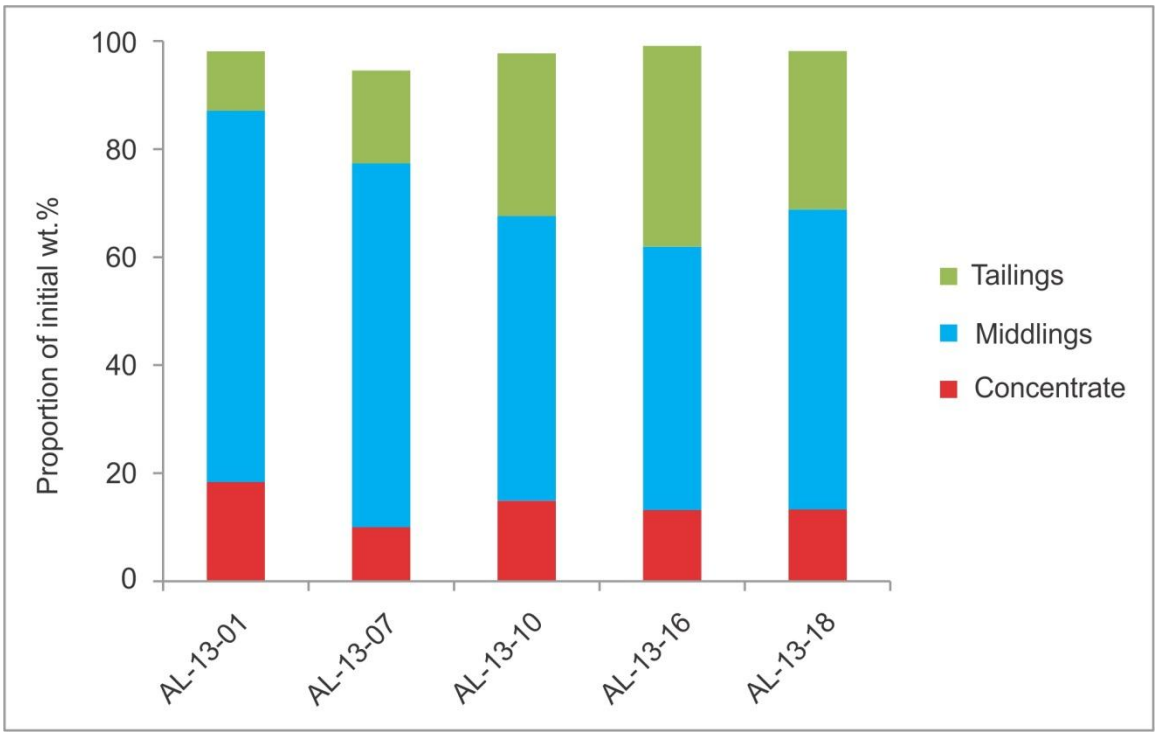

Figure D.3 Proportion of original wt. % in Wilfley table concentrates, middlings, and tailings for Aley carbonatite area stream sediments.

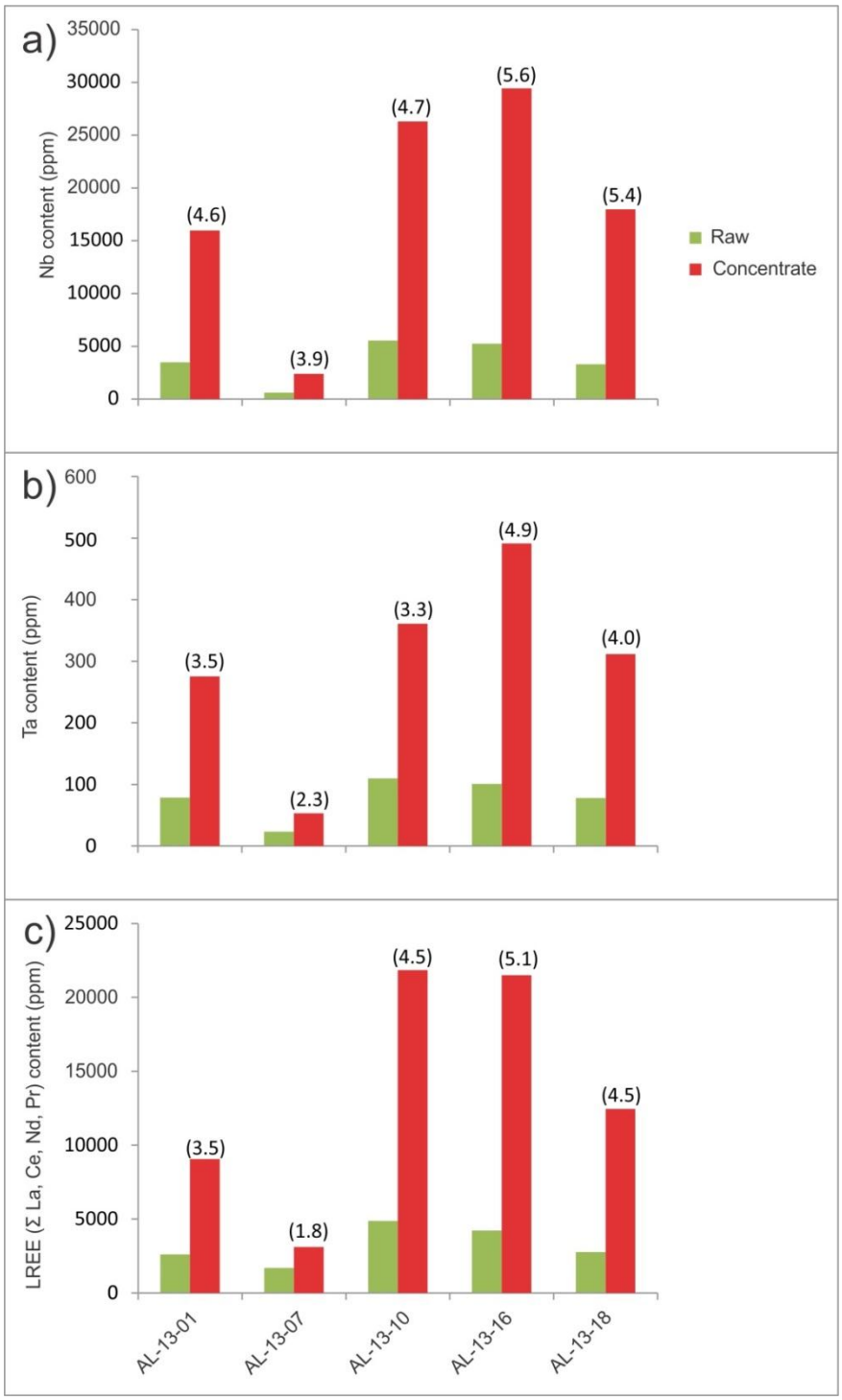

Figure D.4 Comparison of a) Nb, b) Ta, and c) LREE (Σ La, Ce, Nd, Pr) concentrations in Wilfley table concentrates relative to corresponding raw samples from Aley. Concentration factors for each element or group of elements for individual samples are shown in parentheses.

Table D.1 Selected major and minor elemental composition (ppm) of the 125–250 µm size fraction of stream sediments from the Aley area, analysed by portable XRF. Phosphorous content was determined by lab analysis using fused bead, acid digestion, and ICP-AES analysis. Modified from Section 3.1.1.

Sample no.	Split Size (g)	Nb	Ta	LREE	La	Ce	Pr	Nd	Y	Ba	Sr	P*	U	Th	Fe	Ca
AL-13-01	380.4	3495	79	2602	596	936	346	724	72	670	711	10822	26	266	40852	78201
AL-13-07	383.1	615	23	1690	316	505	289	580	34	244	688	6327	6	68	22375	160338
AL-13-10	510.1	5543	110	4879	1280	1918	520	1161	104	505	944	14619	40	376	65852	154081
AL-13-16	938.4	5246	101	4229	1083	1648	470	1028	93	910	745	12000	36	355	59782	156997
AL-13-18	503.7	3311	78	2763	662	1025	355	721	71	688	747	10997	26	255	42845	166097

*Lab analysis by ICP-AES

Table D.2 Selected major and trace element composition (ppm) of Wilfley table concentrates from the Aley area, analysed by portable XRF. Phosphorous was determined by ICP-AES analysis.

Sample no.	Nb	Ta	LREE	La	Ce	Pr	Nd	Y	Ba	Sr	P*	U	Th	Fe	Ca
AL-13-01	15977	275	9058	2528	3885	769	1876	238	1473	988	25964	112	926	128372	164276
AL-13-07	2387	53	3107	754	1156	374	823	71	251	888	14837	14	184	37174	206324
AL-13-10	26293	361	21845	6692	10006	1367	3779	368	1055	943	26052	147	1209	265897	126498
AL-13-16	29441	491	21493	6516	9902	1370	3706	396	3327	861	24743	162	1371	273248	118279
AL-13-18	17983	312	12451	3621	5534	904	2392	274	1912	1006	26663	109	993	167279	155281

*Lab analysis by ICP-AES

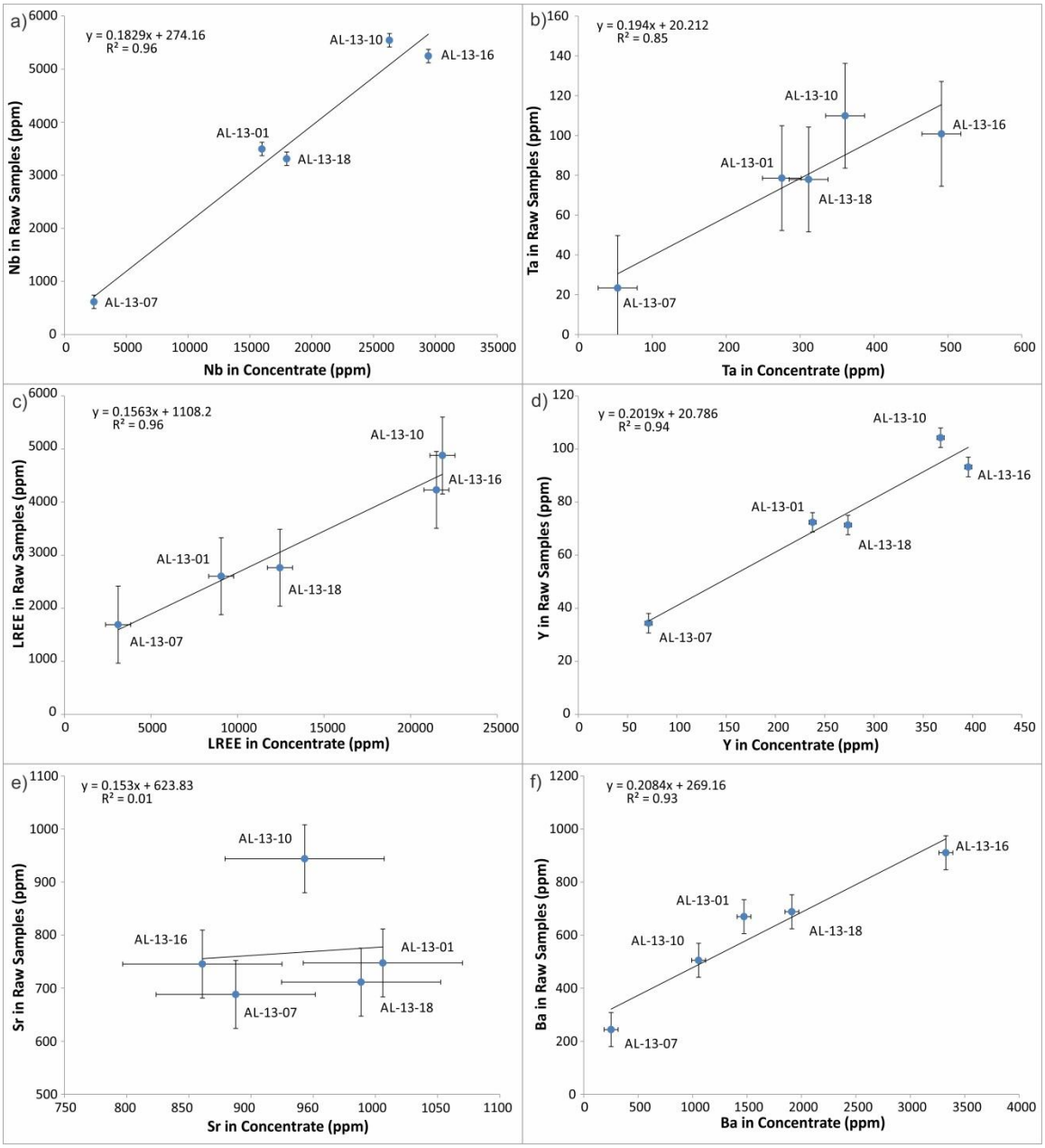

Figure D.5 Comparison of Wilfley table concentrates relative to raw samples from the Aley carbonatite. a) Nb. b) Ta; for raw samples Ta is near the lower detection limit, resulting in large errors relative to the concentrates. c) LREE; error propagation for ΣLREE results in larger margins relative to La, Ce, Pr, and Nd individually. d) Y. e) Sr. f) Ba. Error bars (2σ) are based on repeated analyses of standards as described in Appendix B.

D.6 Conclusions

The Wilfley shaking table successfully concentrated carbonatite pathfinder elements in the 125–250 μm size fraction of stream-sediment samples from the Aley carbonatite drainage. Niobium content of Wilfley table concentrates increased relative to raw samples by a factor of 4.8 (in the range of 600–30000 ppm). Similarly, Ta increased by 3.6 times (in the range of 20–500 ppm), and LREE by 3.9 times (in the range of 1700–22000 ppm). This indicates that the Wilfley table effectively concentrates the Nb-, Ta-, and LREE bearing heavy minerals targeted by this study (e.g. pyrochlore, columbite-[Fe], fersmite, REE-fluorocarbonates, monazite, zircon, apatite, and allanite). High coefficients of determination between pathfinder element concentrations in raw samples and Wilfley table concentrates suggests predictable relationships between indicator mineral counts in raw sediments and Wilfley table concentrates.